

Micro- and Nano- Fabrication and Replication Techniques



Why do we have to write thing
small and replicate fast ?





Plenty of Room at the Bottom

Richard P. Feynman, December 1959

How do we *write* it? We have no standard technique to do this now. But let me argue that it is not as difficult as it first appears to be. We can **reverse the lenses of the electron microscope** in order to demagnify as well as magnify. A source of **ions**, sent through the microscope lenses in reverse, could be focused to a very small spot. We could write with that spot like we write in a TV cathode ray oscilloscope, by going across in lines, and having an adjustment which determines the amount of material which is going to be deposited as we scan in lines. **This method might be very slow** because of space charge limitations. There will be more rapid methods. We could first make, perhaps by some **photo process**, a screen which has holes in it in the form of the letters. Then we would strike an arc behind the holes and draw metallic ions through the holes; then we could again use our system of lenses and make a small image in the form of ions, which would deposit the metal on the pin.





Plenty of Room at the Bottom

Richard P. Feynman, December 1959

A simpler way might be this (though I am not sure it would work): **We take light and, through an optical microscope running backwards**, we focus it onto a very small photoelectric screen. Then electrons come away from the screen where the light is shining. These electrons are focused down in size by the electron microscope lenses to impinge directly upon the surface of the metal. Will such a beam etch away the metal if it is run long enough? I don't know. If it doesn't work for a metal surface, it must be possible to find some surface with which to coat the original pin so that, where the electrons bombard, a change is made which we could recognize later.





Plenty of Room at the Bottom

Richard P. Feynman, December 1959

There is no intensity problem in these devices---not what you are used to in magnification, where you have to take a few electrons and spread them over a bigger and bigger screen; it is just the opposite. The light which we get from a page is concentrated onto a very small area so it is very intense. The few electrons which come from the photoelectric screen are demagnified down to a very tiny area so that, again, they are very intense. **I don't know why this hasn't been done yet!**



Fabrication of Nanomaterials

- Top-down
 - Begin with bulk materials that are reduced into nanoparticles
- Bottom-up
 - Begin with atoms and molecules that can grow into zero, one, two and three-dimensional nanostructures
- Hybrid



Top-down

- Mechanical energy
 - Ball milling, polishing, grinding
- Thermal
 - Annealing, evaporation, pyrolysis
- High energy
 - Arch, laser, ion milling, reactive ion etching
- Chemical
 - Chemical etching, CMP, electropolishing, anodizing
- Lithographic
 - Photo, e-beam, EUV, X-ray, μ -cp, NIL, Nanosphere
- Nature
 - Erosion, decomposition, digestion



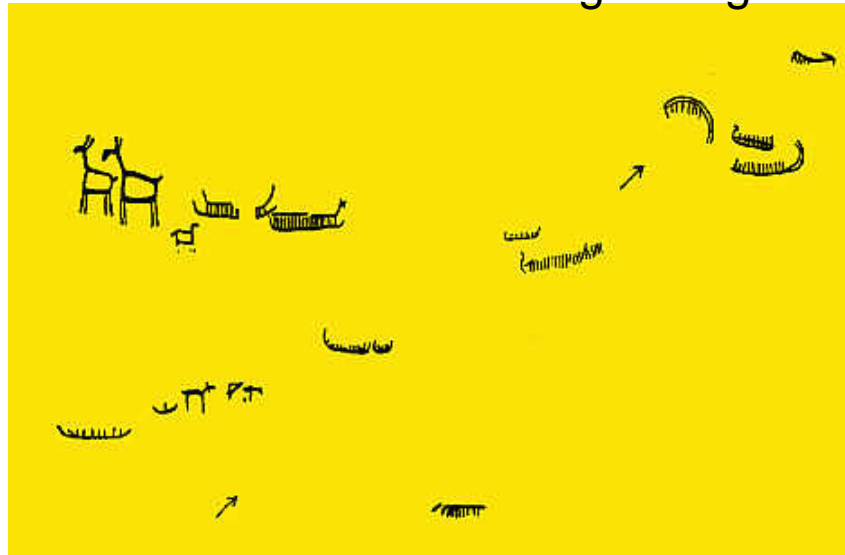
Bottom-up

- Gas
 - Chemical vapor deposition, atomic layer deposition, MOCVD, MBE, ion implantation
- Liquid
 - Self-assembly, supermolecule, reduction, template synthesis
- Lithographic
 - Dip-pen, block co-polymer, STM writing
- Biological
 - Protein, nuclear acid, crystal formation



Ancient Patterning

"This is the Elks' land". A greeting at the mouth of Dalbergsaa, Southern Dal.



It seems that the carvings of Northern Scandinavia's including Kola Peninsula are the oldest.
Large figures of ritual animals characterise the Mesolithic period mostly before c.4200 BC



Writing by Inks

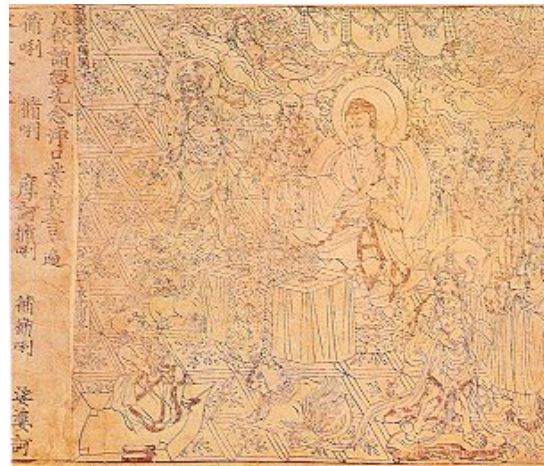
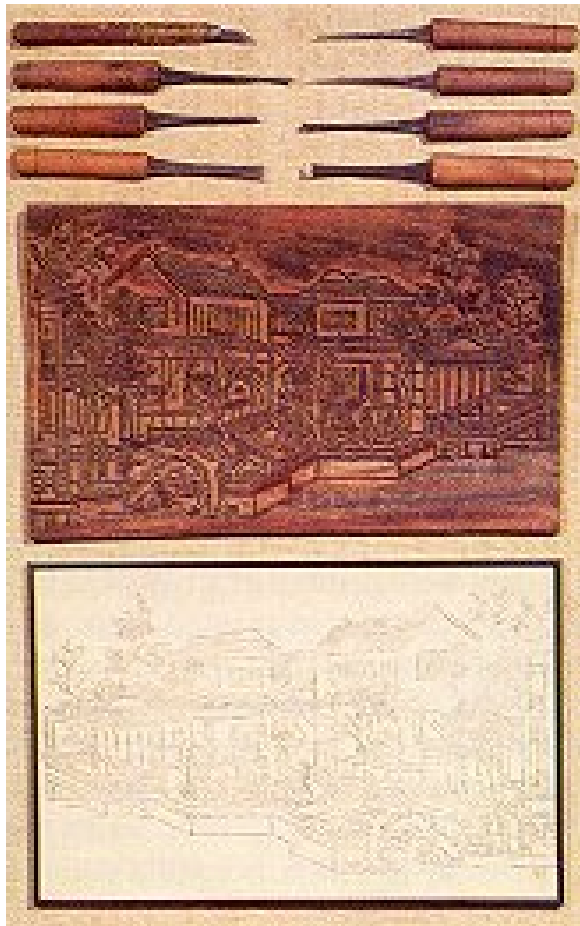


Writing Brush ~2000 Ys

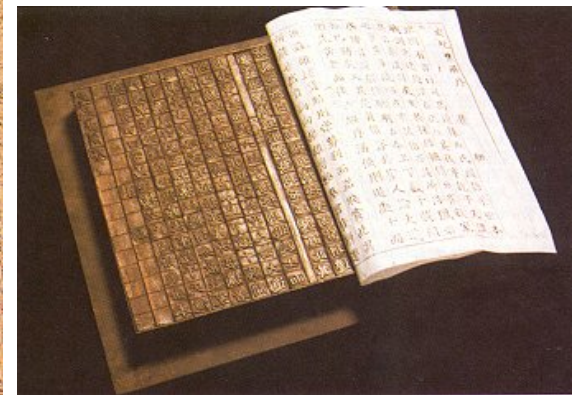
Quill Pen ~1000 Ys



Chinese Replication



868



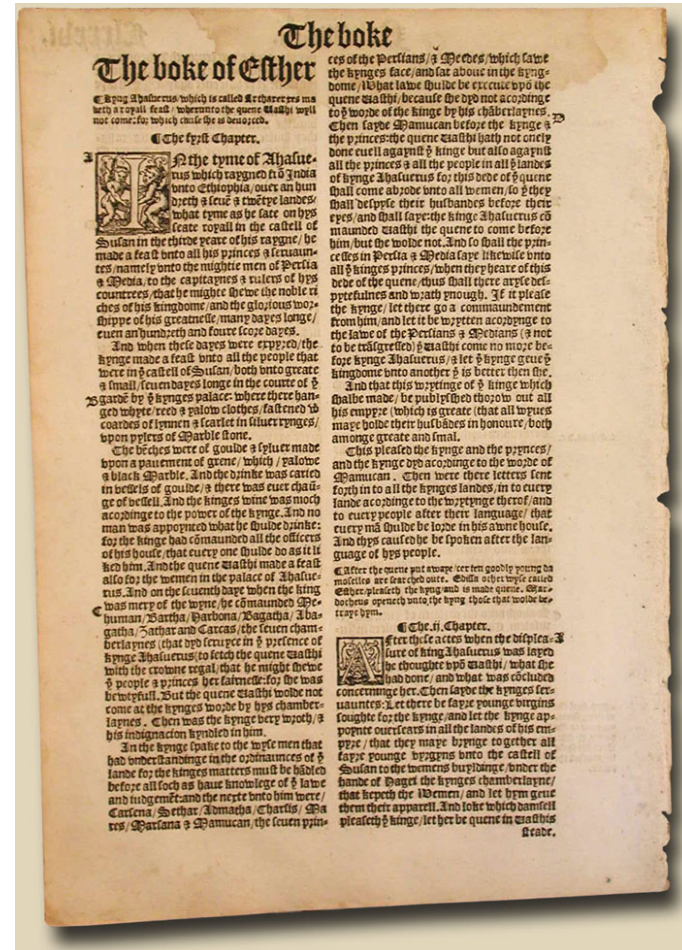
1041 and 1048



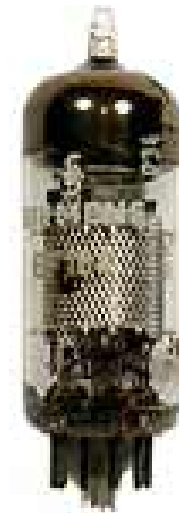
Western Replication



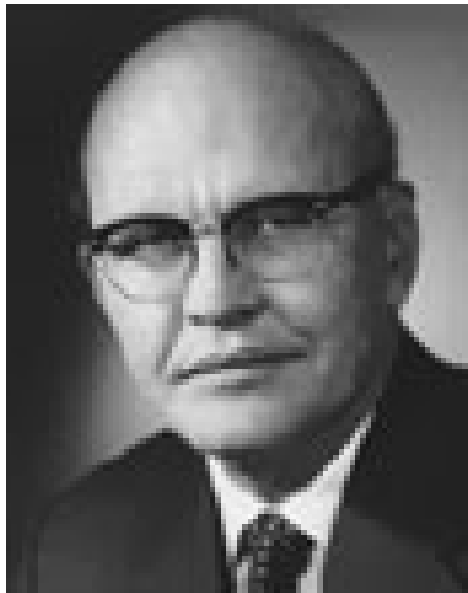
1543 - 1610



Building a computer

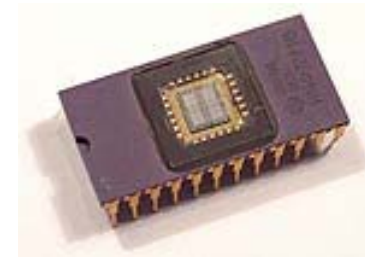


First Integrated Circuit

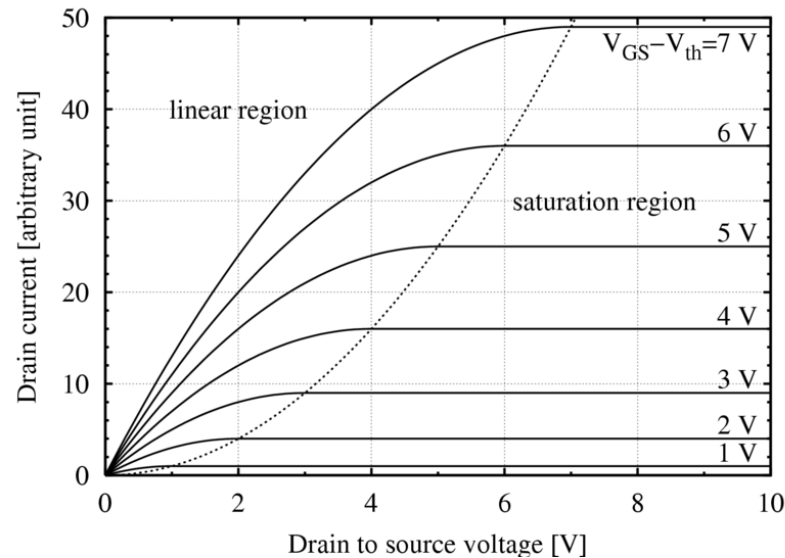
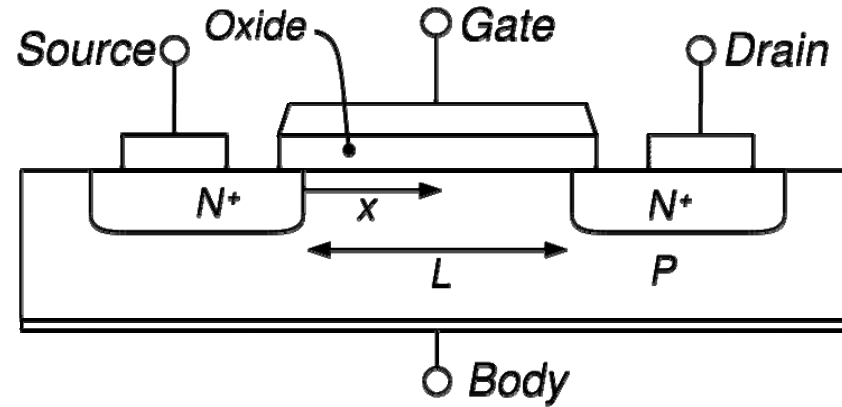
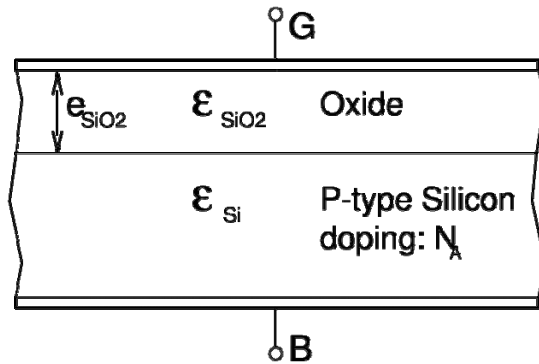


"What we didn't realize then was that the integrated circuit would reduce the cost of electronic functions by a factor of a million to one, nothing had ever done that for anything before" - Jack Kilby 2000 Nobel Prize

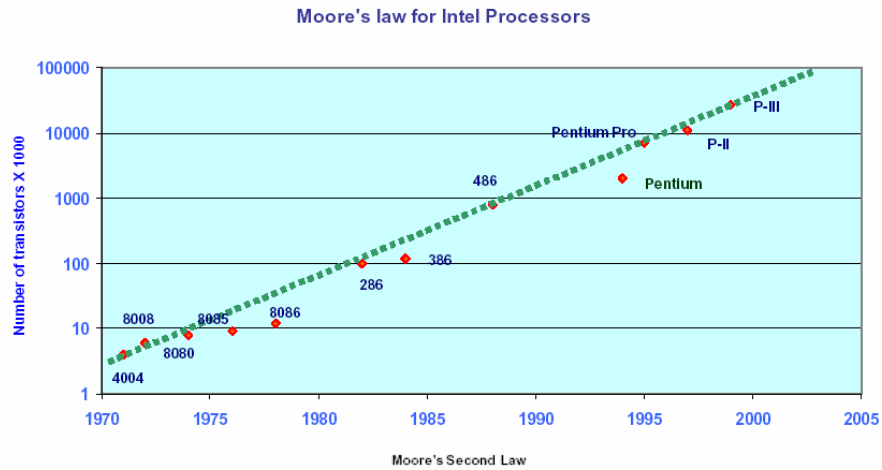
1958 Texas Instruments



metal-oxide-semiconductor field-effect transistor (MOSFET)



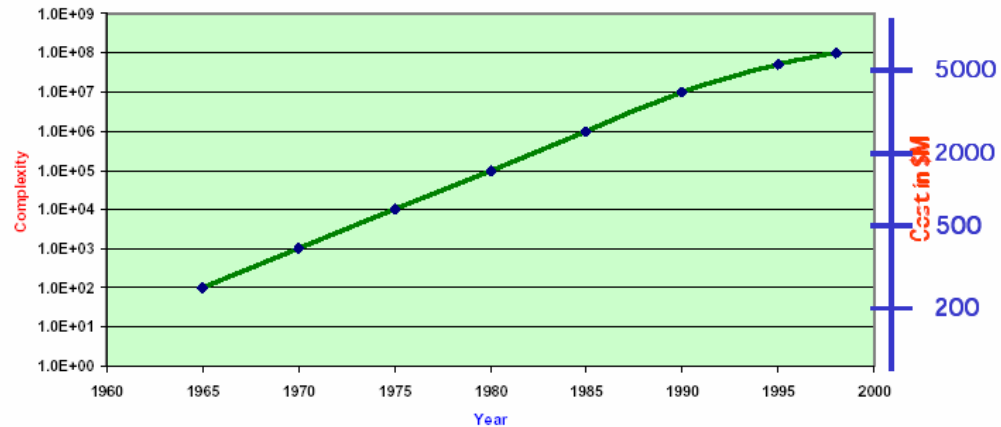
Moore's Law



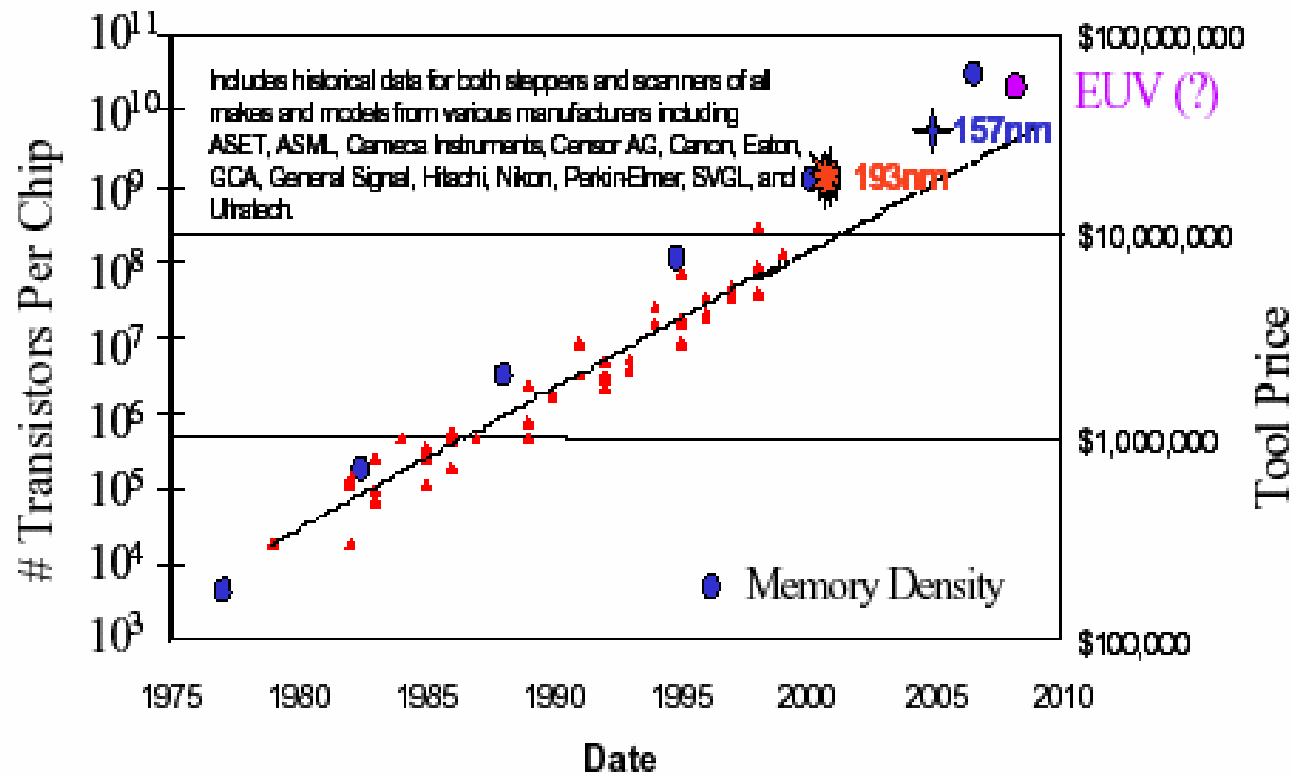
Moore's Laws

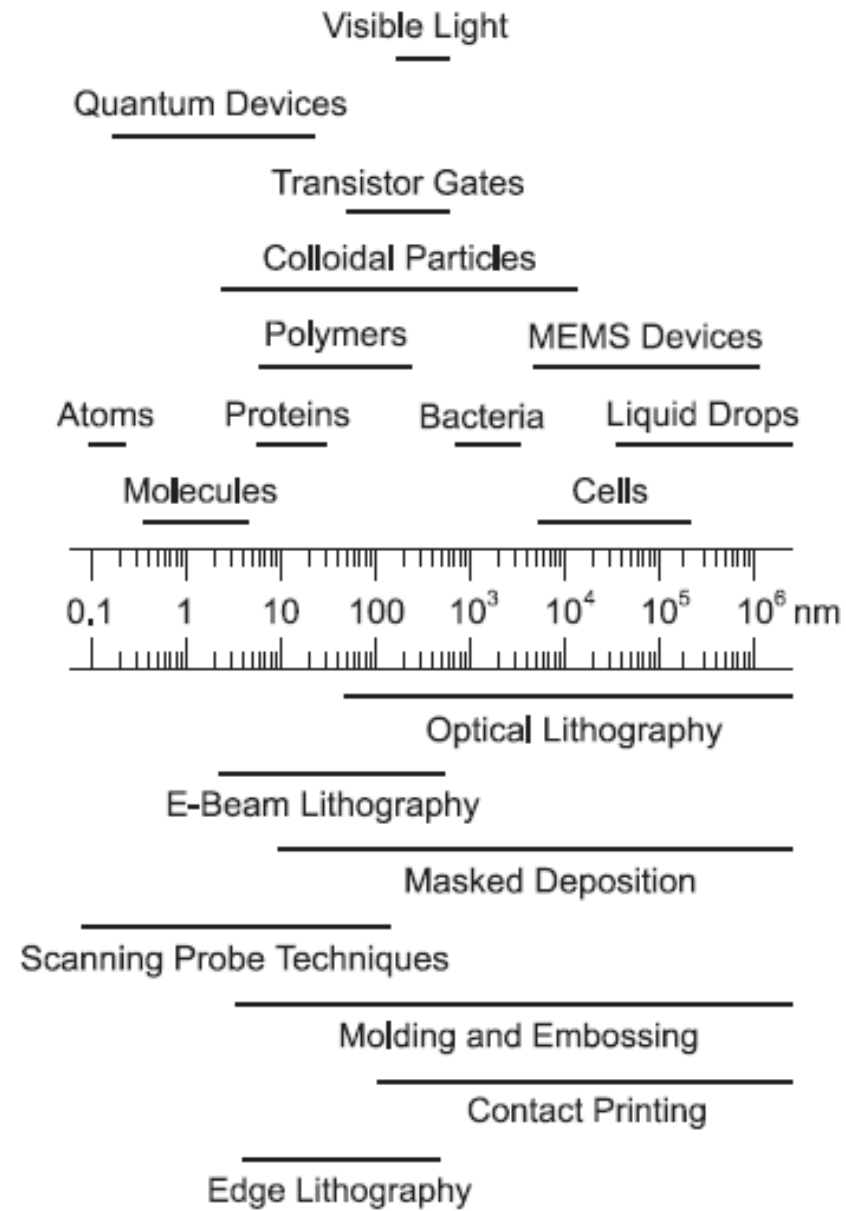
First Law: Number of components in a chip (IC) will double roughly every 18 months (1965, in *Electronics*). This has held true more or less since then.

Second Law: Facility costs increase on a semilog scale (terminology due to Eugene Meieran, Intel Fellow). Fab costs double approximately every four years.



Tool Cost



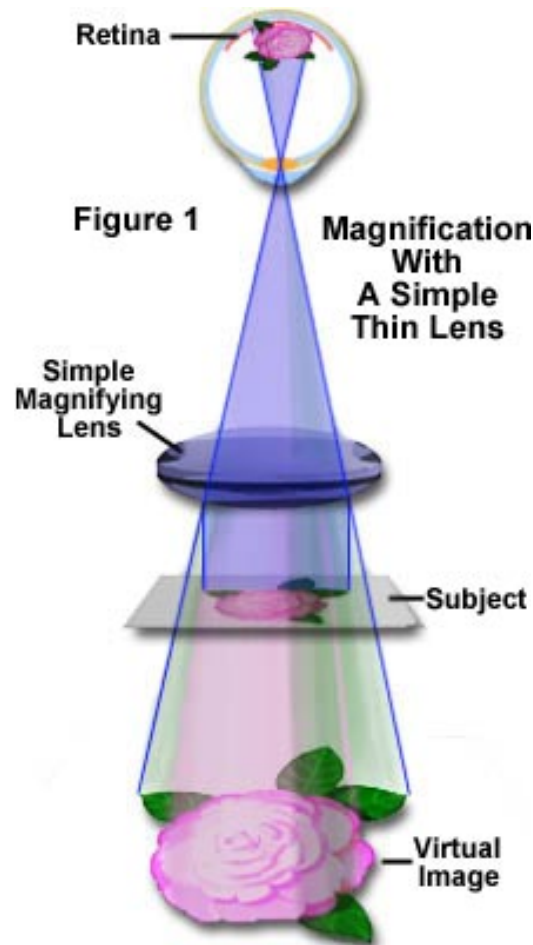


Industrial Process

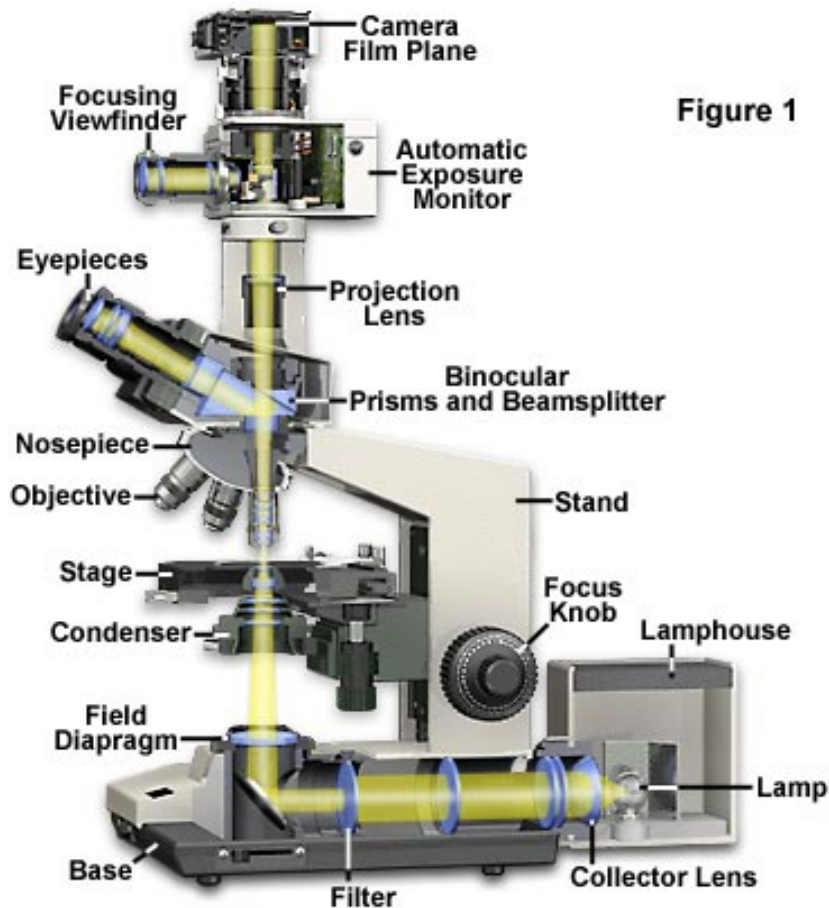
- Lithography
- Deposition
- Etching
- Planization
- Packaging



Optical Microscope

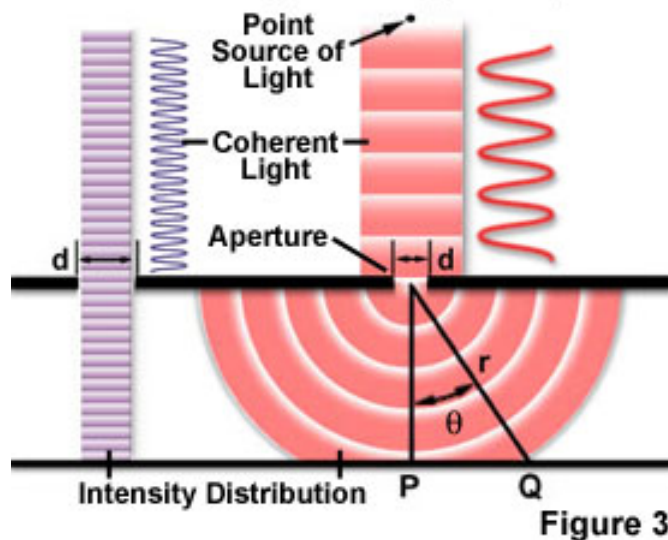


Modern Microscope Component Configuration

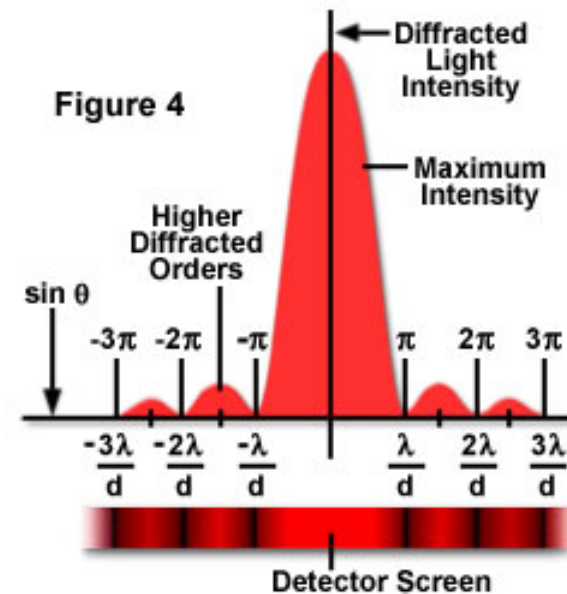


Limit of Photolithography

Diffraction of Light Through an Aperture



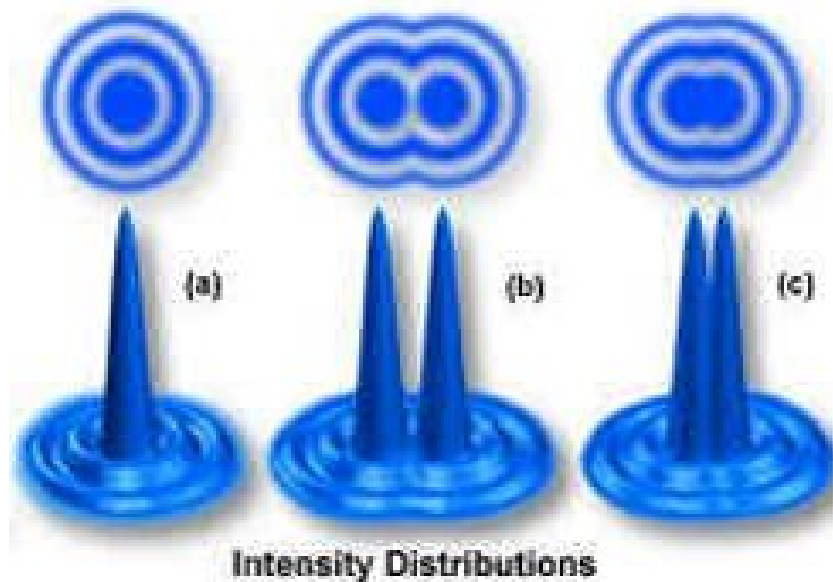
Intensity Distribution of Diffracted Light



$$r = 1.22 \times \lambda / (2 \times \text{N.A.})$$
$$\text{N.A.} = n \times \sin(\theta)$$



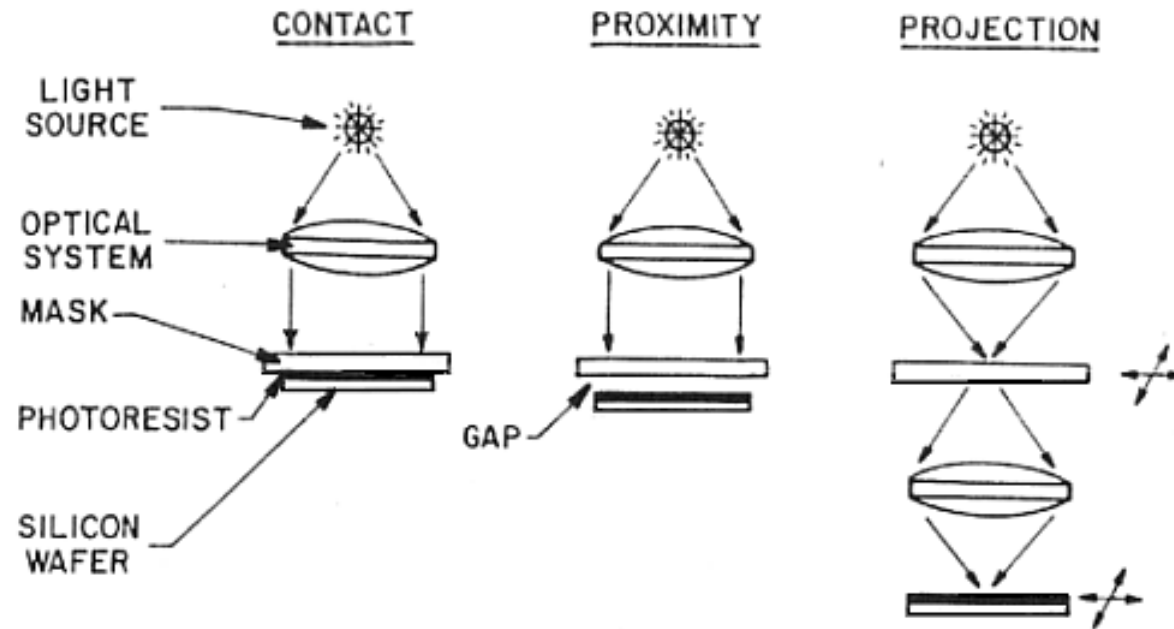
Diffraction Limit



$$\text{Resolution} = K \times \lambda / (\text{N.A.})$$
$$\text{Depth of Focus} = \lambda / (\text{N.A.})^2$$
$$K = 0.61$$



Methods of Photolithography

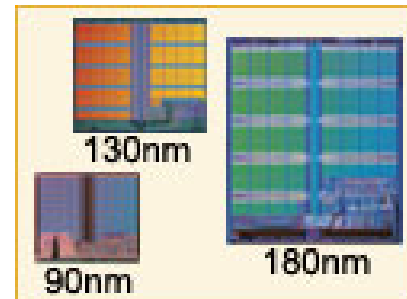
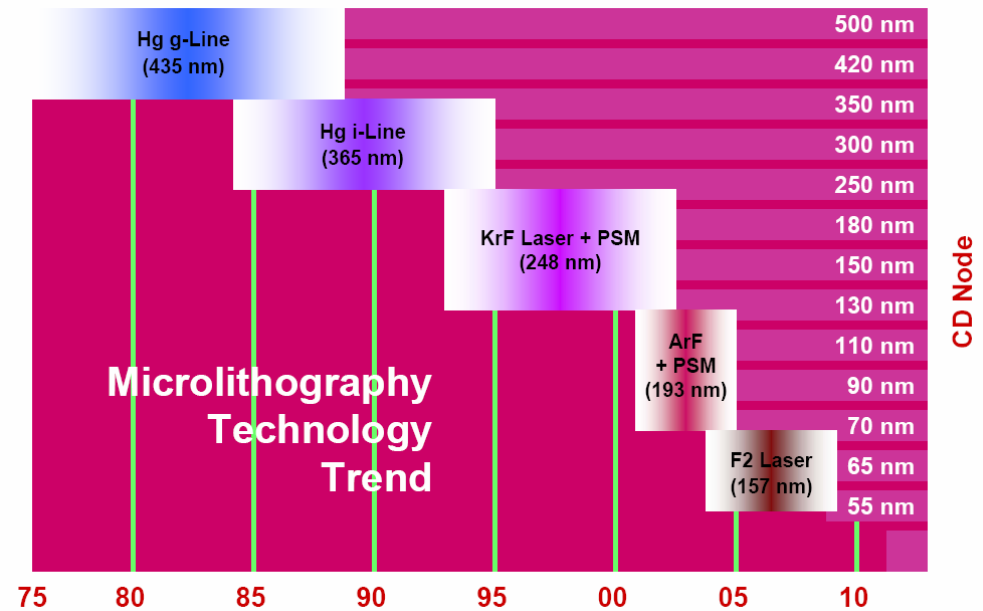


$$W_{\min} = k_1 \sqrt{\lambda d}$$

$$W_{\min} = k_1 \lambda / \text{NA}$$



Photolithography



UV Wavelength (nm)	Wavelength Name	UV Emission Source
436	g-line	Mercury arc lamp
405	h-line	Mercury arc lamp
365	i-line	Mercury arc lamp
248	Deep UV (DUV)	Mercury arc lamp or Krypton Fluoride (KrF) excimer laser
193	Deep UV (DUV)	Argon Fluoride (ArF) excimer laser
157	Vacuum UV (VUV)	Fluorine (F ₂) excimer laser

Year	Linewidth (nm)	Wavelength (nm)
1986	1,200	436
1988	800	436/365
1991	500	365
1994	350	365/248
1997	250	248
1999	180	248
2001	130	248
2003	90	248/193
2005 (fcst)	65	193
2007 (fcst)	45	193



Water Immersion Lithography

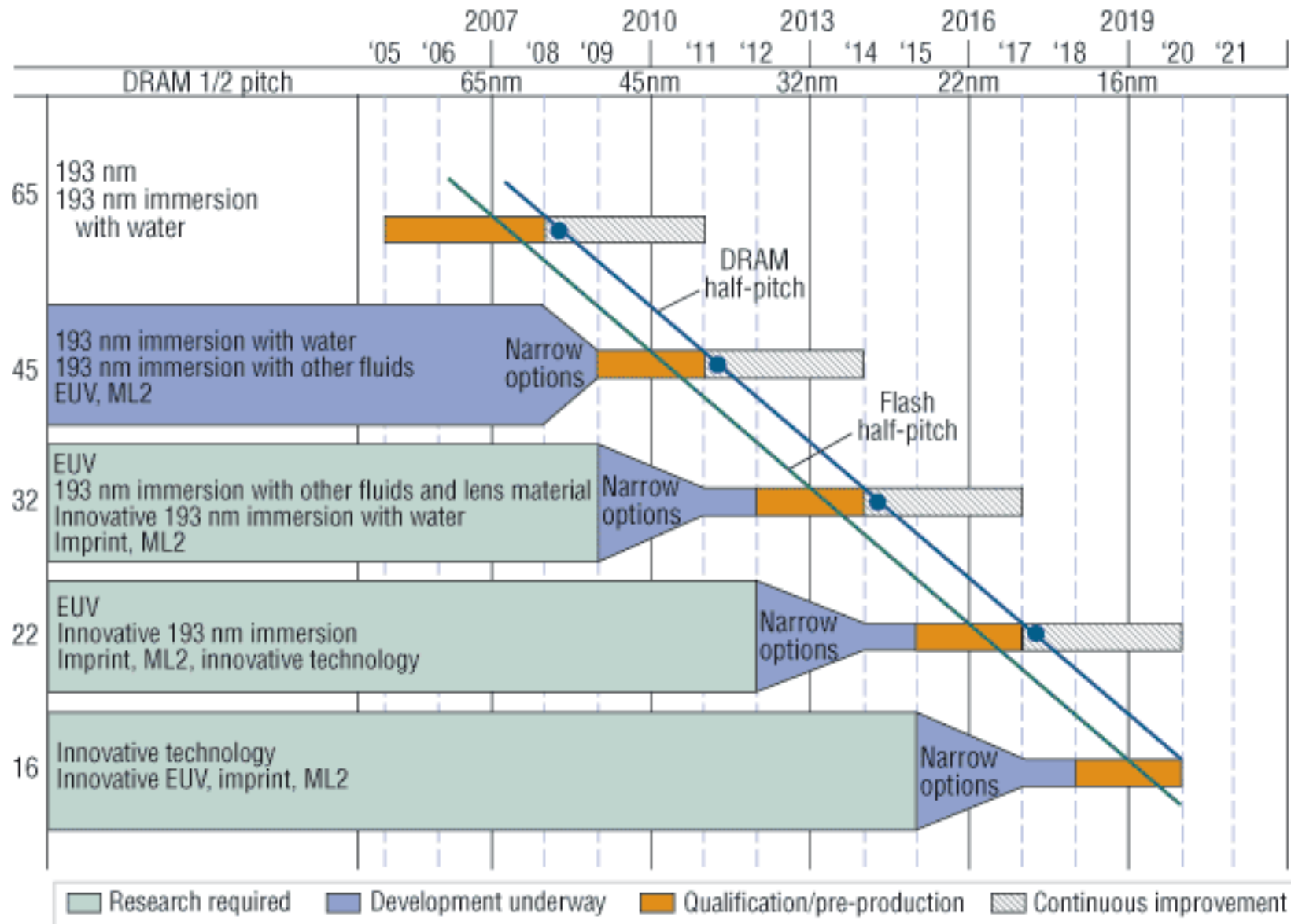
Year	Linewidth (nm)	Wavelength (nm)
1986	1200	436 g-line mercury lamp
1988	800	436/365
1991	500	365 i-line mercury lamp
1994	350	365/248
1997	250	248 KrF excimer laser
1999	180	248
2001	130	248
2003	90	248/193
2005	65	193 ArF excimer laser
2007	45	193/157

$$\text{Resolution (R)} = K \times \lambda / (\text{N.A.})$$

$K = 0.25$, $NA \sim 1.4$, $\lambda = 193$
 $R = 35 \text{ nm}$

Air $n = 1.0003$
Water $n = 1.437$

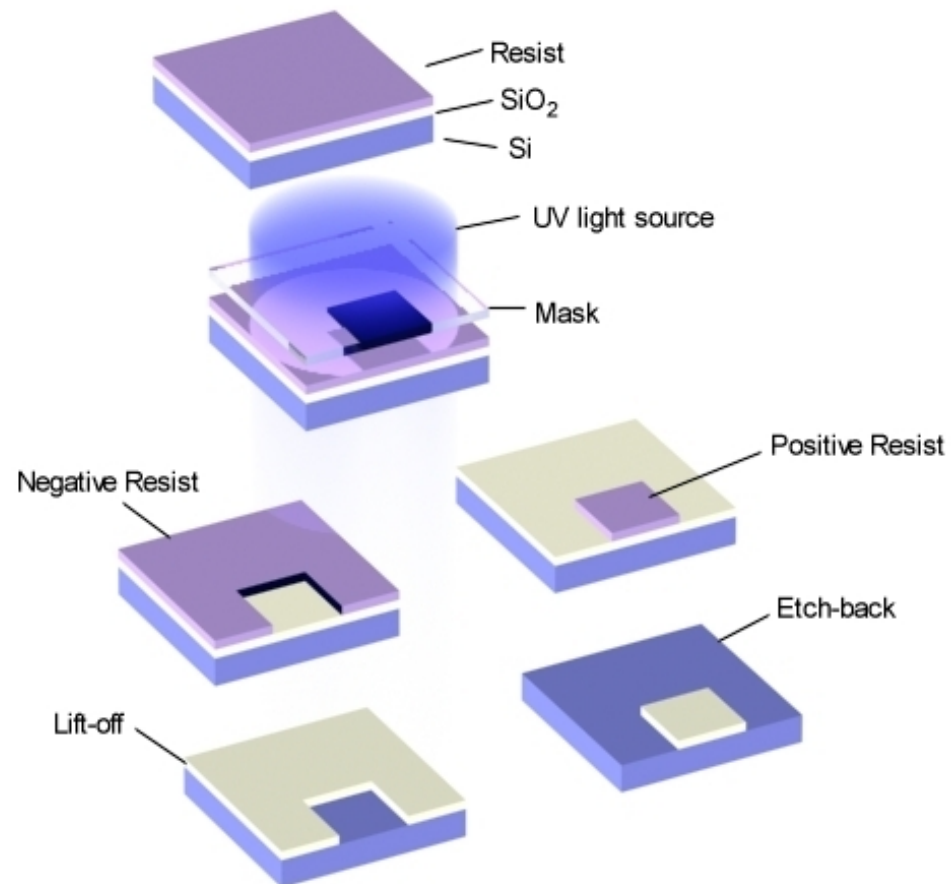




This legend indicates the time during which research, development, and qualification/pre-production should be taking place for the solution.



Photolithography Process



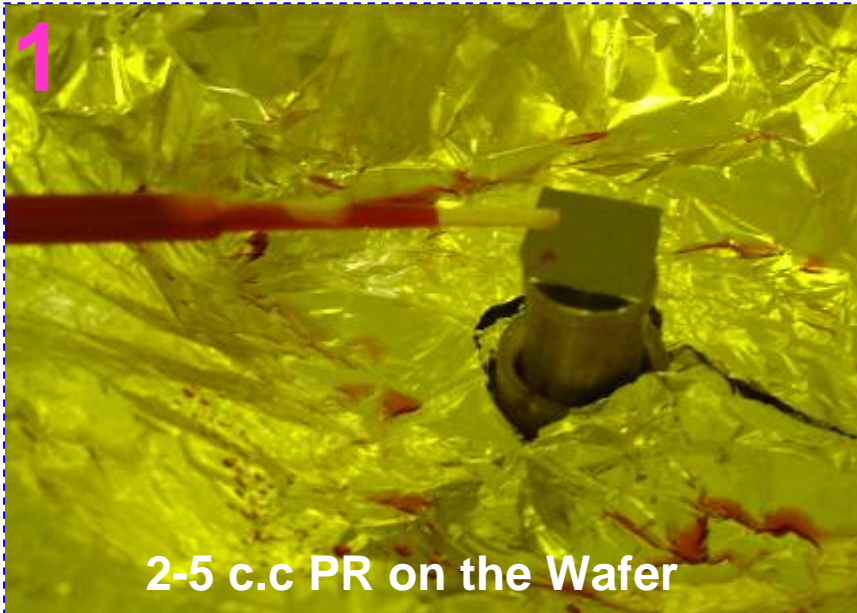
RCA Cleaning (By Radio Corporation of America in 1965)

Chemicals	Volume ratio	Procedure Time (min)	Operation Temperature	Function
Trichloroethane		5	Room T	Dissolve Organic
Acetone		5	Room T	Dissolve Organic
DI Water		5	Room T	Washing
H ₂ SO ₄ (98%)-H ₂ O ₂ (30%) (Piranha Solution)	3:1	10-20	~90°C	Oxide and Dissolve Organic and Metals
DI Water		5	Room T	Washing
HF(49 wt %)-H ₂ O	~2:100	10-20	Room T	Dissolve surface SiO ₂
NH ₄ OH(29%)-H ₂ O ₂ (30%)- H ₂ O	1:1:5	10-20	~90°C	Oxide and Dissolve Metals
DI Water		5	Room T	Washing
HCl(37%)- H ₂ O ₂ (30%)- H ₂ O	1:1:5	10-20	~90°C	Oxide and Dissolve Metals
DI Water		5	Room T	Washing
Spin Dry (In lad – N ₂ blow)				



Spin Coating Photoresist on Wafer

1



2-5 c.c PR on the Wafer

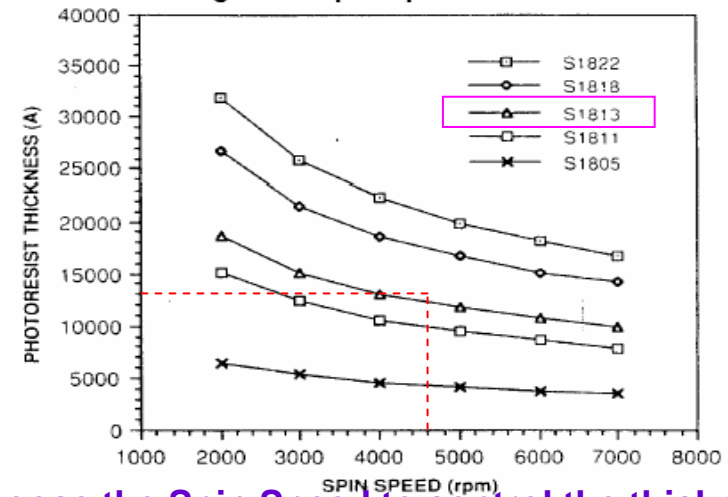
2



Wait for 5 to 15 second

3

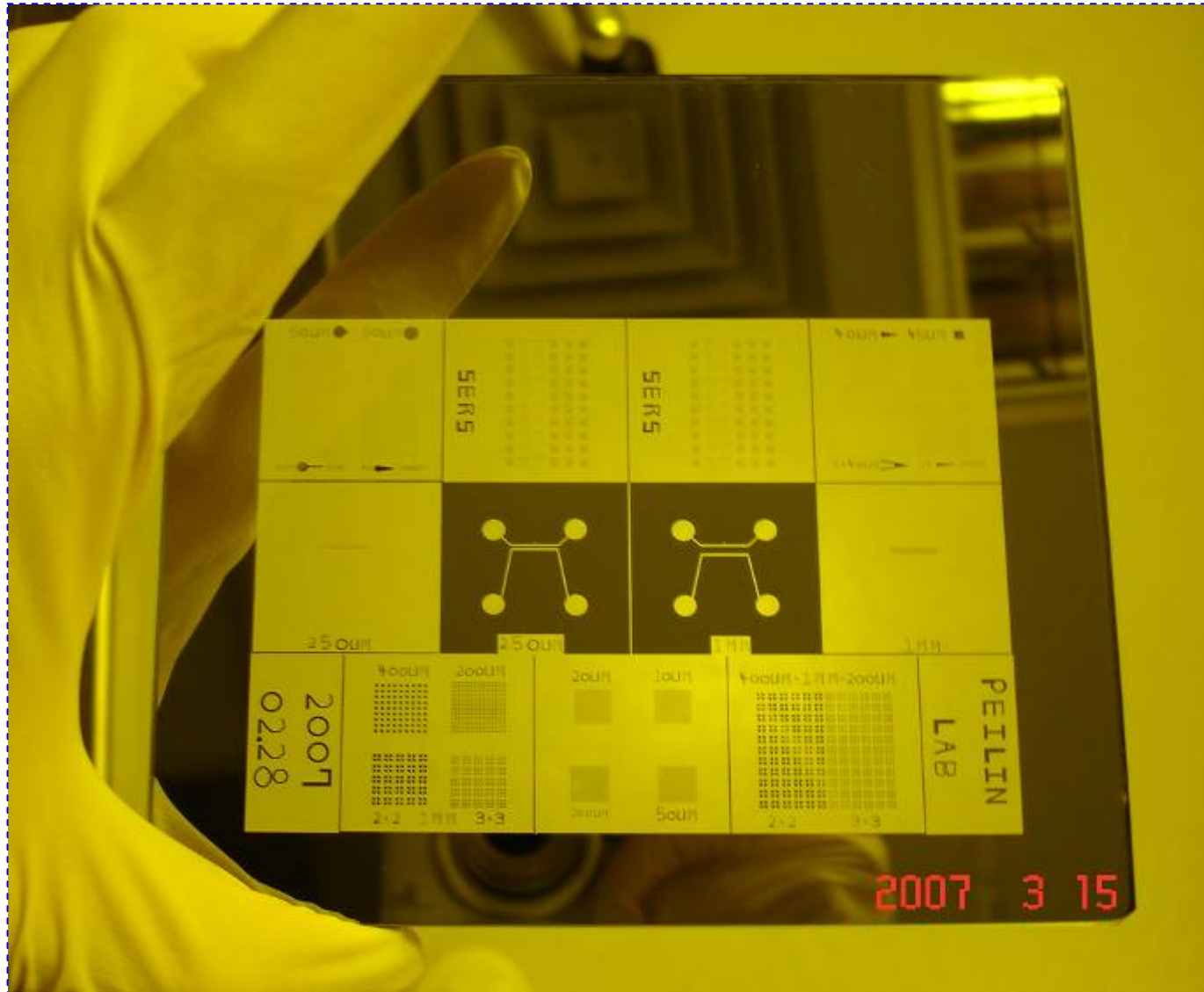
MICROPOSIT S1800 PHOTO RESIST UNDYED SERIES
Figure 1. Spin Speed Curves



Choose the Spin Speed to control the thickness

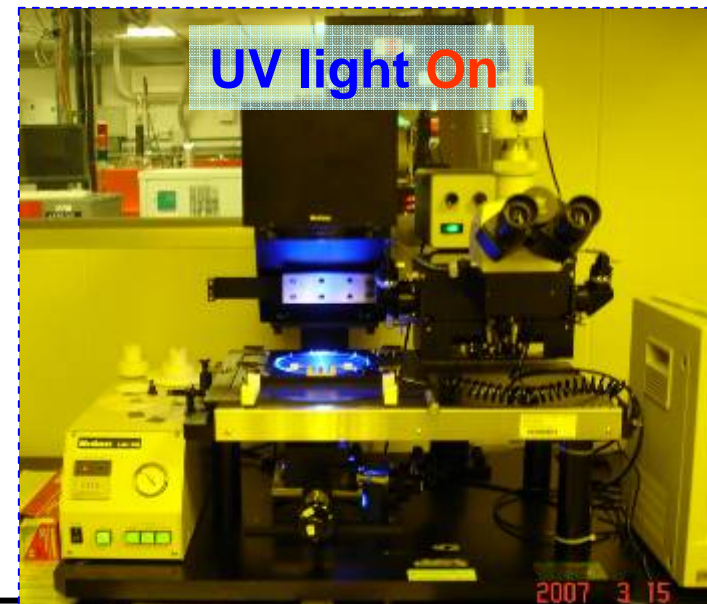
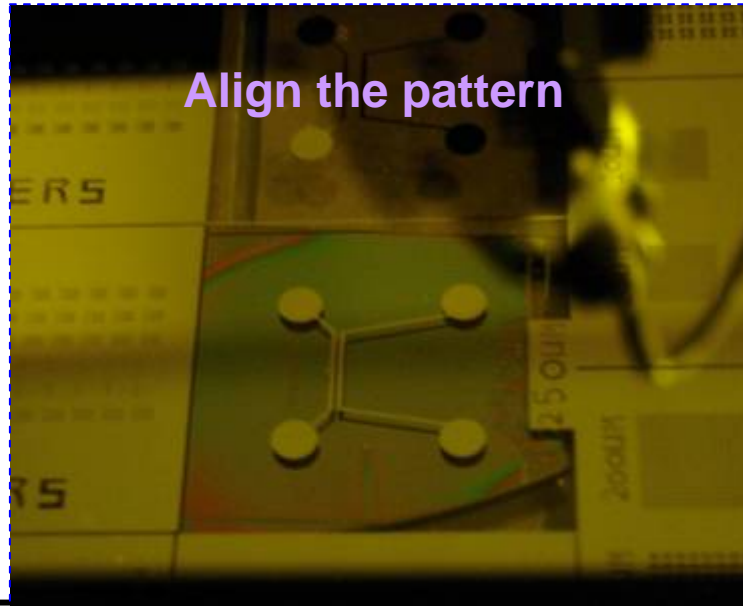
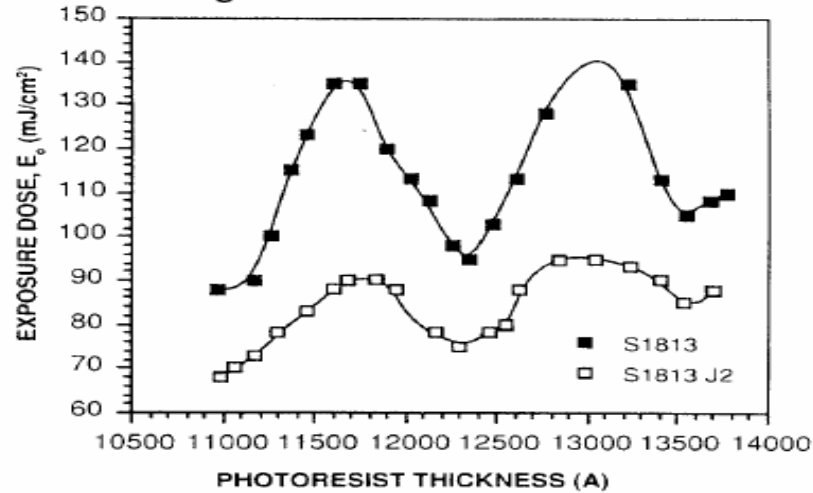
- Photo resist : Shipley 1813
- Spin : 2000 rpm 5 s
4500 rpm 15 s
- Soft Bake : 110°C 60 s
- Exposure : 7 s
- Developed : MF319 for 15 s

Standard Mask Size: 5" x 5"

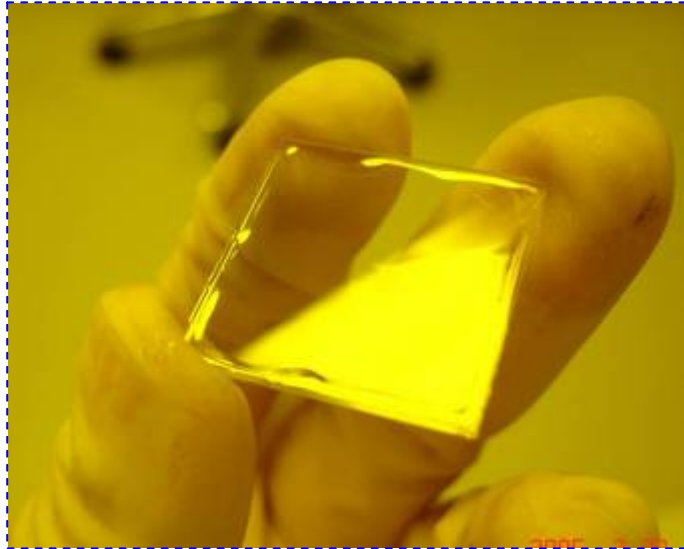


Align the pattern and Exposure

MICROPOSIT S1813 and S1813 J2 PHOTO RESISTS
Figure 4. Interference Curves



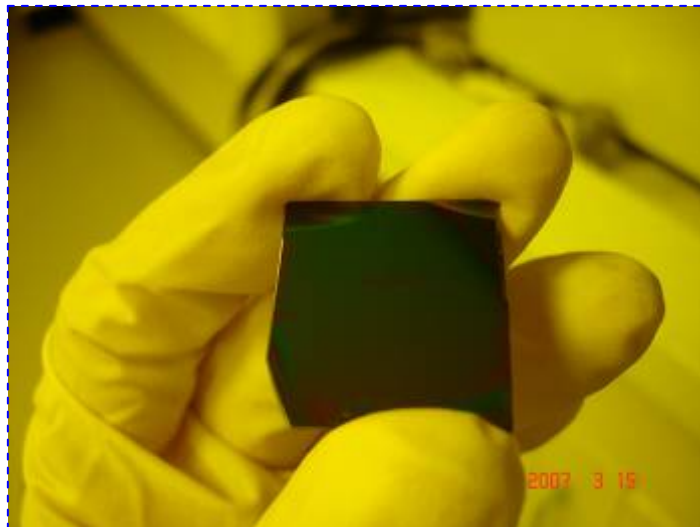
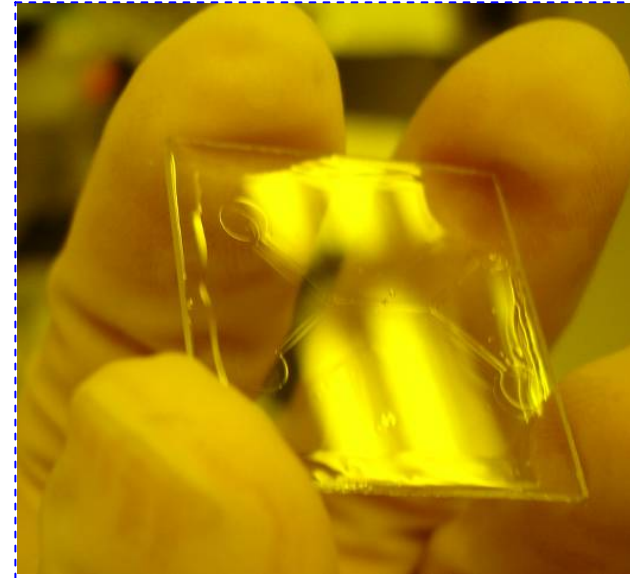
Some Photoresist Need PEB (post exposure Bake)



SU-8 2015

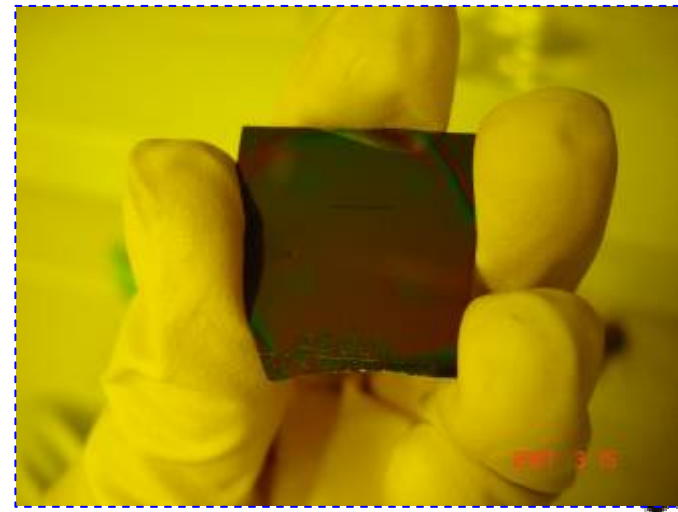
65 °C, 60 s

95 °C, 60 s

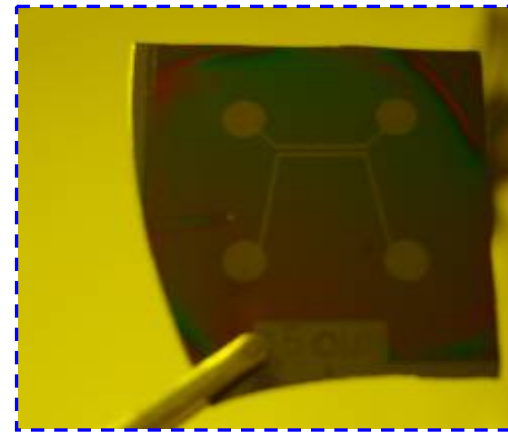
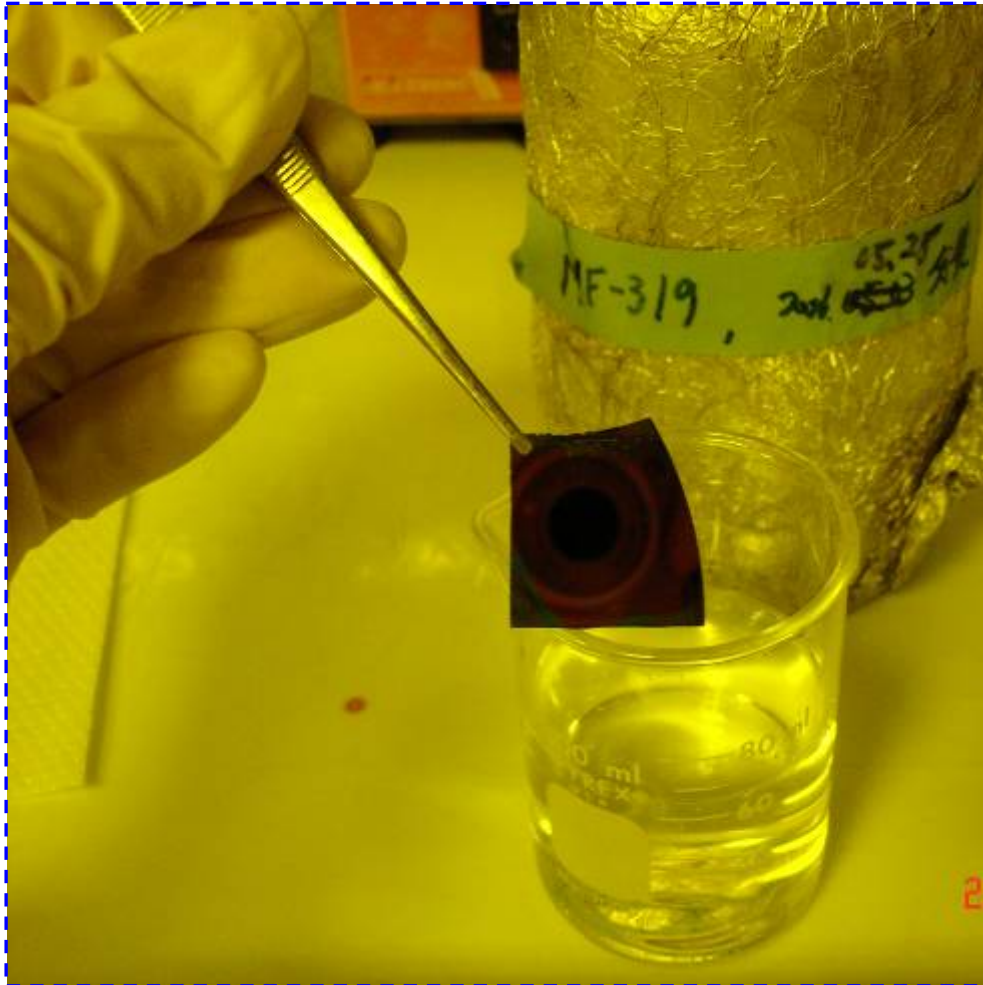


SPR 510A

90 °C, 90 s



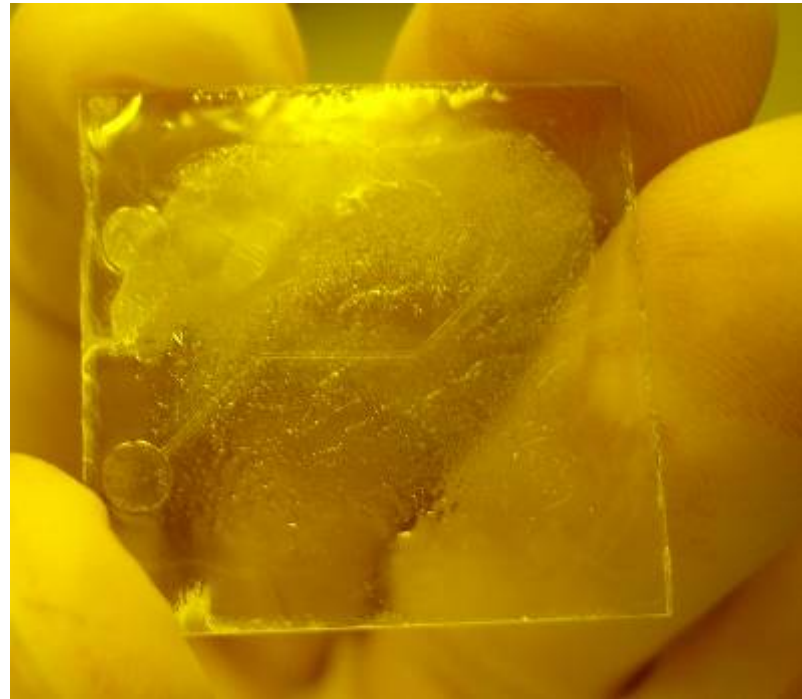
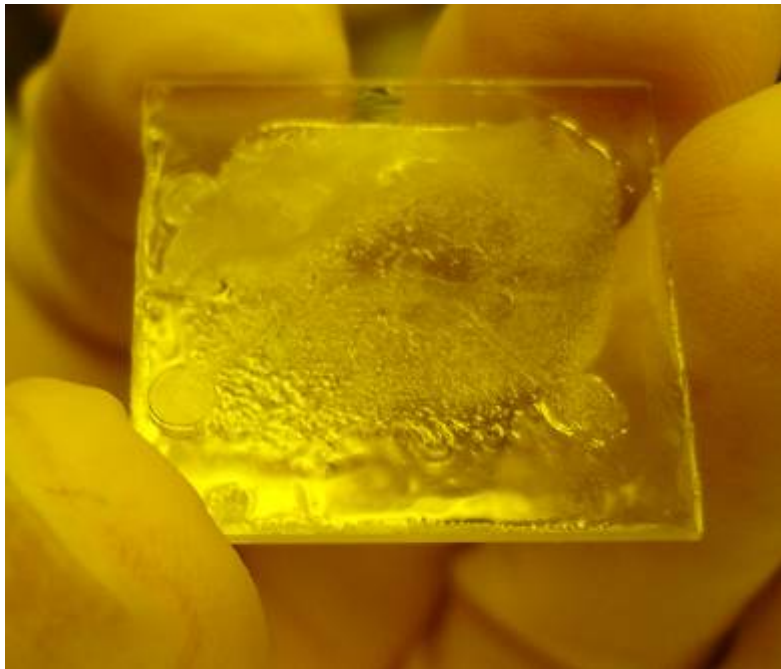
Develop the Photoresist



- Photo resist : **ShIPLEY 1813**
- Spin : 2000 rpm 5 s
4500 rpm 15 s
- Soft Bake : 110°C 60 s
- Exposure : 7 s
- Developed : **MF319 for 15 s**



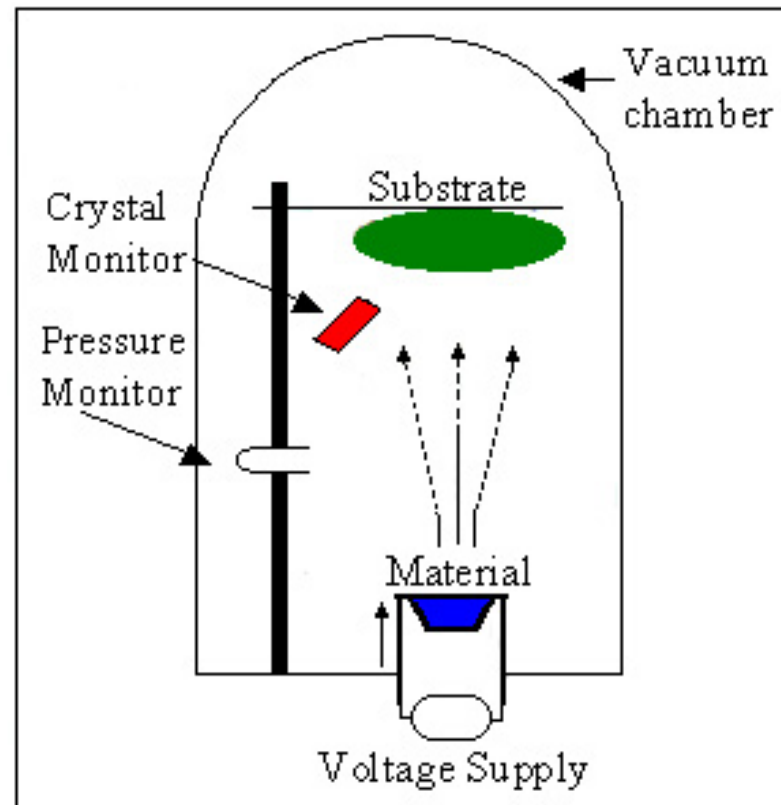
黃光室的黃光是很重要的



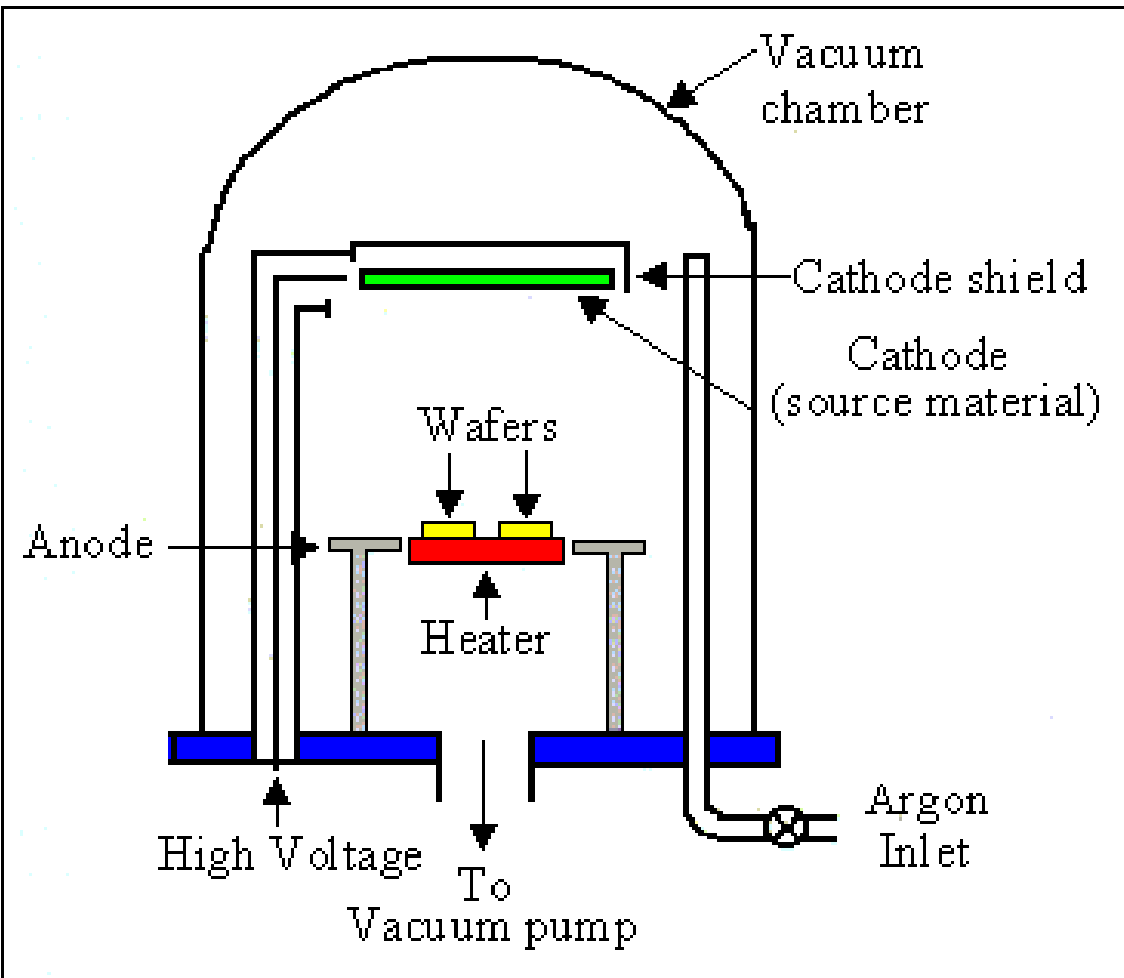
Lift OFF PROCESS BY ACETONE



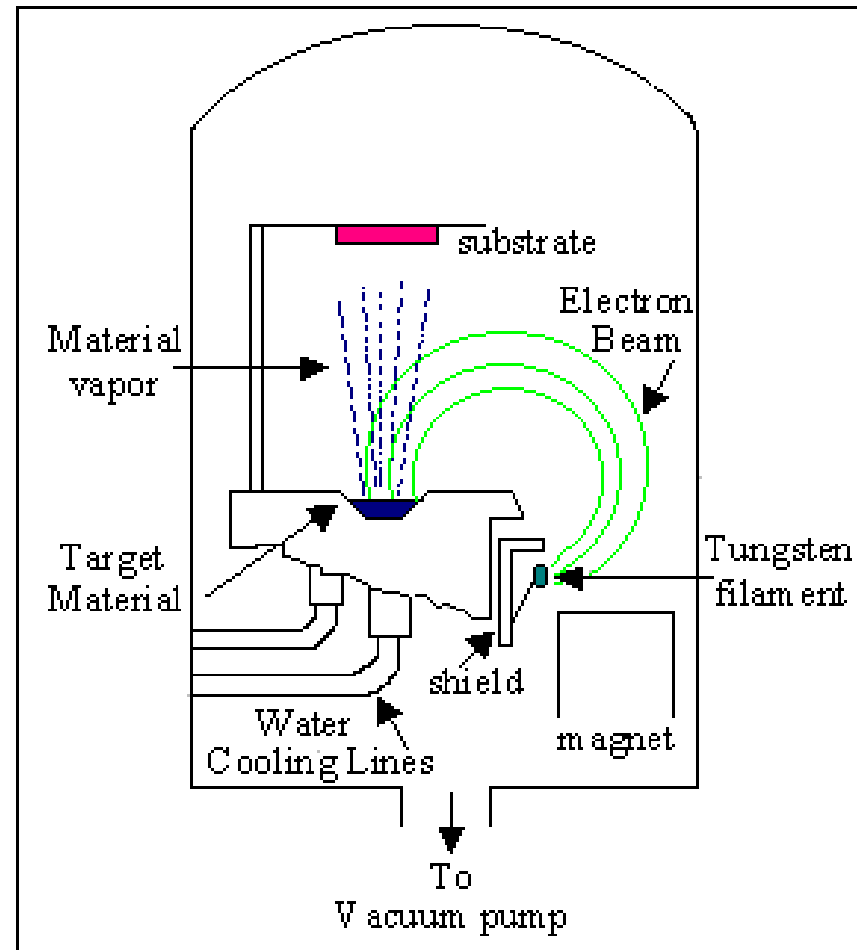
Thermal Evaporator



Sputter



E-beam Evaporator



RCAS E-Beam Evaporator



一. 儀器名稱

中文名稱：電子束蒸鍍系統

英文名稱：E-Beam

二. 儀器廠牌、型號及儀器購置年限

廠牌：聚昌科技 AST

儀器購置年限：民國92年7月

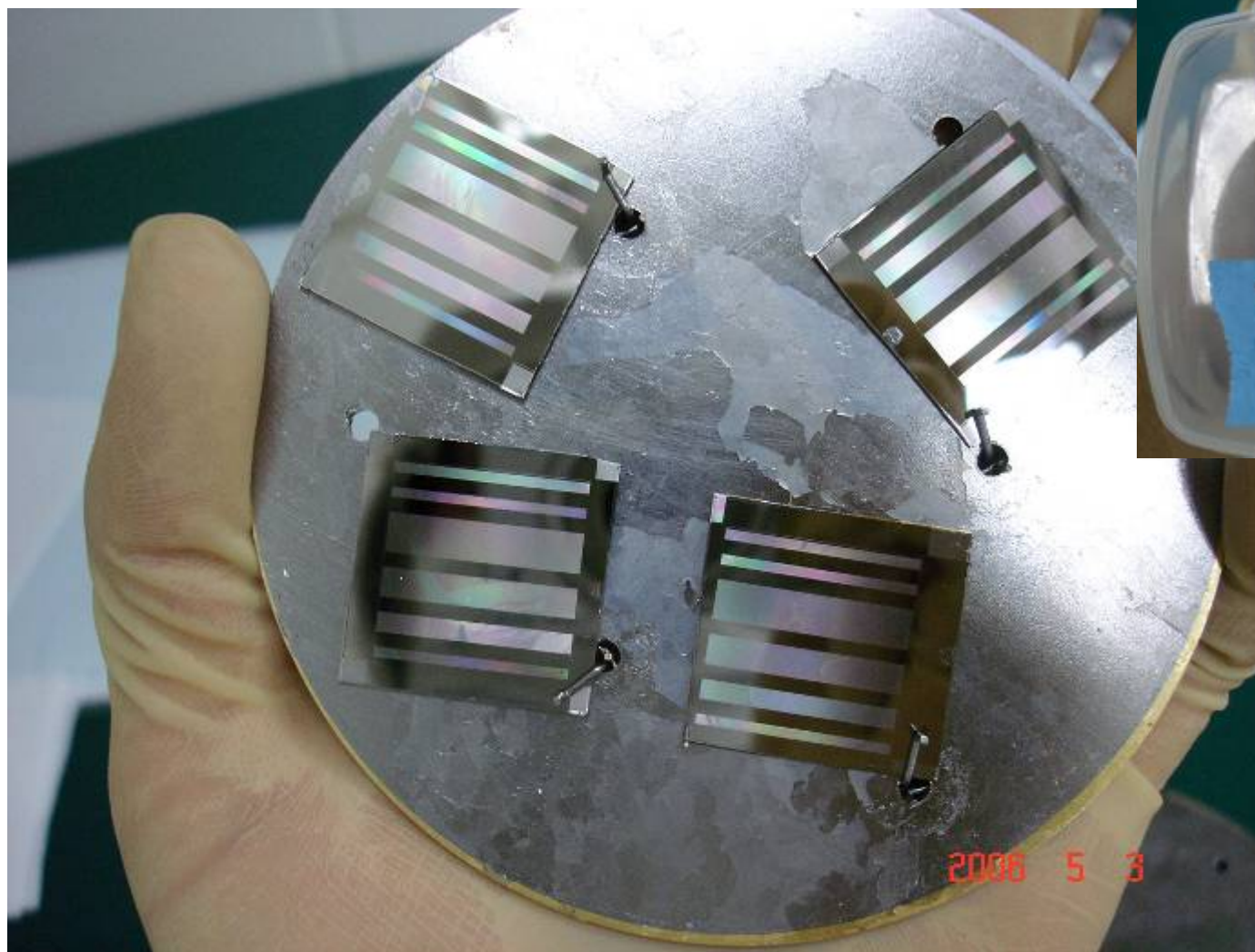
三. 重要規格

蒸鍍金屬: Ni、Ti、Au、Al、Pt、Cr

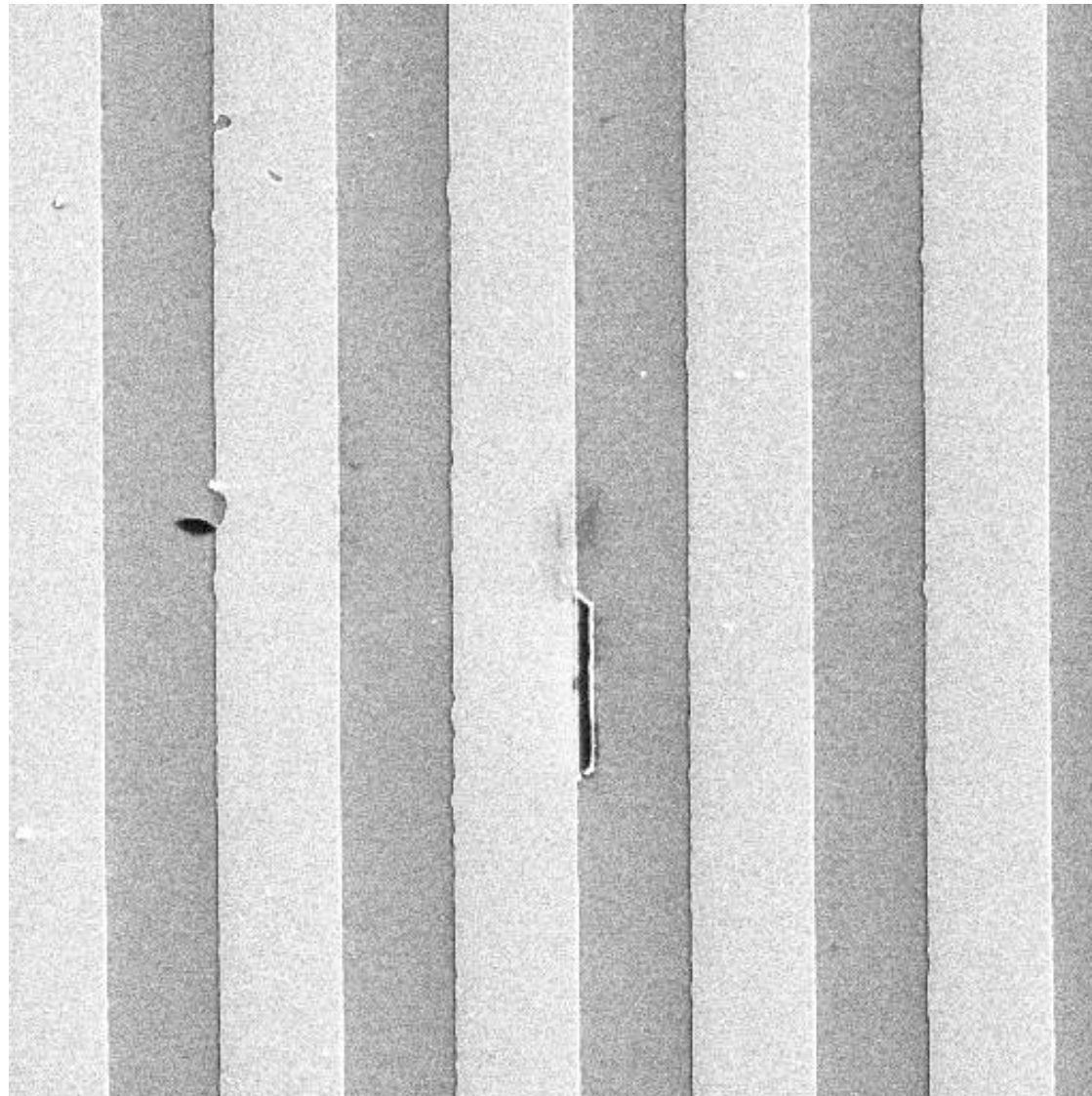
儀器配置圖



Ti 50 nm

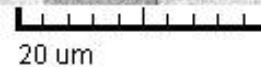


SEM image of Ti 50 nm on Si wafer



SEM MAG: 1.68 kx
View field: 89.76 um
VAC: HiVac

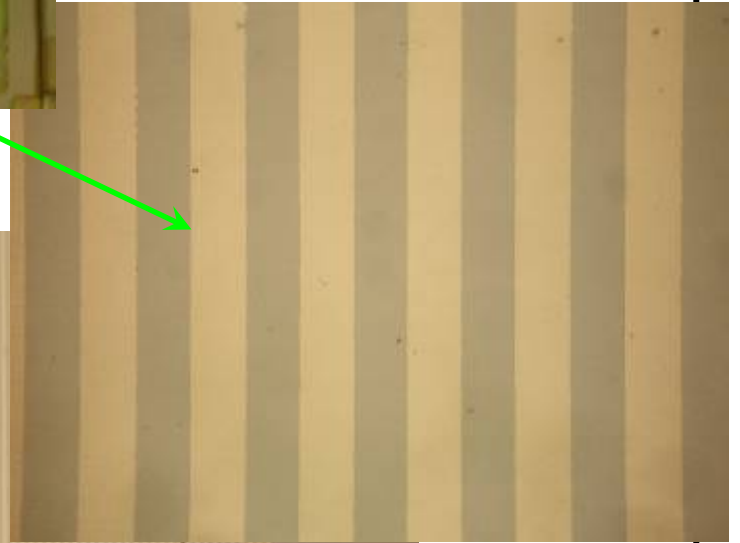
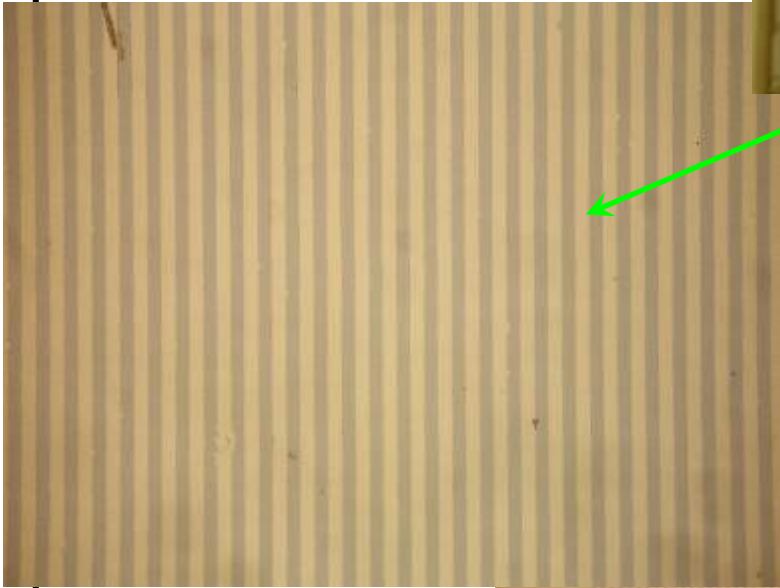
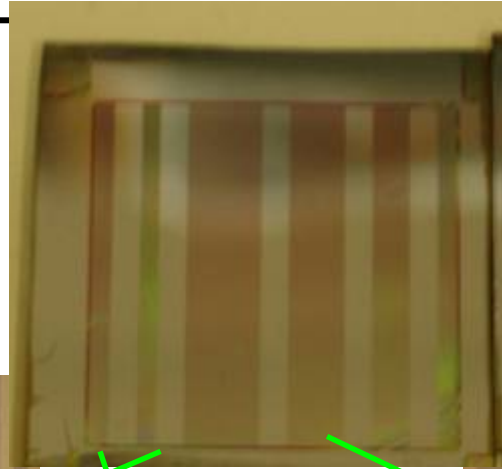
DET: SE Detector
DATE: 05/04/06
SM: RESOLUTION



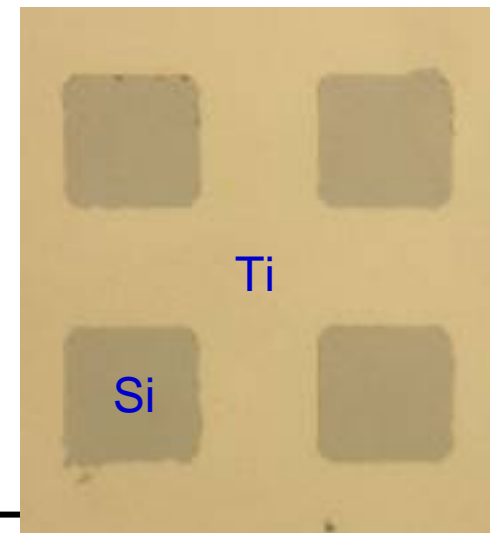
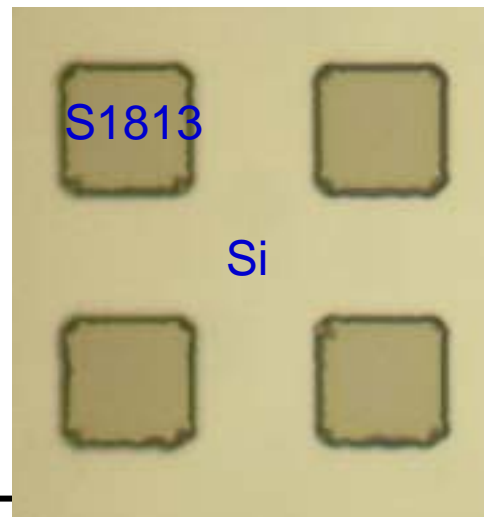
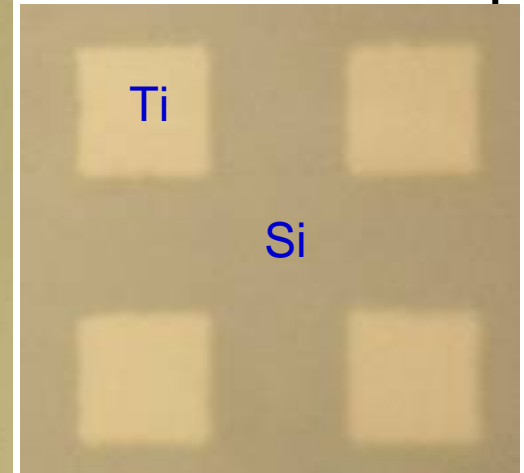
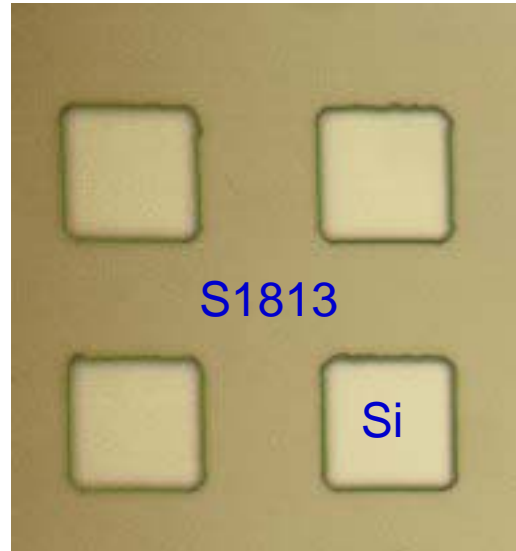
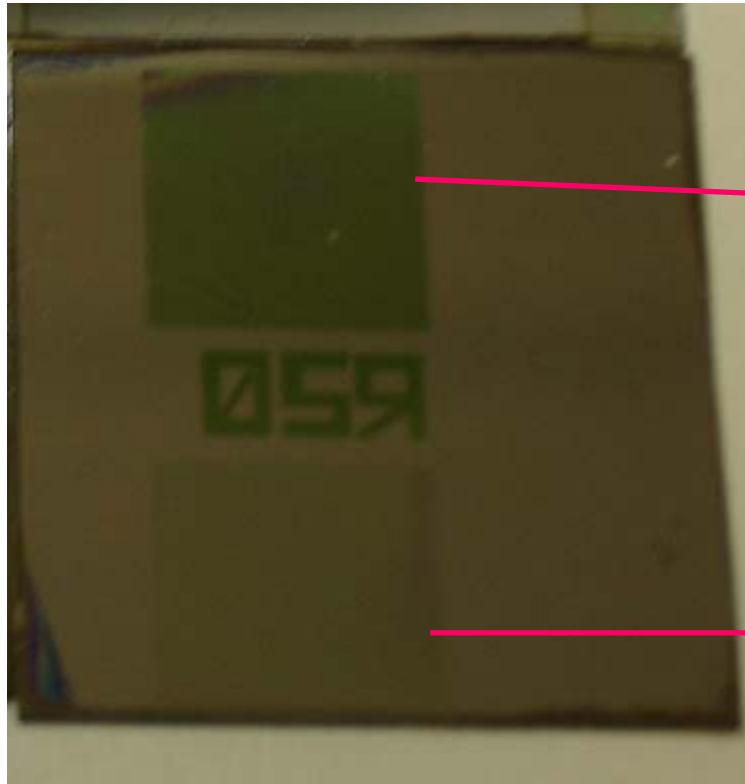
Vega ©Tescan
HARVEST



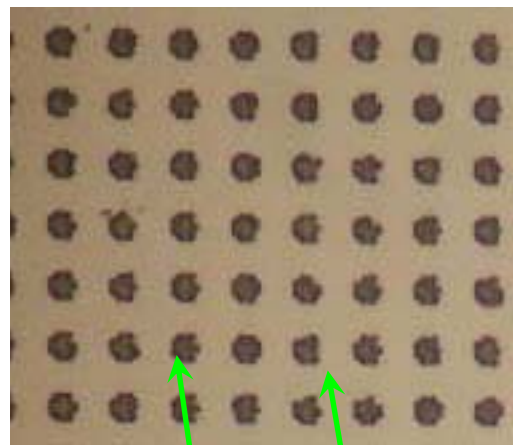
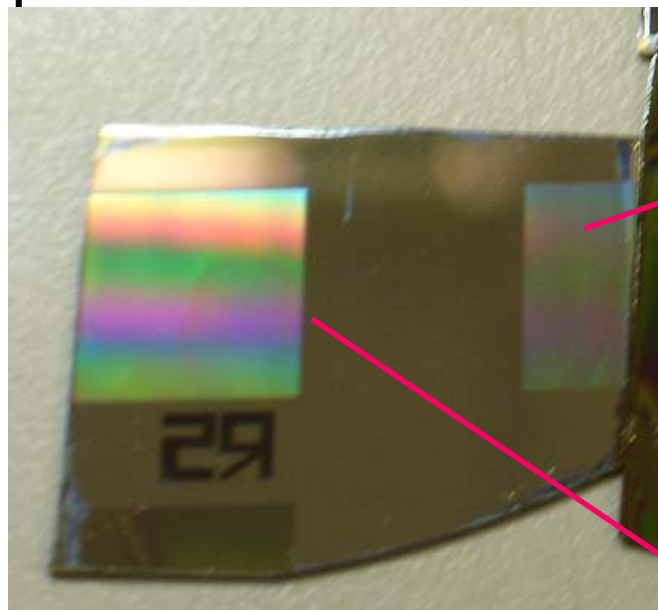
Ti 50 nm
LIFT OFF



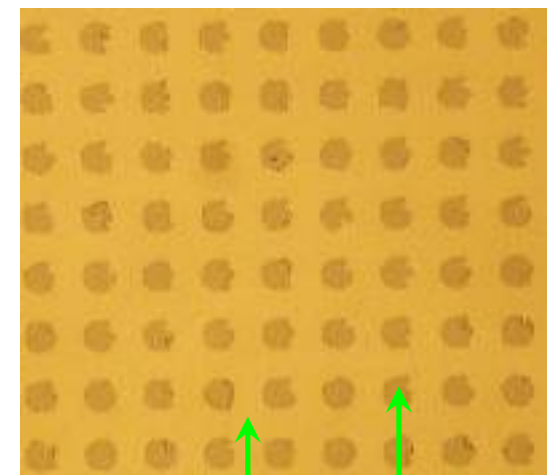
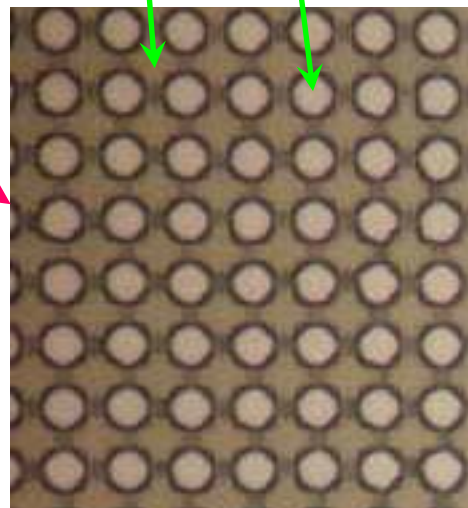
Ti 50 nm on Si 20 um



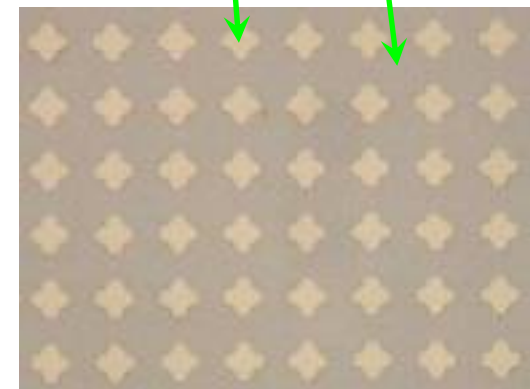
Ti 50 nm on Si 5 um



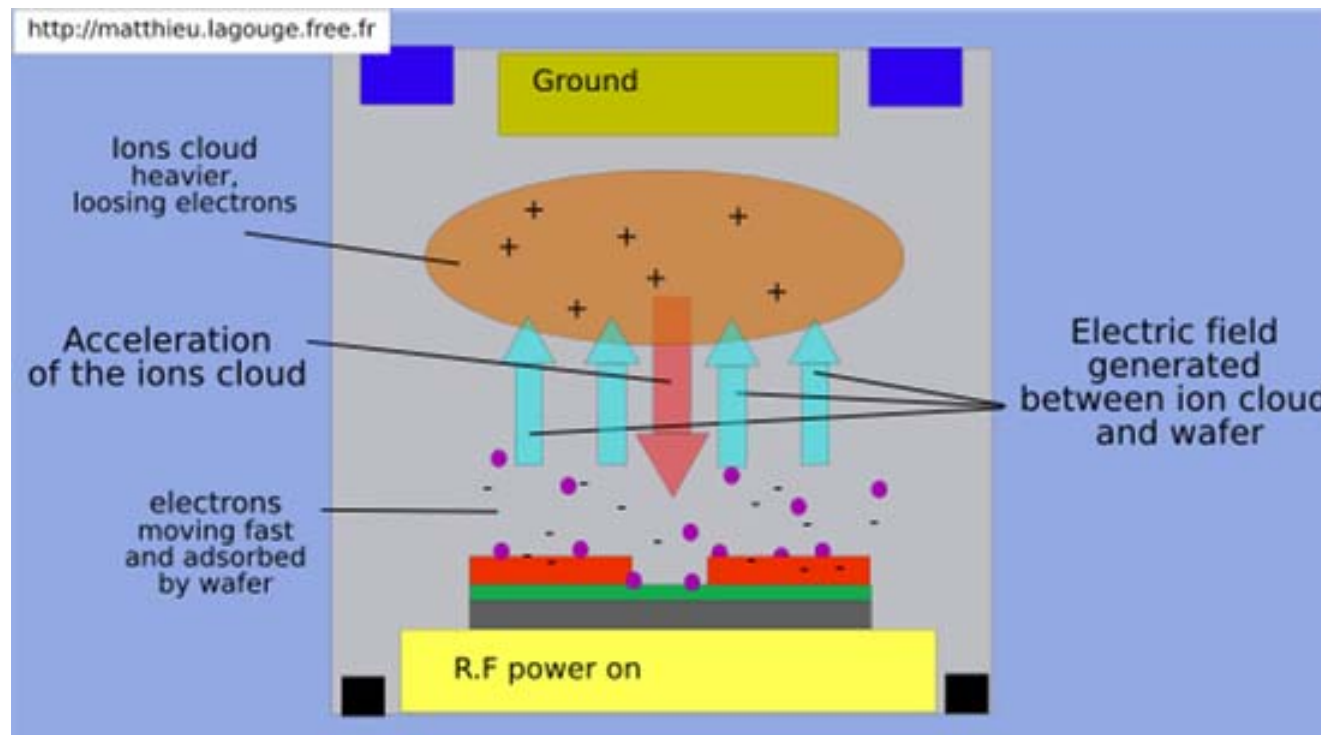
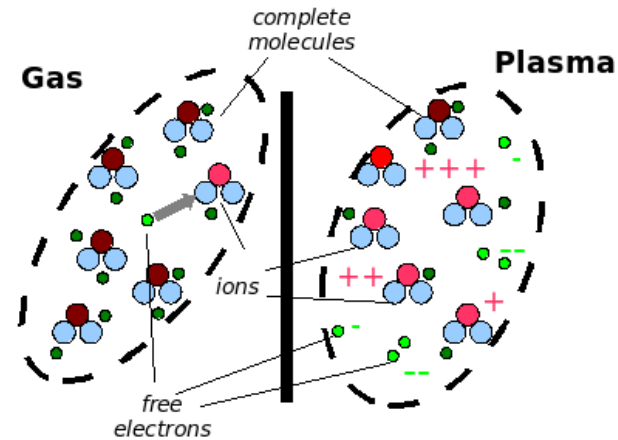
S1813 Si



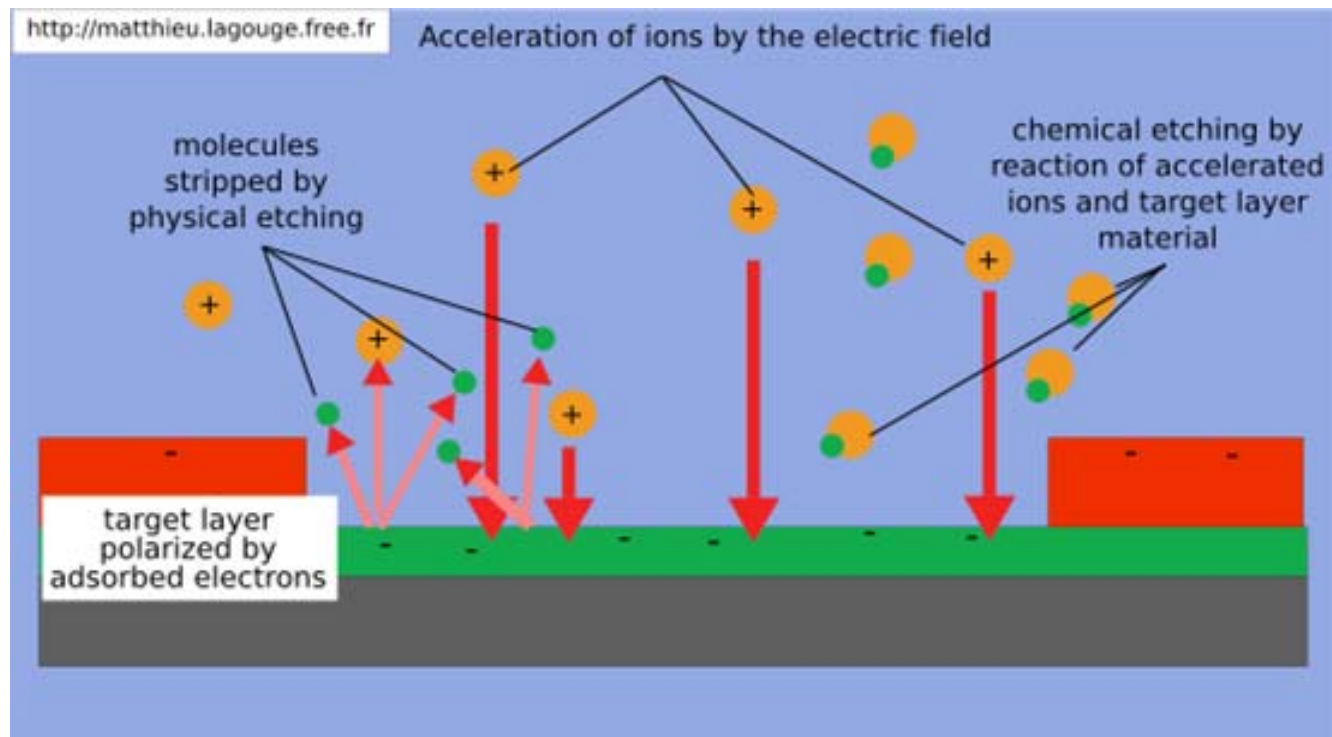
Ti Si

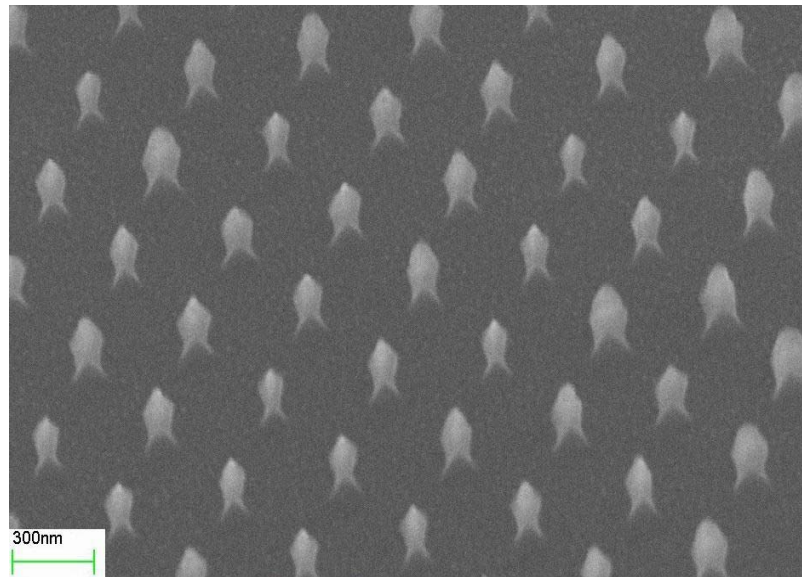
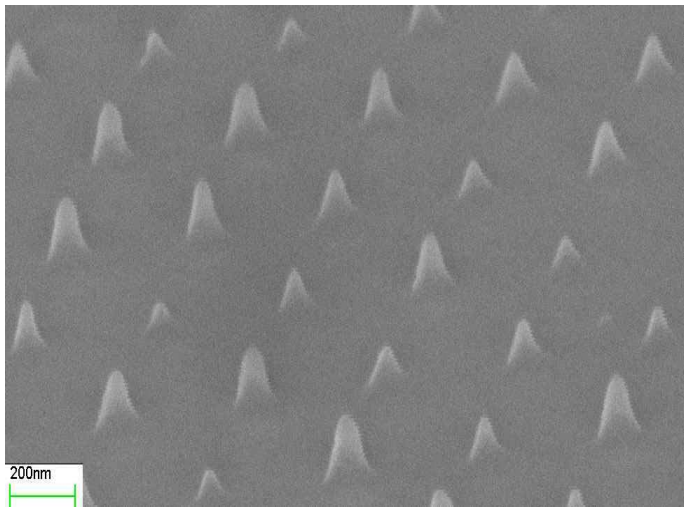
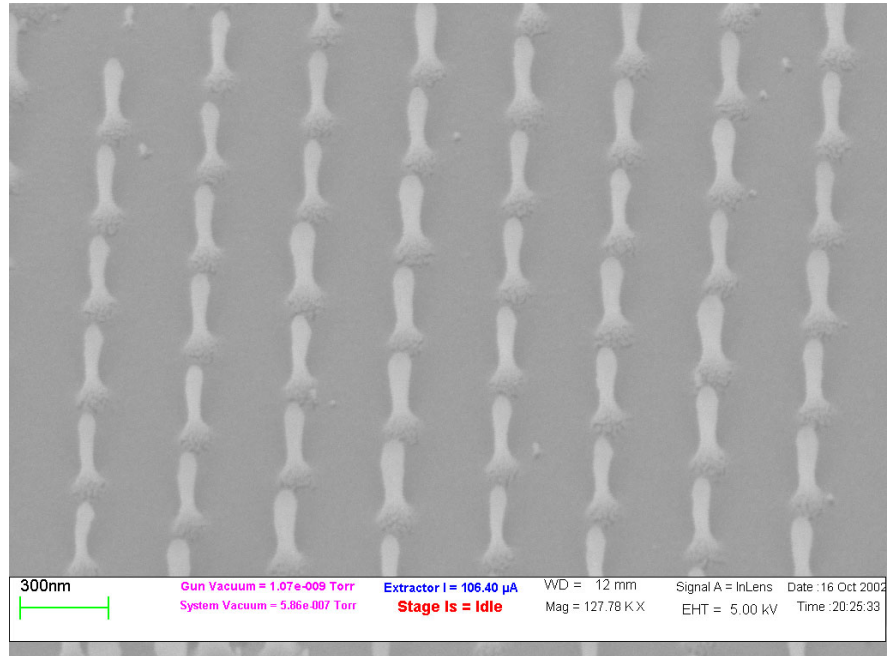
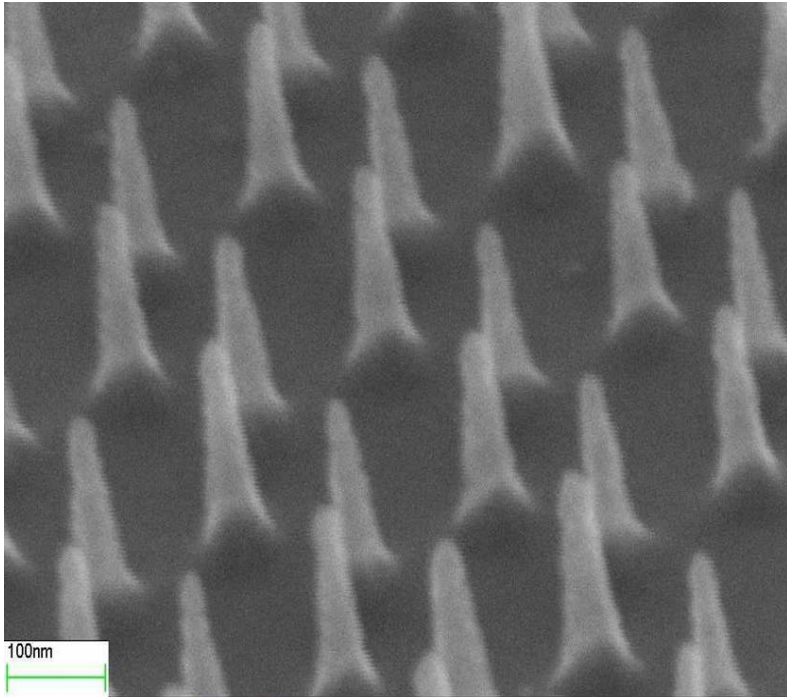


Reactive Ion Etching



Reactive Ion Etching

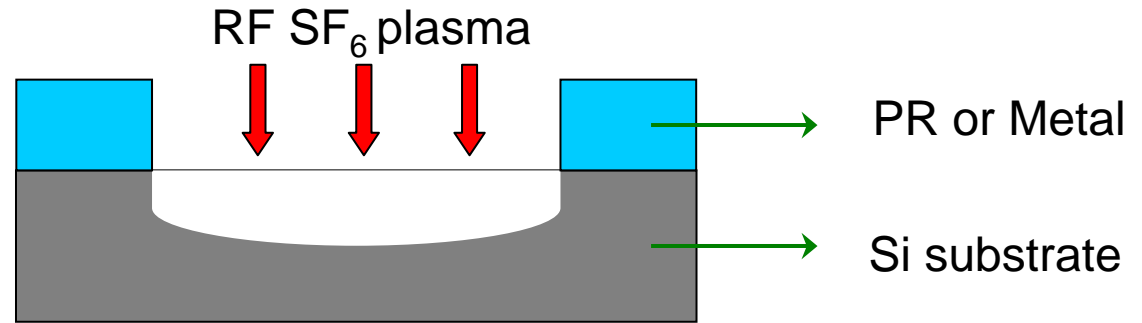




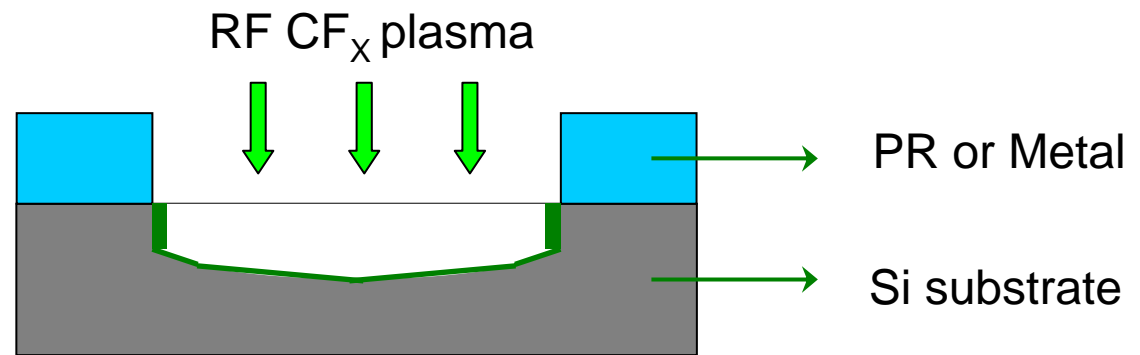
ICP- "BOSCH" Recipe

Etching & Sidewall Passivation Cycle

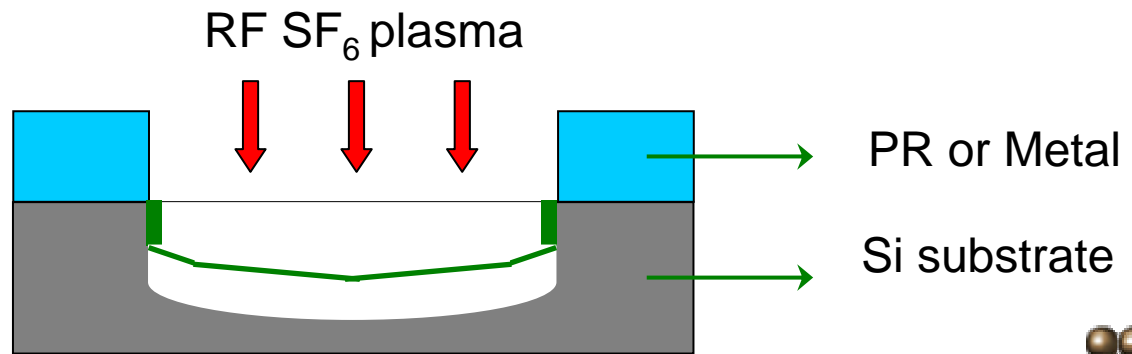
(a) Etch Step

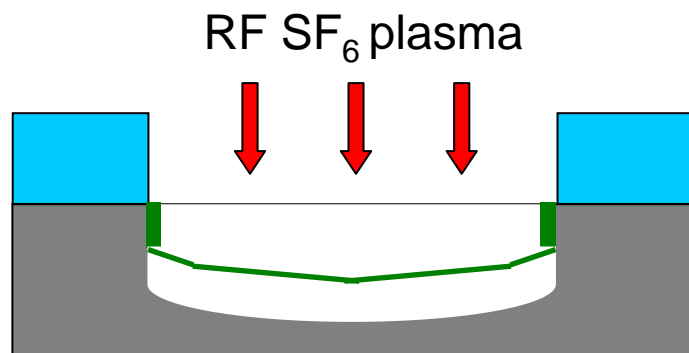
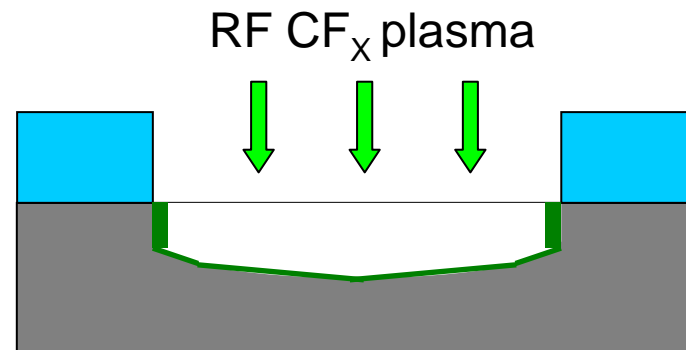
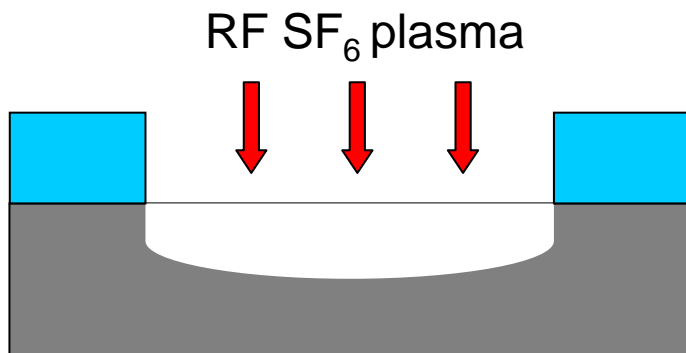


(b) Passivate Step



(a') Etch Step





The gases in RCAS

C₄F₈, CF₄, CHF₃, Ar, O₂

SAMCO ICP (RECIPE)

Si etching CF₄ / O₂ = 30 / 10

SiO₂ (on Si) CHF₃ / Ar = 15 / 30

The gases in NEMSRC

SF₆, C₄F₈, CF₄, O₂

RECIPE

TIME

Etch: 11.5 s

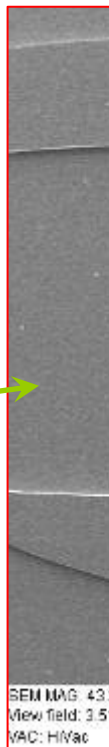
SF₆(130sccm) O₂(13sccm)

Passivate: 7s

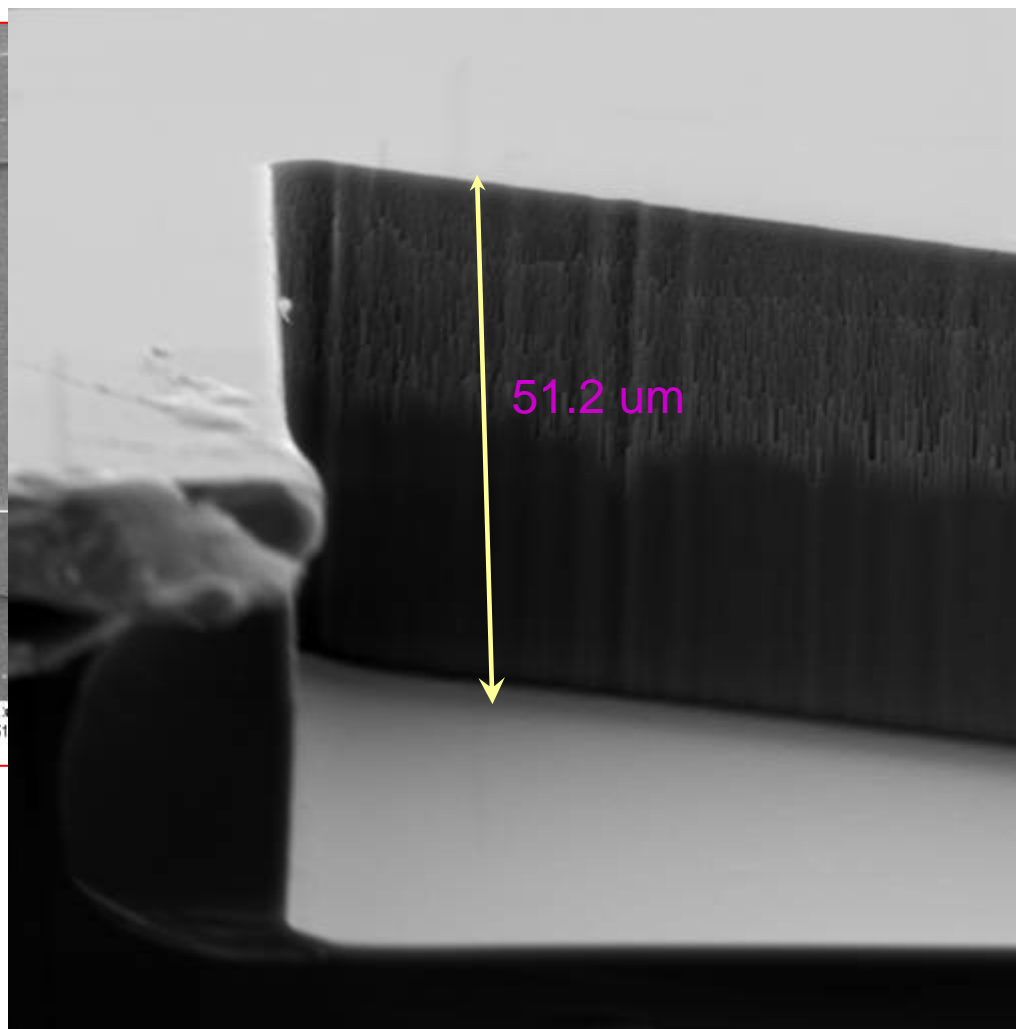
C₄F₈(85sccm)



NEMSRC ICP



SEM MAG: 43.1kx
View field: 3.51 um
VAC: HiVac



SEM MAG: 1.19 kx
View field: 126.40 um
VAC: HiVac

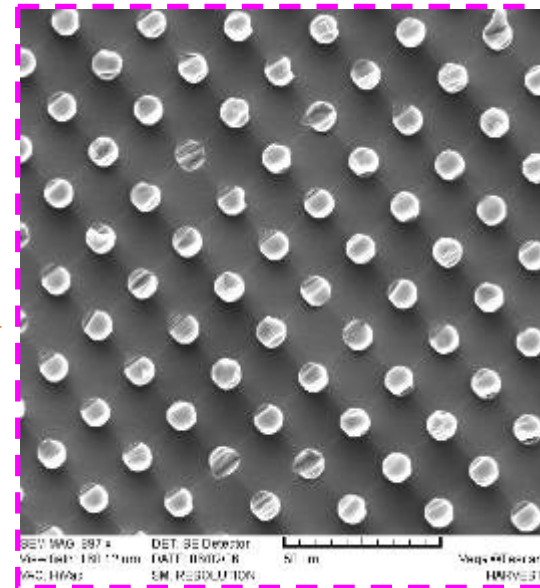
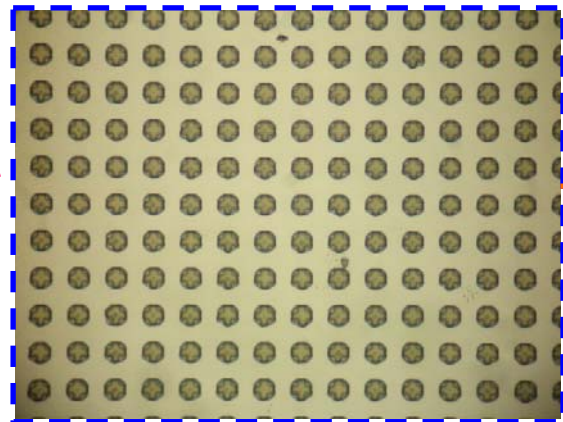
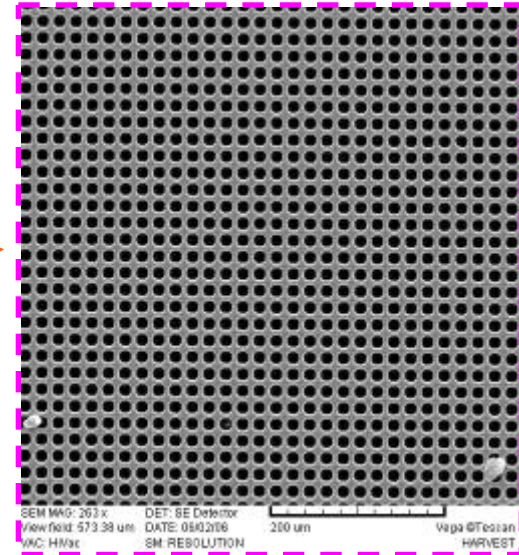
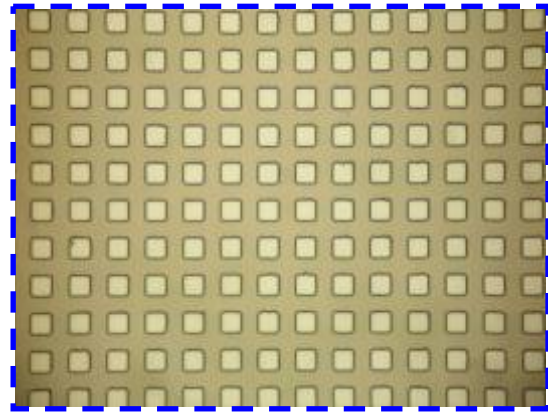
DET: SE Detector
DATE: 06/02/06
SM: RESOLUTION

50 um

Vega ©Tescan
HARVEST



Si ---S1813---ICP



NEMSRC ICP : S1813 on Si

The gases in NEMSRC

SF_6 , C_4F_8 , CF_4 , O_2

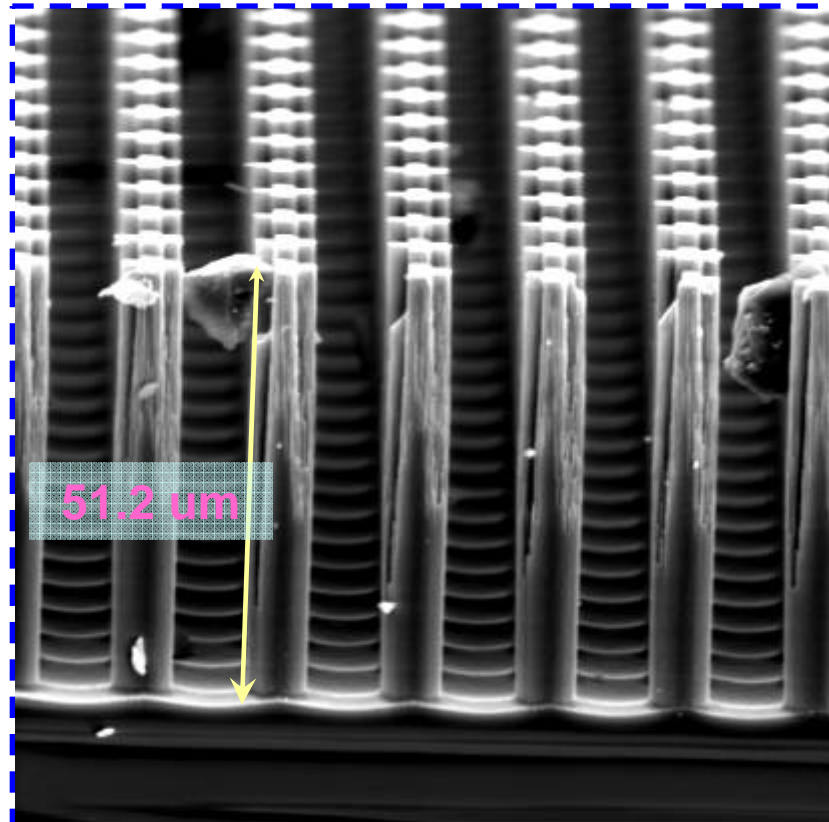
RECIPE

TIME

Etch: 11.5 s SF_6 (130sccm) O_2 (13sccm)
Passivate: 7s C_4F_8 (85sccm)



SEM MAG: 191 x DET: SE Detector
View field: 789.53 um DATE: 06/02/06 200 um Vega ©Tescan
VAC: HiVac SM: RESOLUTION HARVEST



SEM MAG: 1.28 kx DET: SE Detector
View field: 117.35 um DATE: 06/02/06 50 um Vega ©Tescan
VAC: HiVac SM: RESOLUTION HARVEST



NEMSRC ICP : S1813 on Si --20 μ m array

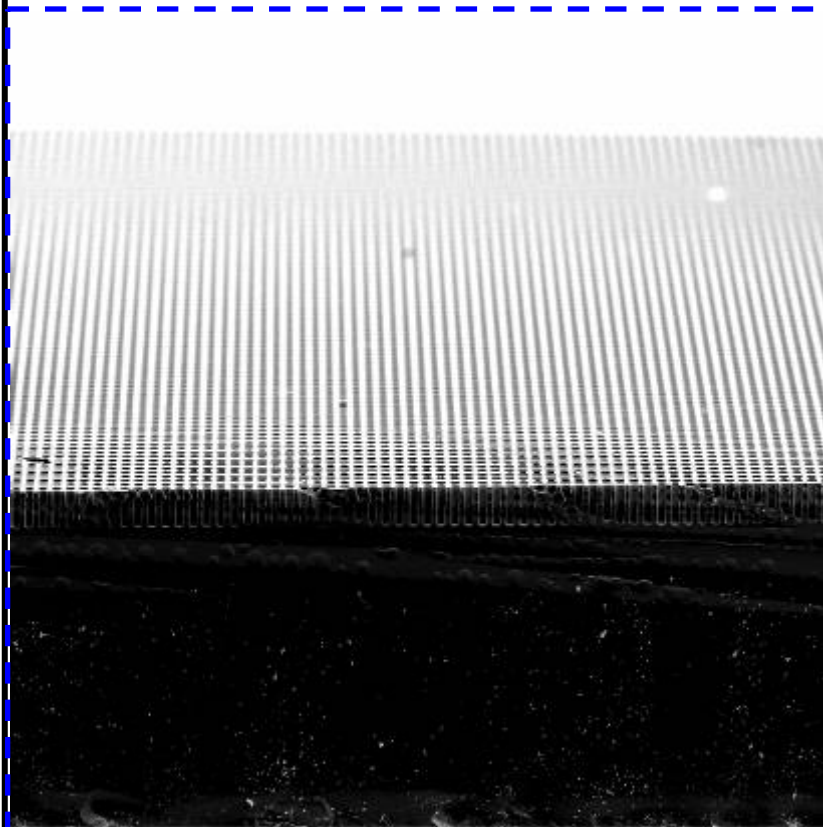
The gases in NEMSRC

SF_6 , C_4F_8 , CF_4 , O_2

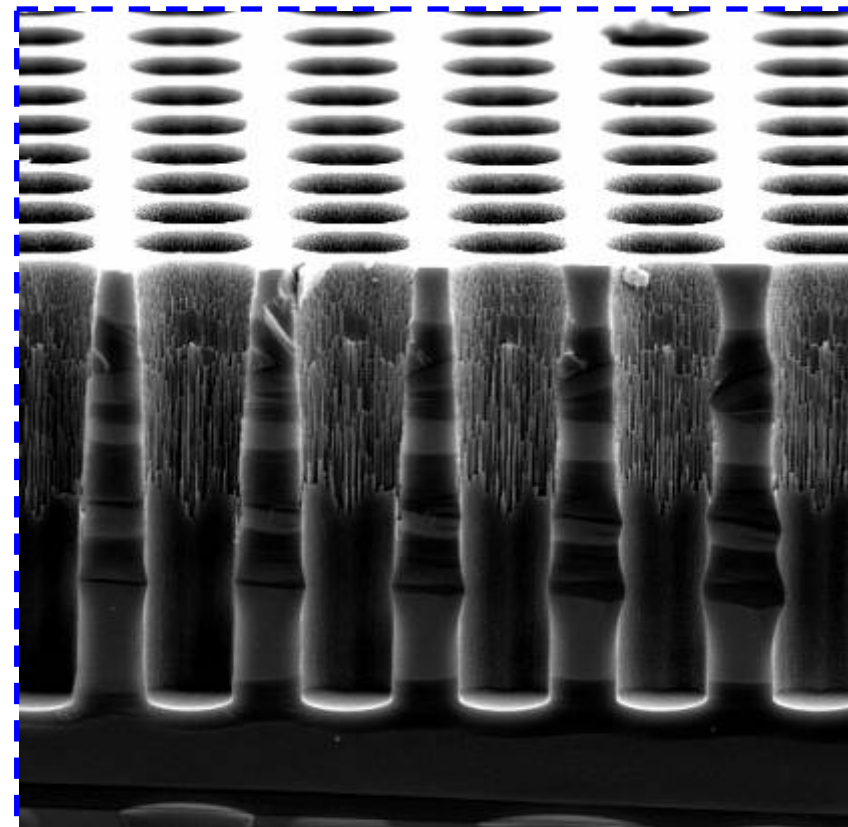
RECIPE

TIME

Etch: 11.5 s SF_6 (130sccm) O_2 (13sccm)
Passivate: 7s C_4F_8 (85sccm)



SEM MAG: 129 x DET: SE Detector
View field: 1.17 mm DATE: 05/02/06 500 μ m Vega@Tescan
VAC: HiVac SM: RESOLUTION HARVEST

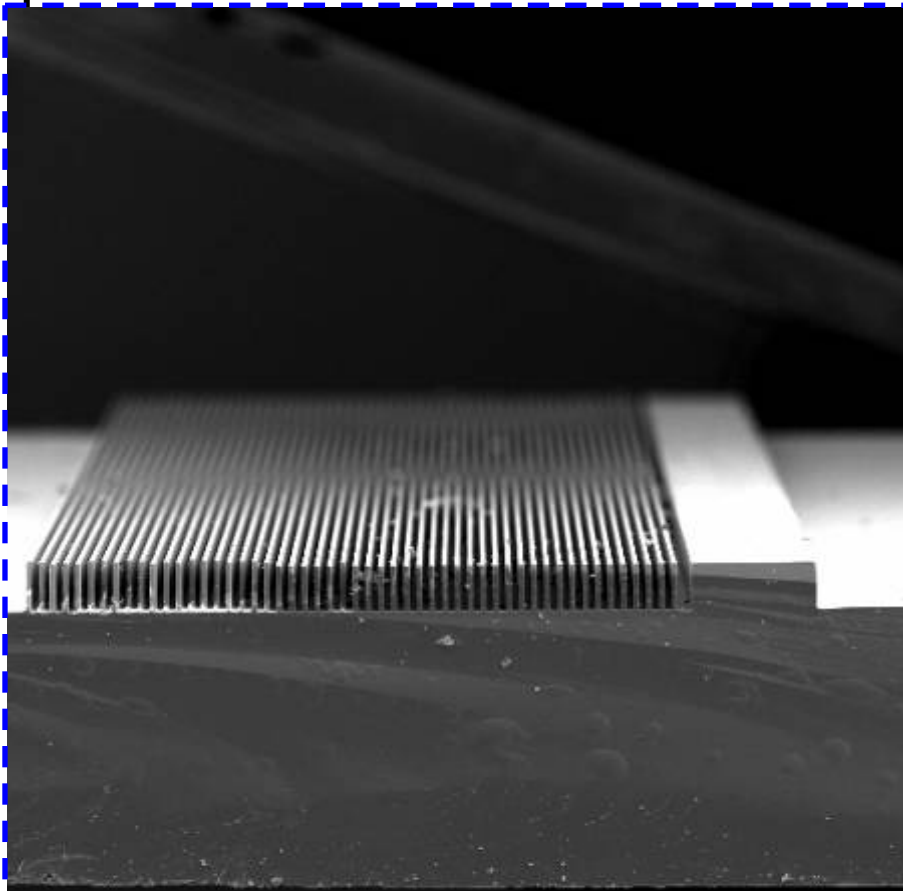


SEM MAG: 1.44 kx DET: SE Detector
View field: 104.43 μ m DATE: 06/02/06 50 μ m Vega@Tescan
VAC: HiVac SM: RESOLUTION HARVEST

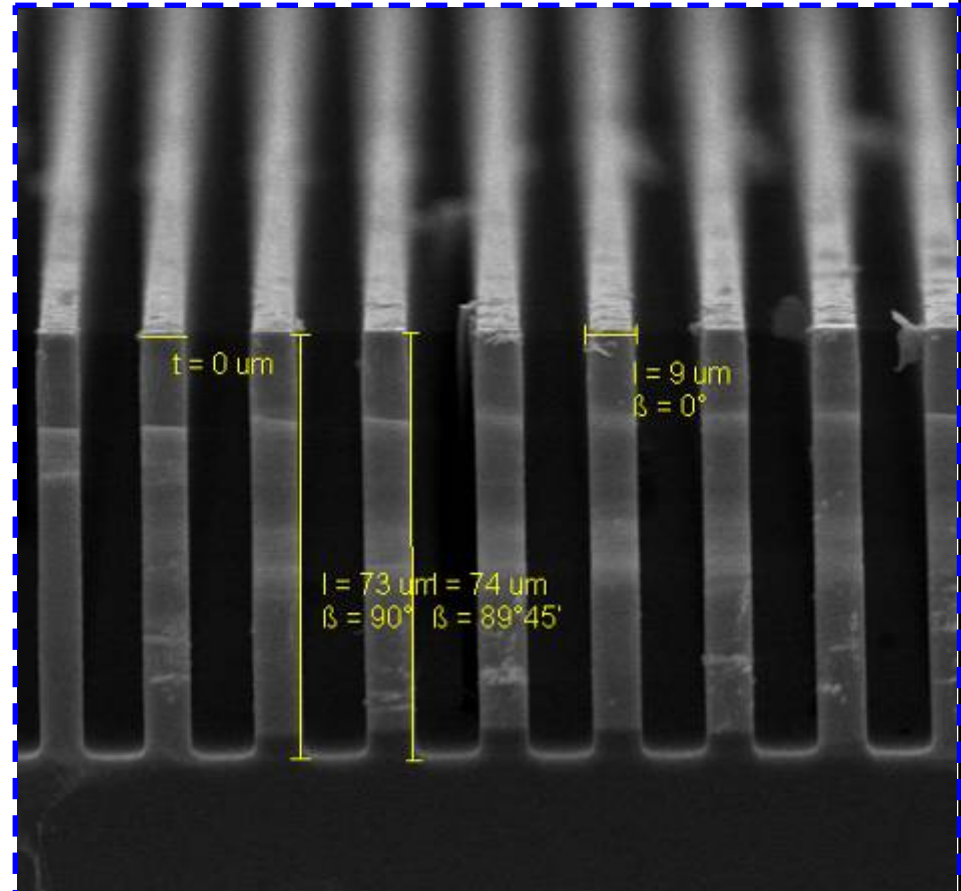


NEMSRC ICP

Si 10 um Line



SEM MAG: 110 x DET: SE Detector 500 um Vega ©Tescan
View field: 1.37 mm DATE: 06/21/06 HARVEST
VAC: HiVac SM: RESOLUTION

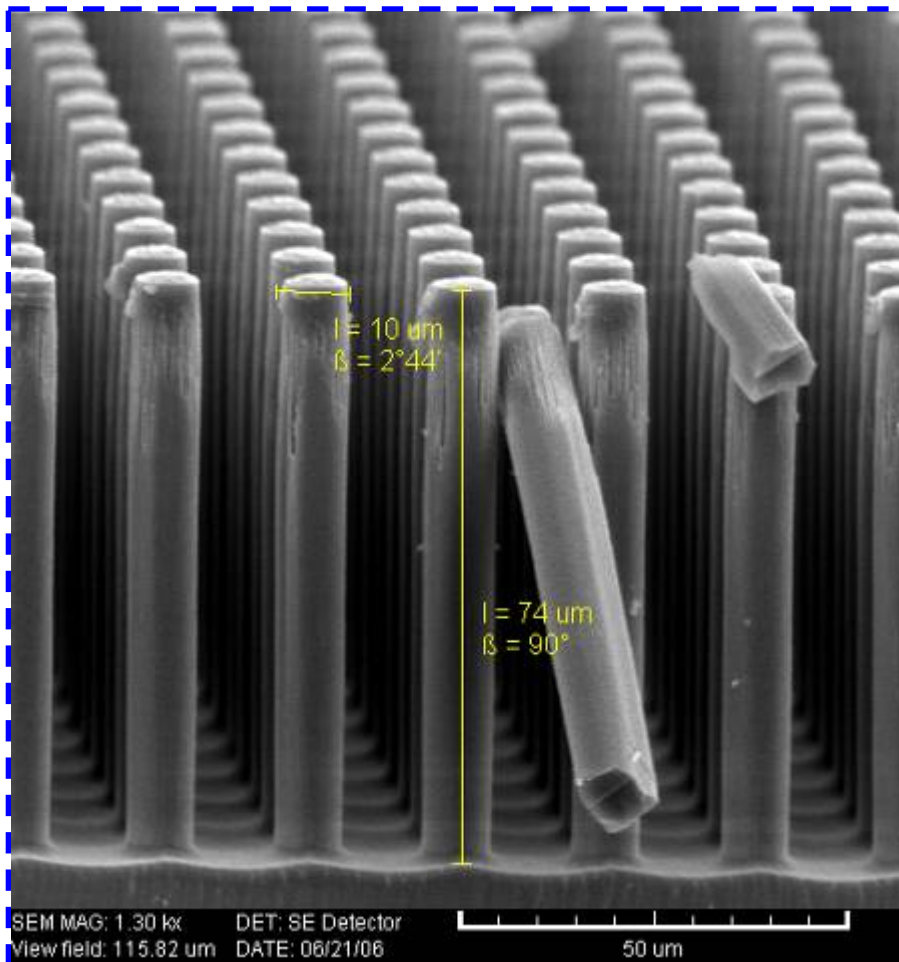
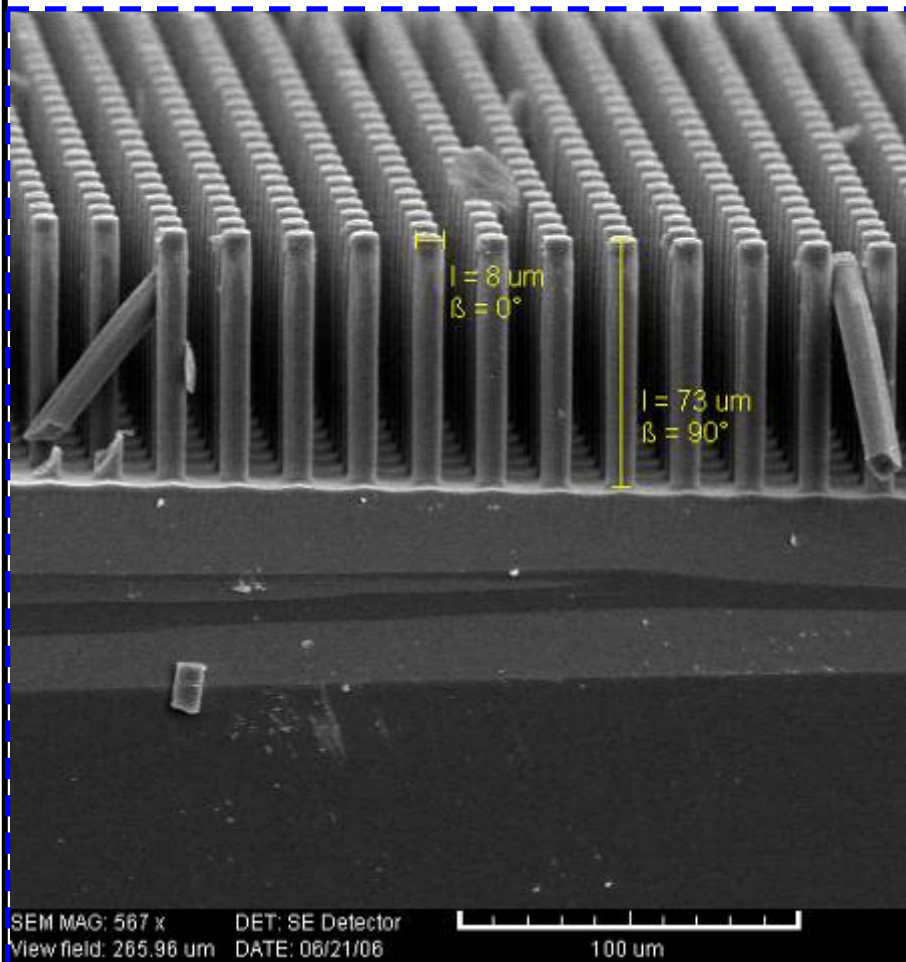


SEM MAG: 928 x DET: SE Detector 50 um
View field: 162.50 um DATE: 06/21/06

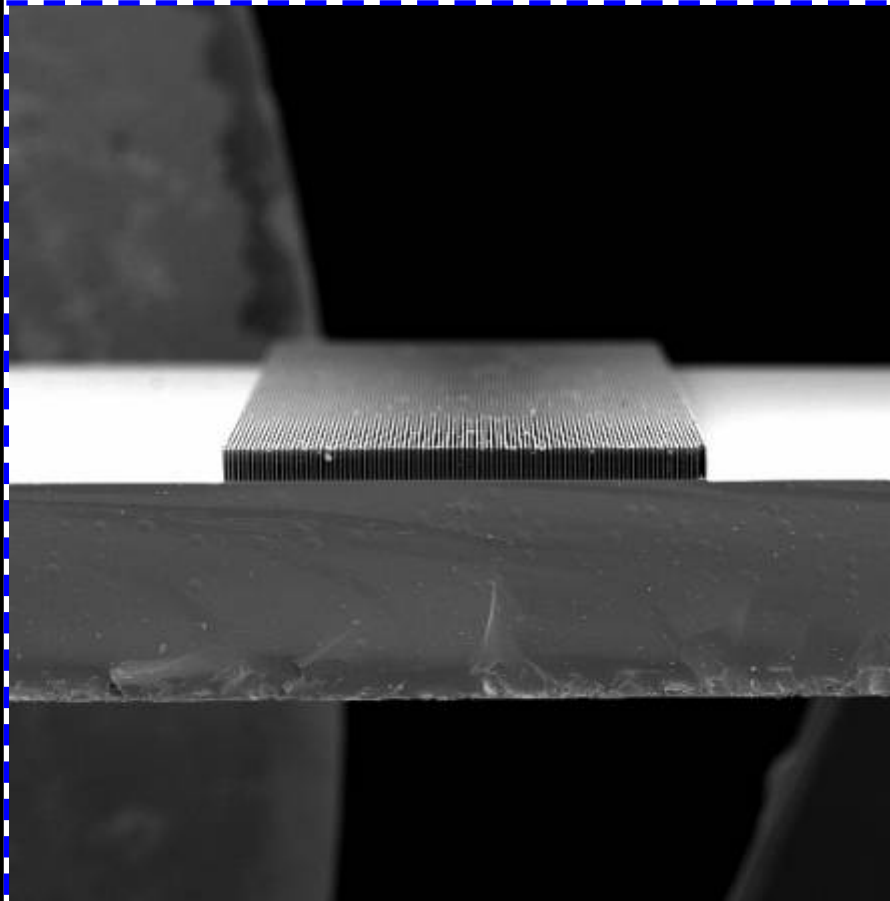


NEMSRC ICP

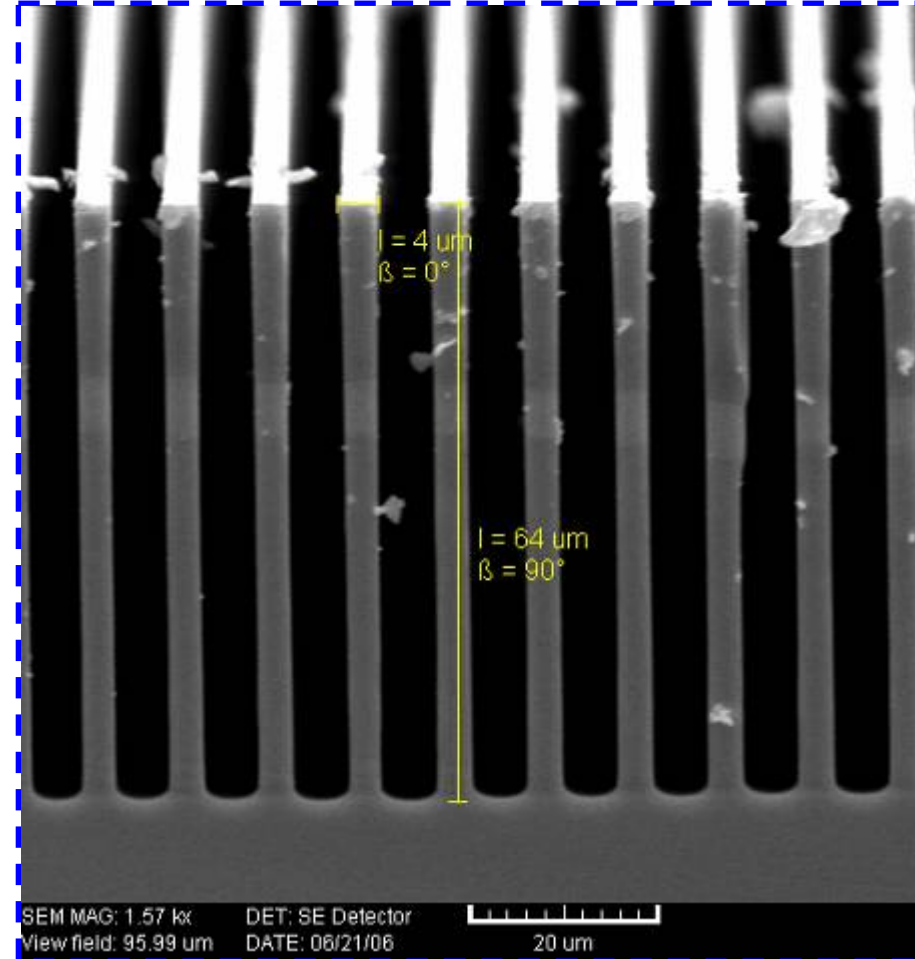
Si 10 um pillar



Si 5um Line



SEM MAG: 83 x DET: SE Detector 500 um
View field: 1.82 mm DATE: 06/21/06
VAC: HiVac SM: RESOLUTION Vega @Tescan
HARVEST



SEM MAG: 1.57 kx DET: SE Detector
View field: 95.99 um DATE: 06/21/06

20 um



NEMSRC ICP : S1813 on Si

5 um pillar

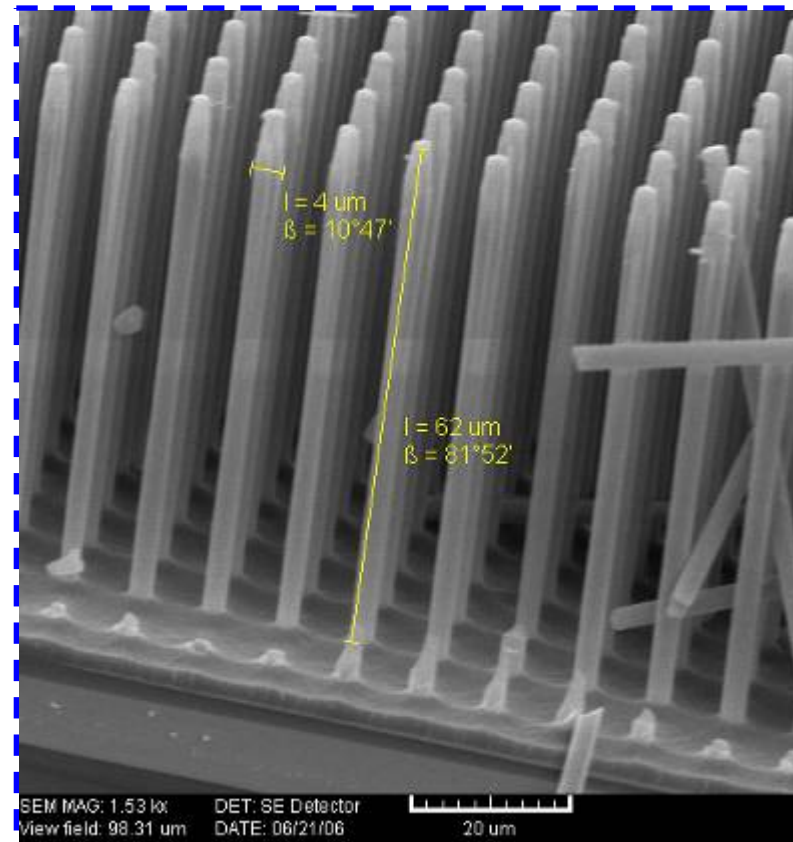
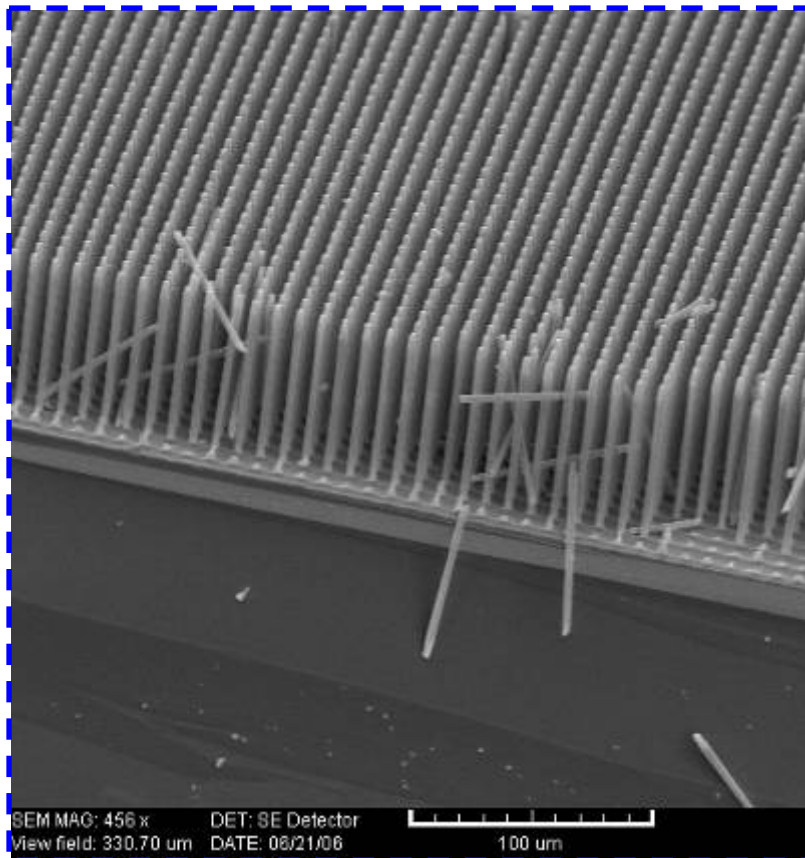
The gases in NEMSRC

SF₆, C₄F₈, CF₄, O₂

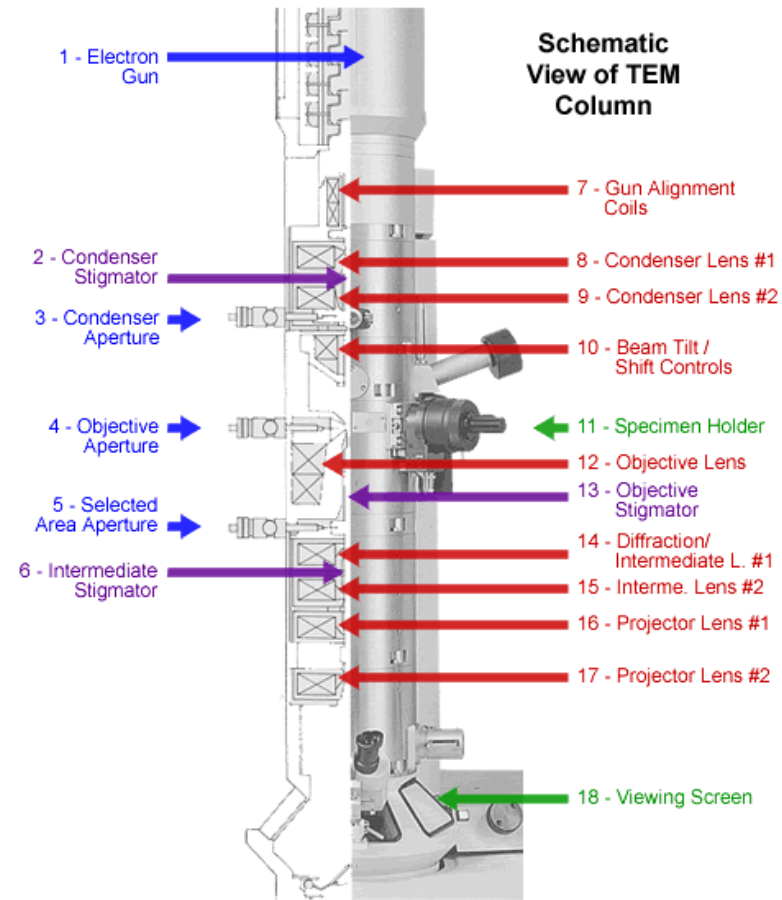
RECIPE

TIME

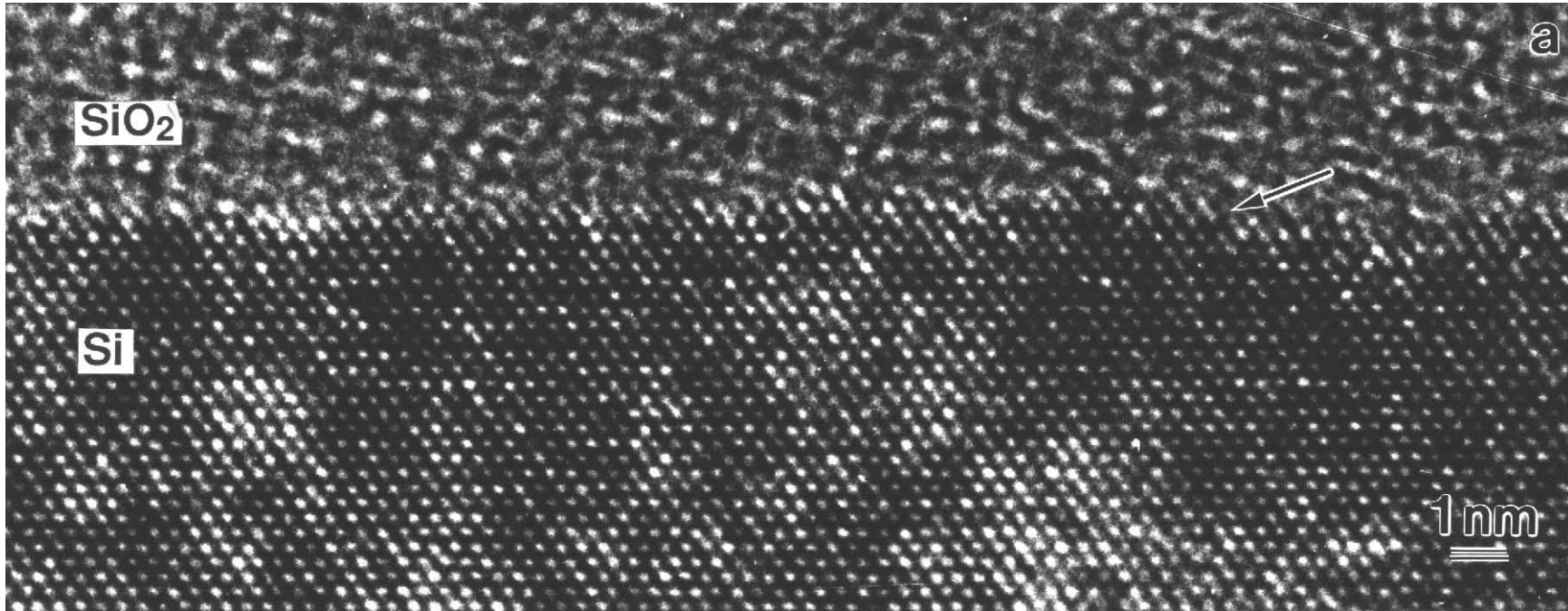
Etch: 11.5 s SF₆(130sccm) O₂(13sccm)
Passivate: 7s C₄F₈(85sccm)



Electron Microscope



TEM Image



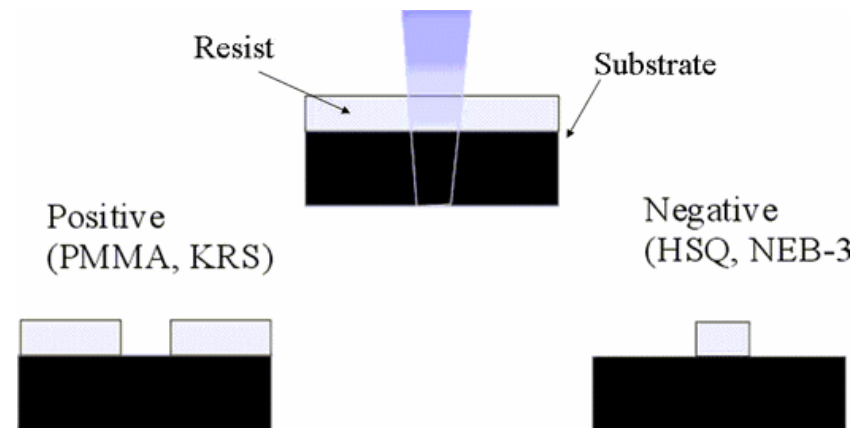
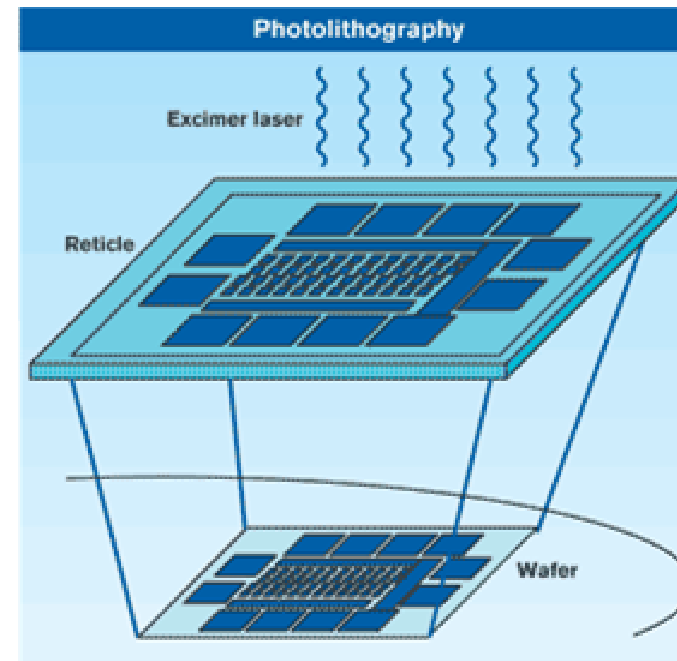
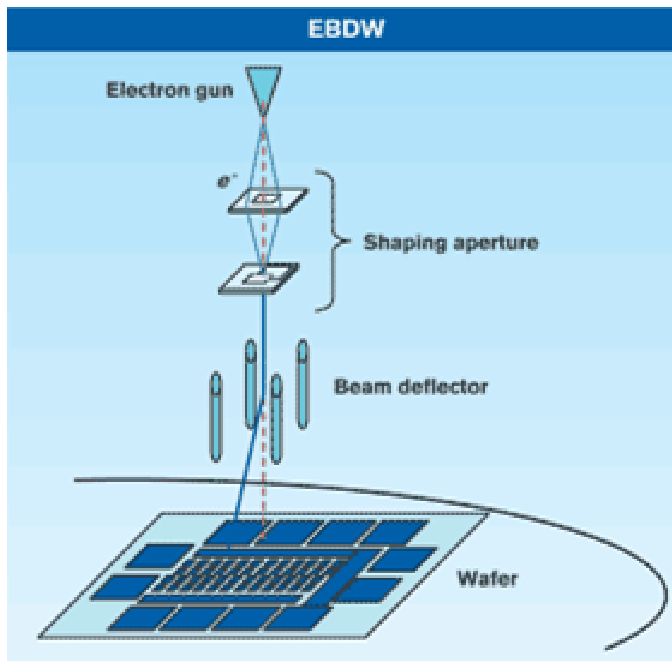
100 kV = 0.00388 nm

$$\lambda = h/p = h/mv \quad h / \text{sqrt}(2 \text{ meV})$$



E-Beam Lithography

E-Beam Direct Writing (EBDW)

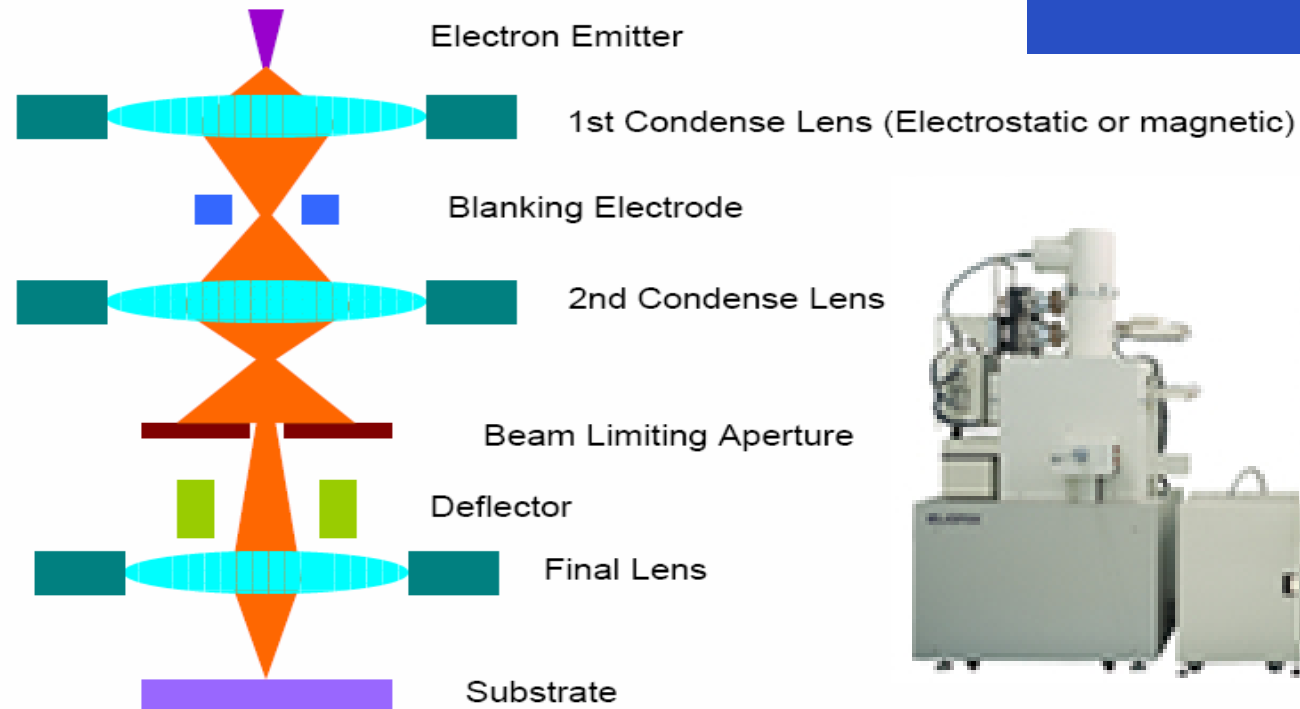


E-Beam Lithography

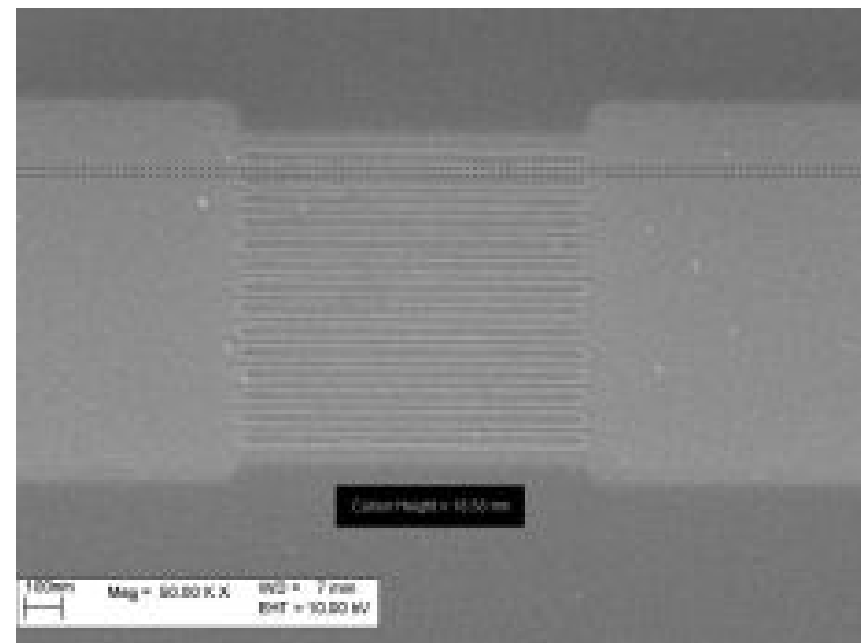
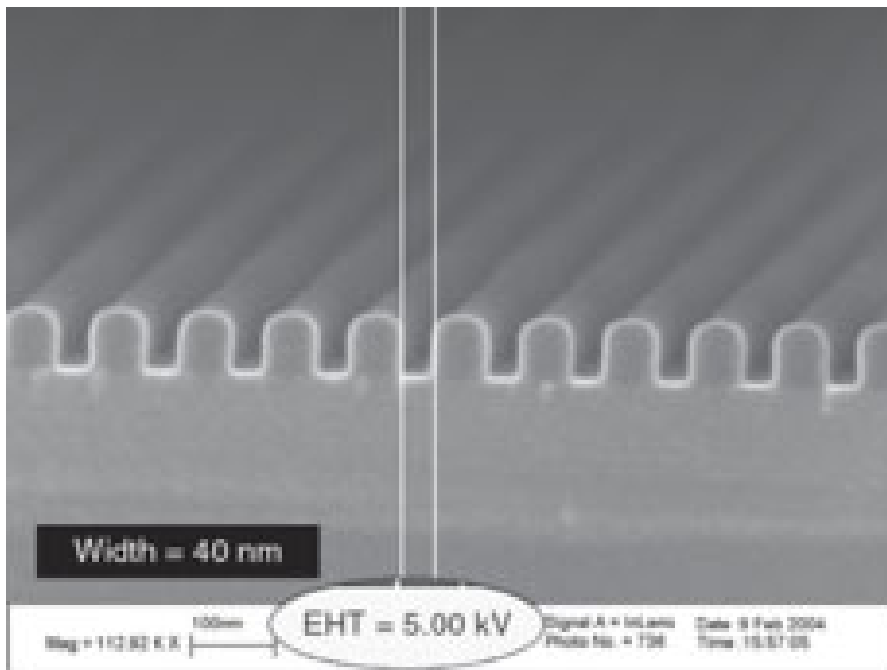
Resolution:

2 nm @ 20 KeV

2 nm @ 1.0 KeV



E-beam Writer

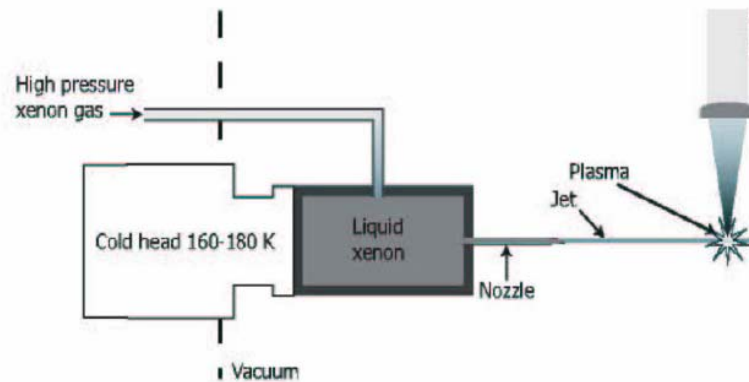


Better than 10 nm lines over 4 inch wafer



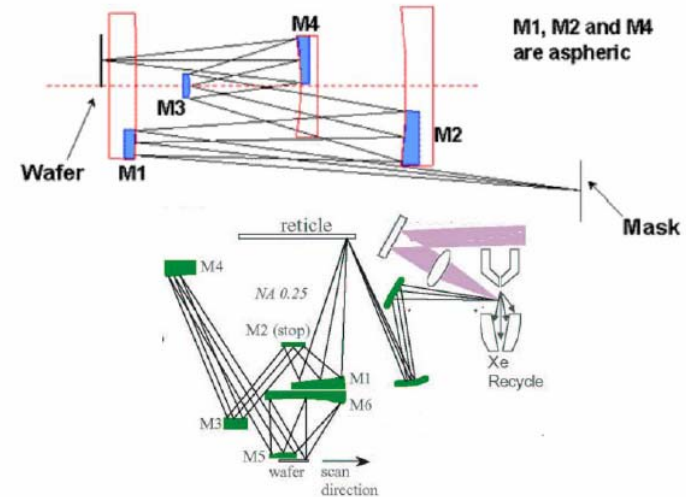
EUV System

EUV Source



1. 13.4nm source.
2. Laser-produced plasma

Reflective Optics for EUV



EUV light ($< 100\text{nm}$) is absorbed by almost all materials \rightarrow No lens.



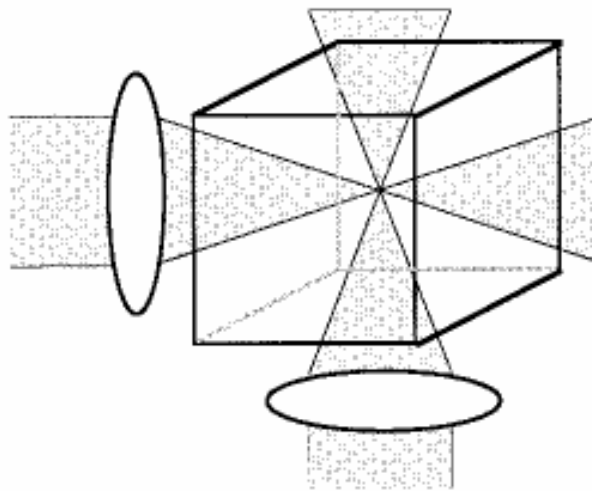
Laser Writing



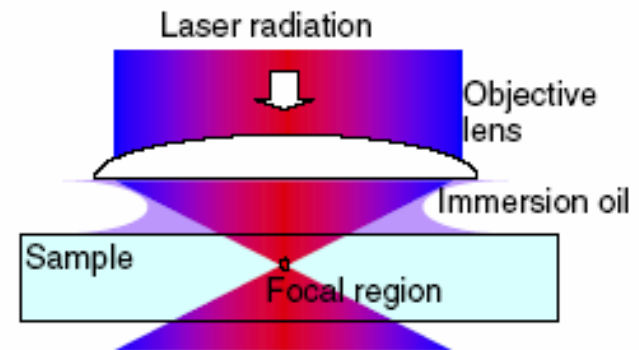
	write head				
	2mm	4mm	10mm	20mm	40mm
min. structure size [μm]	0.6	1.0	2.5	5.0	10.0
address resolution [nm]	20	40	100	200	400
writing speed [mm^2/min]	1.5	5.7	36	119	416
line width uniformity, 3σ [nm]	80	100	220	440	880
edge roughness, 3σ [nm]	60	80	120	180	280



Two Photon Writing



(a)



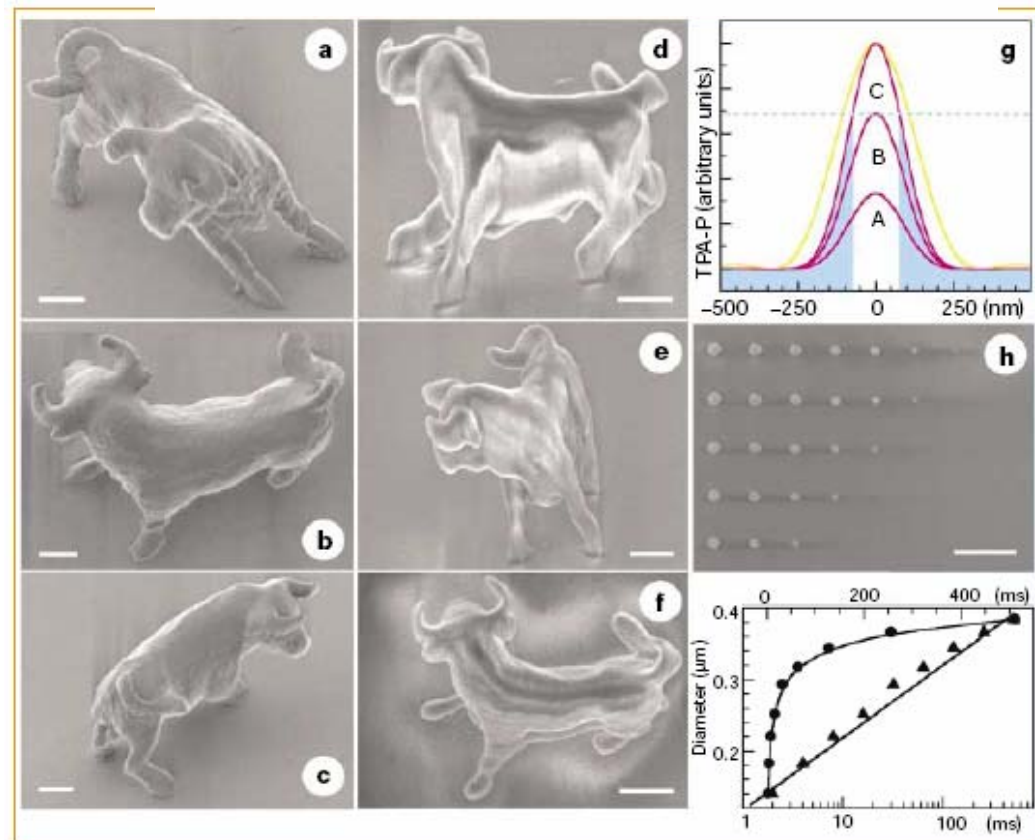
$$D(r) = w_0 \sqrt{2 \ln \left(\frac{I(r)}{I_{th}} \right) \frac{1}{N}},$$

$$L(z) = 2z_R \sqrt{\left(\frac{I(z)}{I_{th}} \right)^{\frac{1}{N}} - 1},$$



Two Photon Writing

NATURE | VOL 412 | 16 AUGUST 2001 |



Two Photon Writing

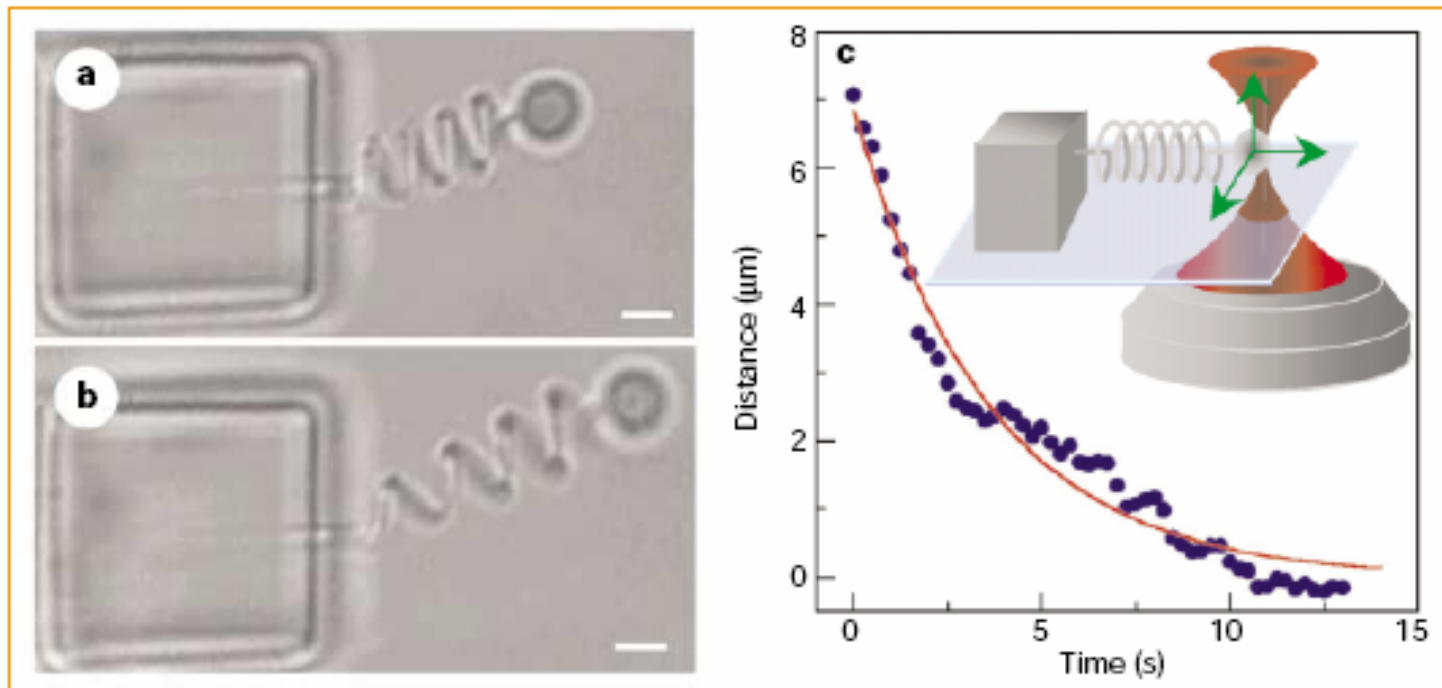


Figure 2 Functional micro-oscillator system, in which not only the spring but also the cubic anchor and the bead were produced using our two-photon absorption system. The oscillator was kept in ethanol so that the buoyancy would balance gravity and eliminate bead-substrate friction. **a, b**, The spring in its original (**a**) and extended (**b**) states. Scale bars, 2 μm . **c**, Restoring curve of the damping oscillation; inset, diagram showing driving of the oscillator by using laser trapping.



Interference

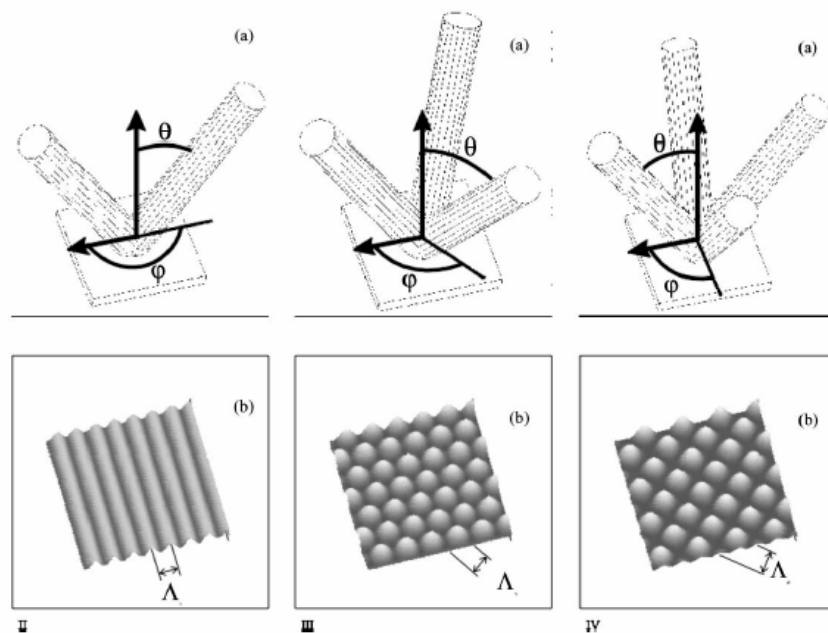


Fig. 1. The orientation of the two (left column), three (middle column) and four (right column) incident beams: (a) and the resulting interference patterns (b).

1. Two beams

$$I'_2 = I_1 + I_2 + 2 \cos(k(R_2 - R_1))$$

2. Three beams

$$I'_3 = I_1 + I_2 + I_3 + 2[\cos(k(R_2 - R_1)) + \cos(k(R_3 - R_1)) + \cos(k(R_3 - R_2))]$$

3. Four beams

$$I'_4 = I_1 + I_2 + I_3 + I_4 + 2[\cos(k(R_2 - R_1)) + \cos(k(R_3 - R_1)) + \cos(k(R_3 - R_2)) + \cos(k(R_4 - R_1)) + \cos(k(R_4 - R_2)) + \cos(k(R_4 - R_3))]$$



Interference

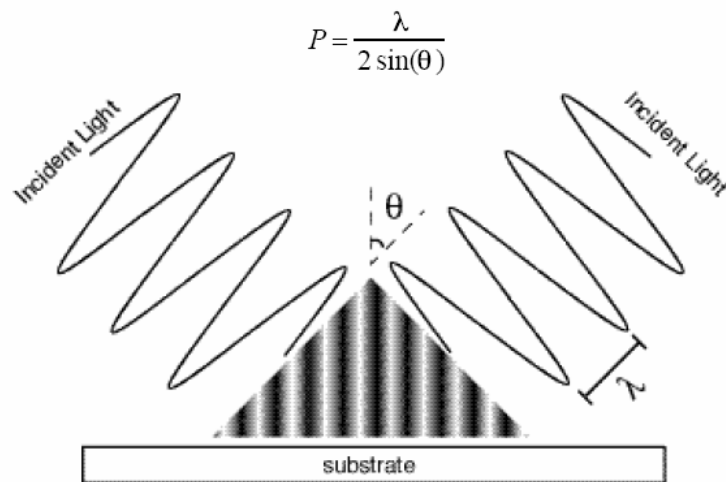


Figure 2.1: Two-beam interference forms a standing wave.

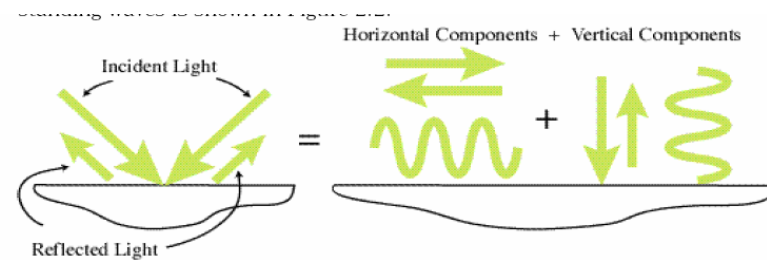


Figure 2.2: The horizontal and vertical components combine separately to create the desired horizontal standing wave and the undesired vertical standing wave



Interference Lithography

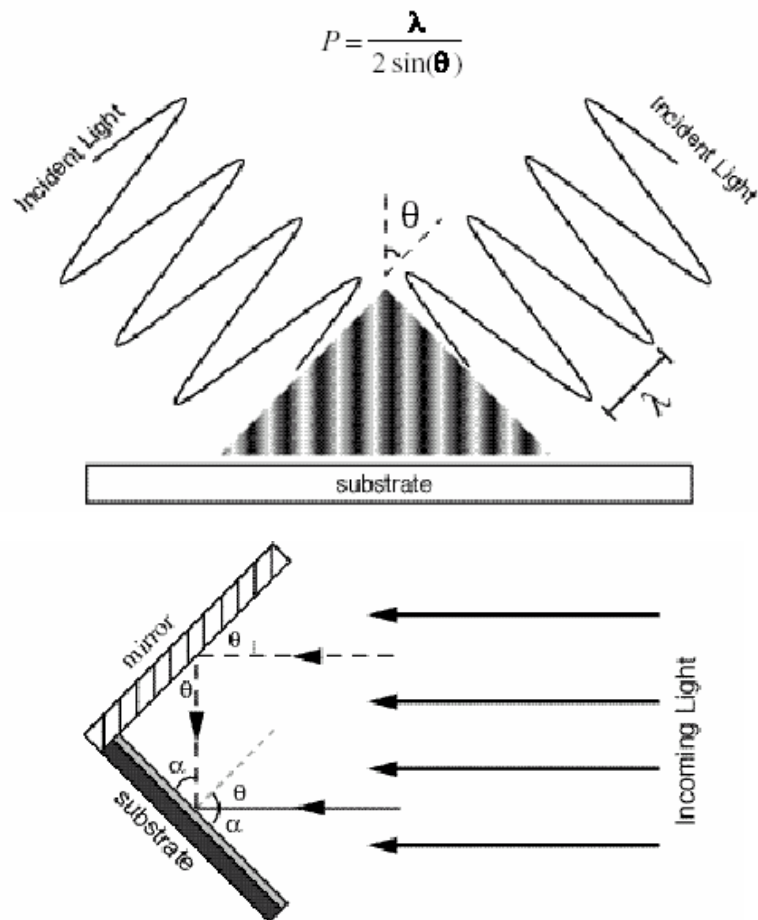
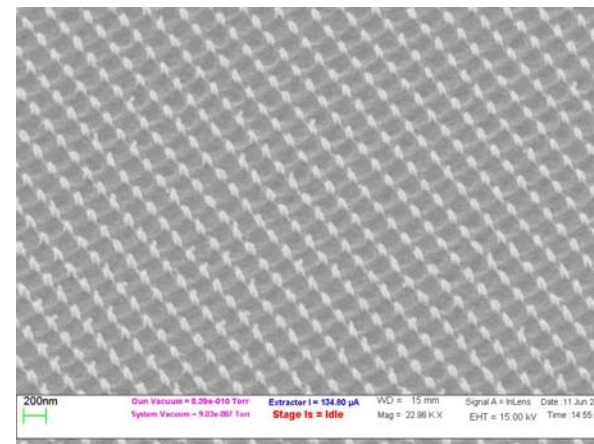


Figure 3.2) Basic Lloyd's mirror configuration



Holographic

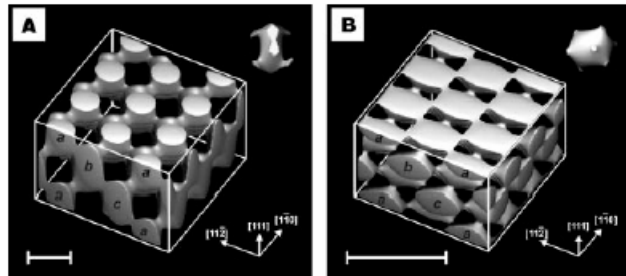


Figure 1 Calculated constant-intensity surfaces in four-beam laser interference patterns designed to produce photonic crystals for the visible spectrum from photoresist. The primitive basis (contents of a Wigner-Seitz unit cell) is shown inset in each case. **A**, f.c.c. pattern with lattice constant 922 nm, used to produce the structures shown in Fig. 3a–d and 4. The close-packed layers of the f.c.c. lattice are indicated on one side of the cube. **B**, f.c.c. pattern with lattice constant 397 nm. Scale bars, 500 nm.

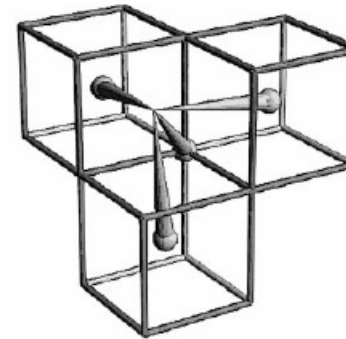


Figure 2 Beam geometry for an f.c.c. interference pattern. The wavevectors of the four laser beams are drawn as cones originating from lattice points in a b.c.c. reciprocal lattice. The differences between the central beam wavevector \mathbf{k}_0 , which originates from the common point of the three cubes shown, and the three wavevectors \mathbf{k}_{1-3} originating from body-centre lattice points, are the primitive set of reciprocal lattice vectors $2\pi/d(\bar{1}11)$.



Holographic

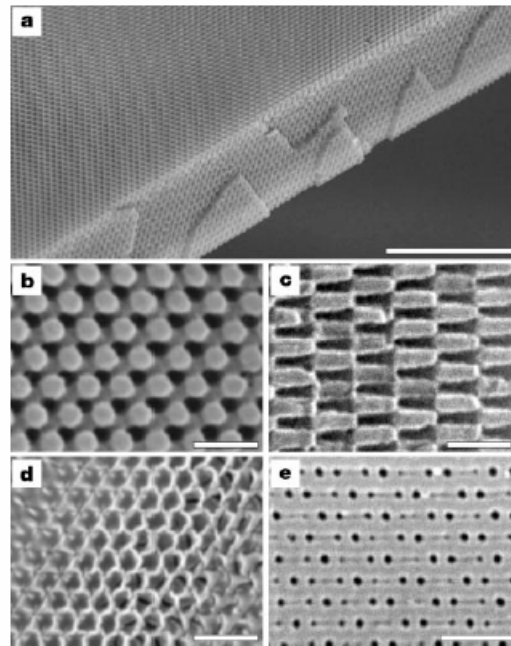


Figure 3 SEM images of photonic crystals generated by holographic lithography. **a**, Polymeric photonic crystal generated by exposure of a 10- μm film of photoresist to the interference pattern shown in Fig. 1A. The top surface is a (111) plane; the film has been fractured along the (11 $\bar{1}$) cleavage planes. Scale bar, 10 μm . **b**, Close-up of a (111) surface. Scale bar, 1 μm . **c**, Close-up of a (11 $\bar{1}$) surface. Scale bar, 1 μm . **d**, Inverse replica in titania made by using the polymeric structure as a template. The surface is slightly tilted from the (111) plane. Scale bar, 1 μm . **e**, (102) surface of a b.c.c. polymeric photonic crystal. Scale bar, 1 μm .

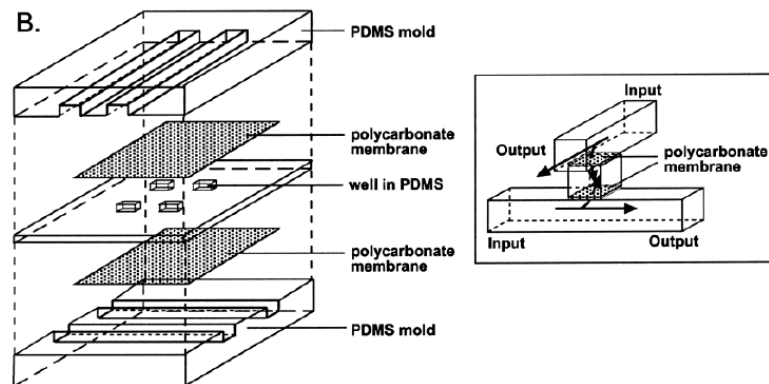
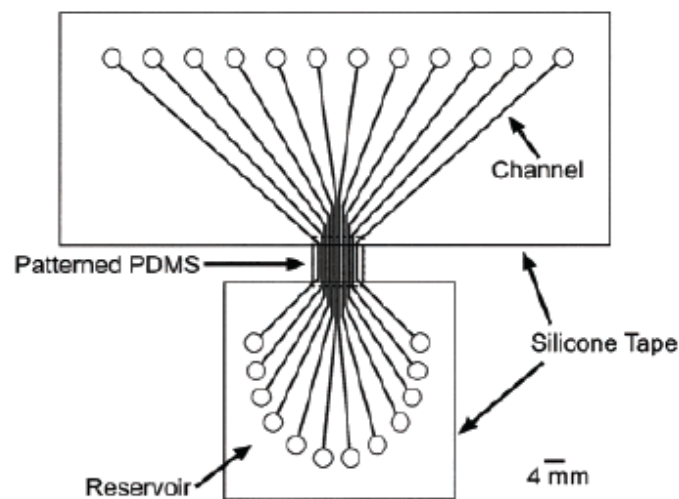


PDMS

ACCOUNTS OF CHEMICAL RESEARCH / VOL. 35, NO. 7, 2002

Table 1. Physical and Chemical Properties of PDMS

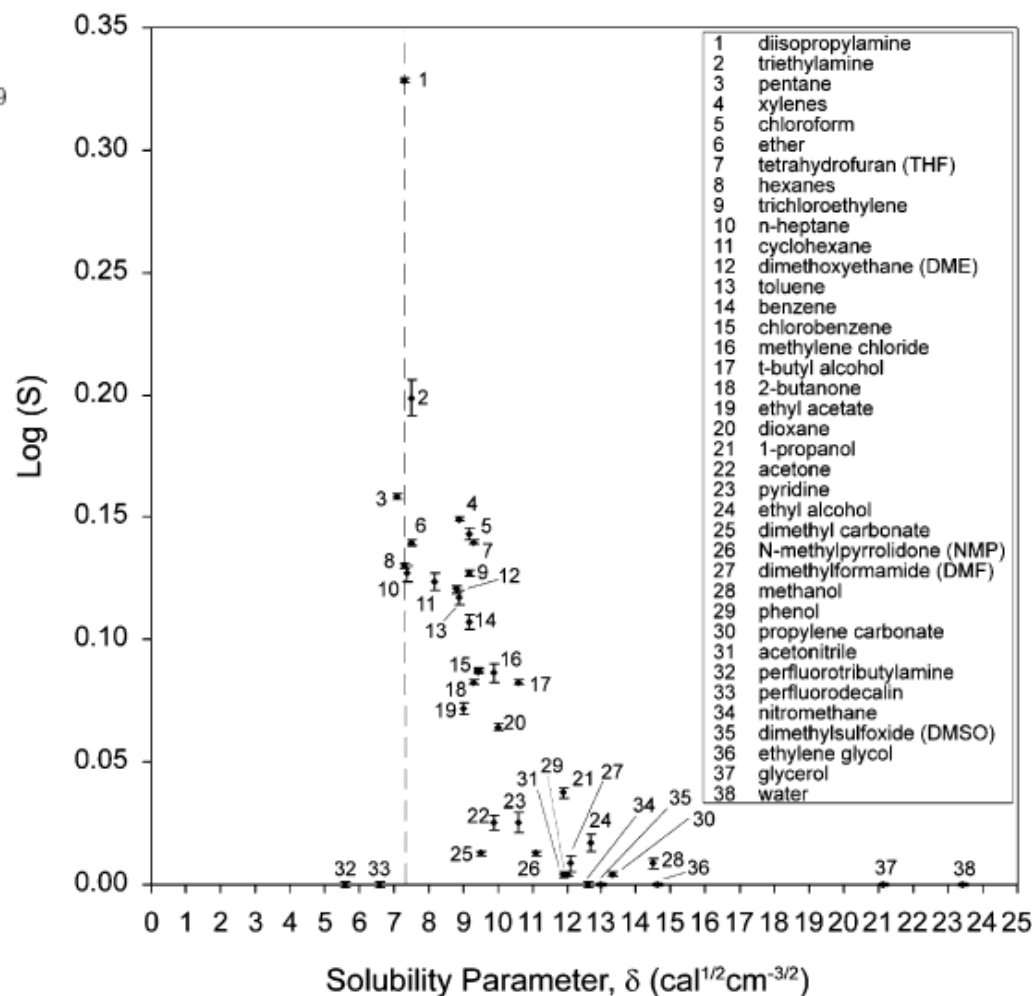
property	characteristic	consequence
optical	transparent; UV cutoff, 240 nm	optical detection from 240 to 1100 nm
electrical	insulating; breakdown voltage, 2×10^7 V/m ⁷¹	allows embedded circuits; intentional breakdown to open connections ⁴³
mechanical	elastomeric; tunable Young's modulus, typical value of ~ 750 kPa ²⁴	conforms to surfaces; allows actuation by reversible deformation; ²⁴ facilitates release from molds
thermal	insulating; thermal conductivity, 0.2 W/(m·K); coefficient of thermal expansion, $310 \mu\text{m}/(\text{m}\cdot^\circ\text{C})$ ⁷¹	can be used to insulate heated solutions; ⁶⁴ does not allow dissipation of resistive heating from electrophoretic separation
interfacial	low surface free energy ~ 20 erg/cm ² ²⁰	replicas release easily from molds; can be reversibly sealed to materials
permeability	impermeable to liquid water; permeable to gases and nonpolar organic solvents	contains aqueous solutions in channels; allows gas transport through the bulk material; incompatible with many organic solvents
reactivity	inert; can be oxidized by exposure to a plasma; $\text{Bu}_4\text{N}^+\text{F}^-$ (TBA)F	unreactive toward most reagents; surface can be etched; can be modified to be hydrophilic and also reactive toward silanes; ²⁰ etching with (TBA)F can alter topography of surfaces ⁵⁹
toxicity	nontoxic.	can be implanted in vivo; supports mammalian cell growth ^{57,59}



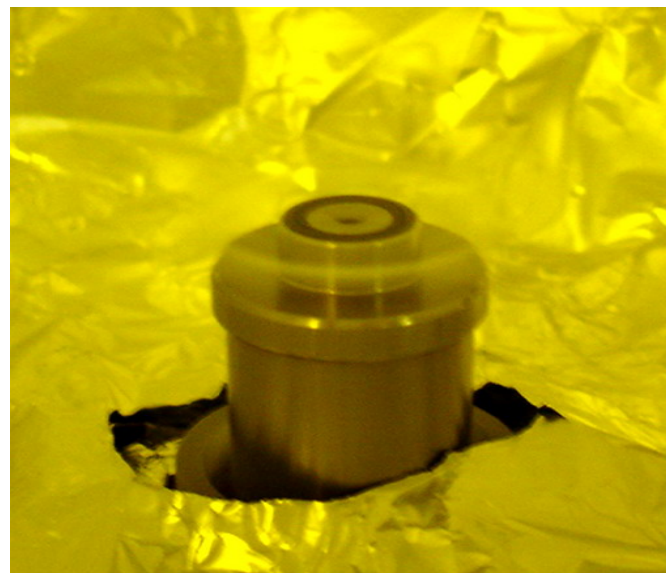
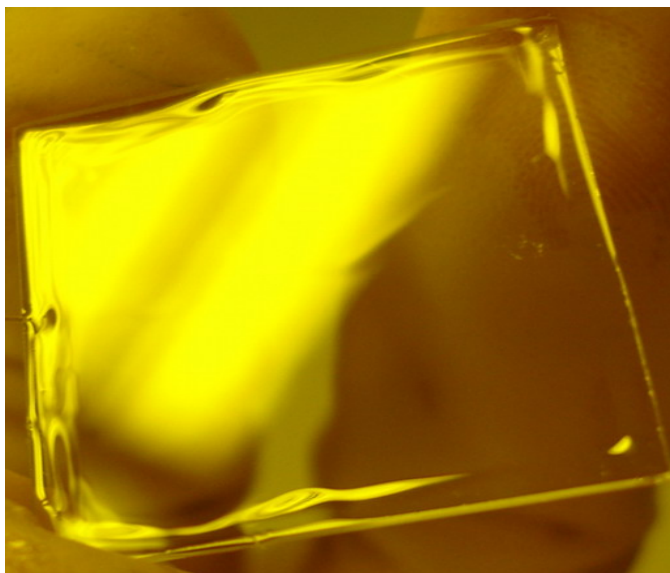
Solvent Compatibility of Poly(dimethylsiloxane)-Based Microfluidic Devices

Anal. Chem. 2003, 75, 6544–6554

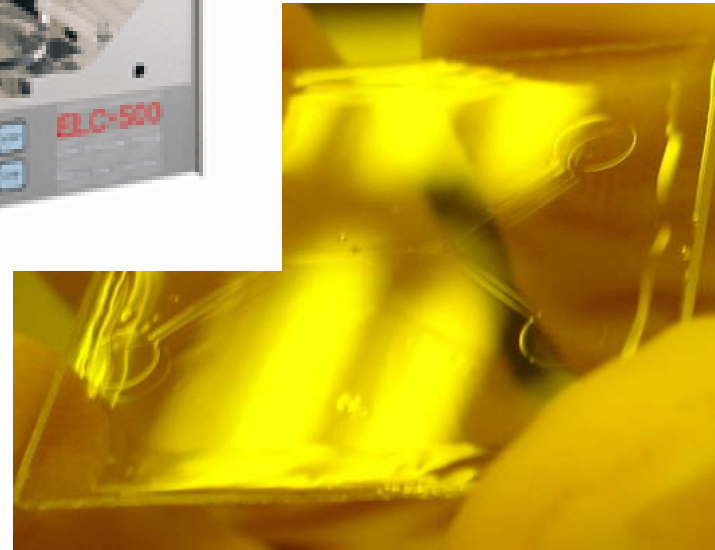
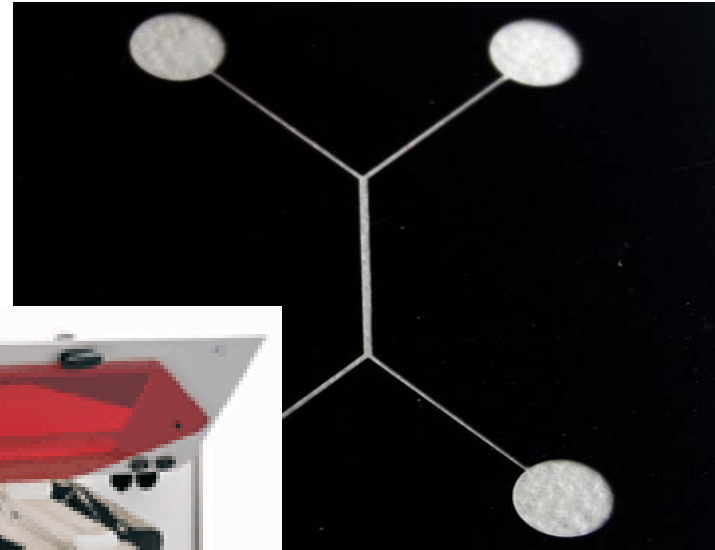
solvent	δ^a	S^b	μ (D)
perfluorotributylamine	5.6	1.00	0.0
perfluorodecalin	6.6	1.00	0.0
pentane	7.1	1.44	0.0
poly(dimethylsiloxane)	7.3	∞	0.6–0.9
diisopropylamine	7.3	2.13	1.2
hexanes	7.3	1.35	0.0
<i>n</i> -heptane	7.4	1.34	0.0
triethylamine	7.5	1.58	0.7
ether	7.5	1.38	1.1
cyclohexane	8.2	1.33	0.0
trichloroethylene	9.2	1.34	0.9
dimethoxyethane (DME)	8.8	1.32	1.6
xylene	8.9	1.41	0.3
toluene	8.9	1.31	0.4
ethyl acetate	9.0	1.18	1.8
benzene	9.2	1.28	0.0
chloroform	9.2	1.39	1.0
2-butanone	9.3	1.21	2.8
tetrahydrofuran (THF)	9.3	1.38	1.7
dimethyl carbonate	9.5	1.03	0.9
chlorobenzene	9.5	1.22	1.7
methylene chloride	9.9	1.22	1.6
acetone	9.9	1.06	2.9
dioxane	10.0	1.16	0.5
pyridine	10.6	1.06	2.2
<i>N</i> -methylpyrrolidone (NMP)	11.1	1.03	3.8
<i>tert</i> -butyl alcohol	10.6	1.21	1.6
acetonitrile	11.9	1.01	4.0
1-propanol	11.9	1.09	1.6
phenol	12.0	1.01	1.2
dimethylformamide (DMF)	12.1	1.02	3.8
nitromethane	12.6	1.00	3.5
ethyl alcohol	12.7	1.04	1.7
dimethyl sulfoxide (DMSO)	13.0	1.00	4.0
propylene carbonate	13.3	1.01	4.8
methanol	14.5	1.02	1.7
ethylene glycol	14.6	1.00	2.3
glycerol	21.1	1.00	2.6
water	23.4	1.00	1.9



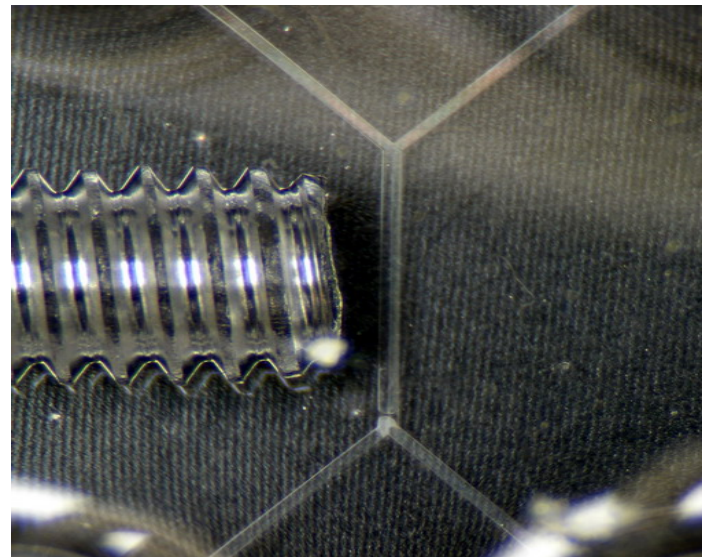
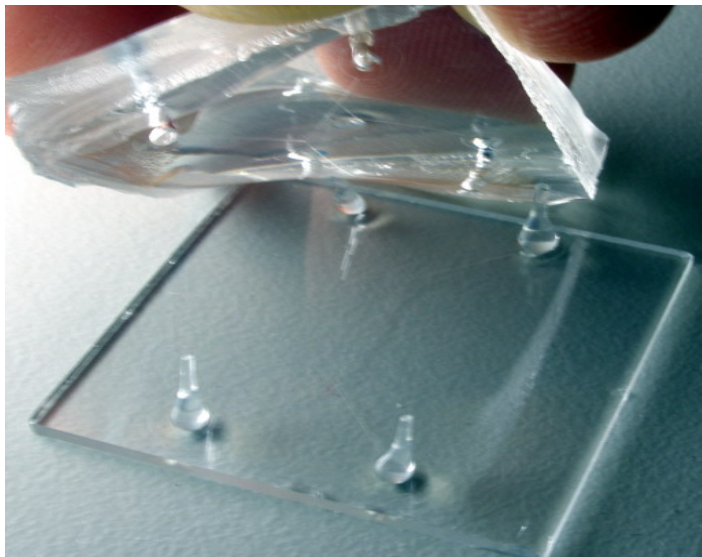
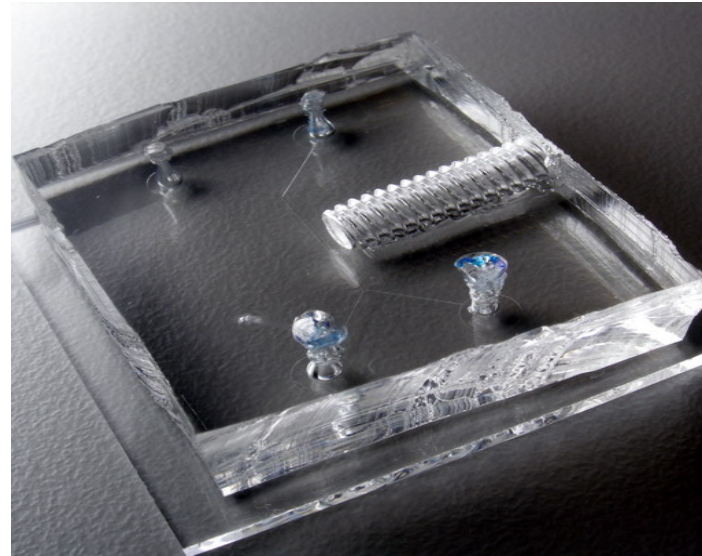
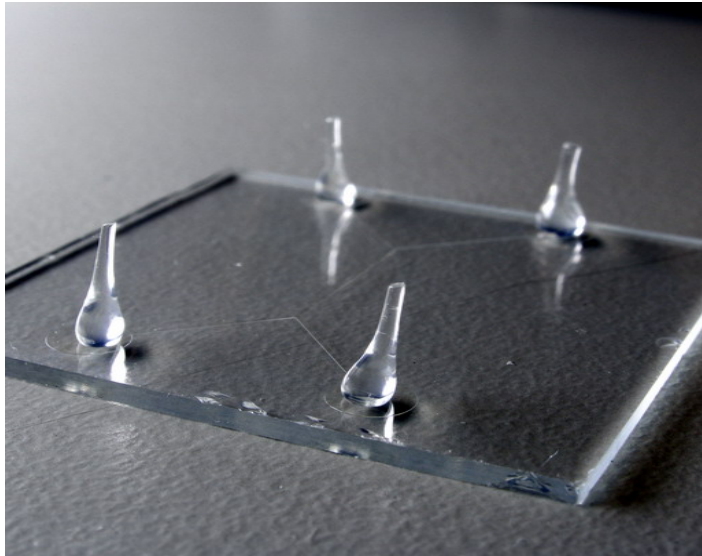
Microfluidics by Soft Lithography



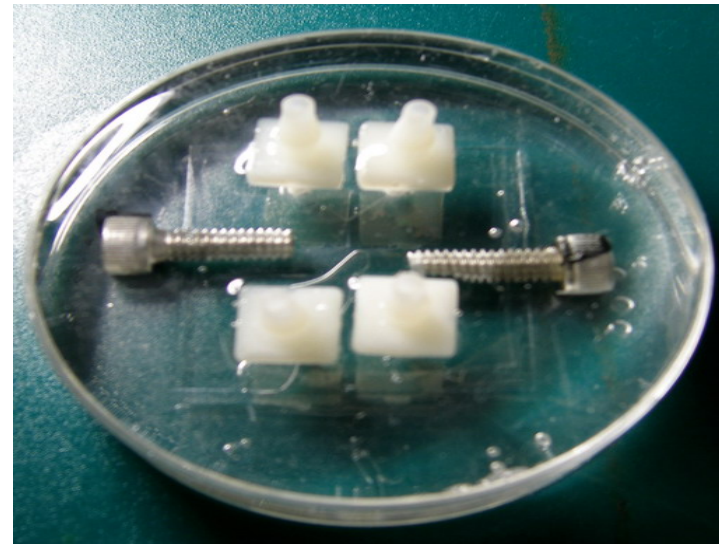
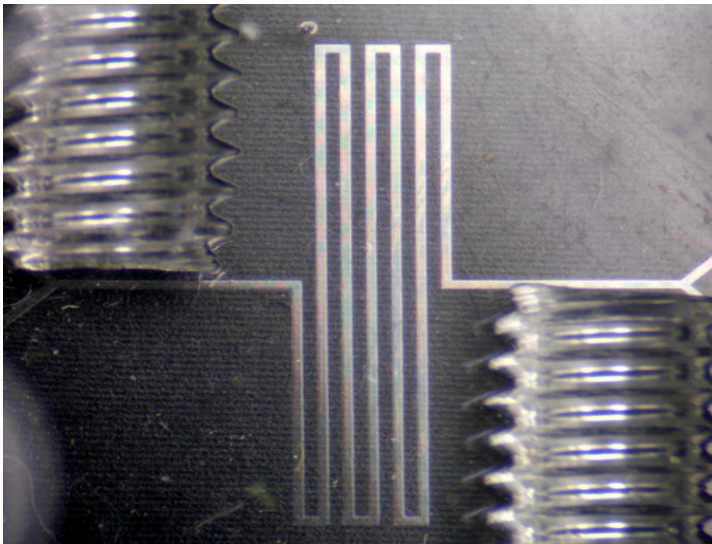
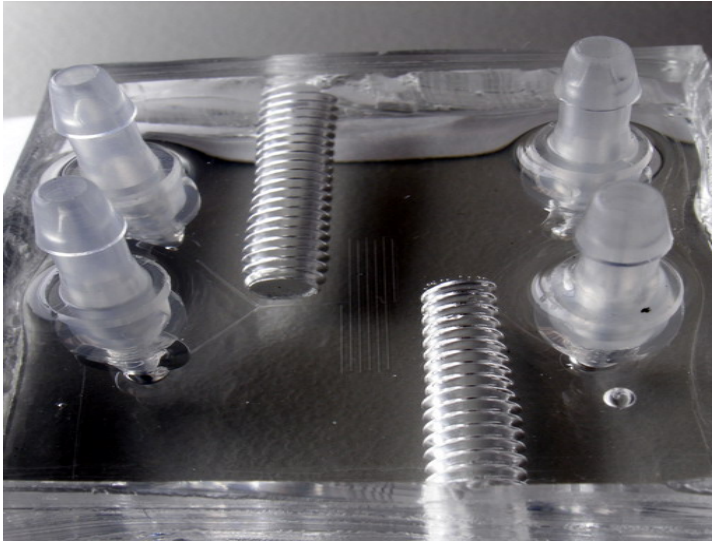
Microfluidics by Soft Lithography



Microfluidics by Soft Lithography

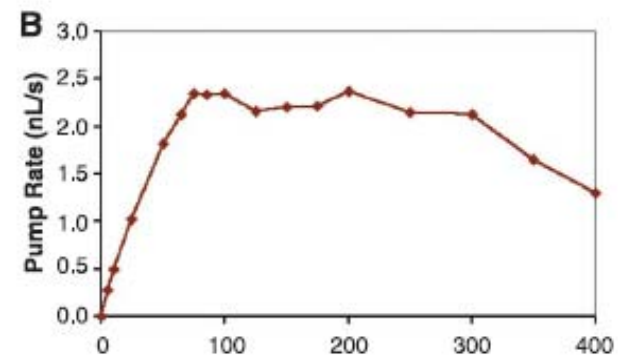
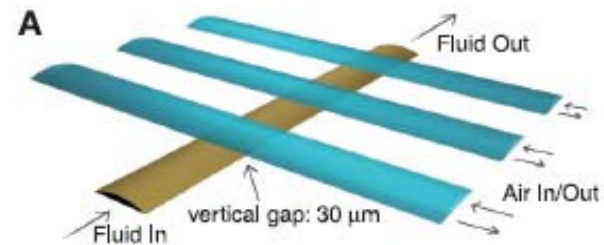
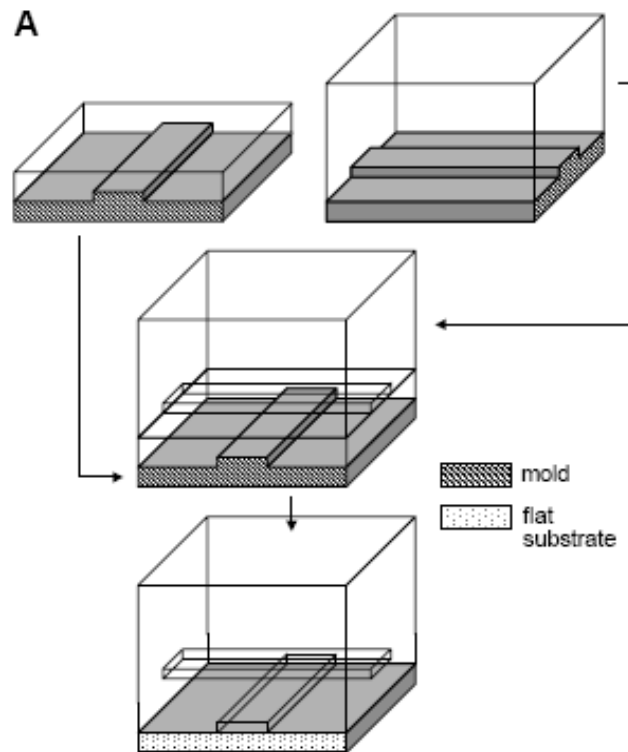


Microfluidics by Soft Lithography



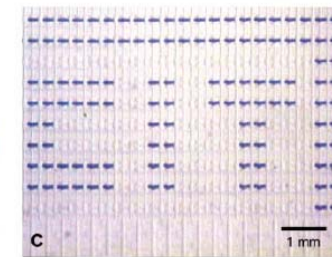
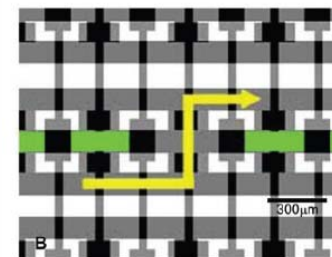
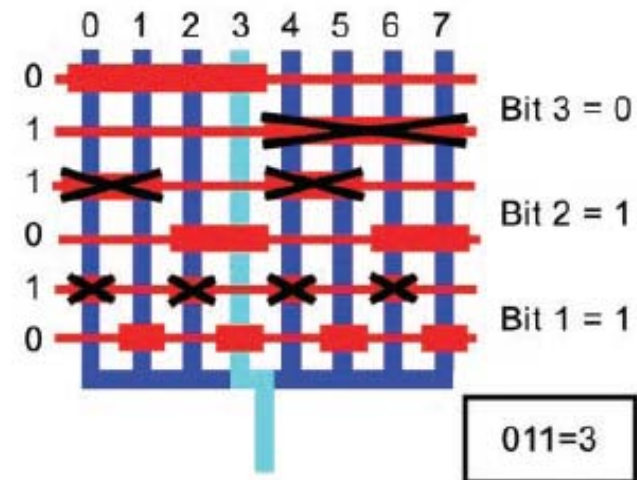
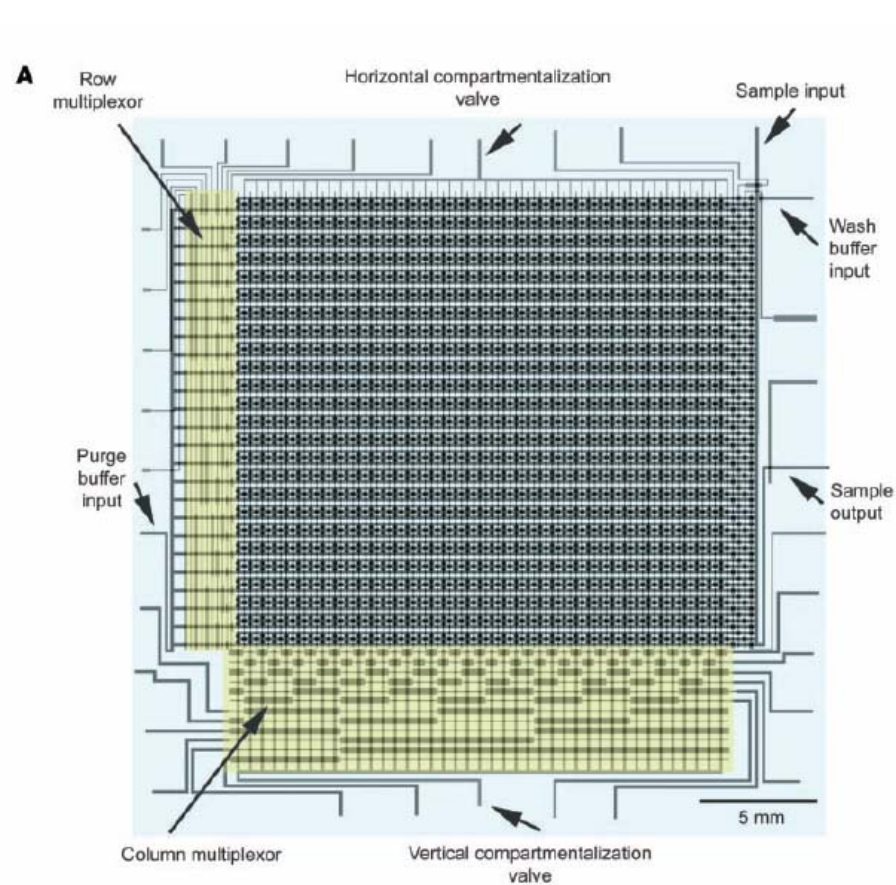
Monolithic Microfabricated Valves and Pumps by Multilayer Soft Lithography

SCIENCE VOL 288 7 APRIL 2000



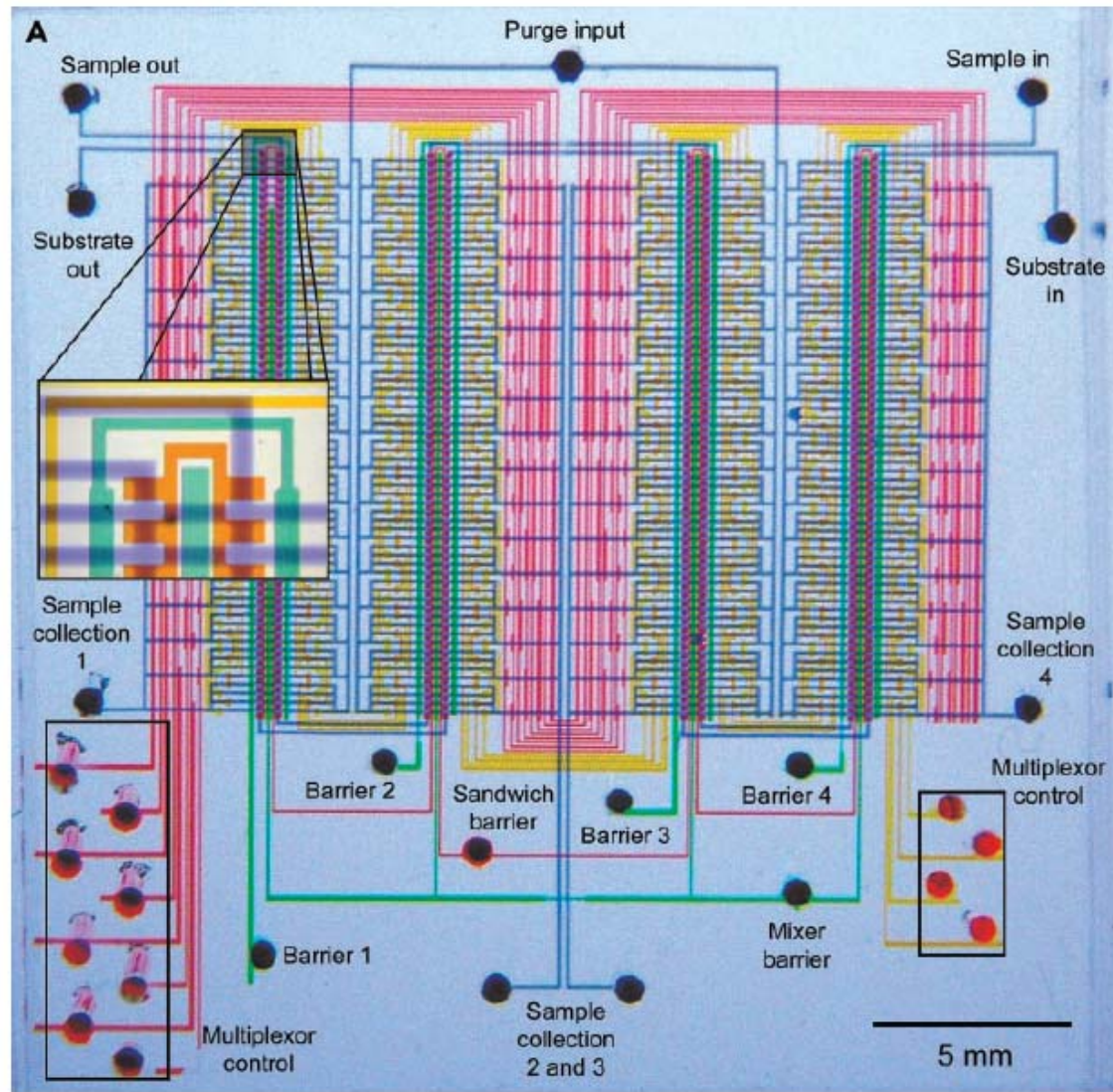
Microfluidic Large-Scale Integration

18 OCTOBER 2002 VOL 298 SCIENCE

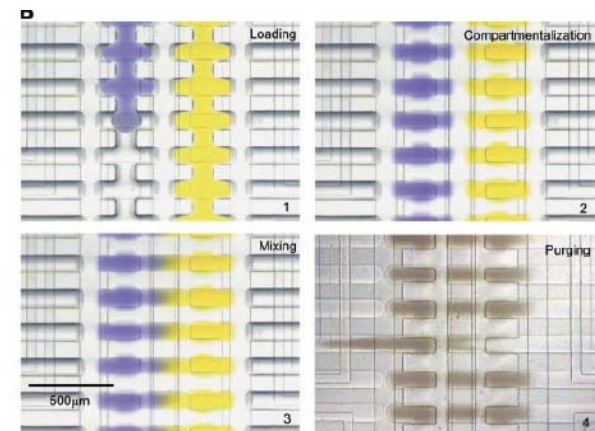


$2 \log_2 n$ control channels.

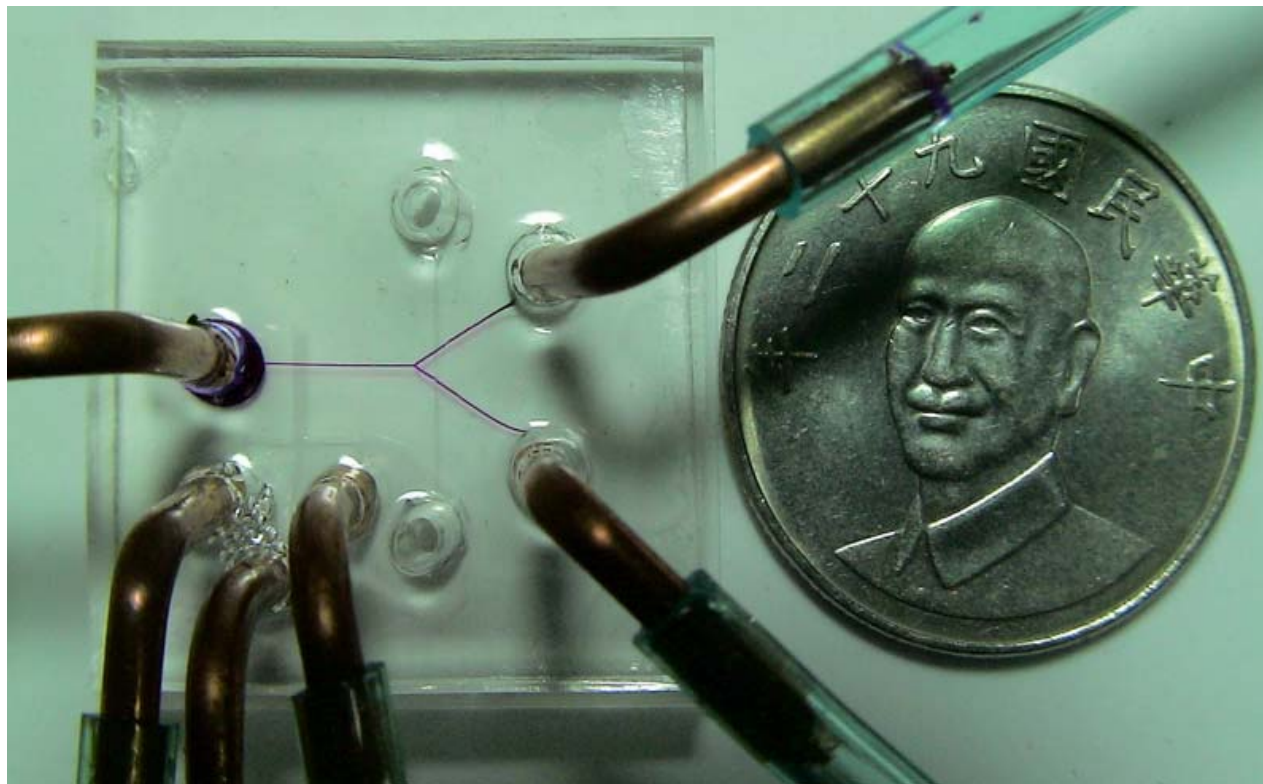




R



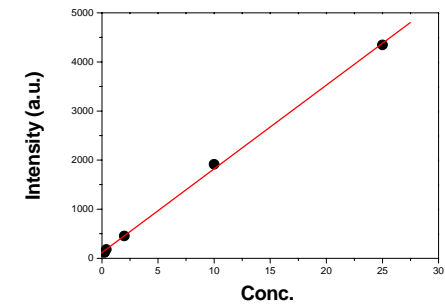
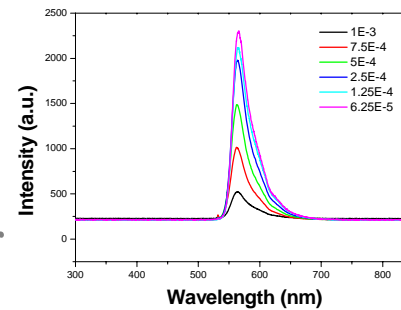
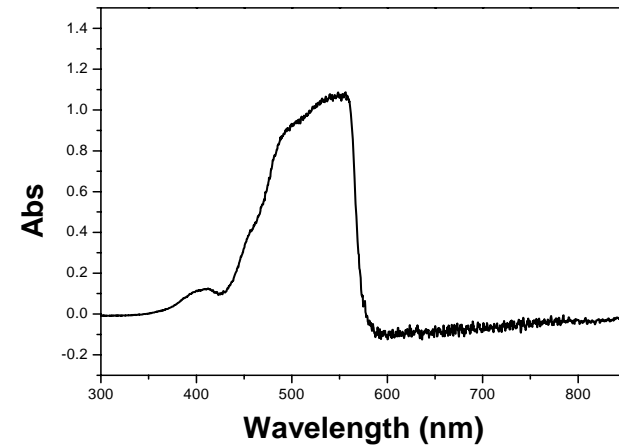
Microfabricated Fluidic System by Soft Lithography



Integrated Detection System in Microchannel



fluidic channel + microlens + fiber

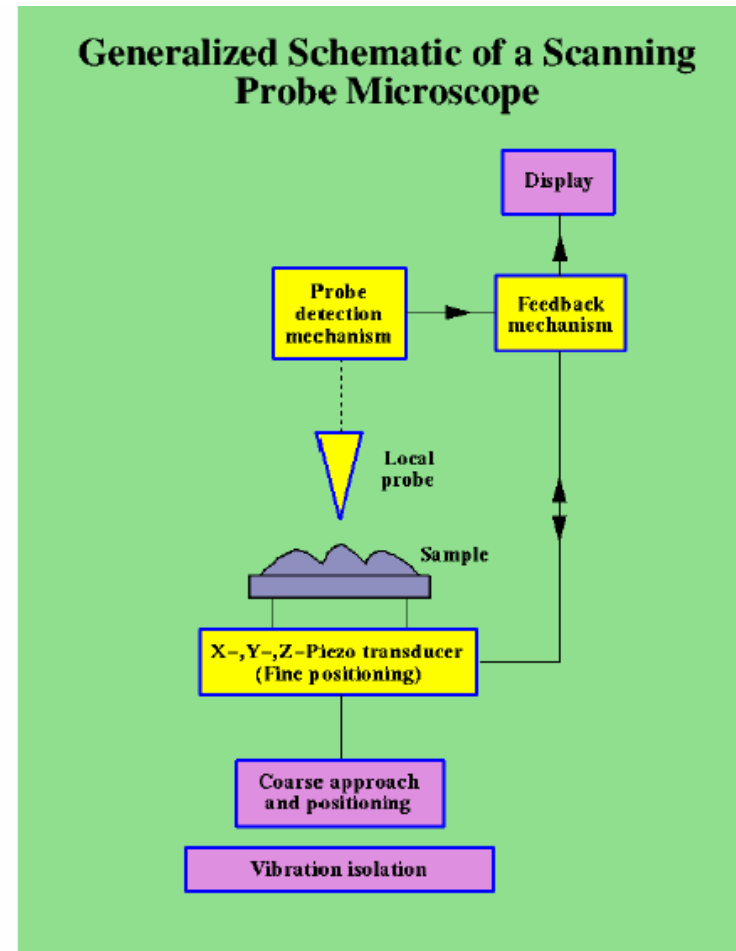


Introduction To Scanning Probe Microscopy

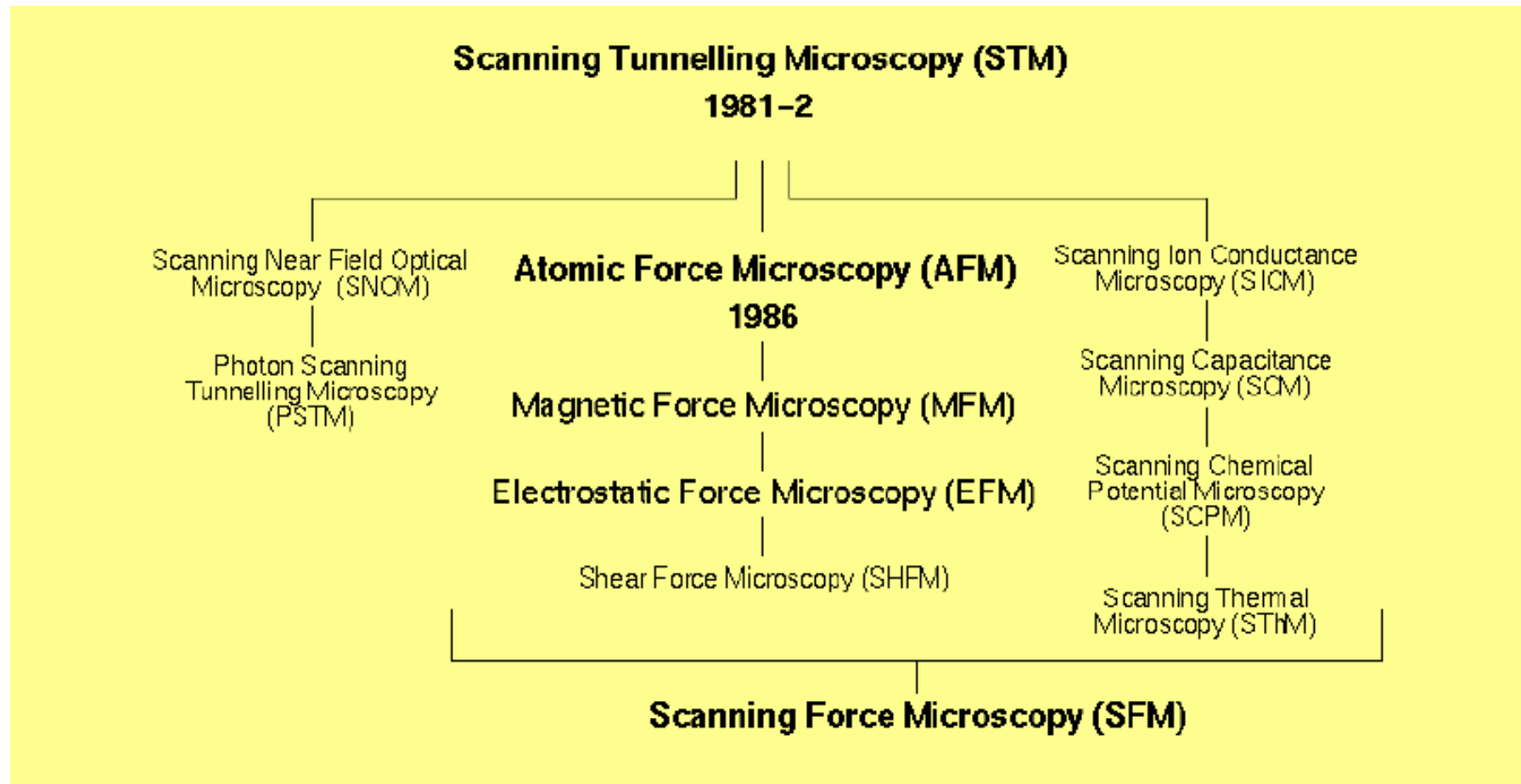
General features of SPM

The first scanning probe microscope was invented in 1981 by Gerd Binnig and Heinrich Rohrer at the IBM laboratory in Zurich. Since that time, a vast family of scanning probe microscopes has been spawned, a few of which are represented in this family tree. Despite the huge number of types of SPM and modes in which they can be operated, the underlying operation is the same for them all. Each different type of SPM is

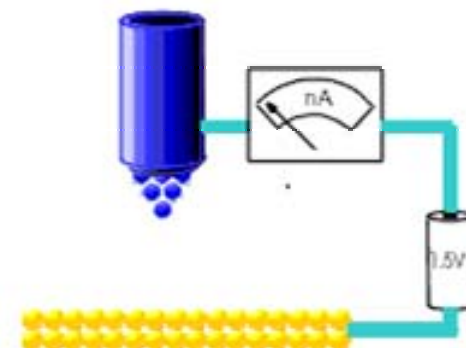
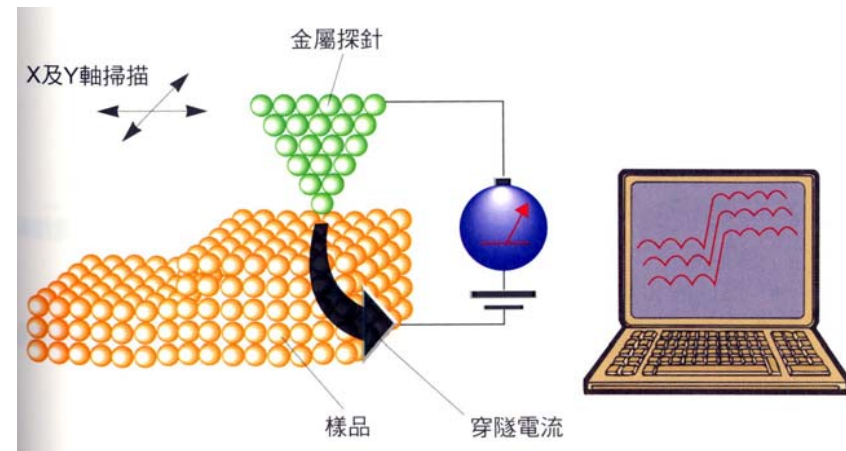
characterized by the nature of the local probe and its interaction with the sample surface.



Scanning Probe Family



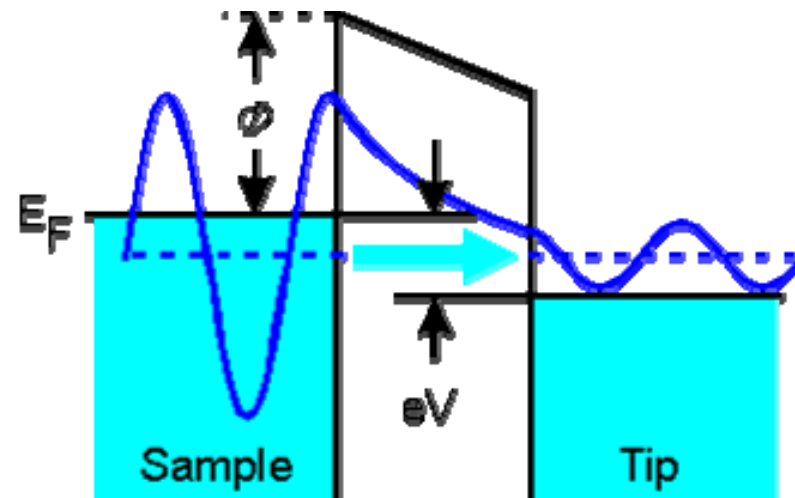
Scanning Tunneling Microscopy



Tunneling Current

$$\Psi(d) = \Psi(0)e^{-\kappa d} \quad \text{where } \kappa = \frac{\sqrt{2m(\Phi - E)}}{\hbar}$$

$$W(d) = |\Psi(d)|^2 = |\Psi(0)|^2 e^{-2\kappa d}$$

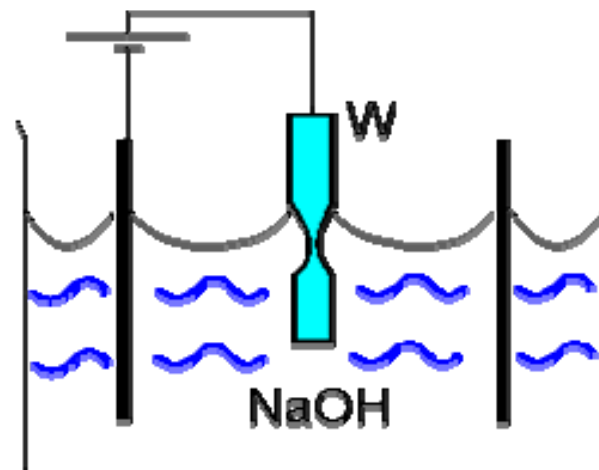
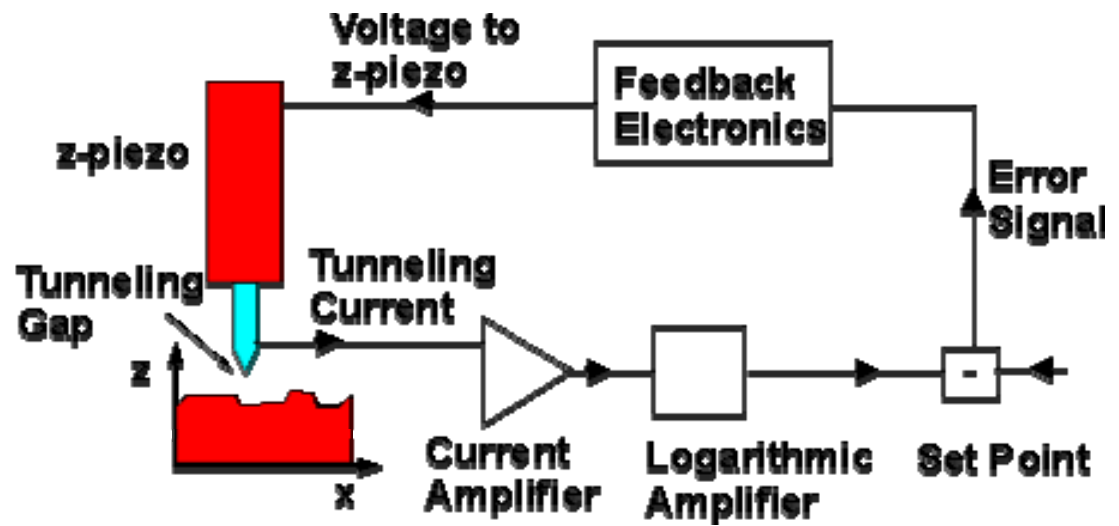
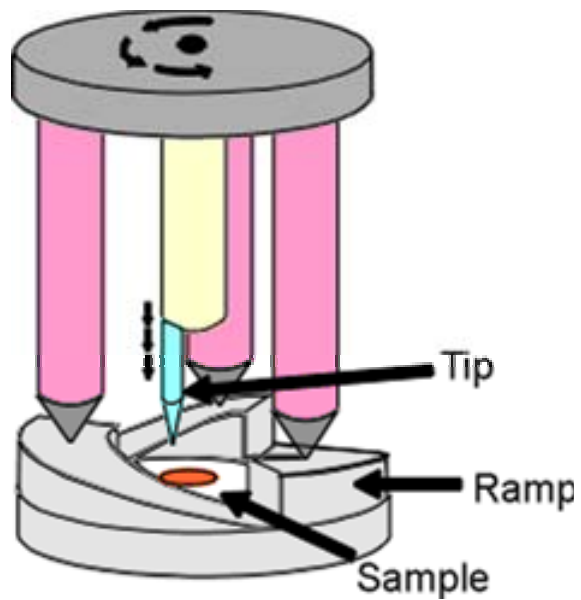


$$I \propto V \rho_{\text{st}}(0, E_F) e^{-2\kappa d} \quad (*)$$

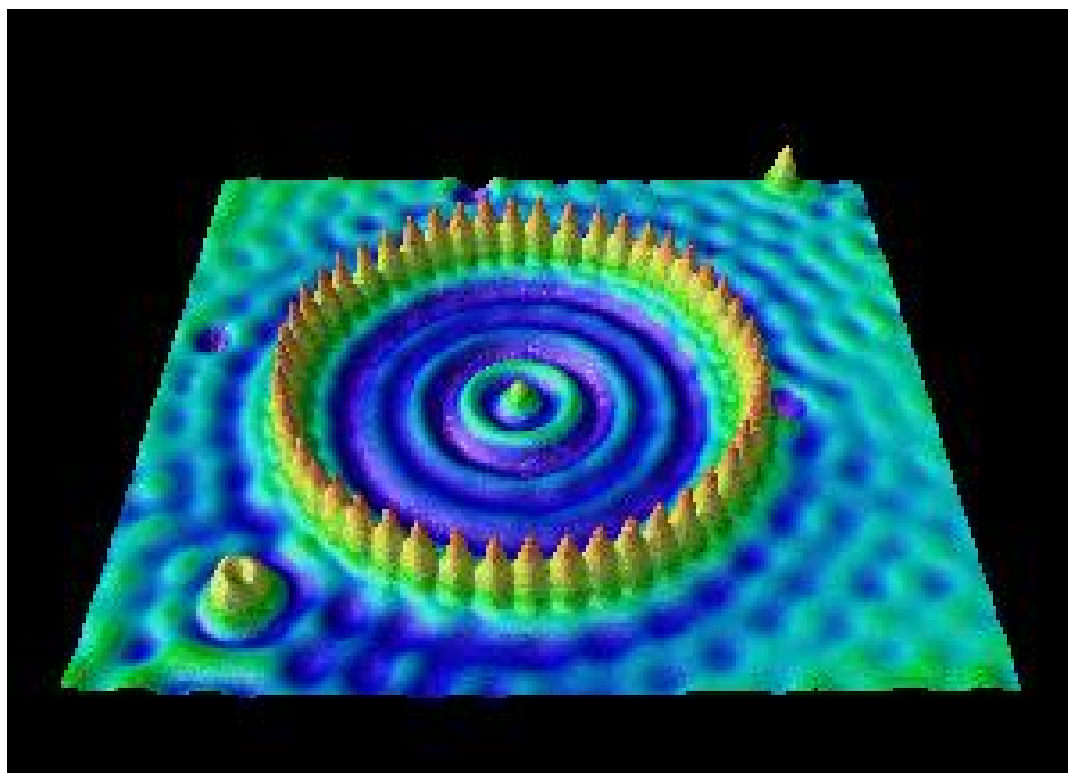
$$\approx V \rho_{\text{st}}(0, E_F) e^{-1.025\sqrt{\Phi}d} \quad \text{where } [d] = \text{\AA}; [\Phi] = \text{eV};$$



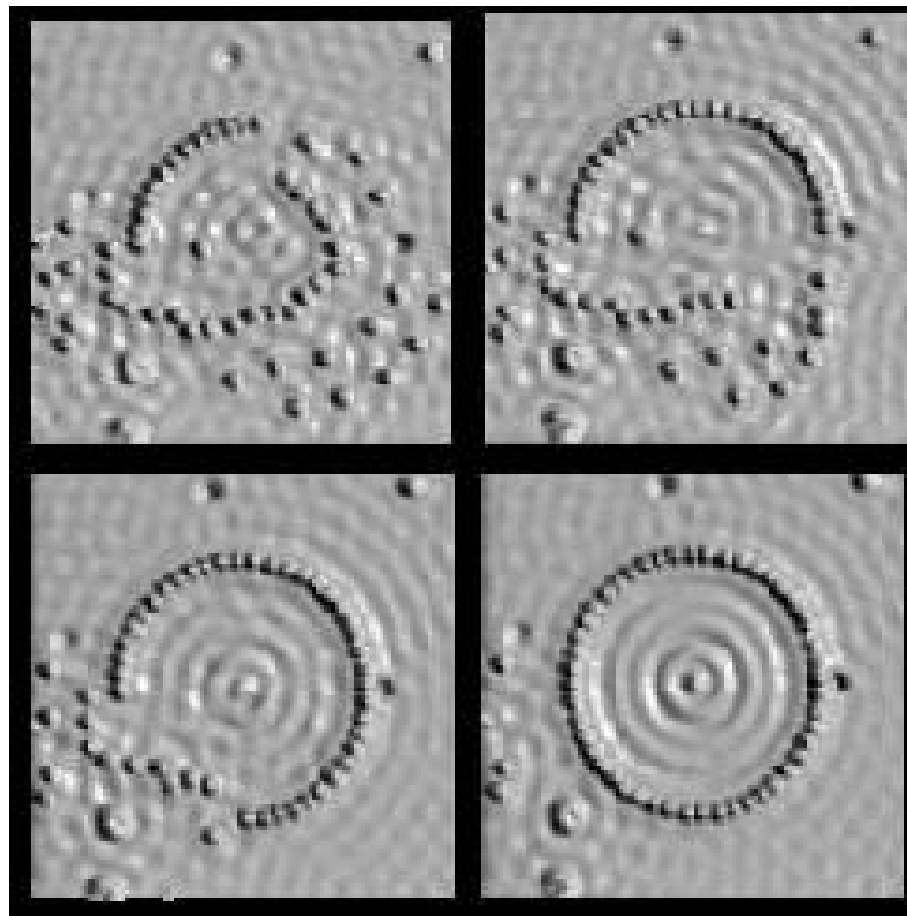
STM



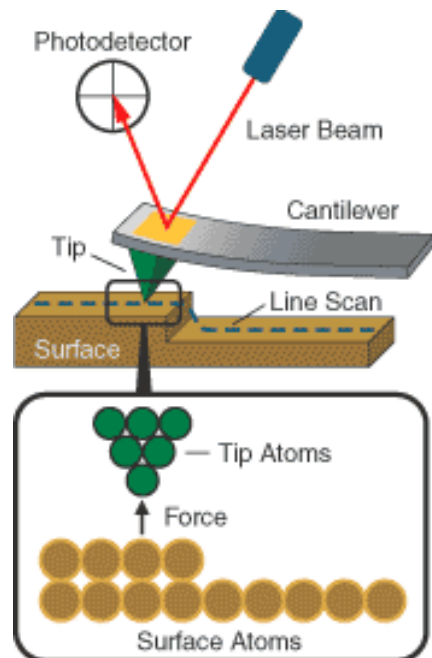
STM

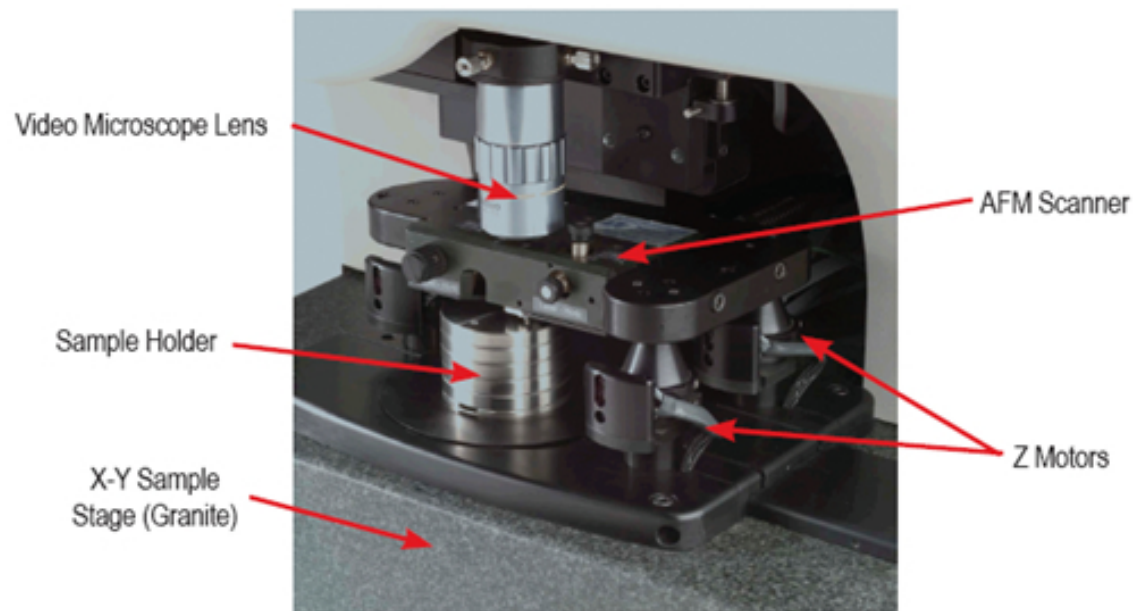
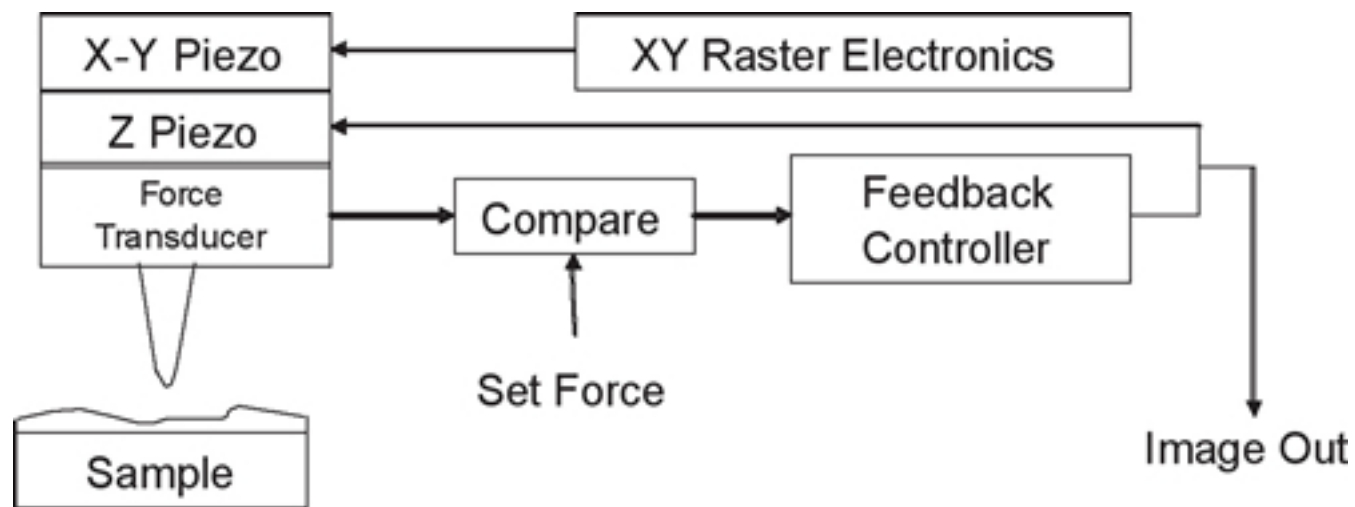


STM

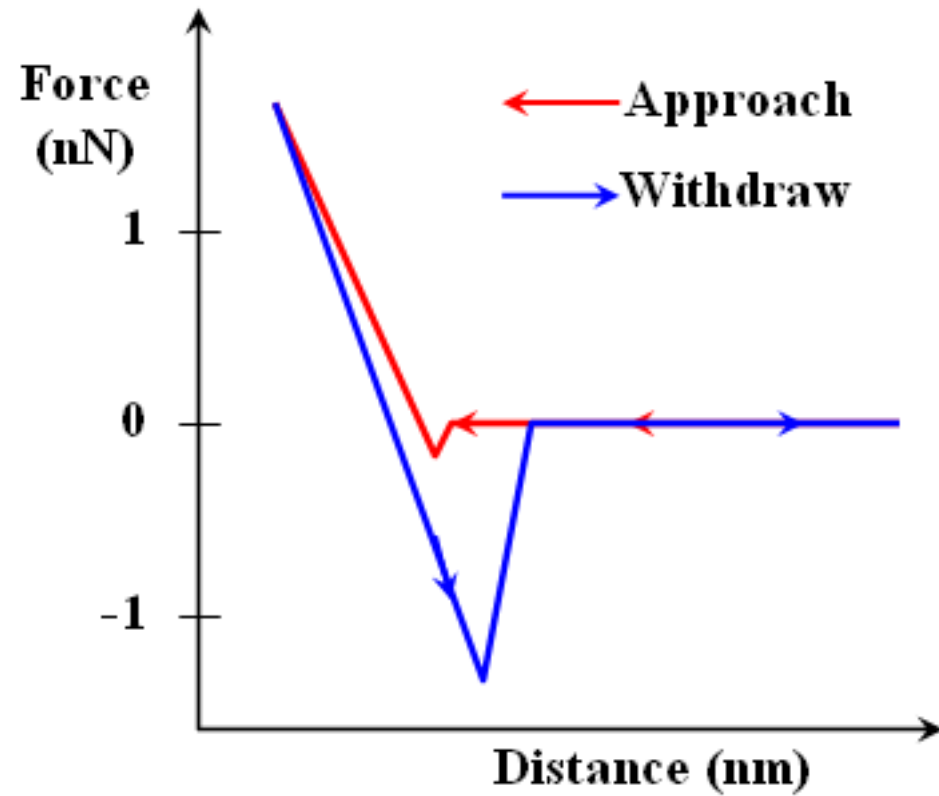
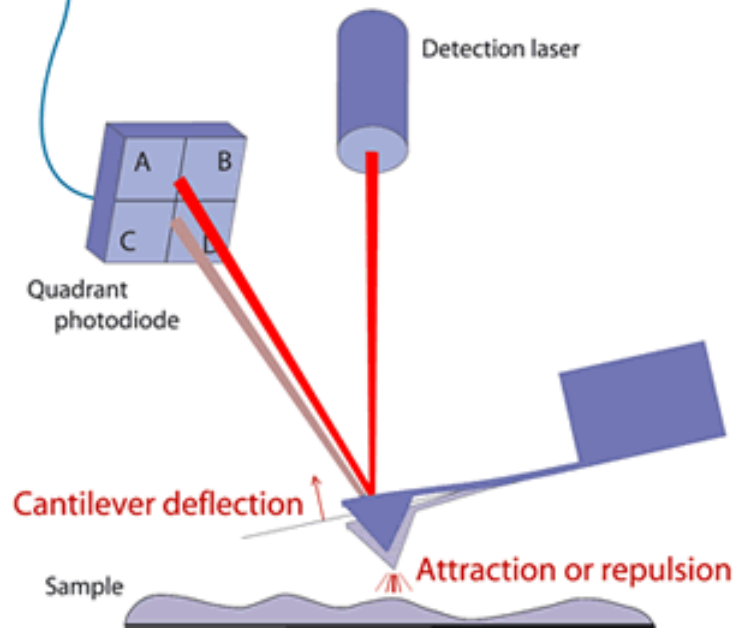


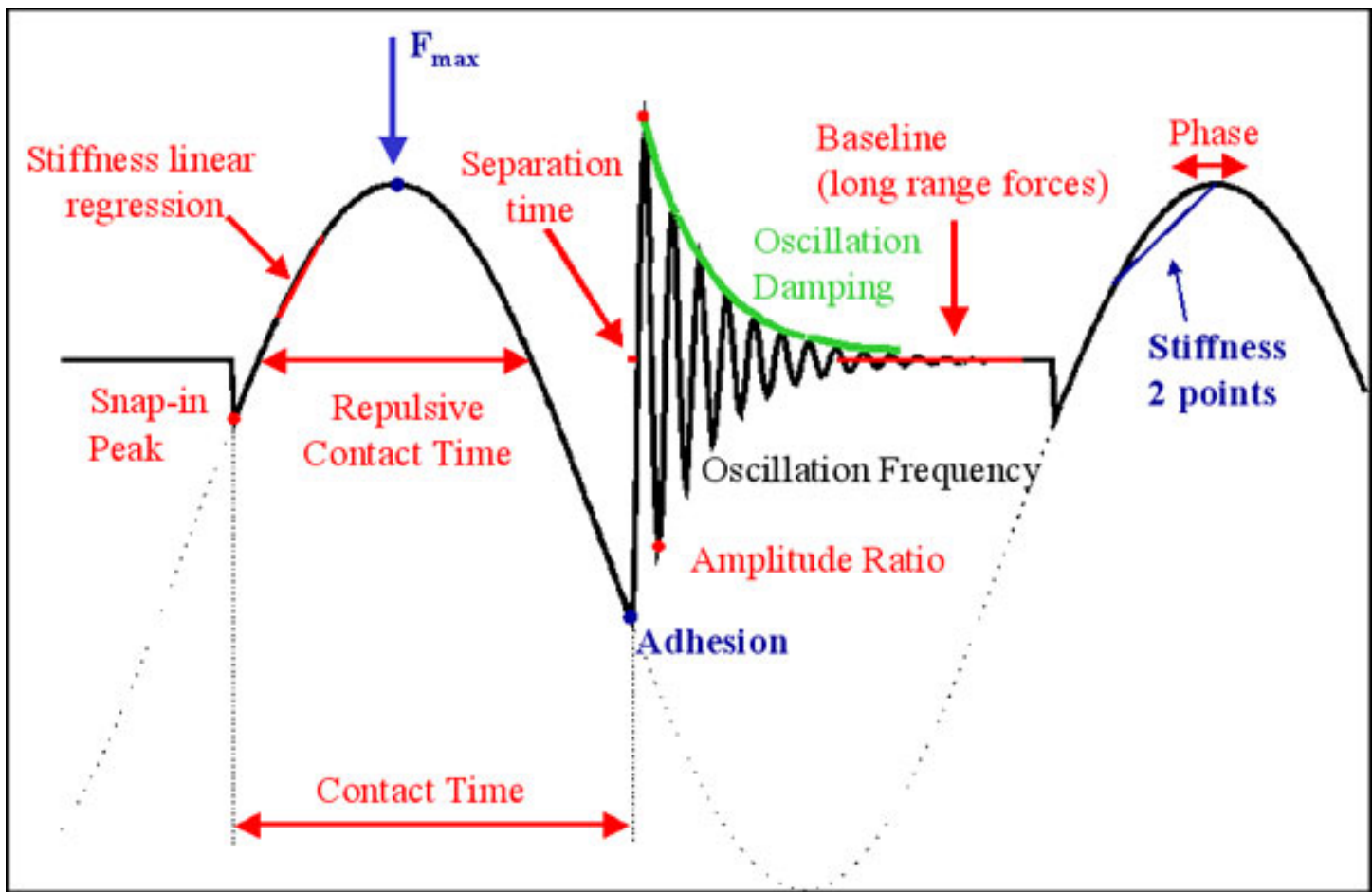
Atomic Force Microscopy

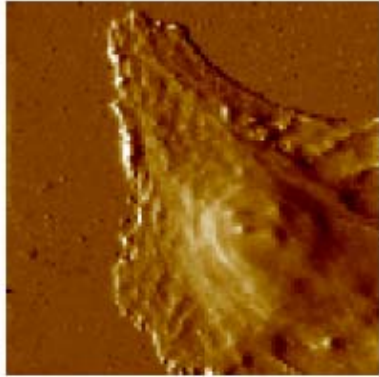




Deflection signal
$$\frac{(A + B) - (C + D)}{(A + B) + (C + D)}$$







Cell surface imaging
AFM imaging of living
and fixed animal cells

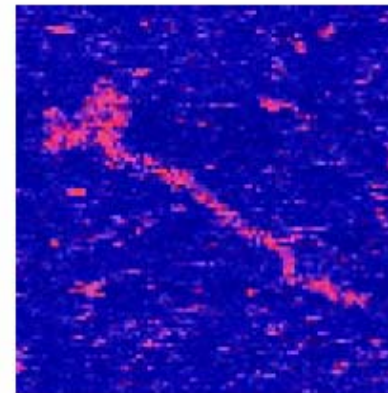


Chromosomes
A large selection of
work on both human
and plant
chromosomes

Scanning Probe Microscope



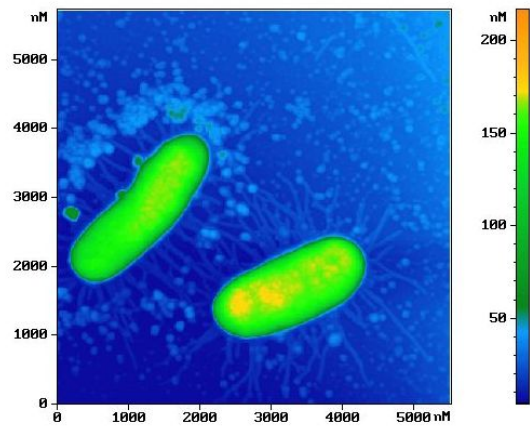
DNA
AFM images of
double-stranded
DNA and of some
special single-
double-stranded
DNA constructs



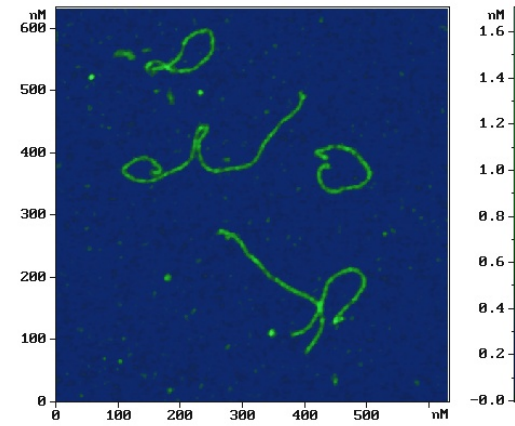
Muscle Proteins
High resolution
AFM images of
myosin and titin



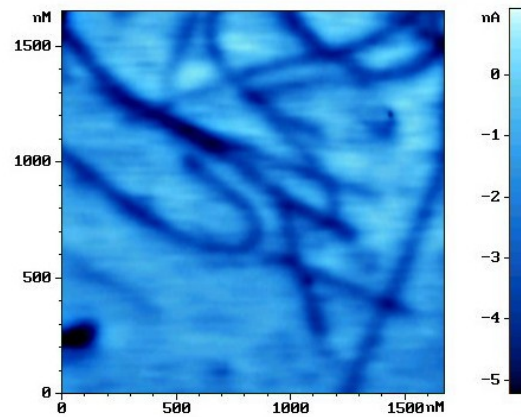
AFM Images



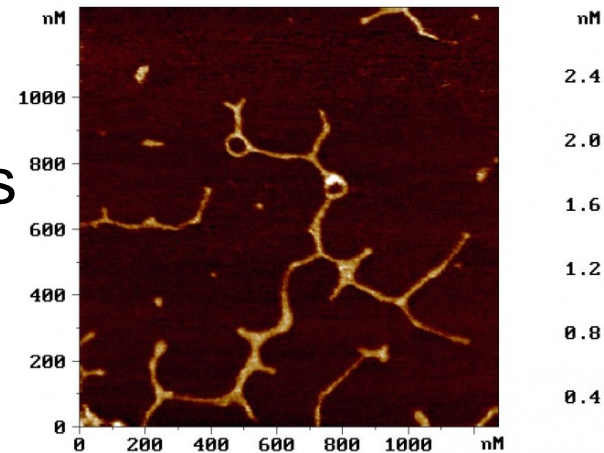
E Coli



Protein



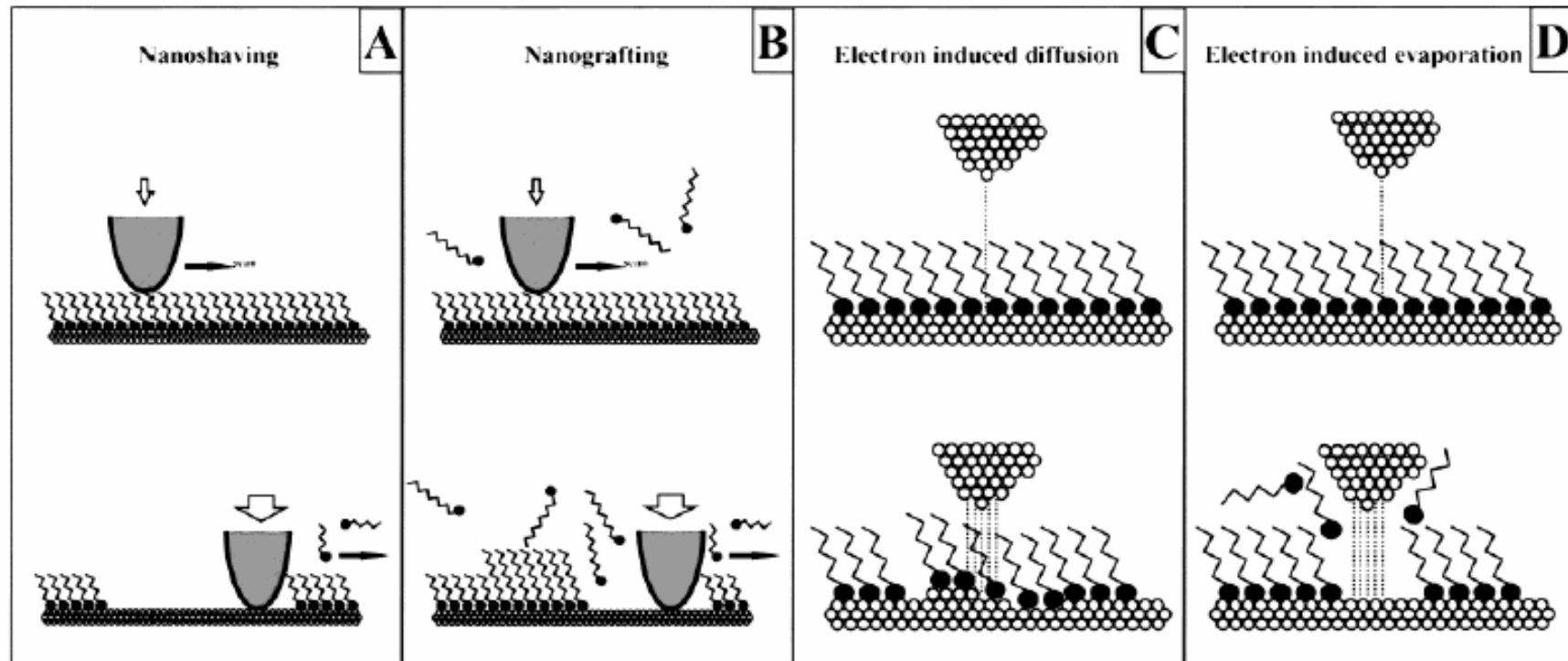
Nanotubes



DNA



STM Lithography



Resist: Thiol



STM Lithography

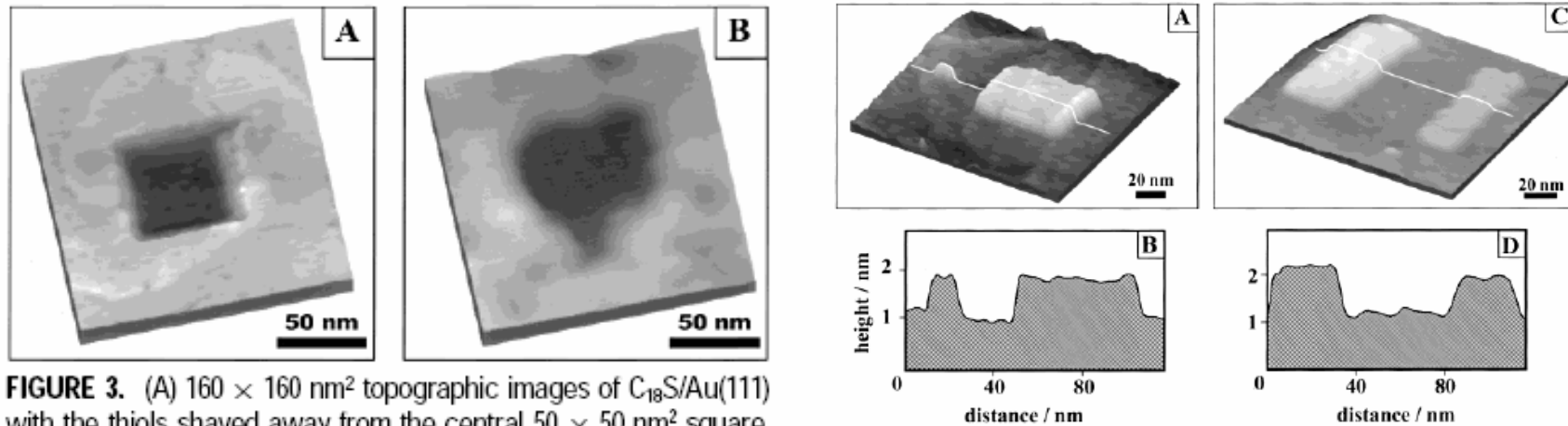


FIGURE 3. (A) $160 \times 160 \text{ nm}^2$ topographic images of $\text{C}_{18}\text{S}/\text{Au}(111)$ with the thiols shaved away from the central $50 \times 50 \text{ nm}^2$ square. (B) $160 \times 160 \text{ nm}^2$ topographic images of OTE/mica containing a heart-shaped pattern produced using nanoshaving.



Oxidation Lithography

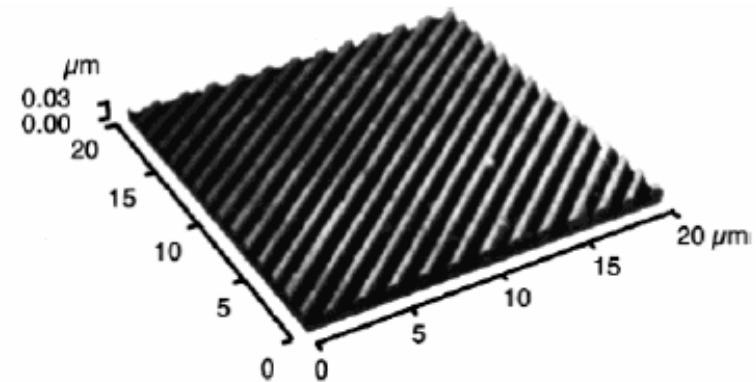
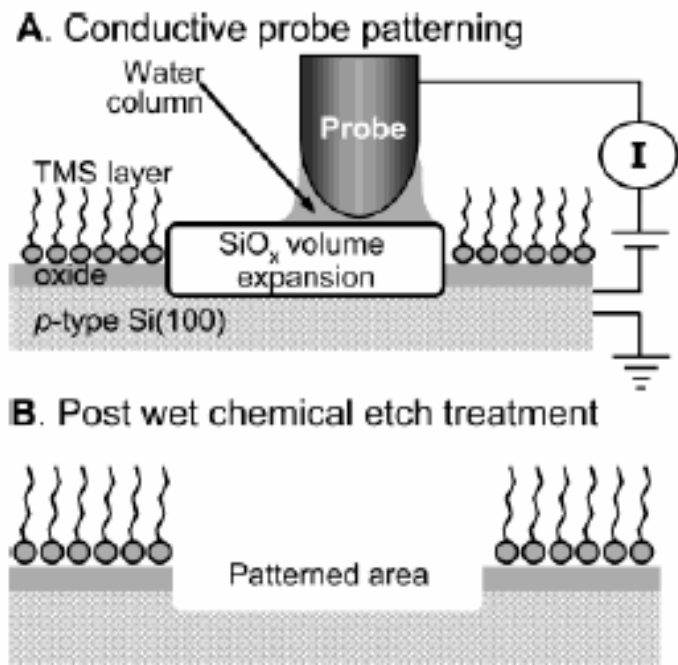


Figure 8. AFM images showing the results of AFM anodic oxidation and wet etching of a pattern in an ODS-SAM on a multilayer resist: scan speed, $10 \mu\text{m/s}$; probe current, 5 nA ; etching steps with 0.5 wt \% hydrofluoric acid (0.5 min) and 25 wt \% tetraammonium hydroxide (3 min). Reprinted with permission from ref 111. Copyright 1999 Society of the American Institute of Physics.



AFM Lithography

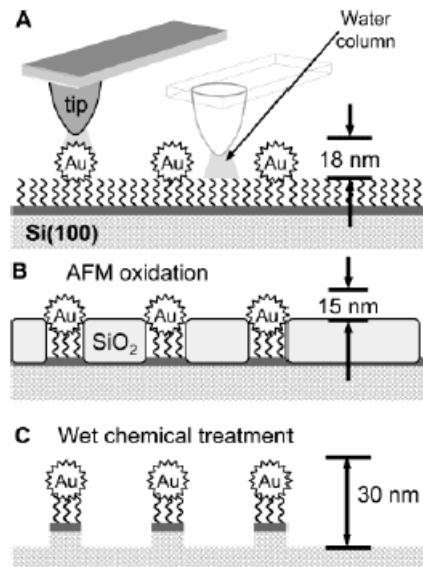


Figure 10. Schematic diagram of (A) selective anodization of the silicon regions not masked by nanoparticles. (B) The volume expansion of the silicon led to a decreased height contrast between the particles and the substrate. (C) After a wet etching step, silicon columns capped with a nanoparticle were formed.

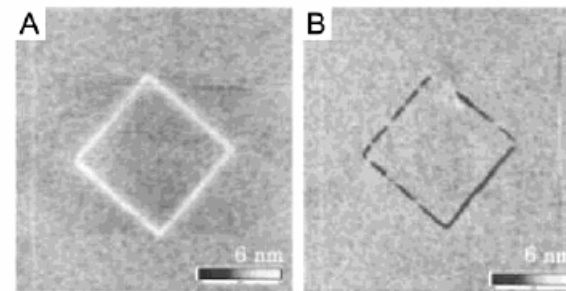


Figure 12. AFM images showing a lithographically defined pattern in a palmitic acid LB layer adsorbed to a SiO_x/Si substrate. Diamond pattern with protruding lines was written with -10 V applied tip bias (A), and that with grooves, with +10 V applied tip bias (B) (z-scale: 6 nm). Reprinted with permission from ref 123. Copyright 2002 American Institute of Physics.



Substitution Lithography

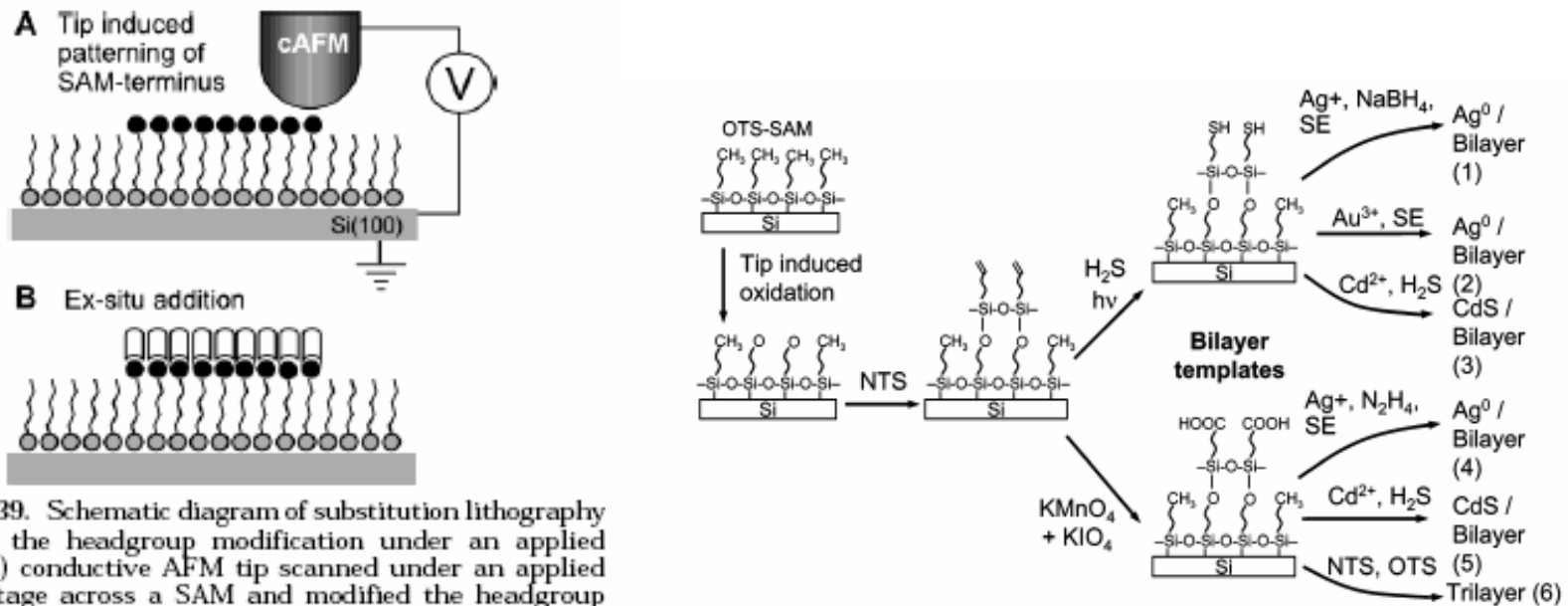
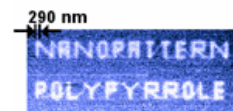
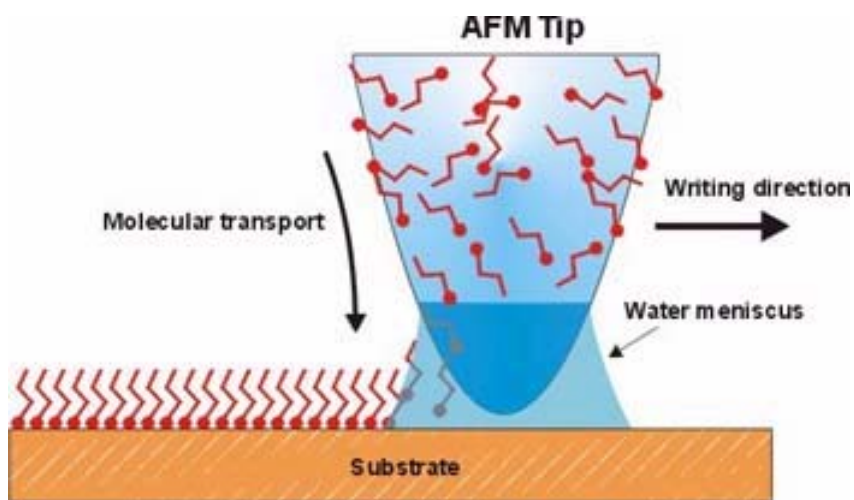


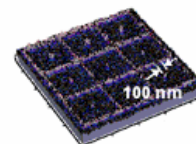
Figure 39. Schematic diagram of substitution lithography through the headgroup modification under an applied bias: (A) conductive AFM tip scanned under an applied bias voltage across a SAM and modified the headgroup without changing the structural integrity of the SAM; (B) altered functionality used for the subsequent binding of a second self-assembly molecule.



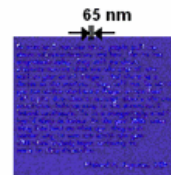
Dip-Pen Lithography



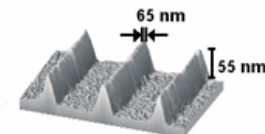
Conducting Polymers



Protein Nanoarrays

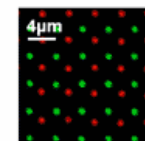
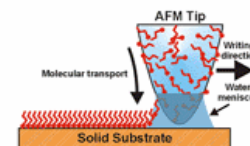


Small Organic Molecules

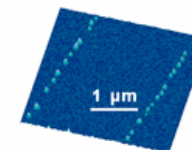


Silicon Nanostructures

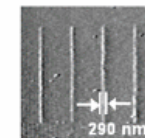
Dip-Pen Nanolithography



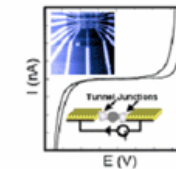
Ultrahigh Density DNA Arrays



Single Nanoparticle Lines



Sol Gel Templates



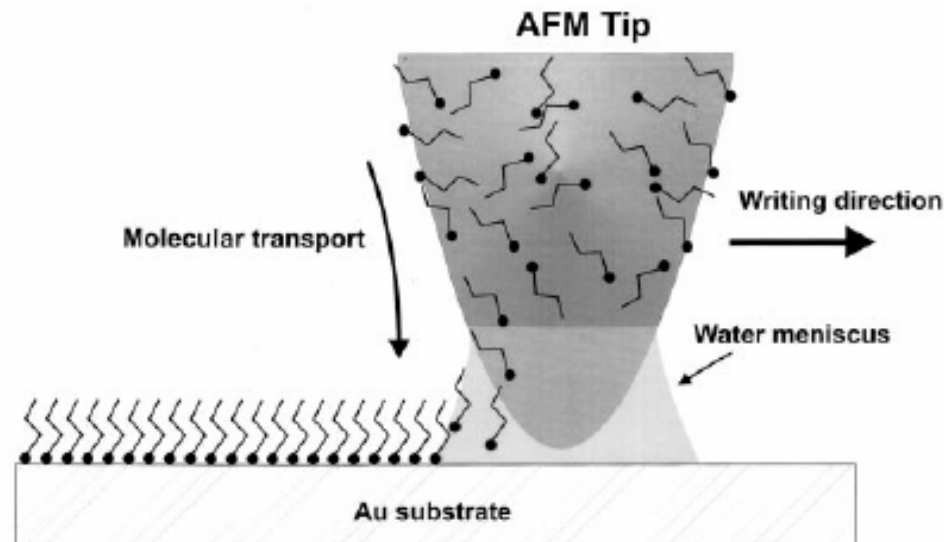
Single Particle Devices



"Dip-Pen" Nanolithography

Richard D. Piner, Jin Zhu, Feng Xu, Seunghun Hong,
Chad A. Mirkin*

Fig. 1. Schematic representation of DPN. A water meniscus forms between the AFM tip coated with ODT and the Au substrate. The size of the meniscus, which is controlled by relative humidity, affects the ODT transport rate, the effective tip-substrate contact area, and DPN resolution.

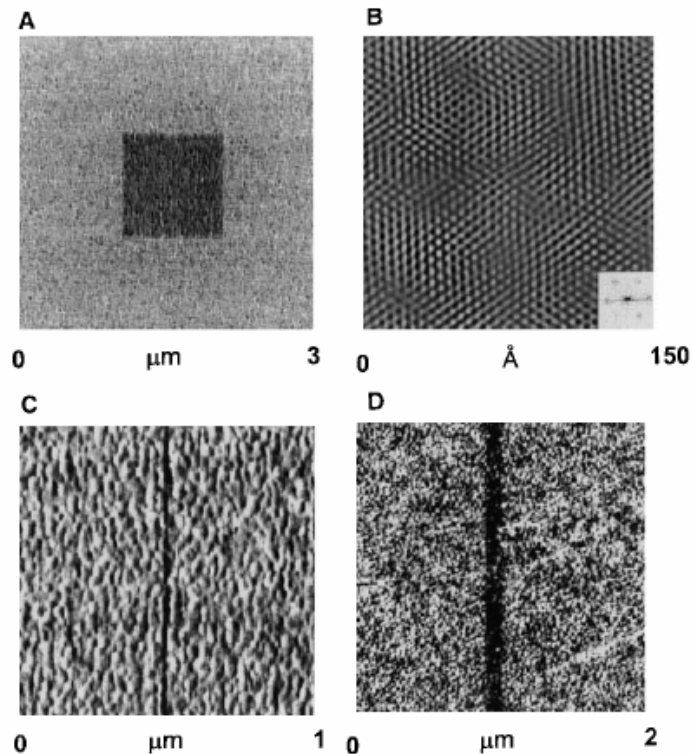


SCIENCE VOL 283 29 JANUARY 1999



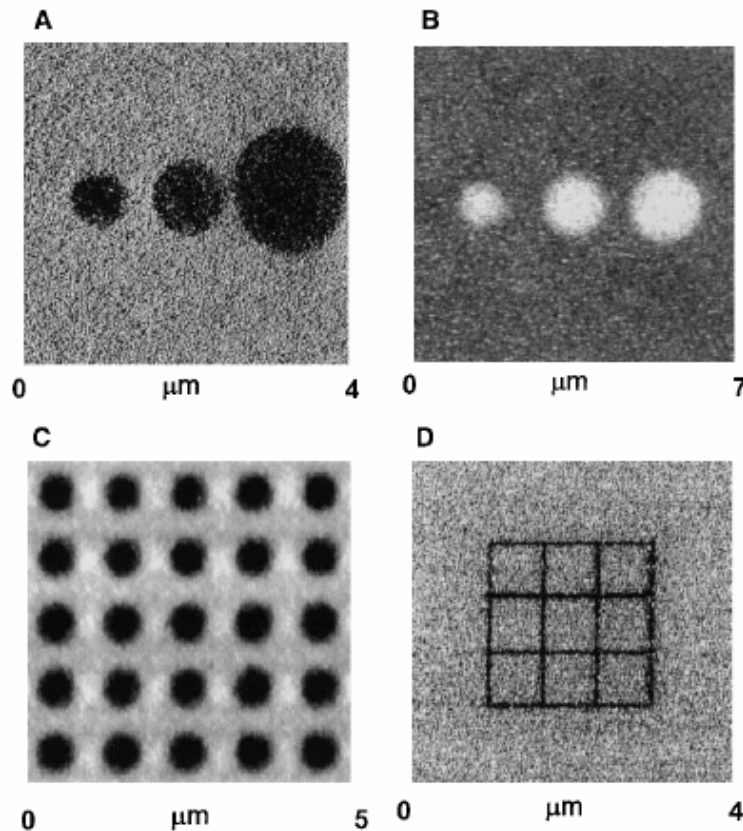
Dip-Pen Lithography

Fig. 2. (A) Lateral force image of a square of ODT measuring $1\ \mu\text{m}$ by $1\ \mu\text{m}$, deposited onto a Au substrate by DPN. This pattern was generated by scanning the $1\text{-}\mu\text{m}^2$ area at a scan rate of 1 Hz for a period of 10 min at a relative humidity of 39%. Then the scan size was increased to $3\ \mu\text{m}$, and the scan rate was increased to 4 Hz while the image was recorded. The faster scan rate prevents ODT transport. (B) Lattice-resolved, lateral force image of an ODT SAM deposited onto Au(111)/mica by DPN. The image has been filtered with a fast Fourier transform (FFT), and the FFT of the raw data is shown in the lower right insert. The monolayer was generated by scanning a $1000\ \text{\AA}$ square area of the Au(111)/mica five times at a rate of 9 Hz at 39% relative humidity. (C) Lateral force image of a 30-nm-wide line ($3\ \mu\text{m}$ long) deposited onto Au/mica by DPN. The line was generated by scanning the tip in a vertical line repeatedly for 5 min at a scan rate of 1 Hz. (D) Lateral force image of a 100-nm line deposited on Au by DPN. The method of depositing this line is analogous to that used to generate the image in (C), but the writing time was 1.5 min. In all images, darker regions correspond to areas of relatively lower friction.



Dip-Pen Lithography

Fig. 3. (A) Lateral force image of an Au substrate after an AFM tip, which was coated with ODT, had been in contact with the substrate for 2, 4, and 16 min (left to right); the relative humidity was held constant at 45%, and the image was recorded at a scan rate of 4 Hz. (B) Lateral force image of dots of 16-mercaptohexadecanoic acid on a Au substrate. To generate the dots, an AFM tip coated with 16-mercaptohexadecanoic acid was held on the Au substrate for 10, 20, and 40 s (left to right). The relative humidity was 35%. The images show that the transport properties of 16-mercaptohexadecanoic acid and of ODT differ substantially. (C) Lateral force image of an array of dots generated by DPN. Each dot was generated by holding an ODT-coated tip in contact with the surface for ~20 s. Writing and recording conditions were the same as in (A). (D) Lateral force image of a molecule-based grid. Each line is 100 nm in width and 2 μm in length and required 1.5 min to write.



Dip-pen Lithography

SCIENCE VOL 288 9 JUNE 2000

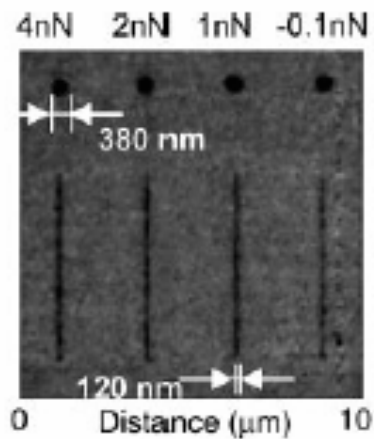
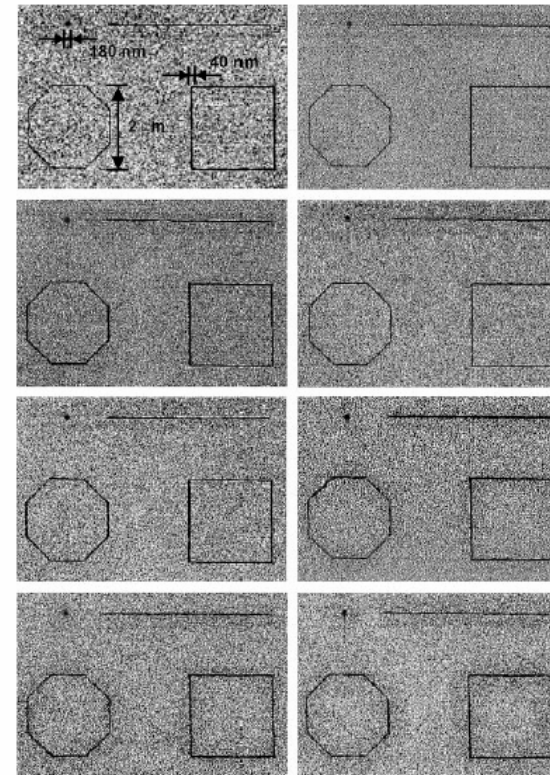


Fig. 1. Lateral force microscopy (LFM) images of ODT monolayer nanodot and line features on gold generated by the same tip but under different tip-substrate contact forces. Feature sizes vary less than 10%.

Fig. 4. LFM images of eight identical patterns generated with one imaging tip and eight writing tips coated with ODT molecules.



Protein Nanoarrays Generated By Dip-Pen Nanolithography

Ki-Bum Lee,¹ So-Jung Park,¹ Chad A. Mirkin,^{1*} Jennifer C. Smith,²
Milan Mrksich^{2*}

1 MARCH 2002 VOL 295 SCIENCE

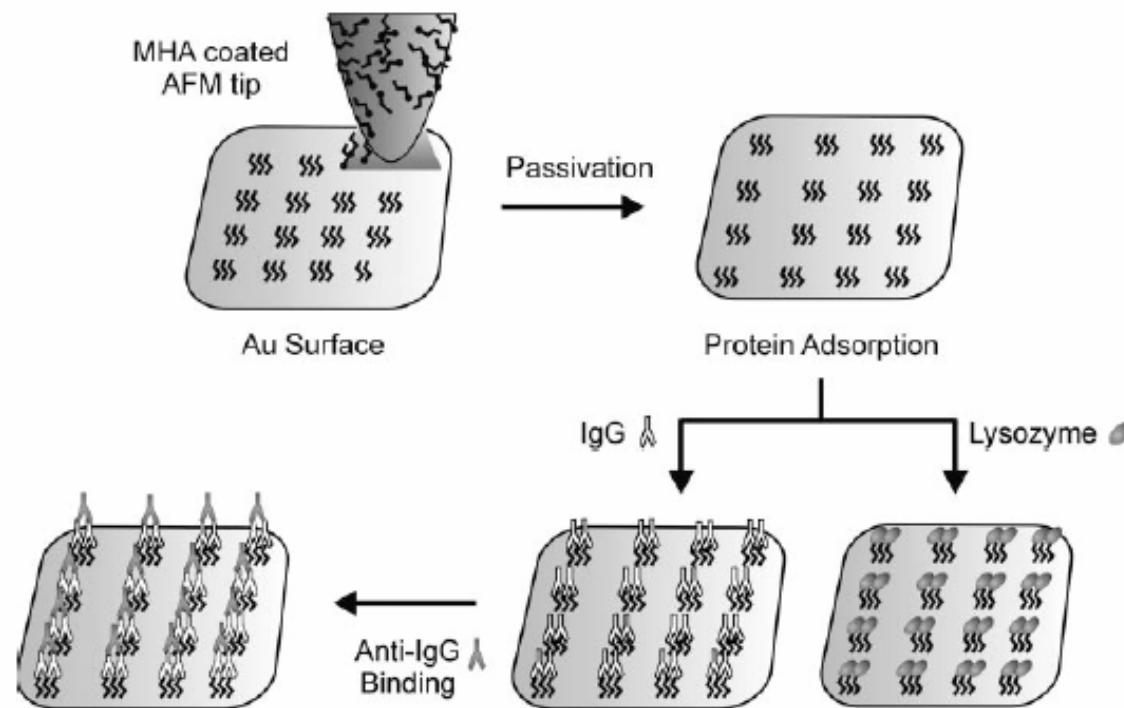
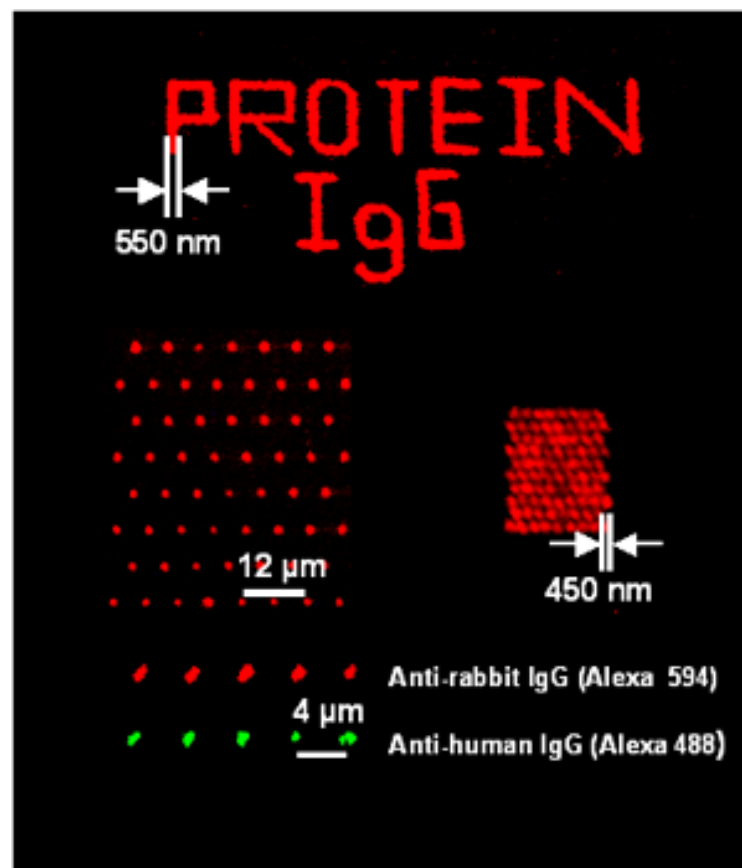


Fig. 2. Diagram of proof-of-concept experiments, in which proteins were absorbed on preformed MHA patterns. The resulting protein arrays were then characterized by AFM.



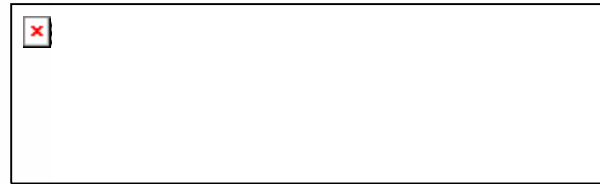
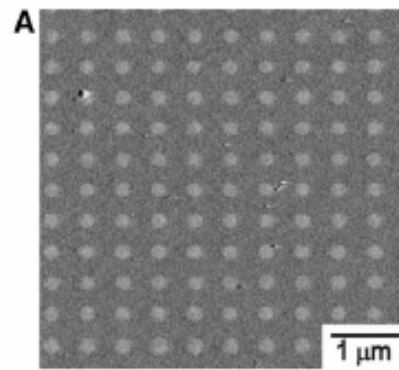
Protein Nanoarrays Generated By Dip-Pen Nanolithography

Ki-Bum Lee,¹ So-Jung Park,¹ Chad A. Mirkin,^{1*} Jennifer C. Smith,²
Milan Mrksich^{2*}

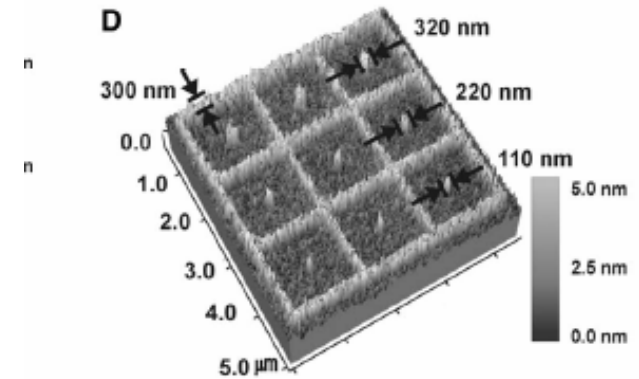
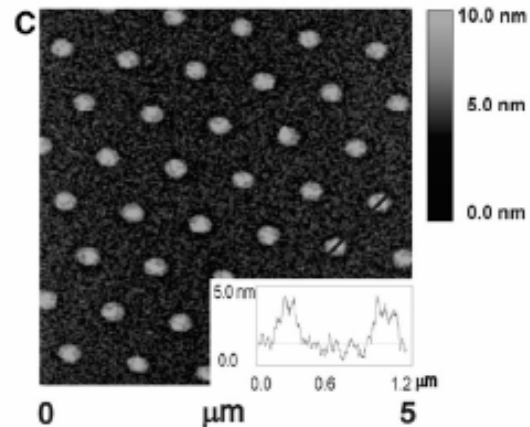
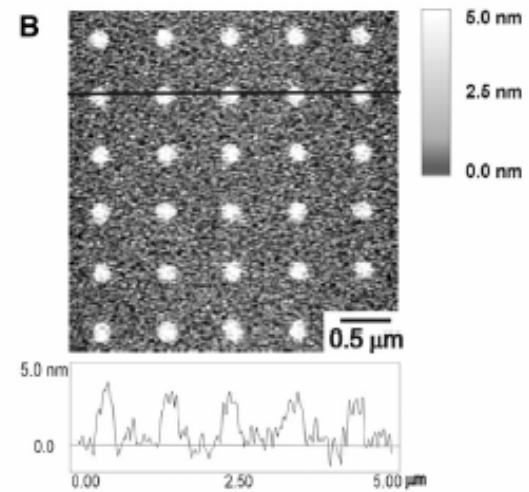


Protein Nanoarrays Generated By Dip-Pen Nanolithography

Ki-Bum Lee,¹ So-Jung Park,¹ Chad A. Mirkin,^{1*} Jennifer C. Smith,² Milan Mrksich^{2*}



5.



Protein Nanoarrays Generated By Dip-Pen Nanolithography

Ki-Bum Lee,¹ So-Jung Park,¹ Chad A. Mirkin,^{1*} Jennifer C. Smith,²
Milan Mrksich^{2*}

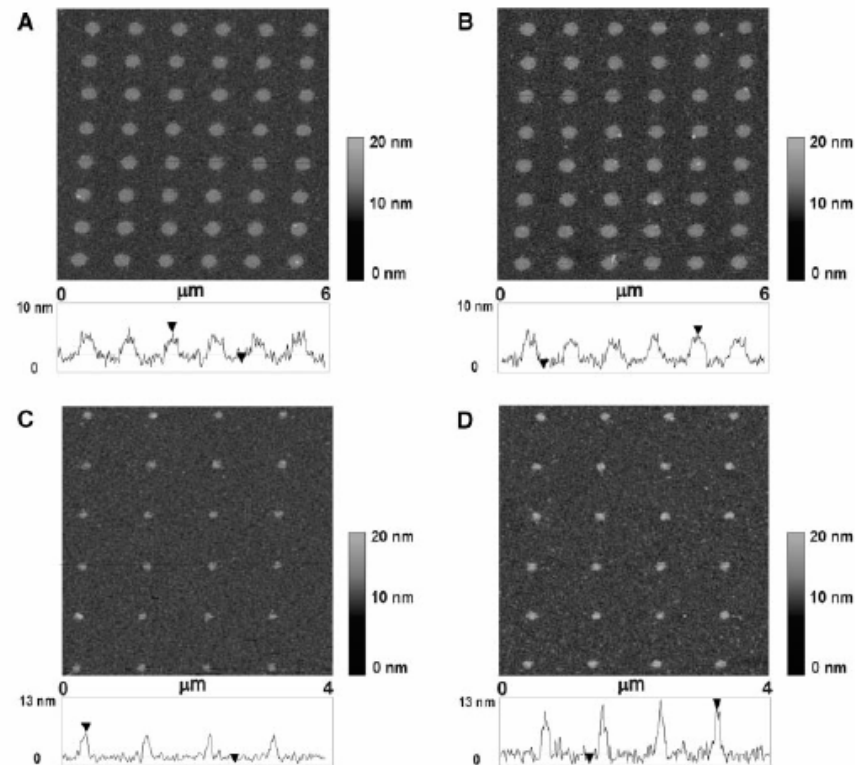


Fig. 3. AFM tapping mode image and height profile of rabbit IgG assembled onto an MHA dot array generated by DPN before (A) and after (B) exposure to a solution containing lysozyme, Retronectin, goat/sheep anti-IgG, and human anti-IgG. An IgG nanoarray before (C) and after (D) treatment with a solution containing lysozyme, goat/sheep anti-IgG, human anti-IgG, and rabbit anti-IgG. All images were taken at a 0.5-Hz scan rate in tapping mode.



Protein Nanoarrays Generated By Dip-Pen Nanolithography

Ki-Bum Lee,¹ So-Jung Park,¹ Chad A. Mirkin,^{1*} Jennifer C. Smith,² Milan Mrksich^{2*}

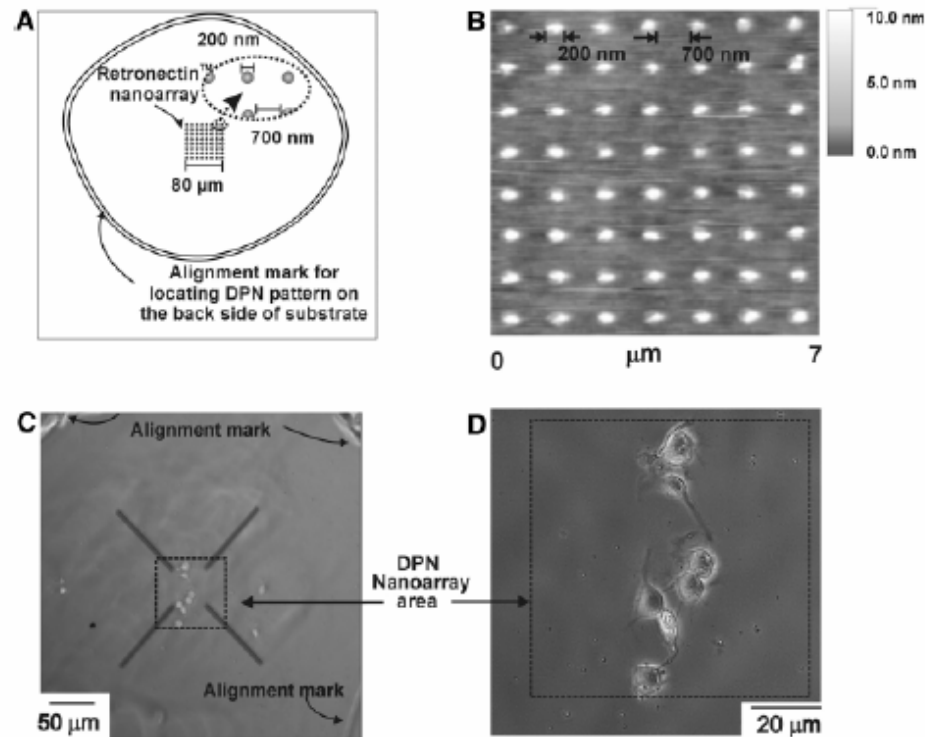


Fig. 4. (A) Diagram describing the cell adhesion experiment on the DPN-generated pattern. The total patterned area is 6400 μm². The alignment marks were generated by scratching a circle into the backside of the Au-coated glass substrate. (B) Topography image (contact mode) of the Retronectin protein array. Imaging conditions were the same as in Fig. 1B. (C) Large-scale optical microscope image showing the localization of cells in the nanopatterned area. (D) Higher resolution optical image of the nanopatterned area, showing intact cells.



Dip-Pen Array

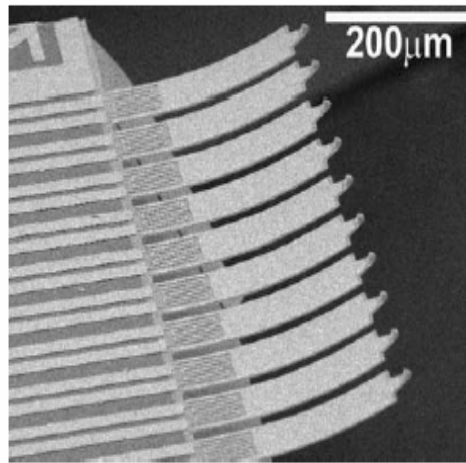


FIG. 2. An array of ten thermally actuated DPN probes showing the power lead and heater layout. Each probe is 300 μm long, 80 μm wide, and 1.3 μm thick.

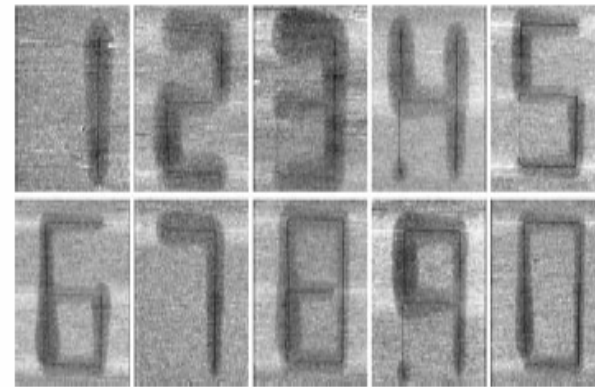
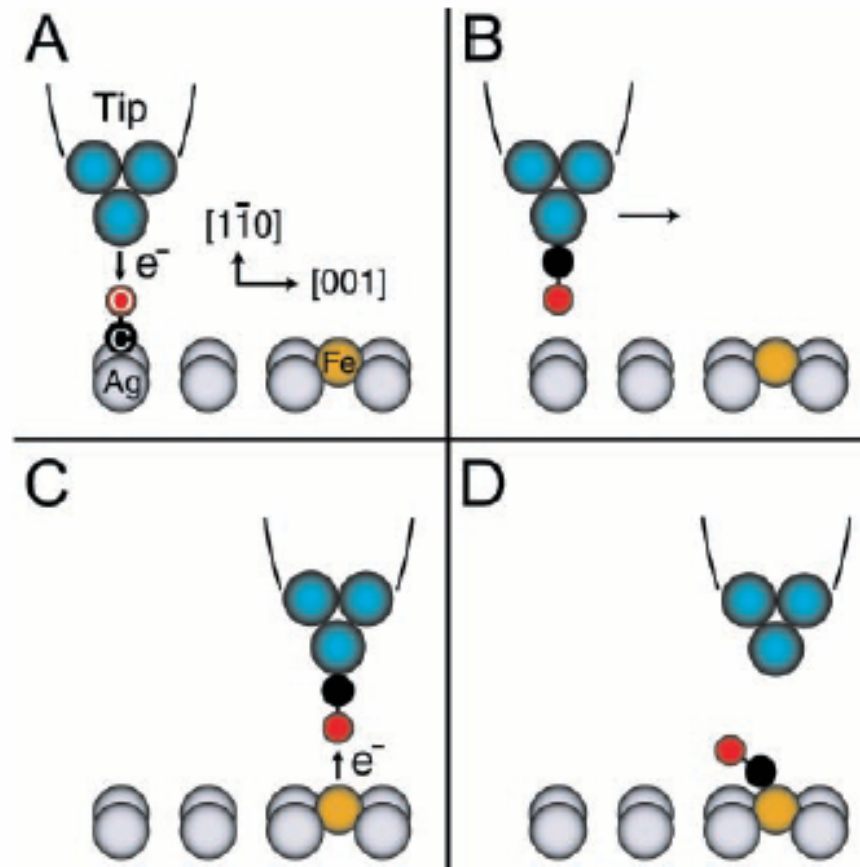


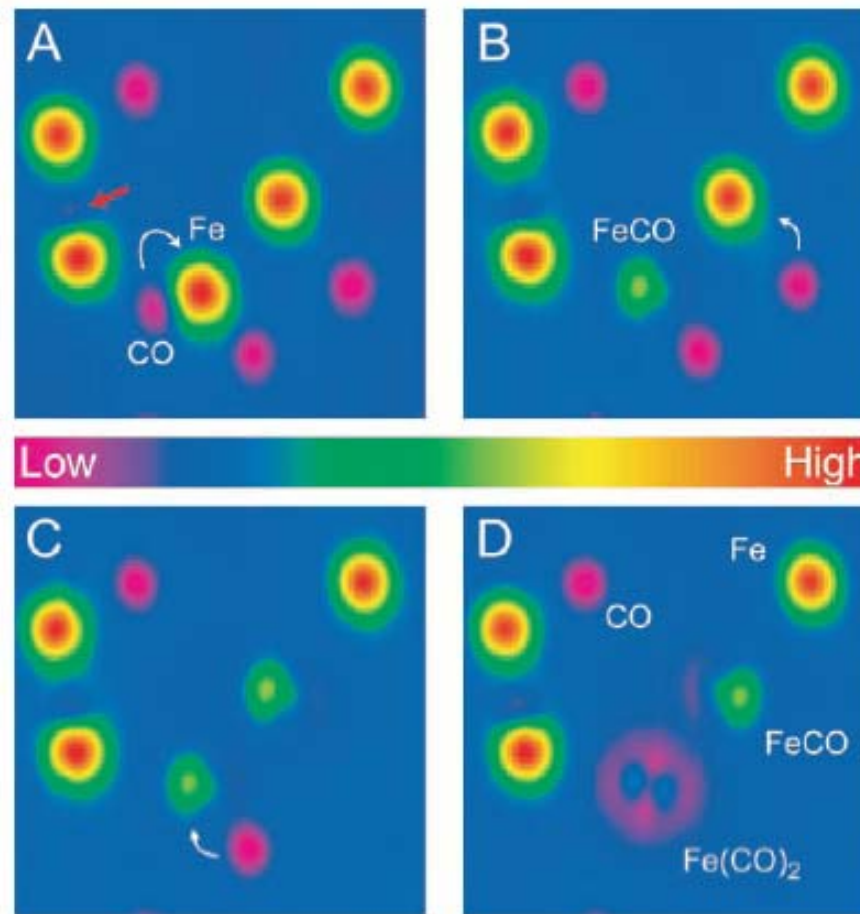
FIG. 4. LFM scans, 8 μm square, of ten simultaneously generated ODT patterns on a gold surface. Each numeral is 6 μm tall, 4 μm wide, and was written at 1 $\mu\text{m}/\text{s}$.



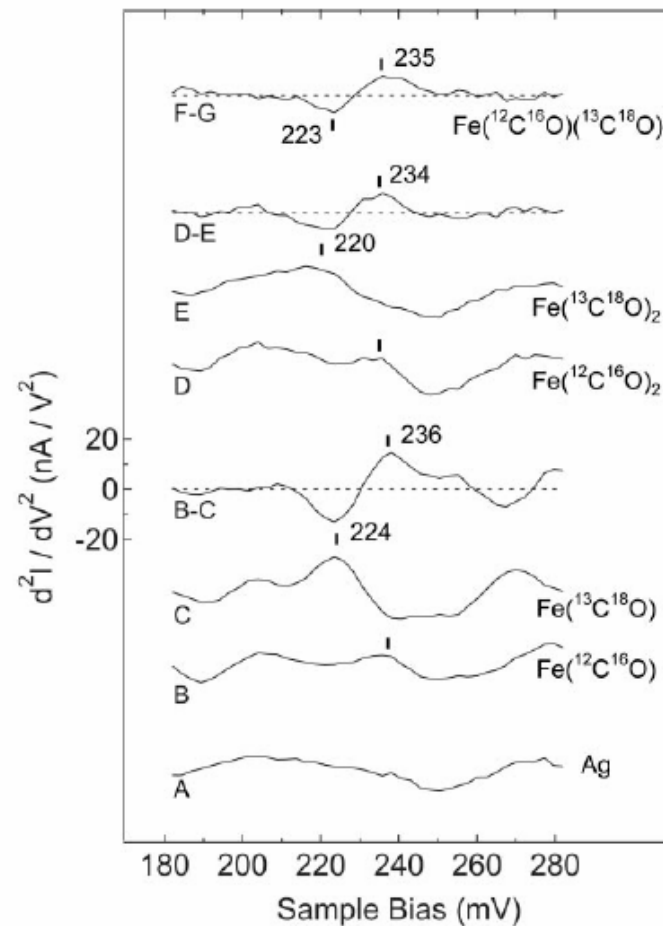
Ultimate STM Lithography



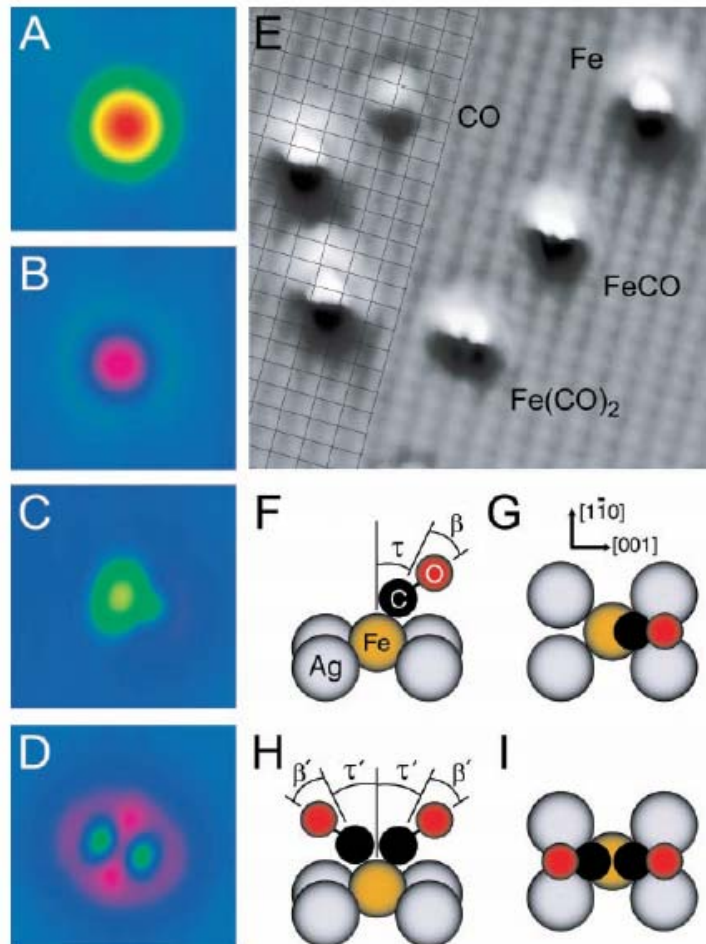
Single Atomic Manipulation



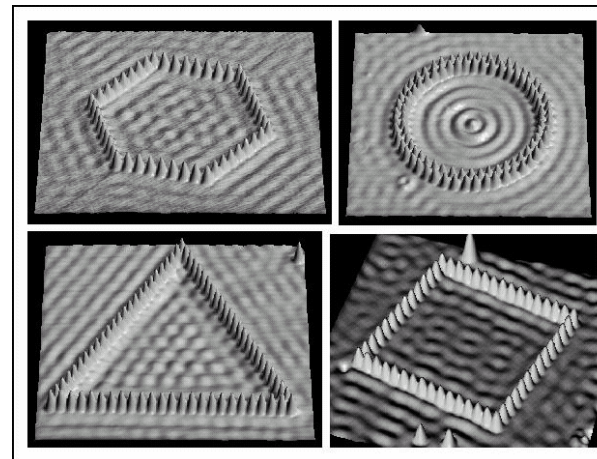
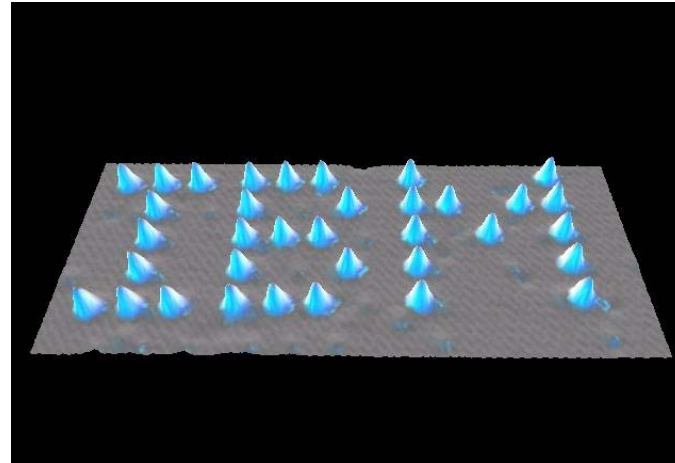
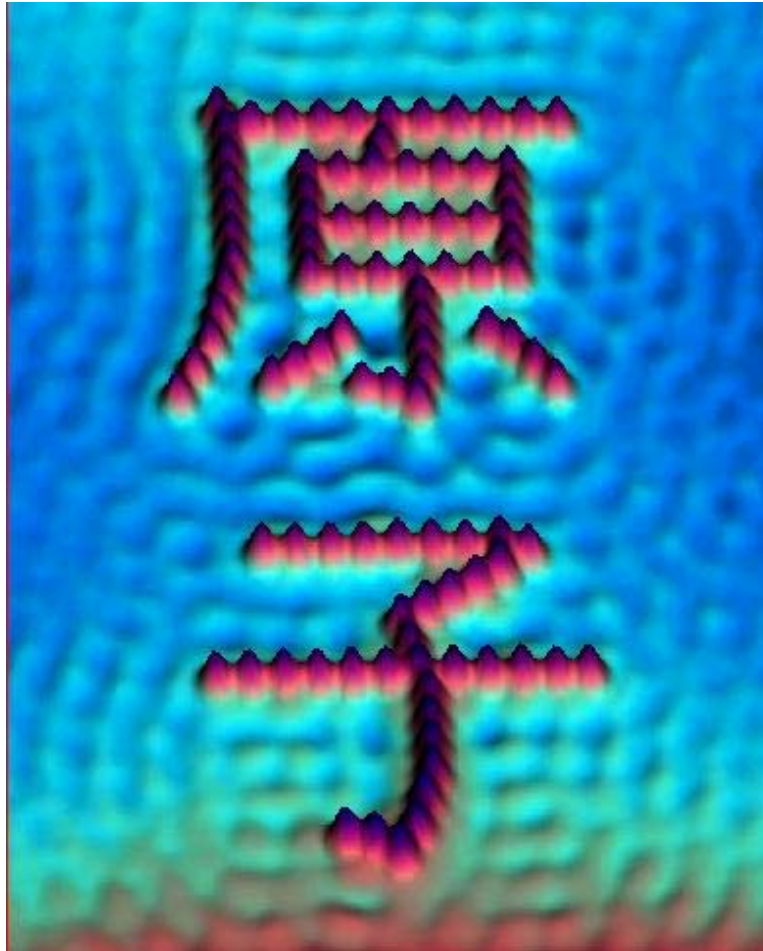
Single Molecular Vibrational Spectra by STM



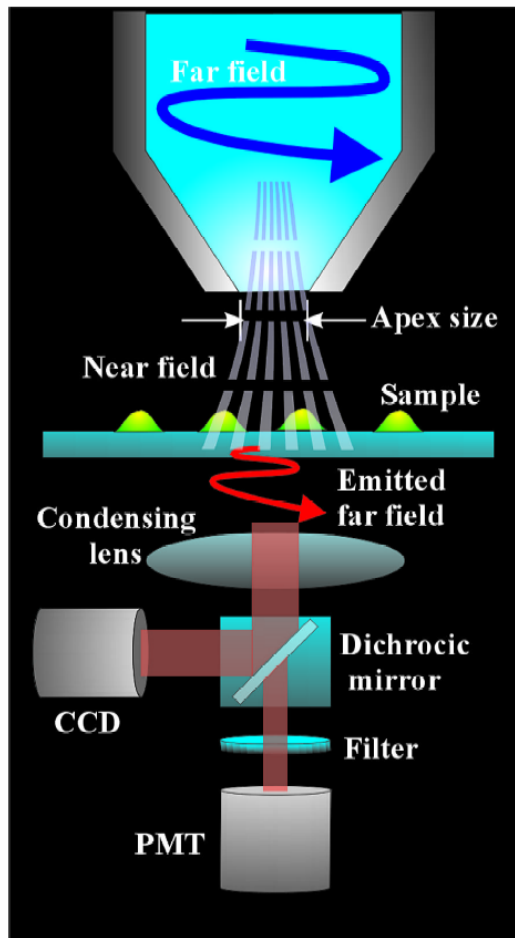
Building Molecule Step by Step



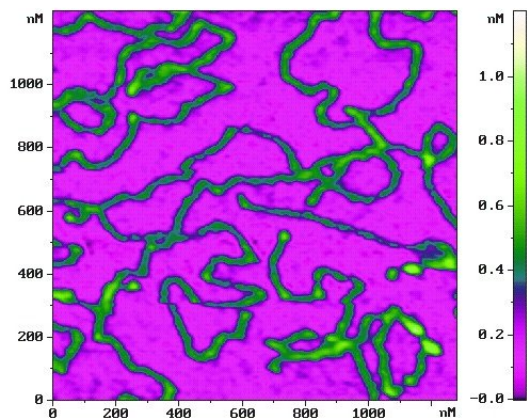
Atomic Manipulation



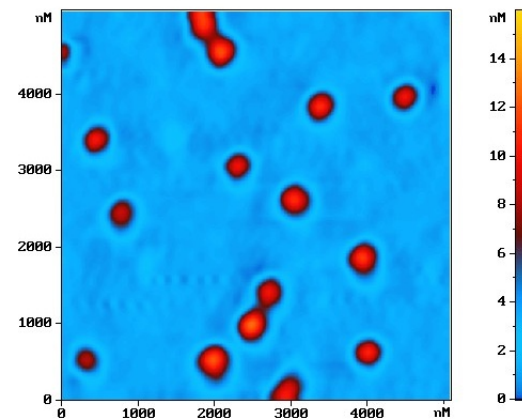
Near-Field Microscope



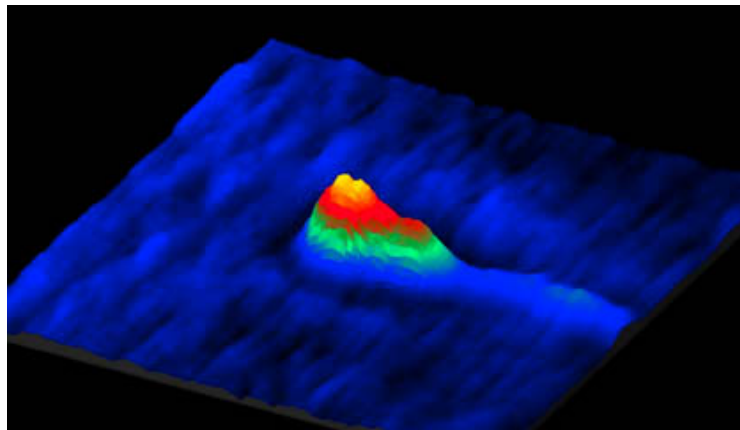
Near-Field Images



DNA



Nanosphere



Sperm



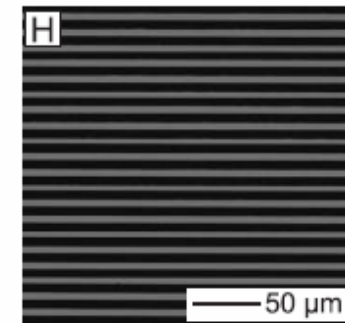
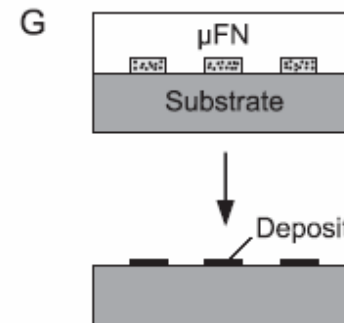
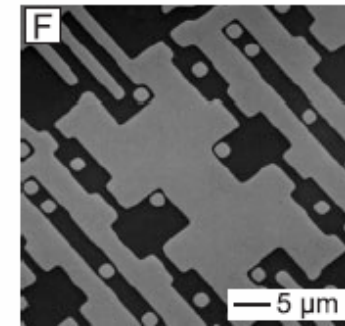
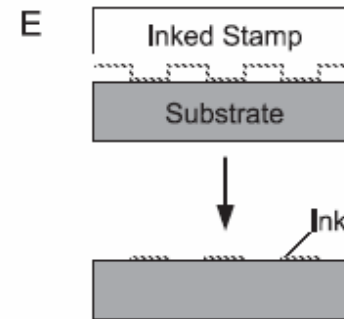
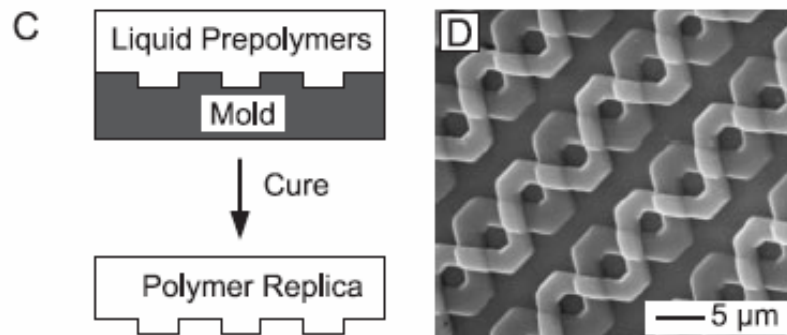
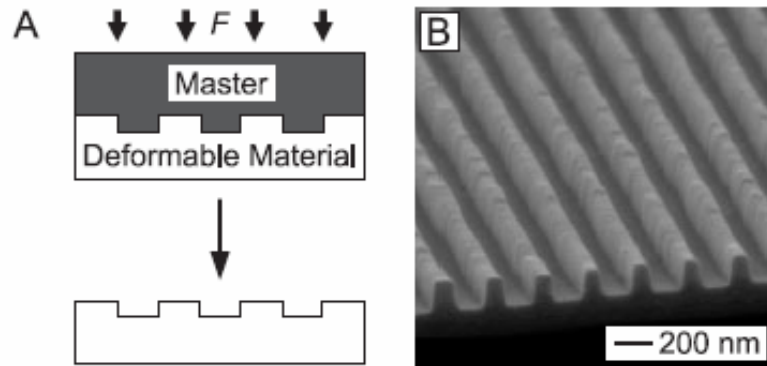
Near-Field Lithography



Figure 2. TappingMode image of a lithography test pattern. The Aurora-3 used nanolithography software to write into S1805 photoresist. 25 μ m scan.

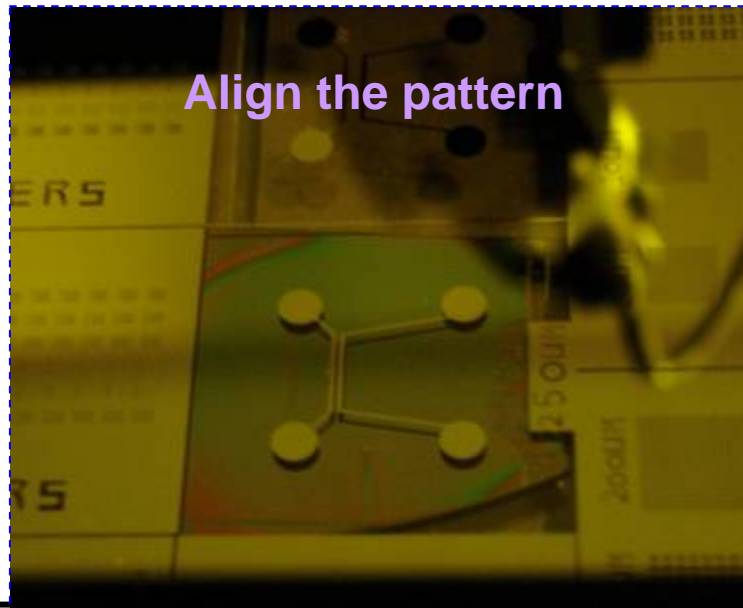
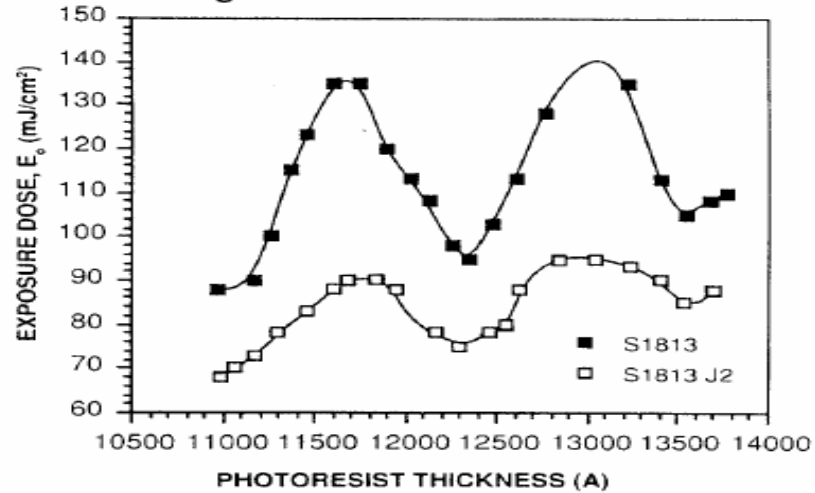


Replication

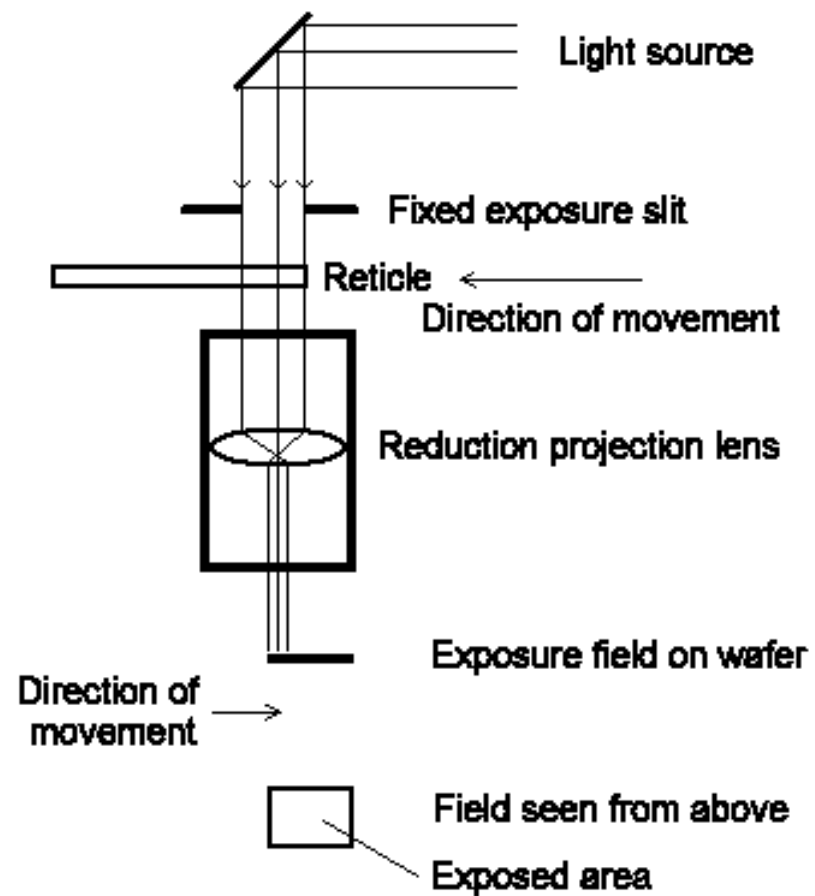
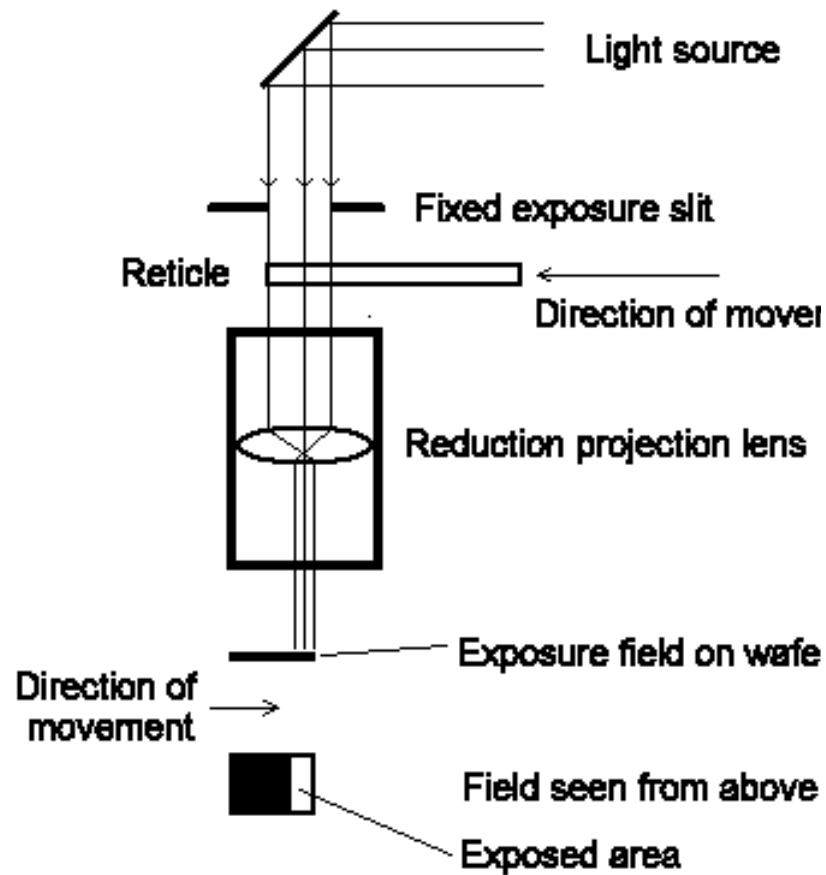


Align the pattern and Exposure

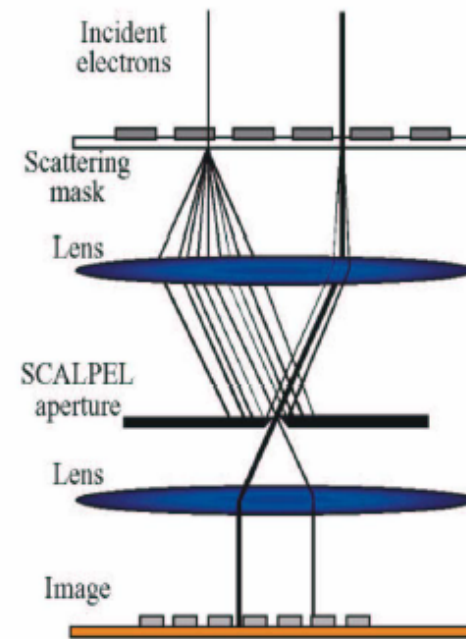
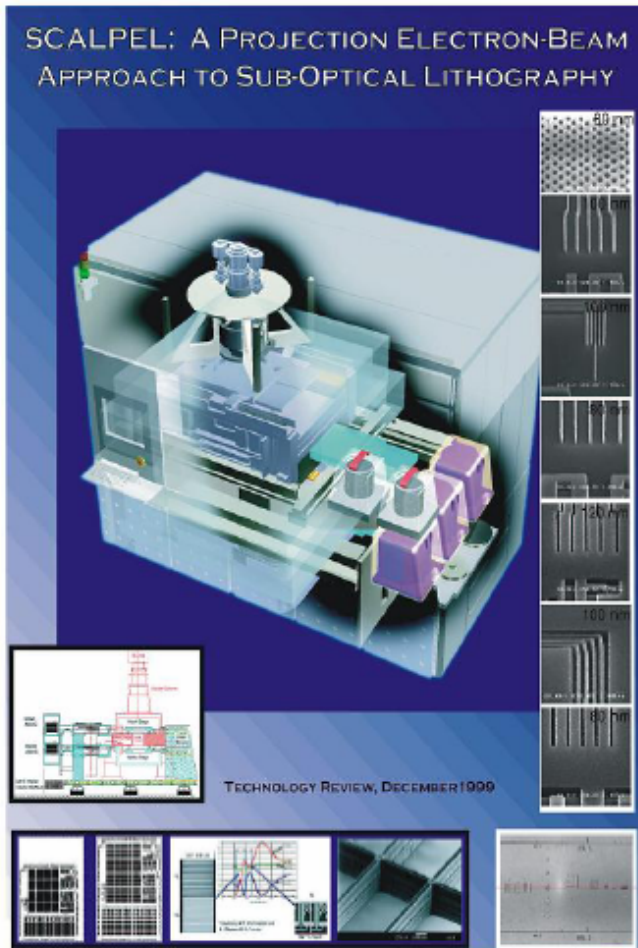
MICROPOSIT S1813 and S1813 J2 PHOTO RESISTS
Figure 4. Interference Curves



Stepper



E-beam Projection



Bell Lab (1999)
There 'was' a consortium including Applied Materials, Inc. and ASM Lithography Holding N.V.; Lucent Technologies Inc.; Motorola, Semiconductor Products Sector; Samsung Electronics Co., Ltd.; and Texas Instruments Incorporated (TI).



Imprint Lithography with 25-Nanometer Resolution

Stephen Y. Chou; Peter R. Krauss; Preston J. Renstrom

Science, New Series, Volume 272, Issue 5258 (Apr. 5, 1996), 85-87.

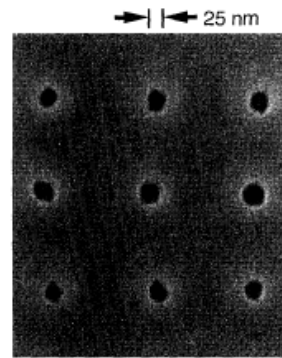


Fig. 2. SEM micrograph of a top view of holes 25 nm in diameter with a period of 120 nm, formed by compression molding into a PMMA film.

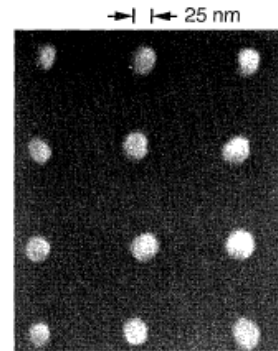


Fig. 5. SEM micrograph of the substrate in Fig. 2, after deposition of metal and a lift-off process. The diameter of the metal dots is 25 nm, the same as that of the original holes created in the PMMA.

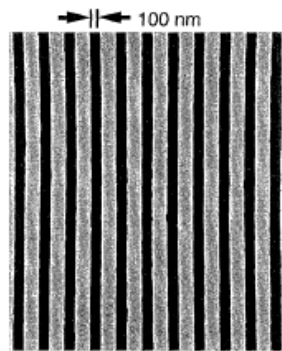


Fig. 3. SEM micrograph of a top view of trenches 100 nm wide with a period of 250 nm, formed by compression molding into a PMMA film.

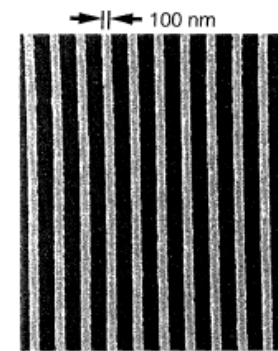
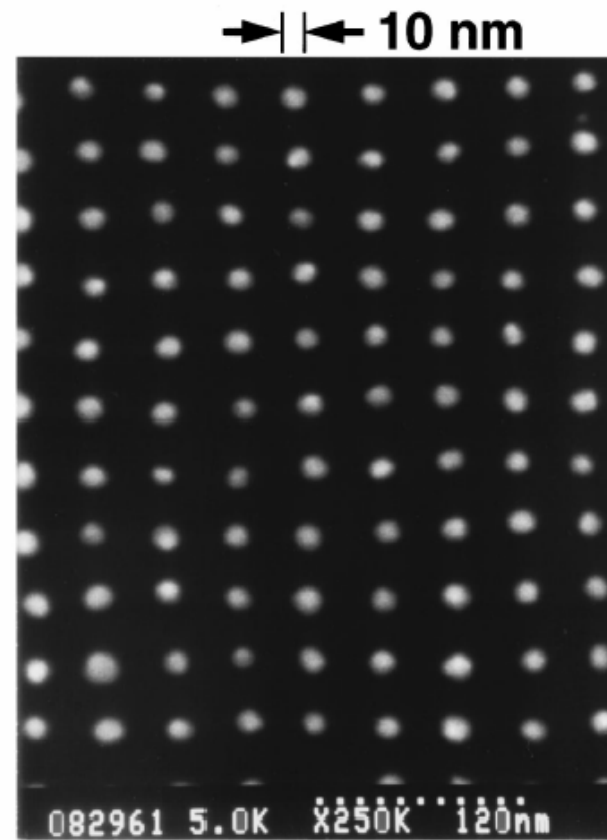
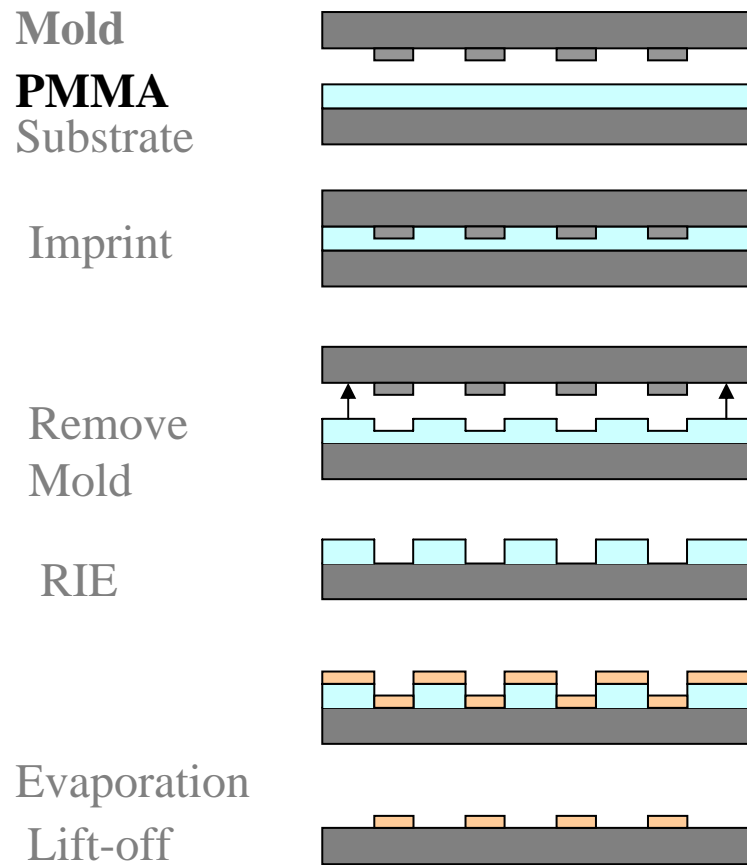


Fig. 6. SEM micrograph of the substrate in Fig. 3, after deposition of metal and a lift-off process. The metal linewidth is 100 nm, the same as the width of the original PMMA trenches.



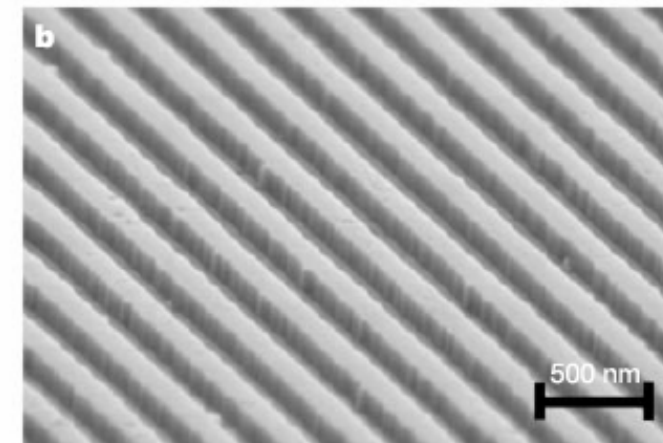
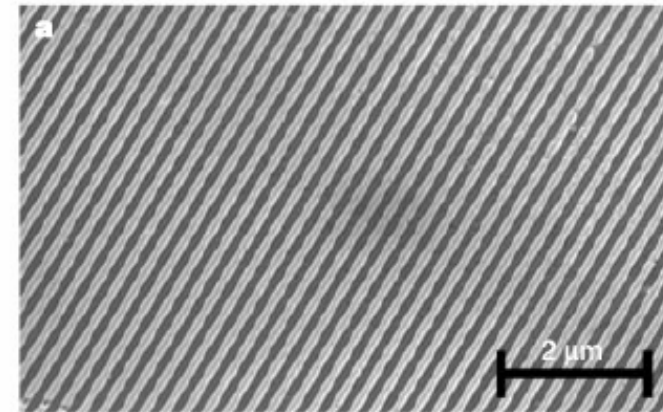
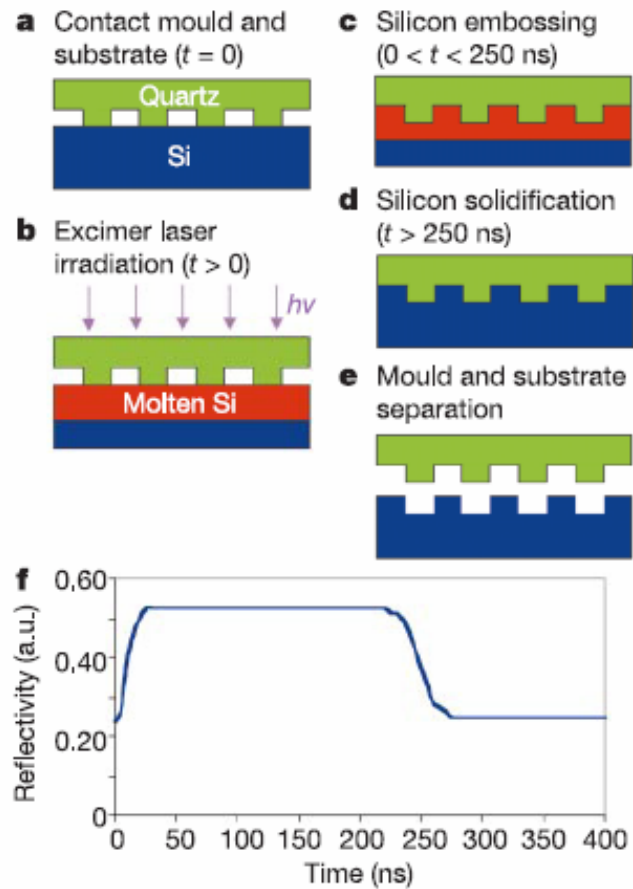
Nanoimprint Lithography



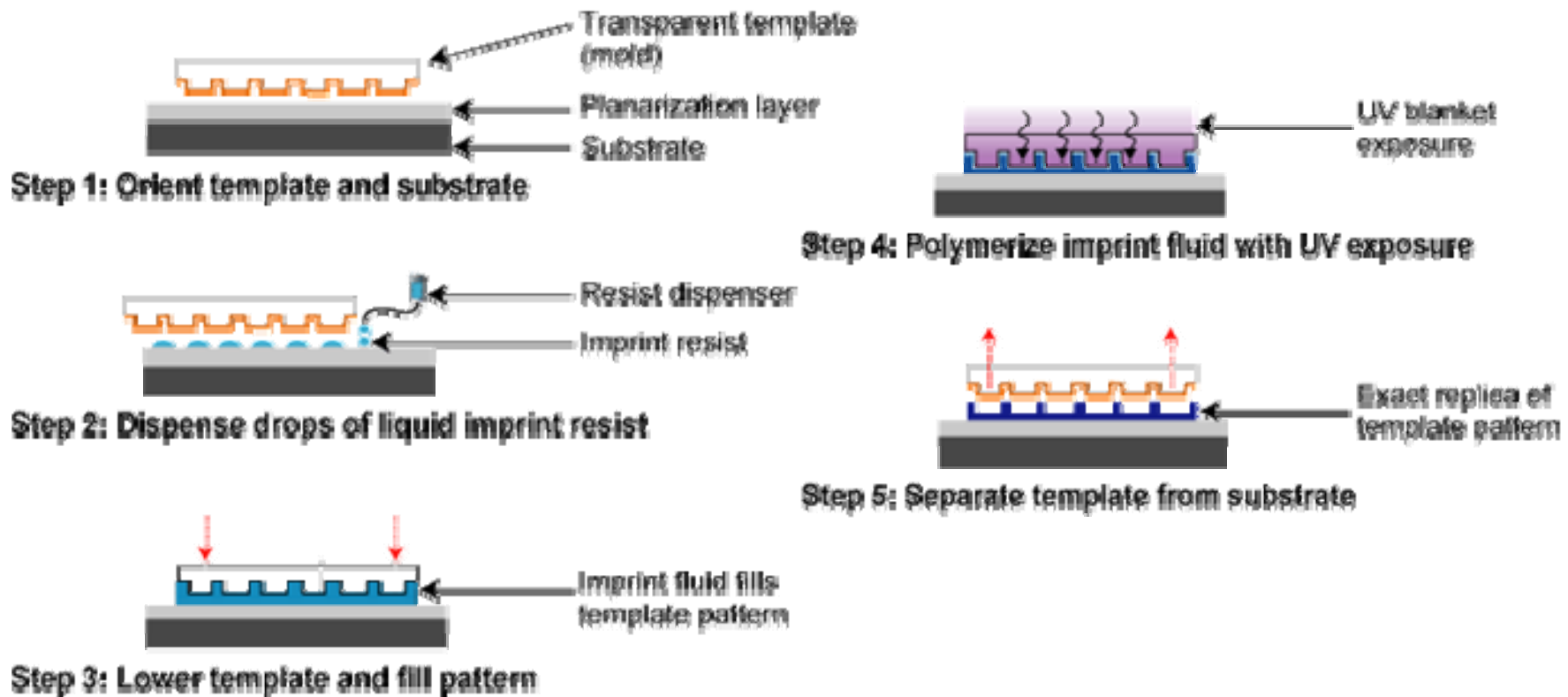
Ultrafast and direct imprint of nanostructures in silicon

NATURE | VOL 417 | 20 JUNE 2002 |

Stephen Y. Chou*, Chris Keimel & Jian Gu



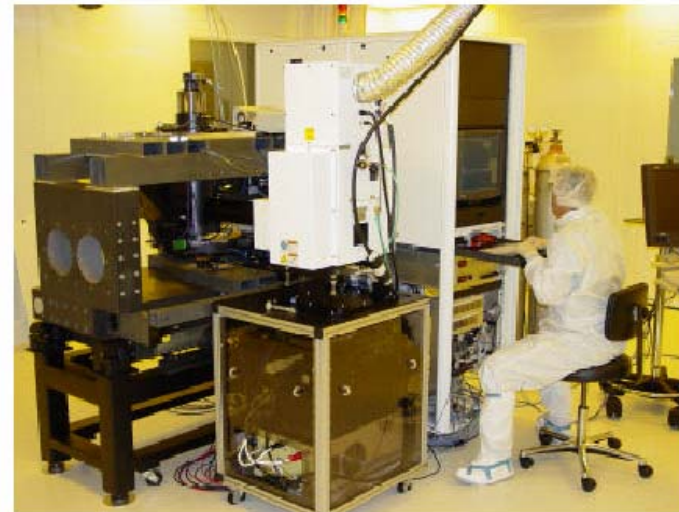
Step and Flash Imprint Lithography



Nanoimprintors



NX-2000, Nanoimprinter, Nanonex



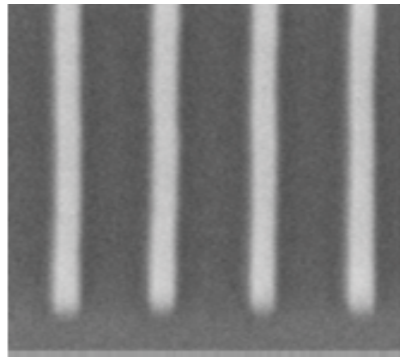

IMPRIO
100



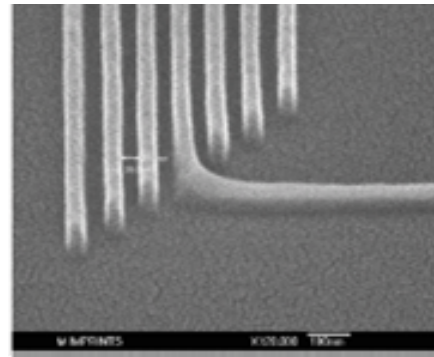
- Resolution: Sub-50 nanometers, imprint template (mold) limited.
- Alignment: < 500 nm, 3σ (X, Y, and Rotation).
- Flexibility: Handles up to 8 inch wafers, including fragile substrates.
- Field size: 25 x 25 mm full active print area, 100 μ m street width.



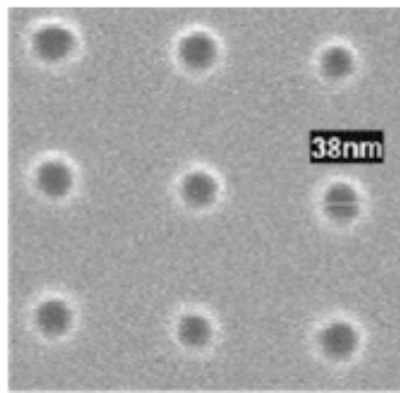
Imprinting Result



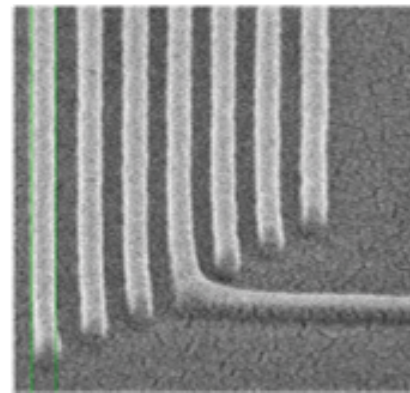
Imprinted 20 nm isolated lines



Imprinted 30 nm dense lines



Imprinted sub-40 nm contacts



Imprinted 50 nm dense lines

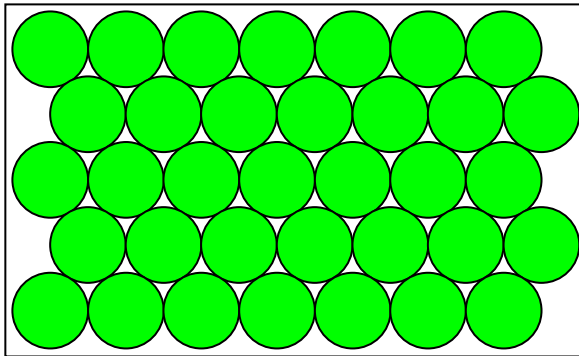


Challenges

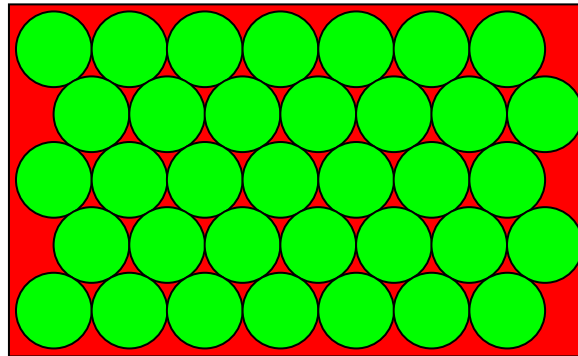
- Mask Fabrication (1:1)
- Lift-off process
- Resist
- Mask Design



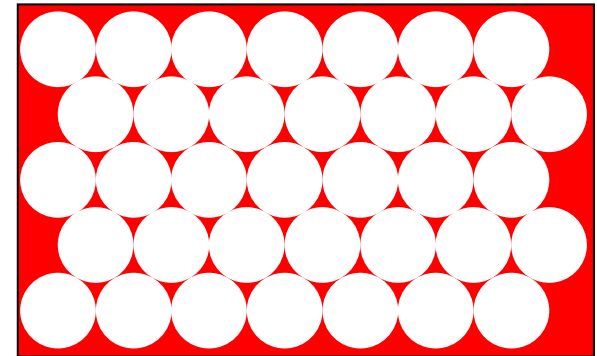
Nanosphere Lithography



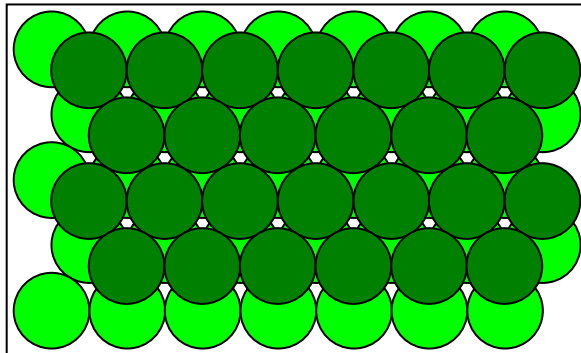
Single layer →



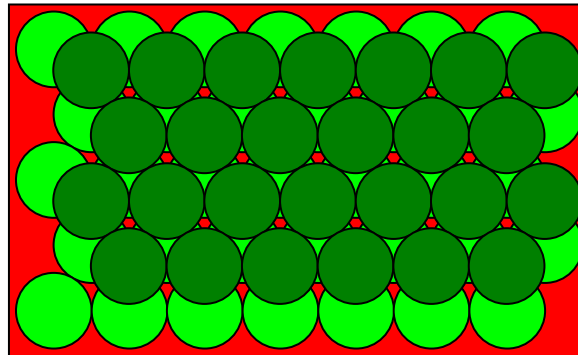
Metal deposition →



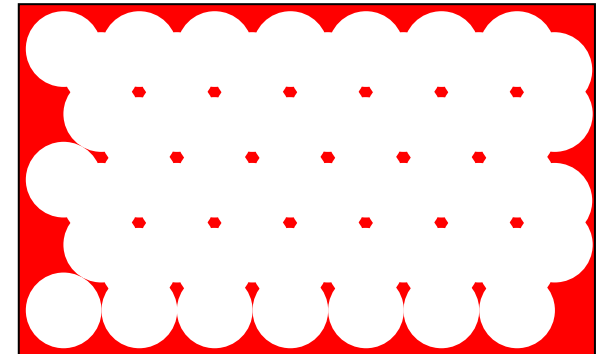
Lift-off



Double layer



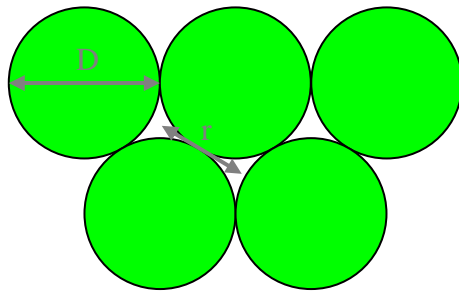
Metal deposition



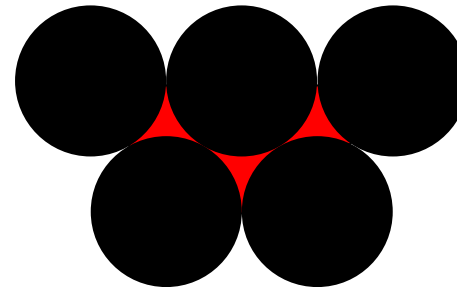
Lift-off



Array Dimension

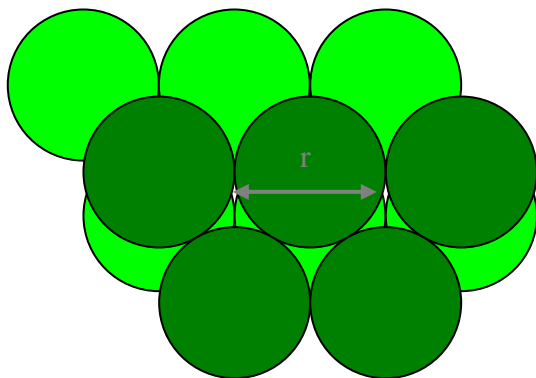


$$r = \frac{1}{\sqrt{3}} D$$

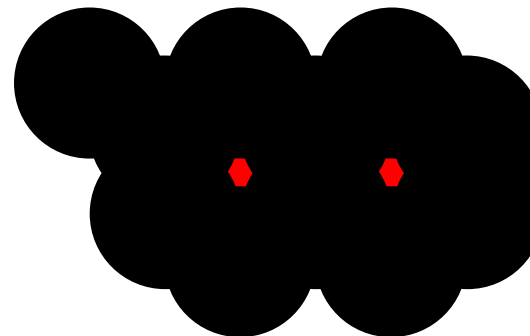


$$a = \frac{3}{2} \left(\sqrt{3} - 1 - \frac{1}{\sqrt{3}} \right) D$$

$$\sim 1/4 D$$



$$r = D$$



$$a = \left(\sqrt{3} - 1 - \frac{1}{\sqrt{3}} \right) D$$

$$\sim 1/7 D$$



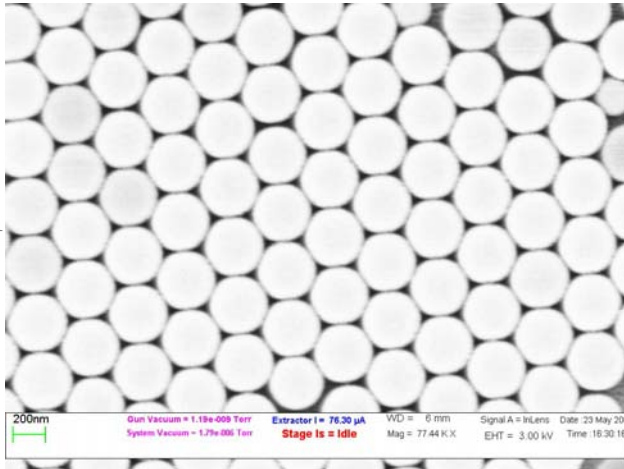
Optical Image of PS Template

800 nm PS

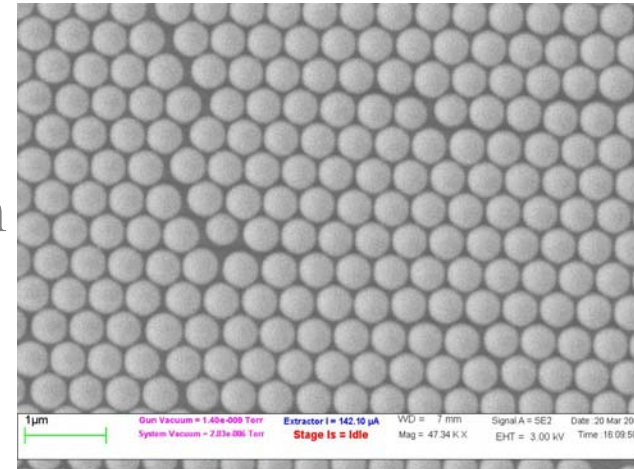


Nanosphere Lithography

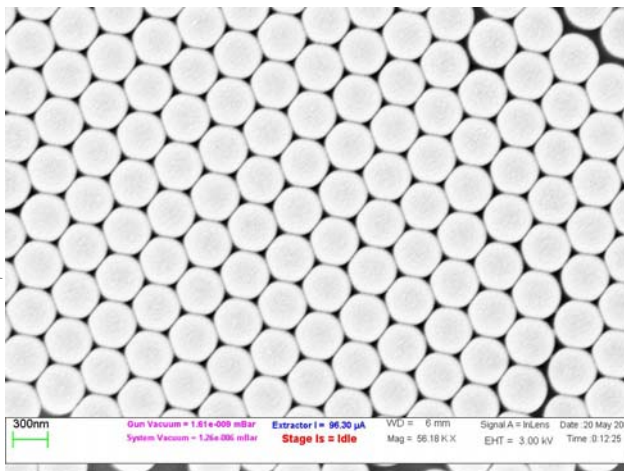
350 nm



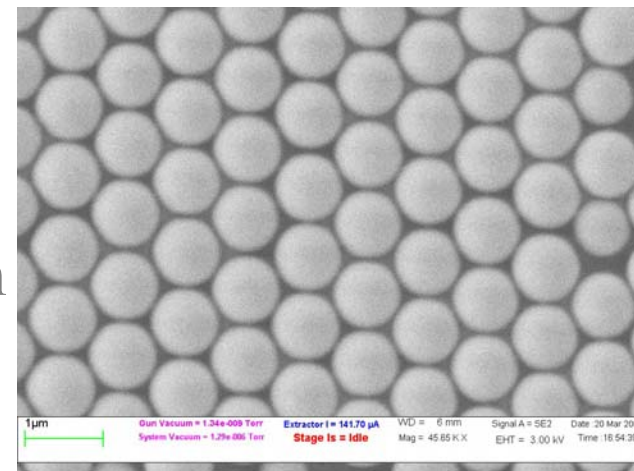
550 nm



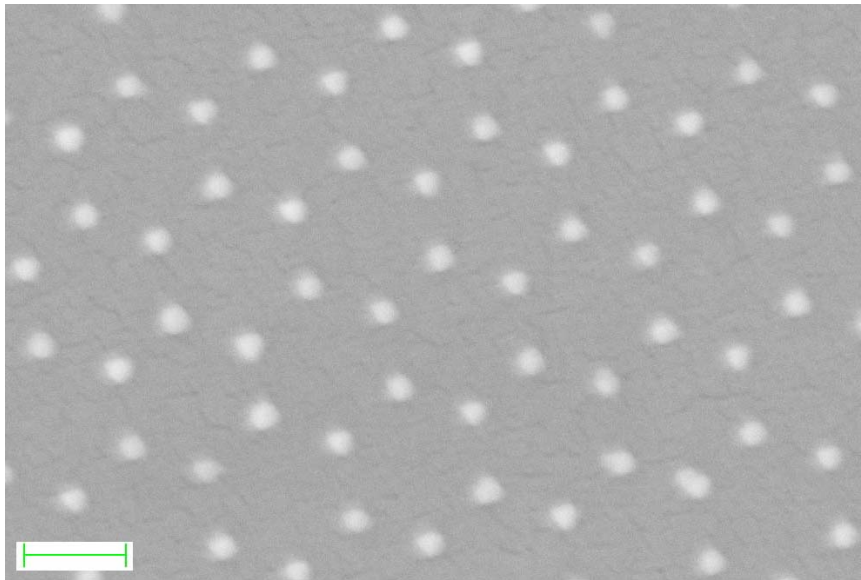
400 nm



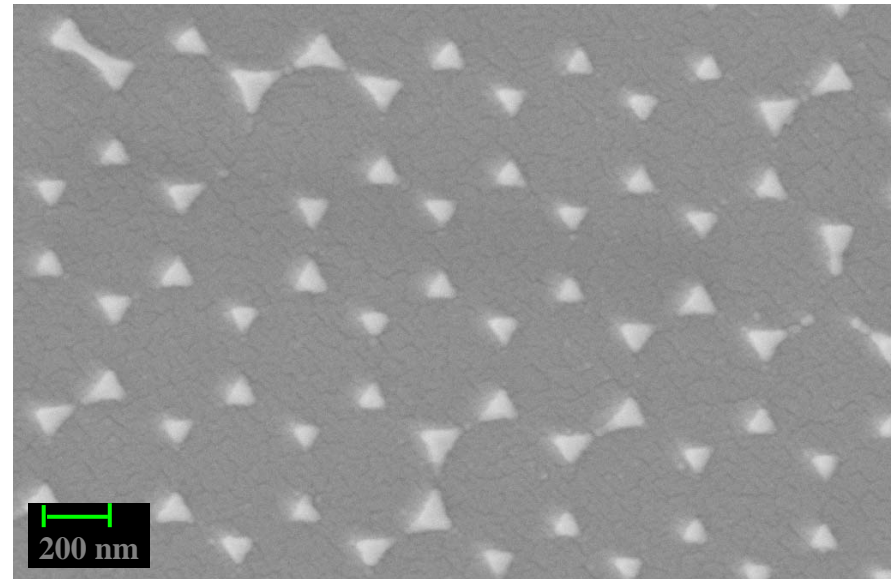
880 nm



Single Layer Templates



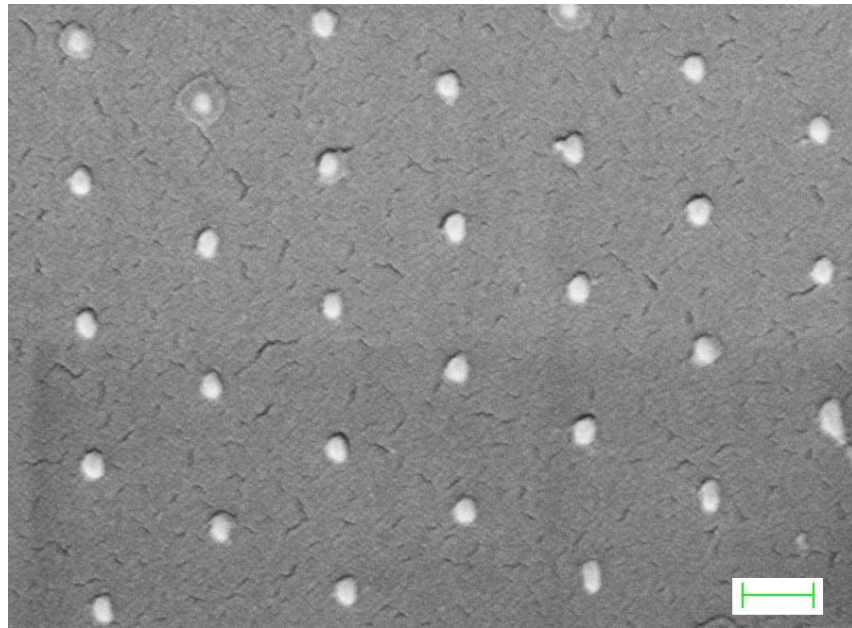
280 nm



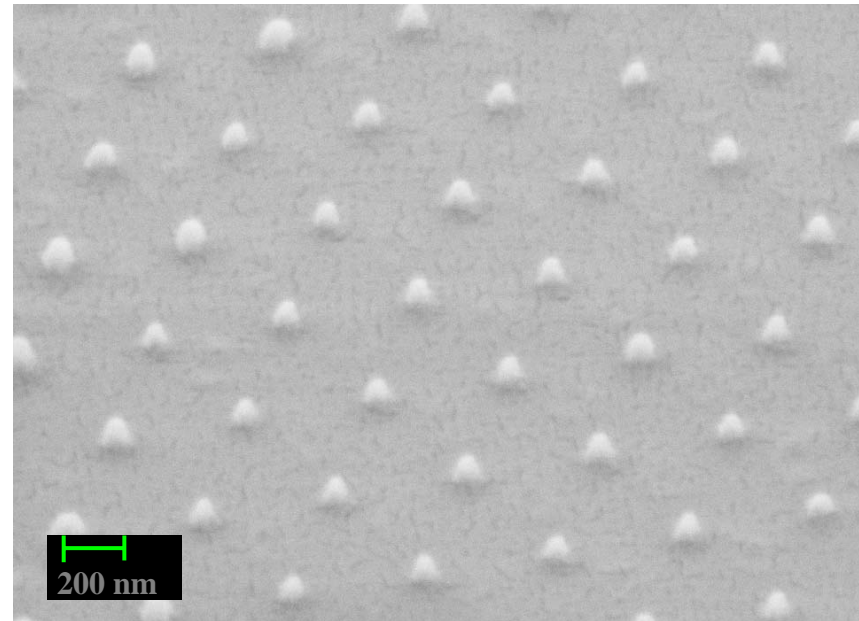
550 nm



Double Layer Templates



400 nm

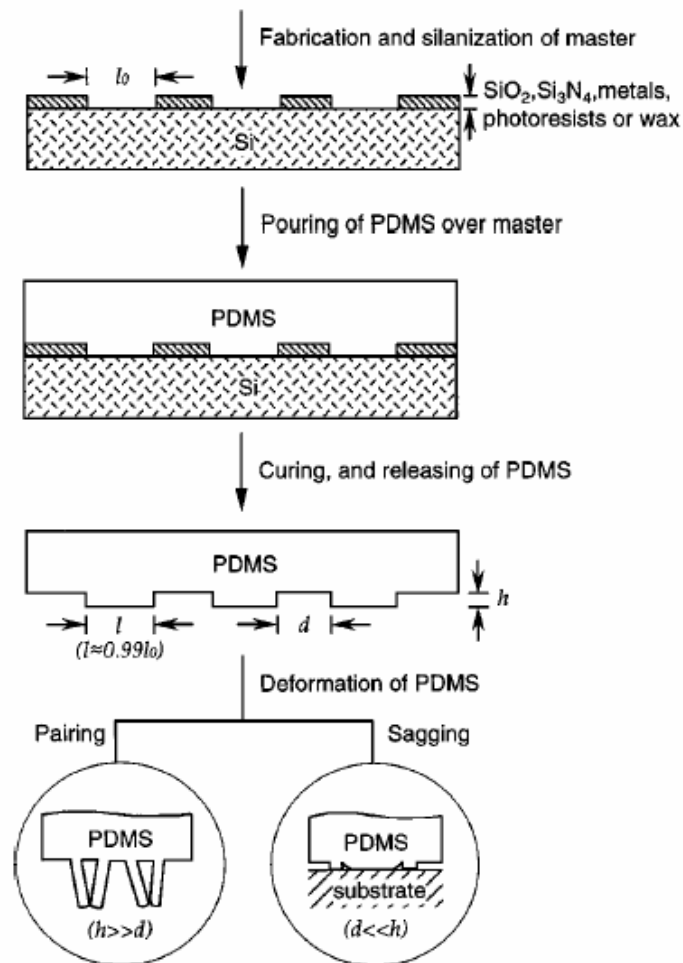


550 nm



Soft Lithography

Annu. Rev. Mater. Sci. 1998. 28:153-84



Soft Lithography

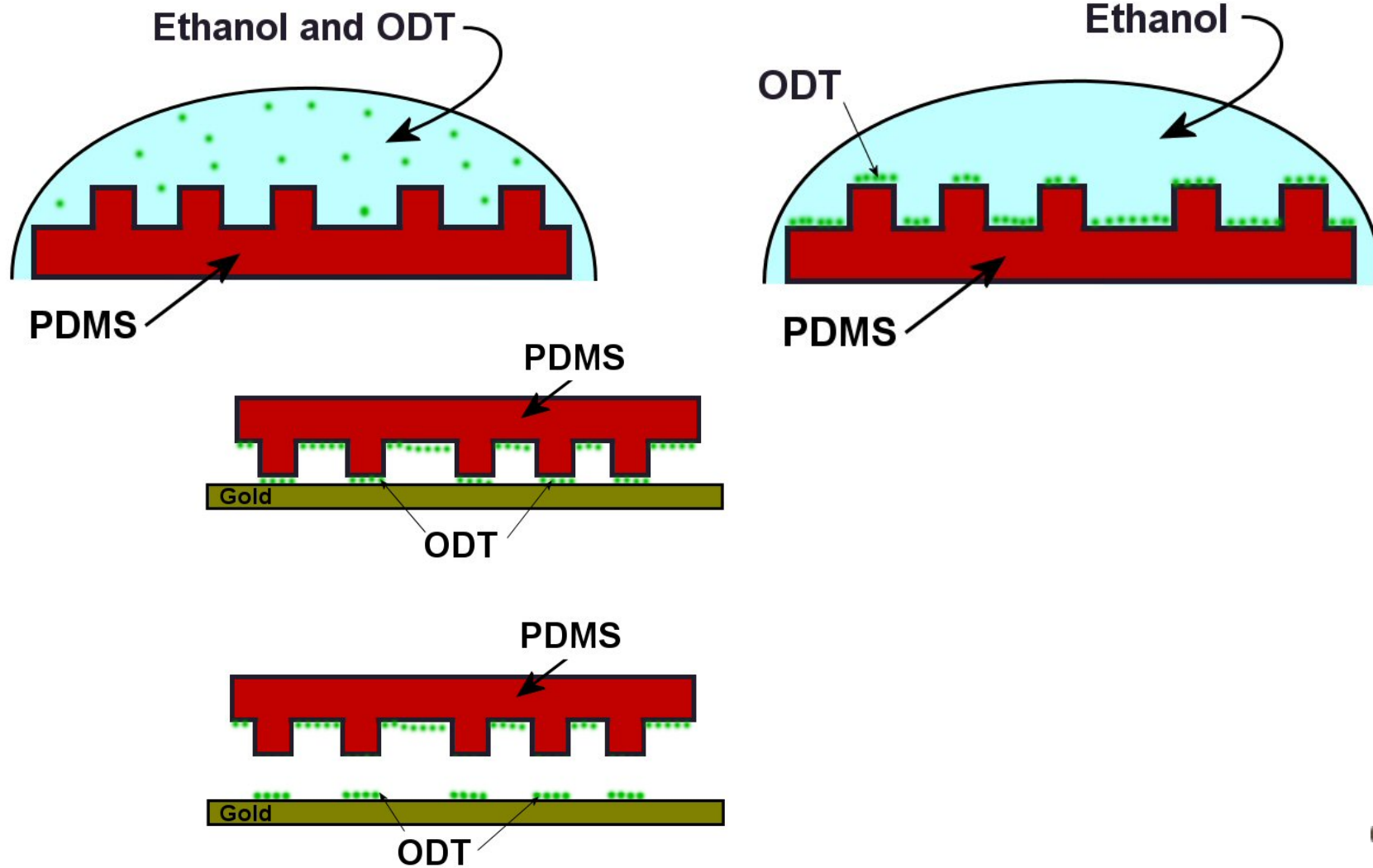


Table 1 Comparison between photolithography and soft lithography

	Photolithography	Soft lithography
Definition of patterns	Rigid photomask (patterned Cr supported on a quartz plate)	Elastomeric stamp or mold (a PDMS block patterned with relief features)
Materials that can be patterned directly	Photoresists (polymers with photo- sensitive additives) SAMs on Au and SiO ₂	Photoresists ^{a,e} SAMs on Au, Ag, Cu, GaAs, Al, Pd, and SiO ₂ ^a Unsensitized polymers ^{b-e} (epoxy, PU, PMMA, ABS, CA, PS, PE, PVC) Precursor polymers ^{c,d} (to carbons and ceramics) Polymer beads ^d Conducting polymers ^d Colloidal materials ^{a,d} Sol-gel materials ^{c,d} Organic and inorganic salts ^d Biological macromolecules ^d
Surfaces and structures that can be patterned	Planar surfaces 2-D structures	Both planar and nonplanar Both 2-D and 3-D structures
Current limits to resolution	~250 nm (projection) ~100 nm (laboratory)	~30 nm ^{a,b} , ~60 nm ^e , ~1 μm ^{d,e} (laboratory)
Minimum feature size	~100 nm (?)	10 (?) - 100 nm

^{a-e}Made by (a) μ CP, (b) REM, (c) μ TM, (d) MIMIC, (e) SAMIM. PU:polyurethane; PMMA: poly(methyl methacrylate); ABS: poly(acrylonitrile-butadiene-styrene); CA: cellulose acetate; PS: polystyrene; PE: polyethylene; and PVC: poly(vinyl chloride)



Micro-contact Printing

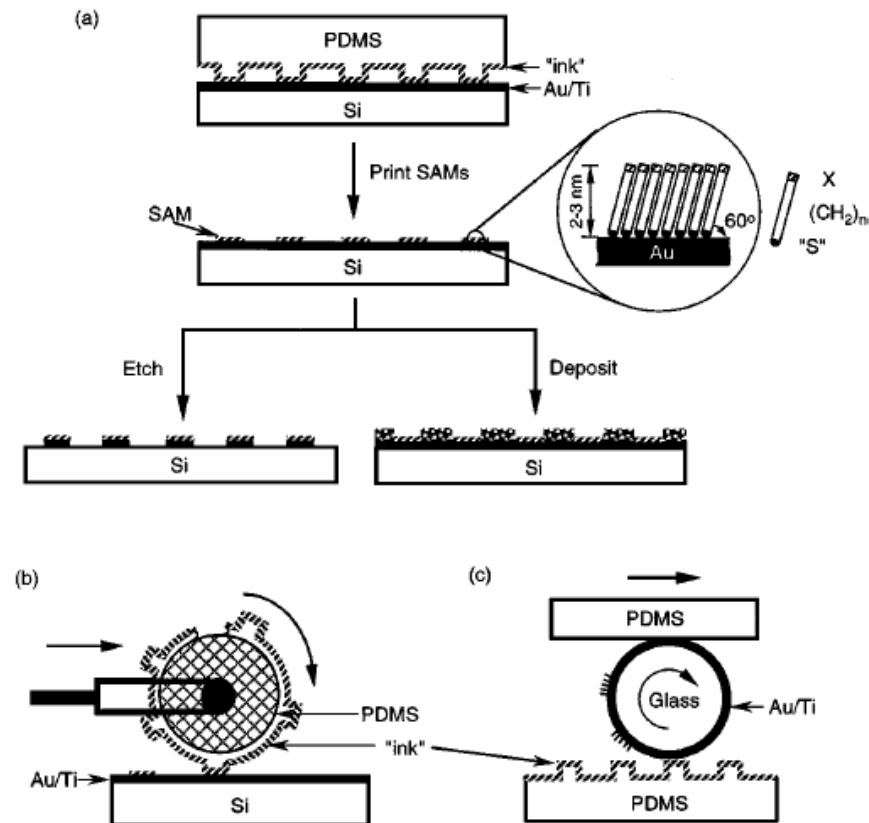


Figure 2 Schematic procedures for μ CP of hexadecanethiol (HDT) on the surface of gold: (a) printing on a planar surface with a planar stamp (21), (b) printing on a planar surface over large areas with a rolling stamp (128), and (c) printing on a nonplanar surface with a planar stamp (174).



Micro-contact Printing

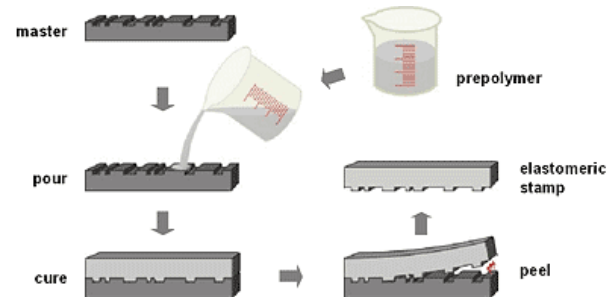


Fig.2 The stamp replication process: A master with a negative of the desired pattern is cast with a pre-polymer. After curing the polymer, the elastomeric stamp is peeled off the master and ready for microcontact printing.

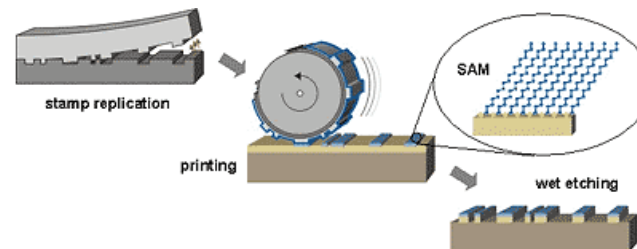
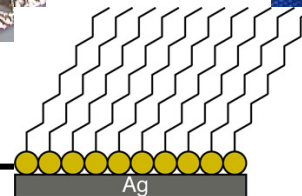
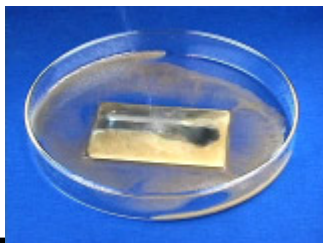
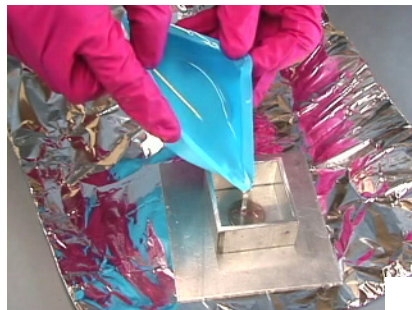
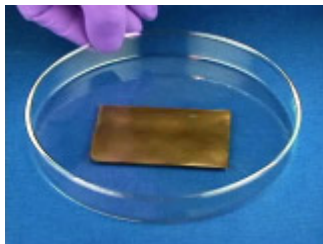
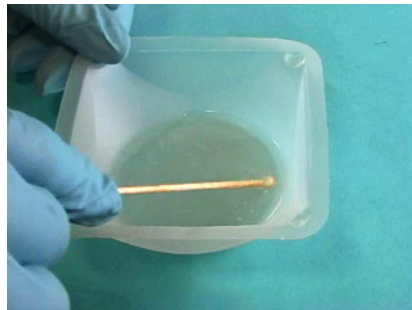
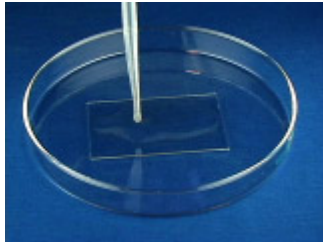


Fig.1 The microcontact printing (μ CP) process: An elastomeric stamp is replicated from a master. After inking of the stamp with a suitable ink, it is fixated on a printing machine with help of which it is brought into conformal contact with a substrate. There the ink forms a self-assembled monolayer (SAM) which can be used as a resist in a subsequent wet etching step.

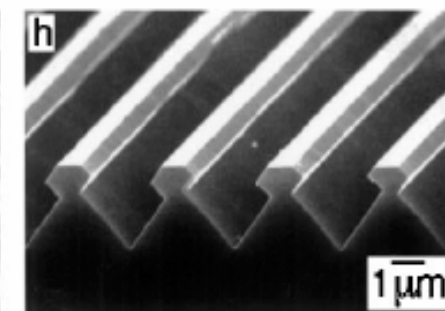
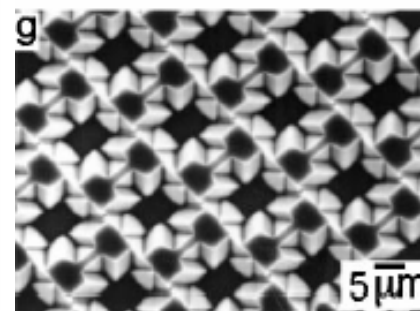
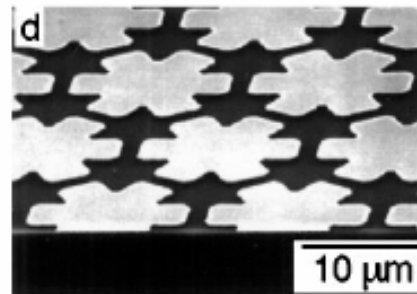
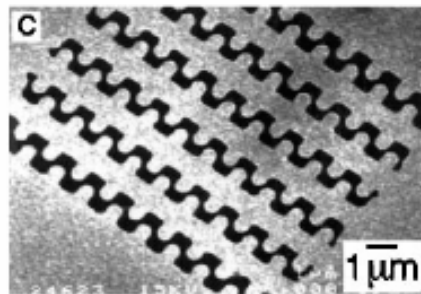
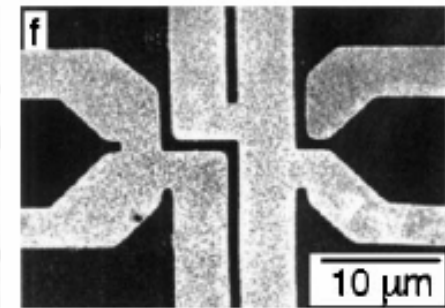
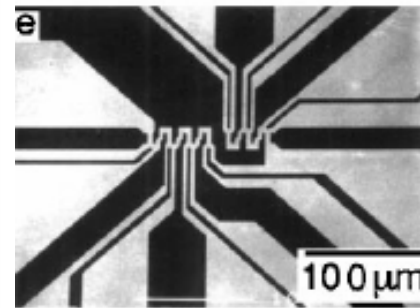
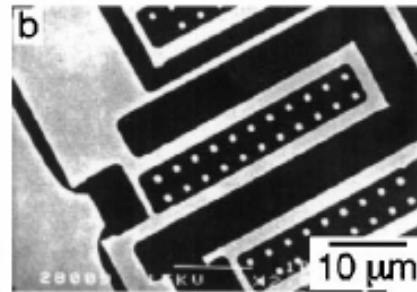
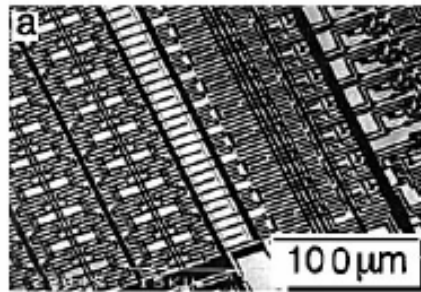


Micro-contact Printing

<http://mrsec.wisc.edu/Edetc/nanolab/print/text.html>



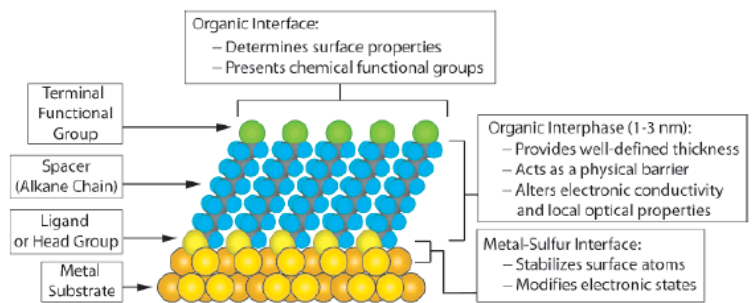
Micro-contact Printing



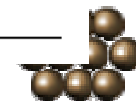
Self-Assemble Monolayer (SAM)

Chem. Rev. 2005, 105, 1103–1169

Ligand	Substrates	Morphology of Substrate		Ligand	Substrates	Morphology of Substrate		
		Thin Films or Bulk Material	Nanoparticles or Other Nanostructures			Thin Films or Bulk Material	Nanoparticles or Other Nanostructures	
ROH	Fe ₂ O ₃	36	35	RSSR'	Ag	89	90	
	Si-H	37			Au	20	90-92	
	Si				CdS		61	
RCOO-/RCOOH	α -Al ₂ O ₃	38,39			Pd	30		
	Fe ₂ O ₃		40		Au	93		
	Ni		41,42					
	Ti/TiO ₂	43						
RCOO-OOCR	Si(111):H	44		RCSsH	Au	94		
	Si(100):H				CdSe		95	
Ene-diol	Fe ₂ O ₃		45	RS ₂ O ₃ ⁻ Na ⁺	Au	96	98	
RNH ₂	FeS ₂	46			Cu	97		
	Mica	47		RSeH	Ag	99		
	Stainless Steel 316L	48			Au	100,101		
	YBa ₂ Cu ₃ O _{7-δ}	49			CdS		60	
	CdSe		50	CdSe		102		
RC \equiv N	Ag	51		RSeSeR'	Au	101		
	Au							
R-N=N'(BF ₄)	GaAs(100)	52		R ₃ P	Au		103	
	Pd	52			FeS ₂	46		
	Si(111):H	52			CdS		104	
RSH	Ag	26	53,54		CdSe		104	
	Ag ₉₀ Ni ₁₀	55			CdTe		104	
	AgS		56	R ₃ P=O	Co		105,106	
	Au	26	57		CdS		104	
	AuAg		58		CdSe		104	
	AuCu		58		CdTe		104	
	Au ₃ Pd _{1-x}		58		RPO ₂ ²⁻ /RPO(OH) ₂	Al	107	
	CdTe		59	Al-OH		108		
	CdSe		60	Ca ₁₀ (PO ₄ CO ₃) ₆ (OH) ₂		109		
	CdS		61,62	GaAs		110		
	Cu	26	58	GaN		110		
	FePt		63-66	Indium tin oxide		111		
	GaAs		67	(ITO)				
	Ge		68	Mica		112		
	Hg		69-71	TiO ₂		113,114		
	HgTe		72	ZrO ₂		114,115		
	InP		73	CdSe		116-118		
	Ir		74	CdTe		118,119		
	Ni		75	RPO ₄ ²⁻	Al ₂ O ₃	120		
	PbS		76-78		Nb ₂ O ₅	120		
Pd	30	74,79	Ta ₂ O ₅		121			
PdAg		58	TiO ₂		120,122			
Pt		80	RN \equiv C		Pt	123	124	
Ru		81			RHC=CH ₂	Si	37	
Stainless Steel 316L	48				RC \equiv CH	Si(111):H	125	
YBa ₂ Cu ₃ O _{7-δ}	82				RSiX ₃ X = H, Cl, OCH ₂ CH ₃	HfO ₂	126	
Zn	83					ITO	127	
ZnSe	84		PtO			128		
ZnS		85	TiO ₂	113,126,129				
			ZrO ₂	126,129				
RSAc	Au	86						
	Au		87					
RSR'	Au	88						



S-Au 25-30 Kcal/mole
 Si-O 190 kcal/mole



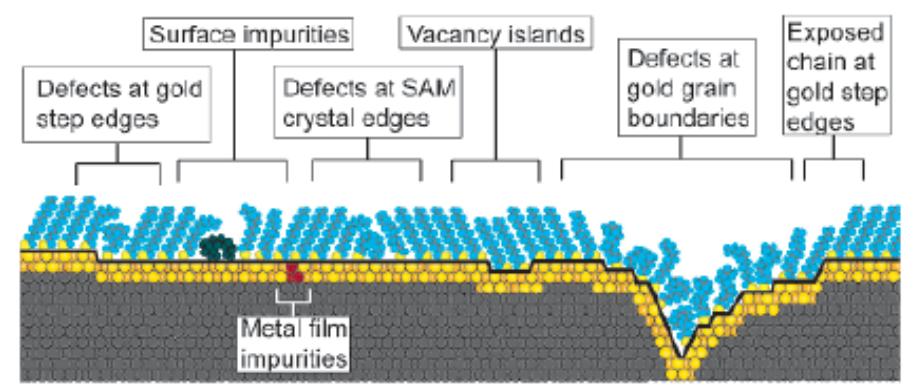
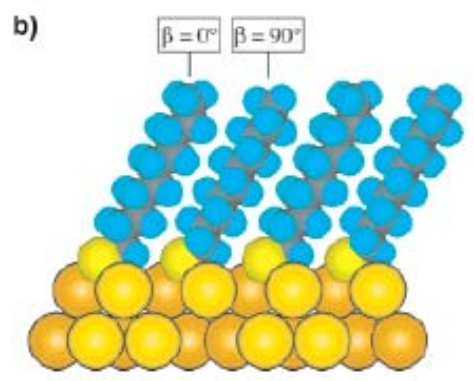
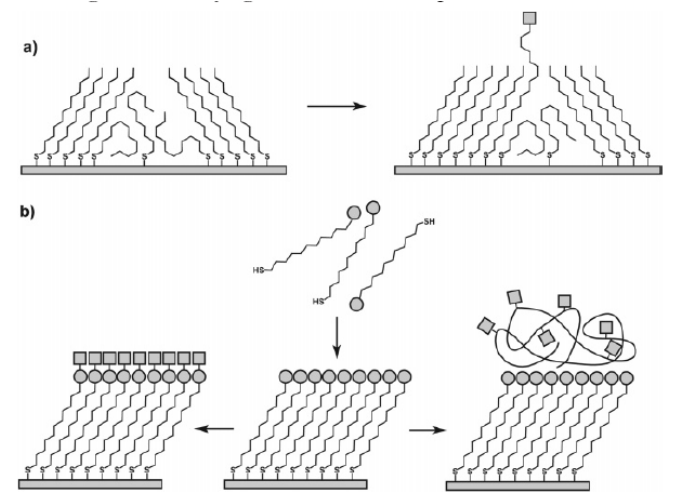
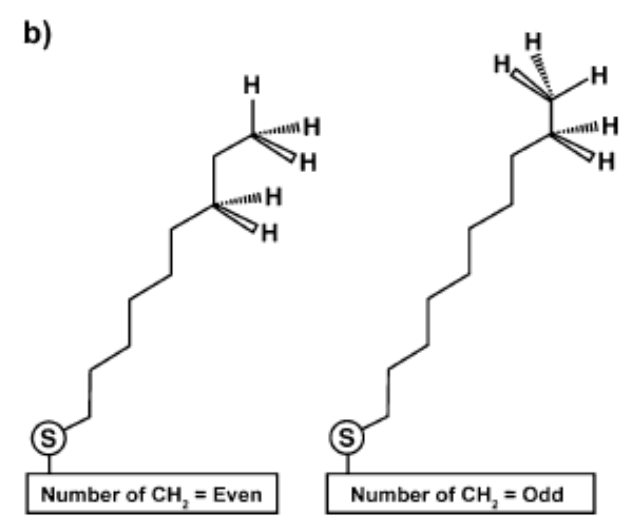


Figure 7. Schematic illustration of some of the intrinsic and extrinsic defects found in SAMs formed on polycrystalline substrates. The dark line at the metal–sulfur interface is a visual guide for the reader and indicates the changing topography of the substrate itself.



^a (a) Insertion of a functional adsorbate at a defect site in a preformed SAM. (b) Transformation of a SAM with exposed functional groups (circles) by either chemical reaction or adsorption of another material.



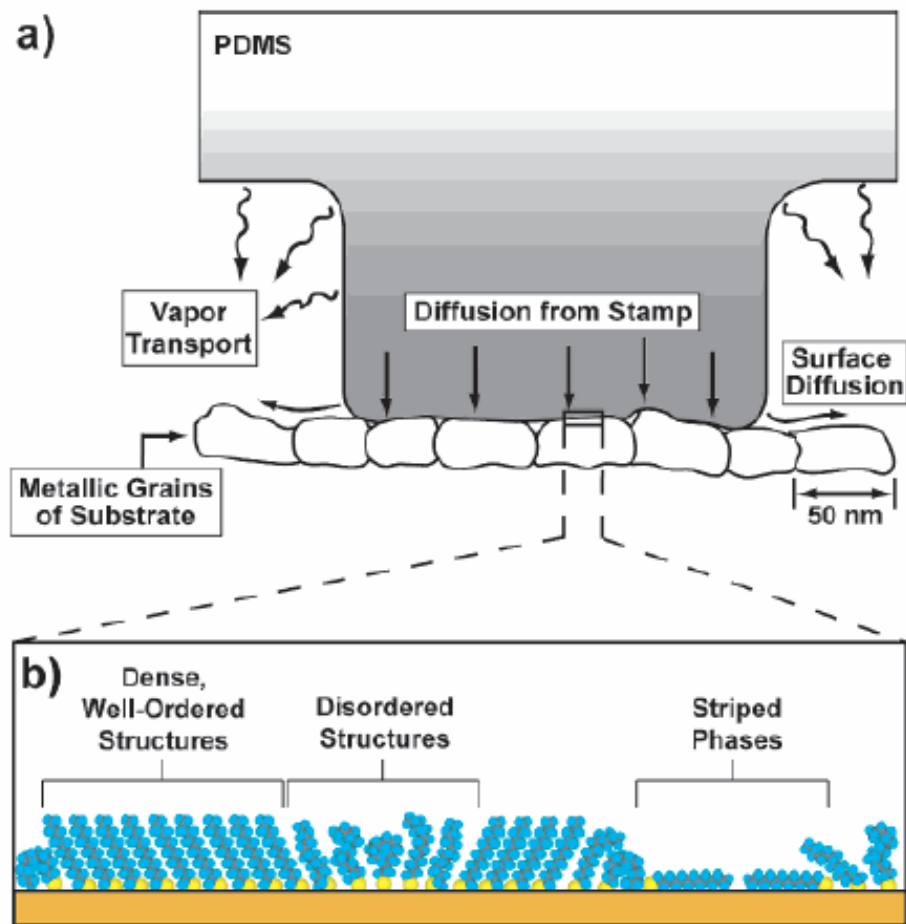


Figure 12. (a) Schematic illustration depicting the application of a PDMS stamp containing thiols to a polycrystalline metal film. The primary mechanisms of mass transport from the stamp to the surface are shown. The grayscale gradient approximates the concentration of thiols adsorbed in the stamp itself. (b) Magnified schematic view that illustrates the variety of structural arrangements found in SAMs prepared by μ CP when the stamp is wetted with a 1–10 mM solution and applied to the substrate for 1–10 s.

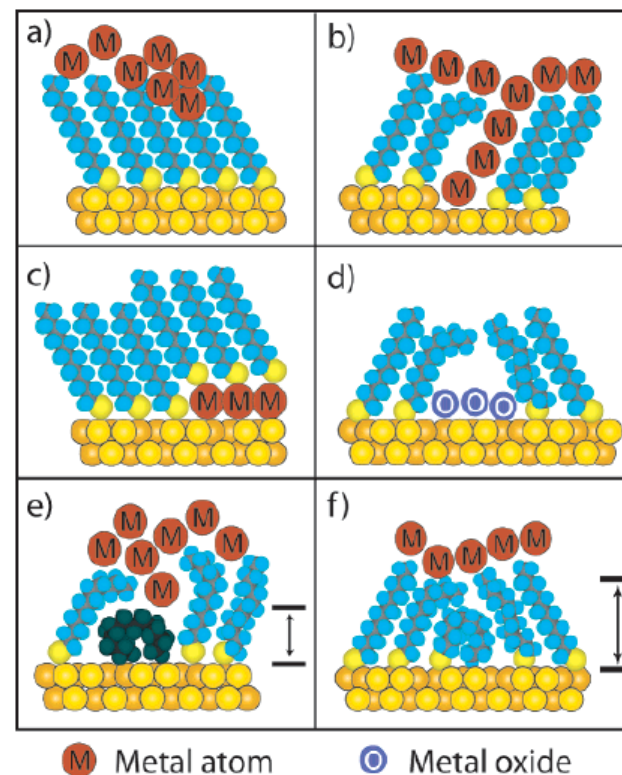


Figure 17. Schematic illustration of the types of defects in SAMs that can influence the rate of electron transfer in two-terminal (or three-terminal) devices. (a) Chemical reaction with the organic component of SAMs during evaporation of metal films. (b) Formation of metallic filaments during evaporation or operation of the device. (c) Deposition of adlayers of metal on the surface of the substrate supporting the SAM. (d) Formation of oxide impurities on the surface. (e) Organic (or organometallic) impurities in the SAM. (f) Thin regions in the SAM resulting from conformational and structural defects. In e and f the dimension normal to the surface that is denoted by the black arrows indicates the approximate shortest distance between the two metal surfaces; note that these distances are less than the nominal thickness of the ordered SAM.



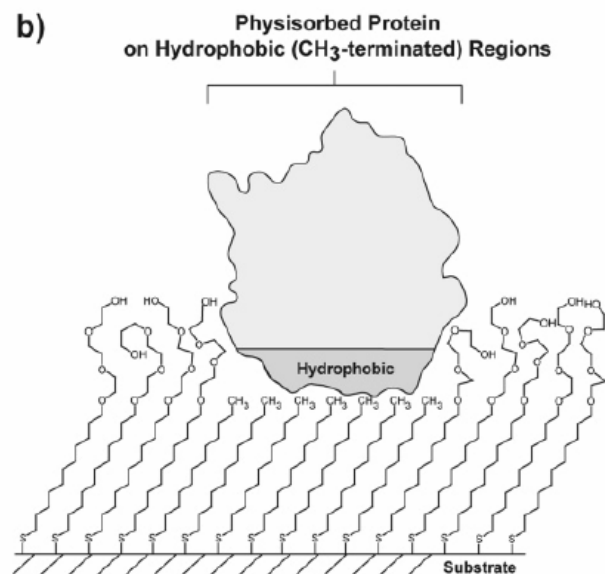
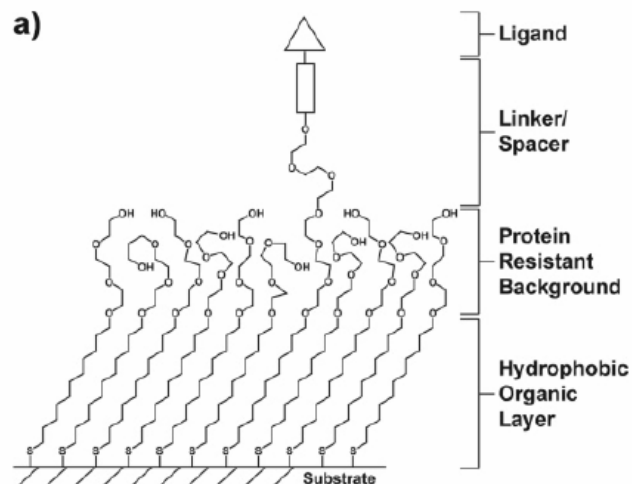


Figure 21. Schematic illustrations of (a) a mixed SAM and (b) a patterned SAM. Both types are used for applications in biology and biochemistry.

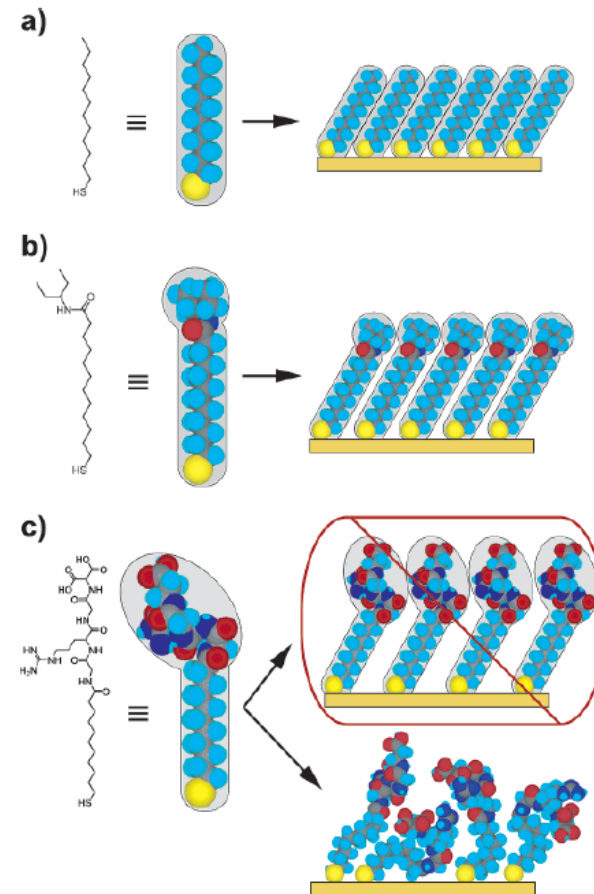


Figure 22. Schematic diagram illustrating the effects that large terminal groups have on the packing density and organization of SAMs. (a) Small terminal groups such as -CH₃, -CN, etc., do not distort the secondary organization of the organic layer and have no effect on the sulfur arrangement. (b) Slightly larger groups (like the branched amide shown here) begin to distort the organization of the organic layer, but the strongly favorable energetics of metal-sulfur binding drive a highly dense arrangement of adsorbates. (c) Large terminal groups (peptides, proteins, antibodies) sterically are unable to adopt a secondary organization similar to that for alkanethiols with small terminal groups. The resulting structures probably are more disordered and less dense than those formed with the types of molecules in a and b.



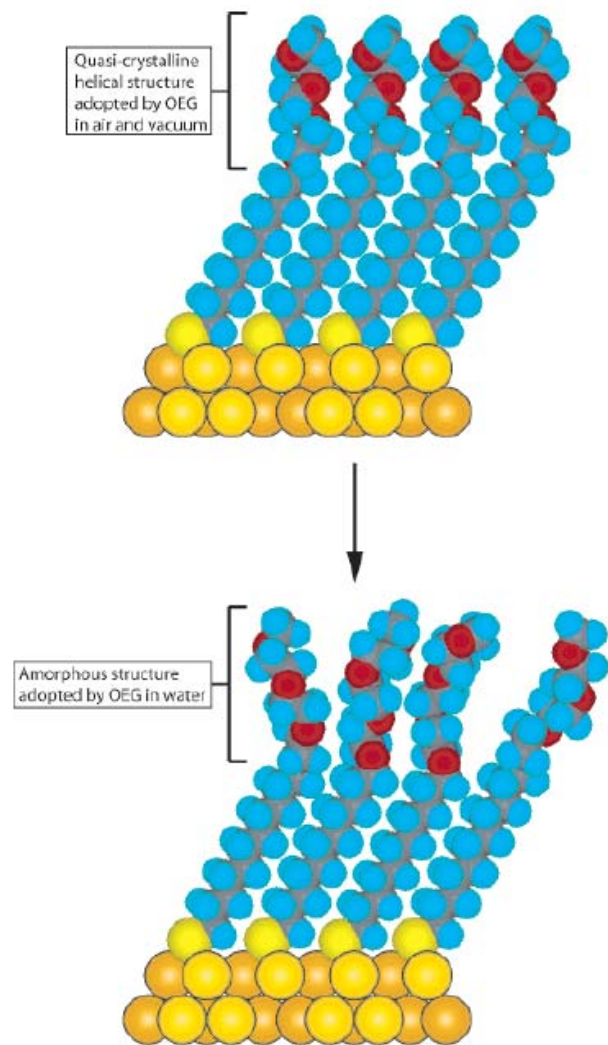
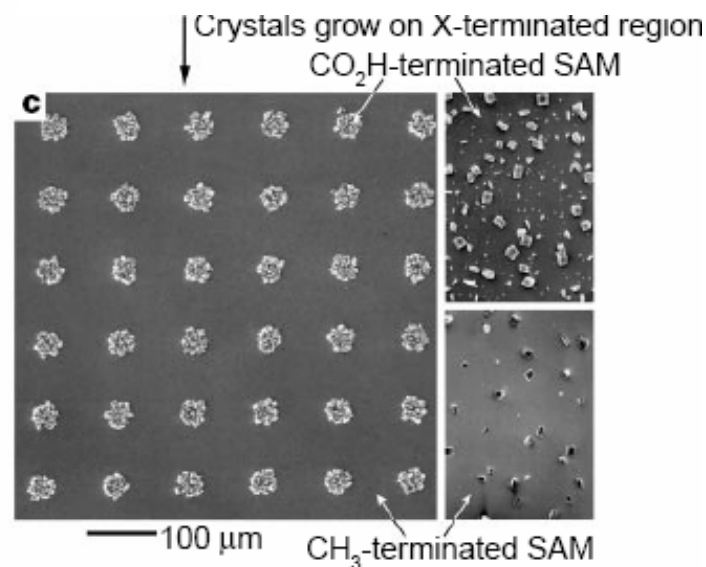
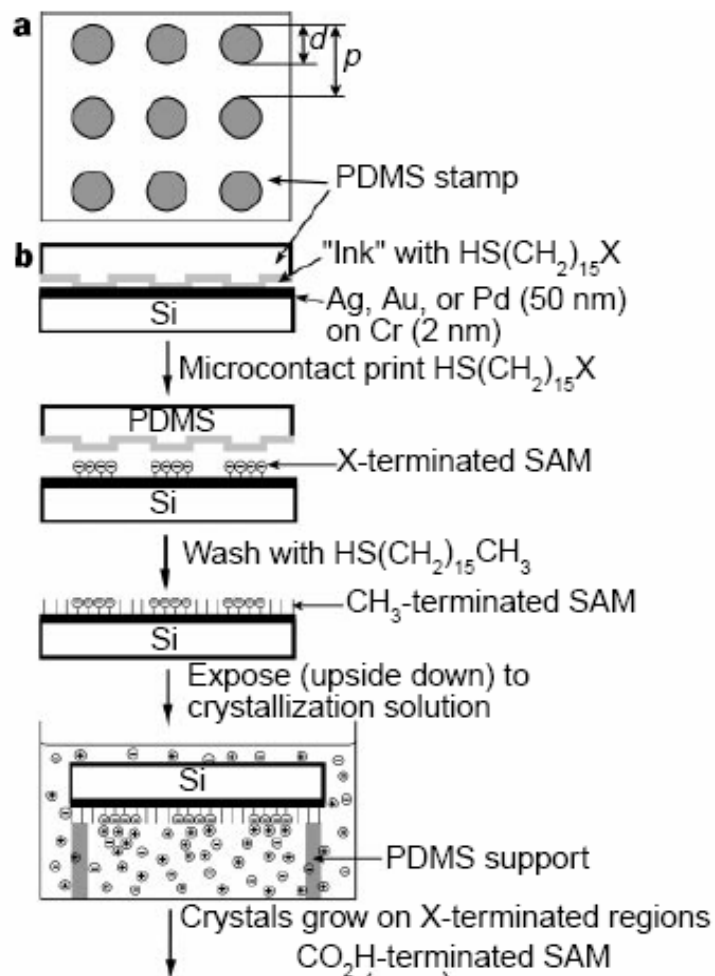


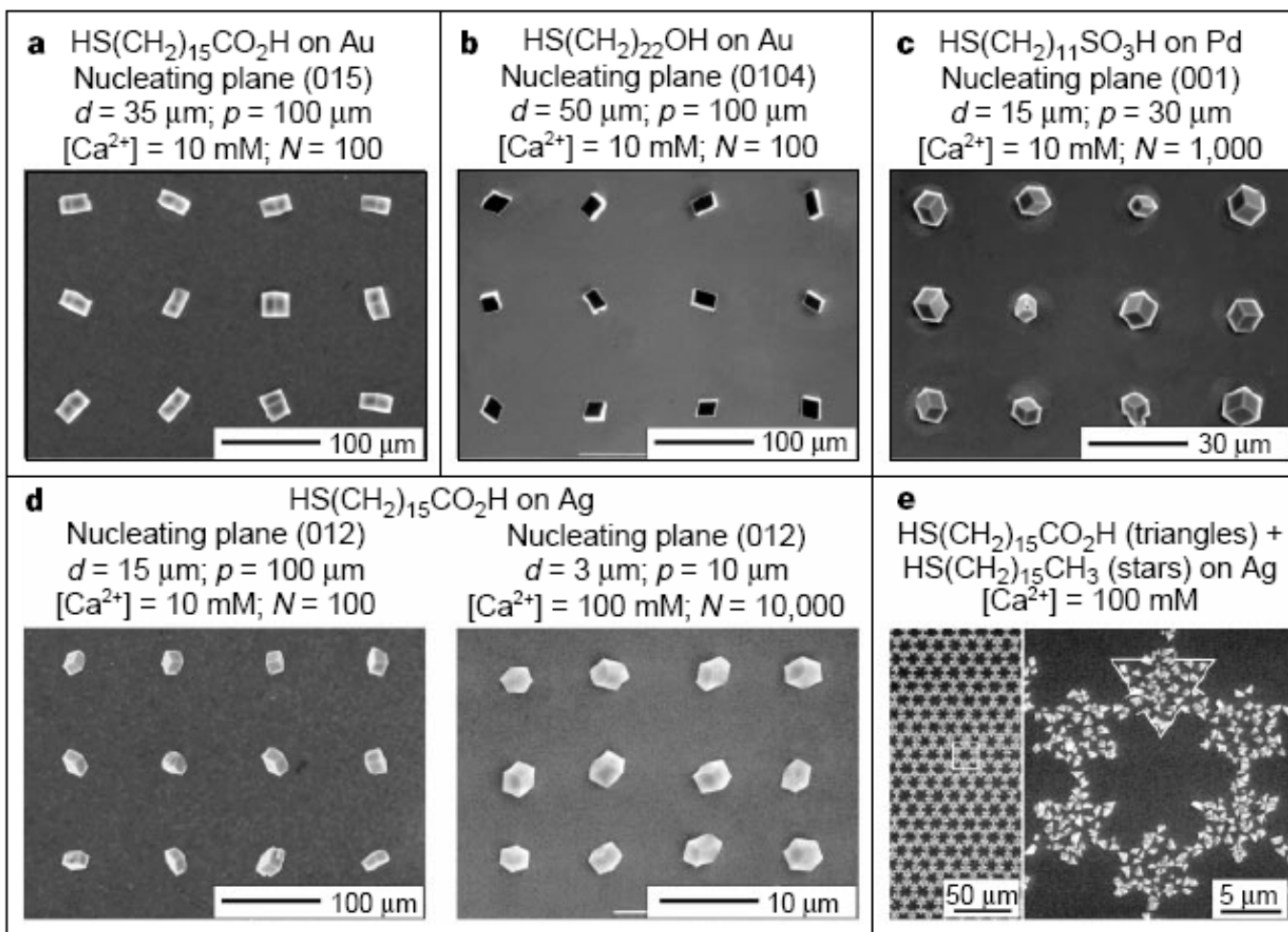
Figure 23. Schematic illustration of the order–disorder transition evidenced by SAMs of alkanethiolates terminated with triethylene glycol. The EG₃ group loses conformational ordering upon solvation in water.



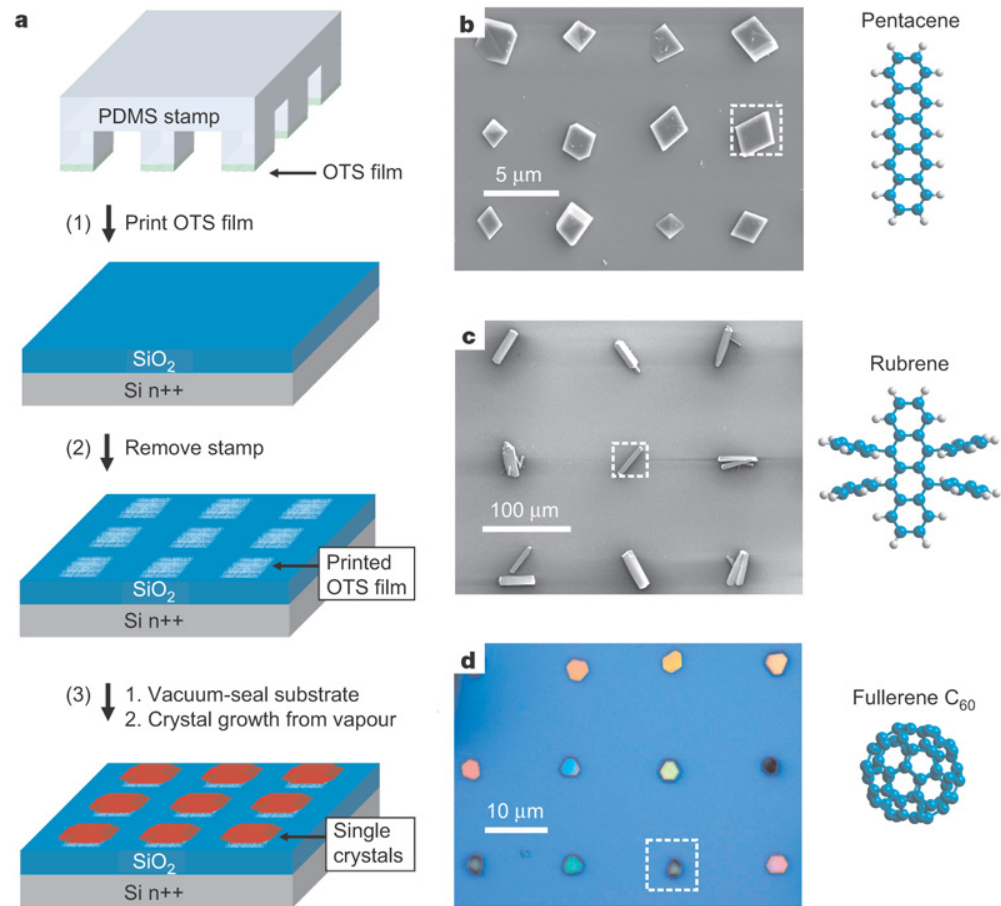
Control of crystal nucleation by patterned self-assembled monolayers

NATURE | VOL 398 | 8 APRIL 1999





Patterning of organic single crystals



Nature 444, 913-917(14 December 2006)



Large On-Off Ratios and Negative Differential Resistance in a Molecular Electronic Device

J. Chen,¹ M. A. Reed,^{1*} A. M. Rawlett,² J. M. Tour^{2*}

19 NOVEMBER 1999 VOL 286 SCIENCE

Fig. 1. Schematics of device fabrication. (A) Cross section of a silicon wafer with a nanopore etched through a suspended silicon nitride membrane. (B) Au-SAM-Au junction in the pore area. (C) Blowup of (B) with 1c sandwiched in the junction. (D) Scanning electron micrograph (SEM) of pyramid Si structure after anisotropic Si etching [that is, the bottom view of (A)]. (E) SEM of an etched nanopore through the silicon nitride membrane. (F) The active molecular compound 1c and its precursors the free thiol 1b and the thiol-protected system 1a.

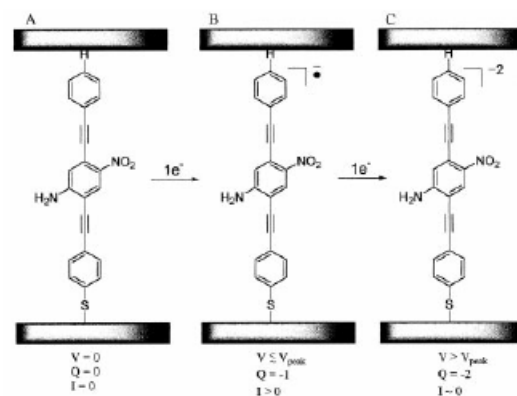
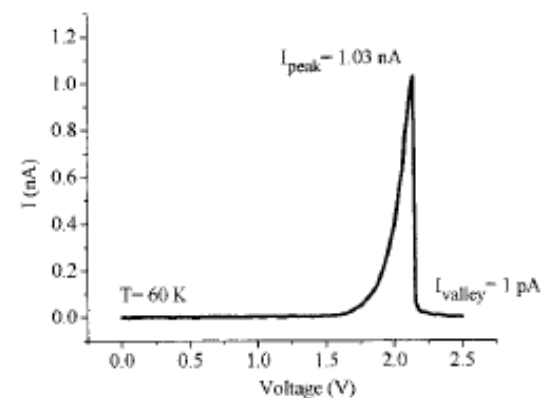
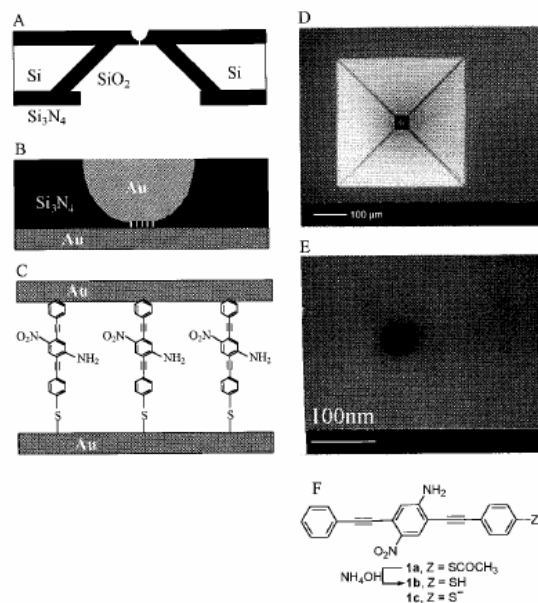


Fig. 4. Potential mechanism for the NDR effect. As voltage is applied, the molecules in the SAM (A) undergo a one-electron reduction to form the radical anion (B) that provides a conductive state. Further increase of the voltage causes another one-electron reduction to form the dianion insulating state (C). Q is the charge.



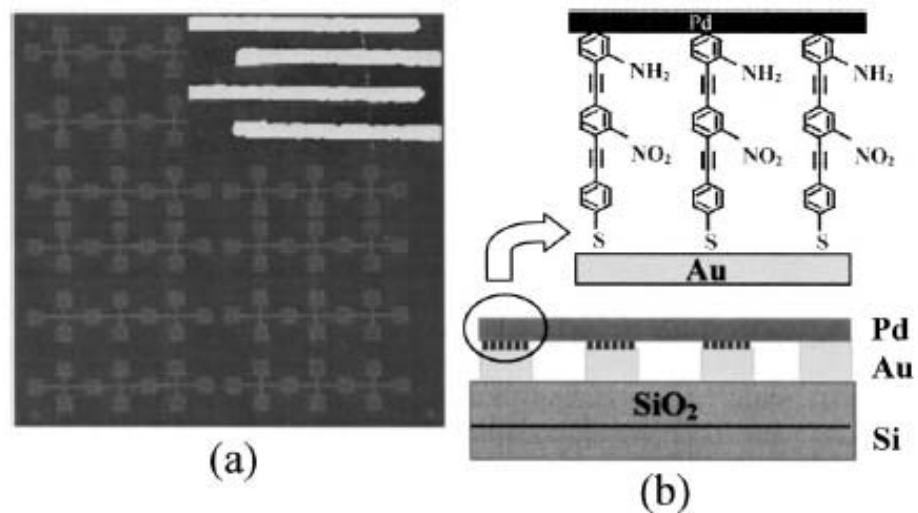


FIG. 1. (a) Optical micrograph of the nanoelectrode array. Inset: AFM image of four Au nanoelectrodes with a Pd nanowire lying across. (b) Schematic diagram of the Pd/molecular wires/Au junctions on a Si/SiO₂ substrate.

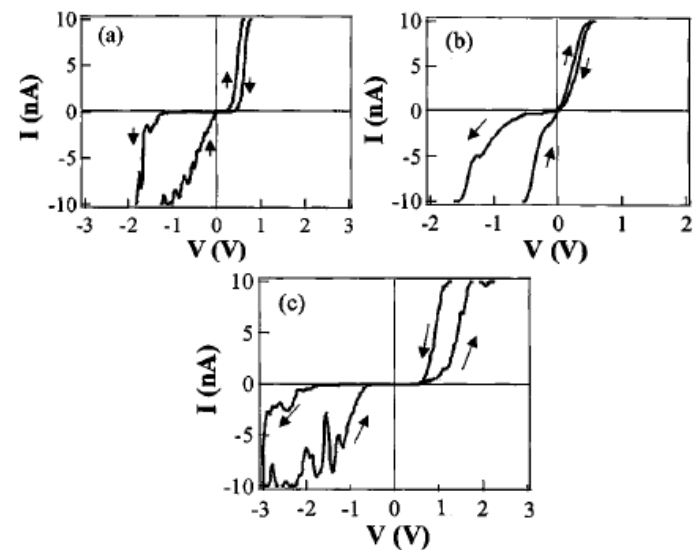
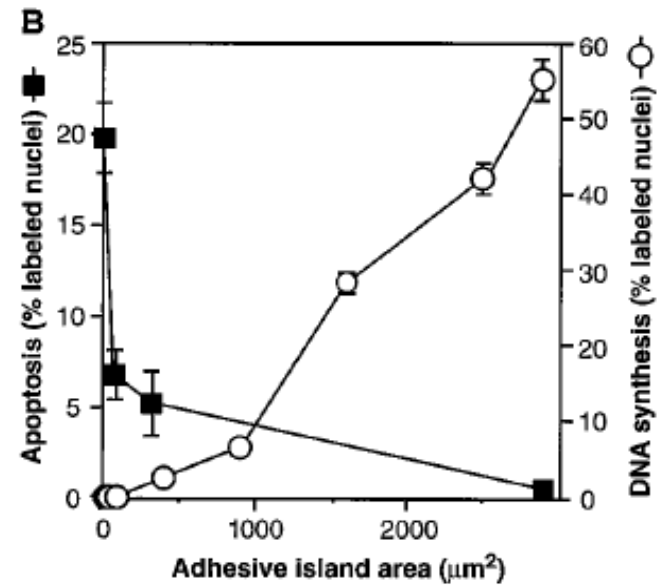
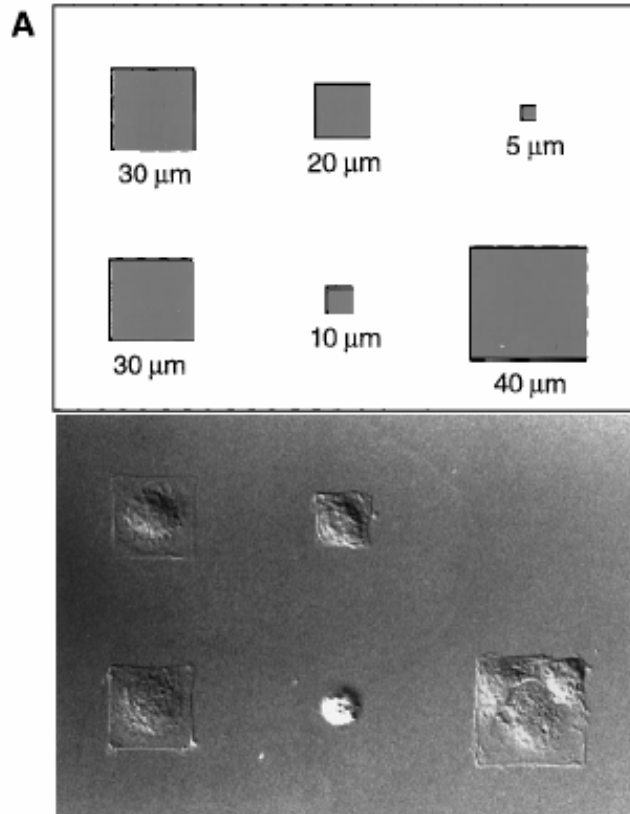


FIG. 3. Typical I - V curves of molecular devices. (a), (b), and (c) correspond to molecules a, b, and c shown in Fig. 2, respectively.



Geometric Control of Cell Life and Death

• SCIENCE • VOL. 276 • 30 MAY 1997



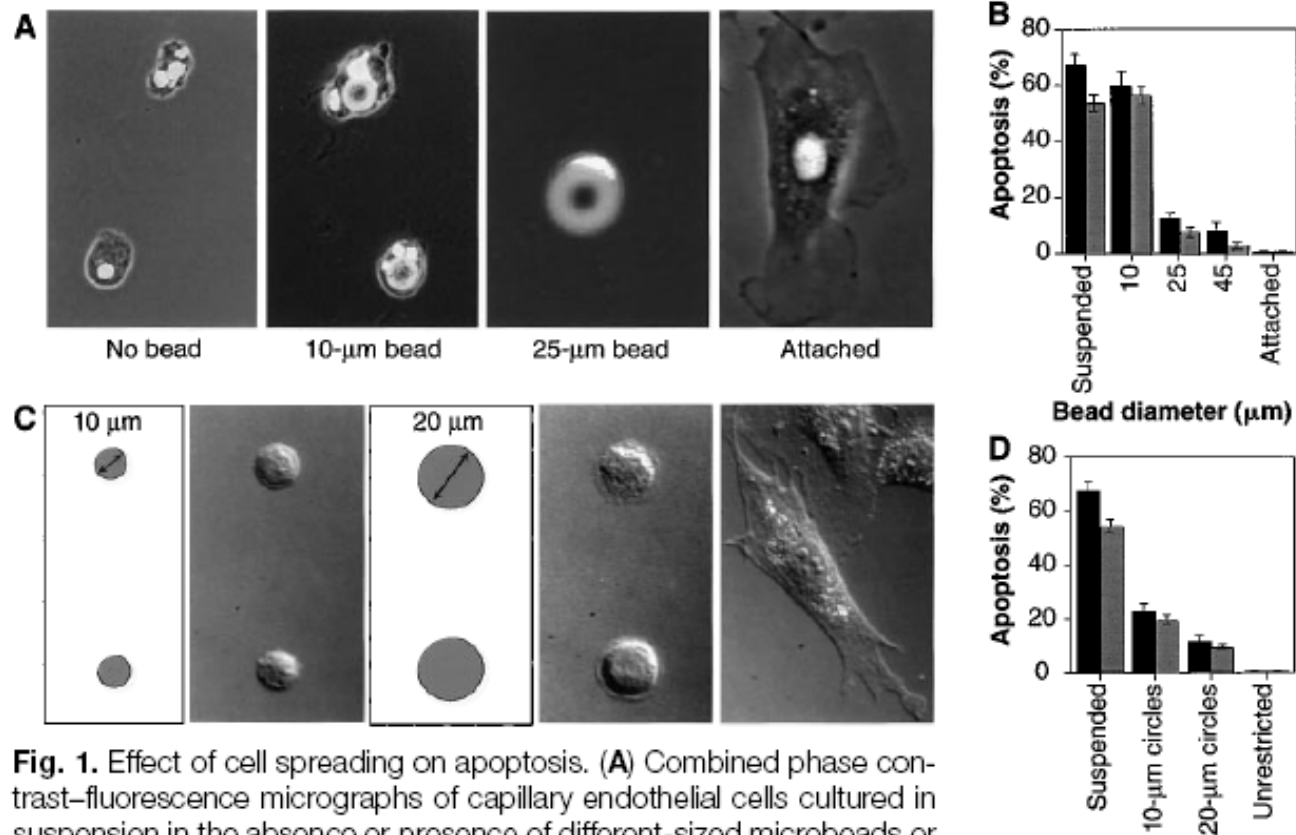


Fig. 1. Effect of cell spreading on apoptosis. **(A)** Combined phase contrast–fluorescence micrographs of capillary endothelial cells cultured in suspension in the absence or presence of different-sized microbeads or attached to a planar culture dish coated with FN for 24 hours (28). In the highly spread cell on the 25- μm bead, only the flattened 4',6'-diamidino-2-phenylindole (DAPI)–stained nucleus is clearly visible. **(B)** Apoptosis in cells attached to different-sized beads, in suspension, or attached to a dish. The apoptotic index was quantitated by measuring the percentage of cells exhibiting positive TUNEL staining (black bars) (Boehringer Mannheim), which detects DNA fragmentation; similar results were obtained by analyzing changes in nuclear condensation and fragmentation in cells stained with DAPI at 24 hours (gray bars). Apoptotic indices were determined only within single cells bound to single beads. Error bars indicate SEM. **(C)** Differential interference-contrast micrographs of cells plated on substrates micropatterned with 10- or 20- μm -diameter circles coated with FN (left), by a microcontact printing method (29) or on a similarly coated unpatterned substrate (right). **(D)** Apoptotic index of cells attached to different-sized adhesive islands coated with a constant density of FN for 24 hours; similar results were obtained with human and bovine capillary endothelial cells (28). Bars same as in (B).



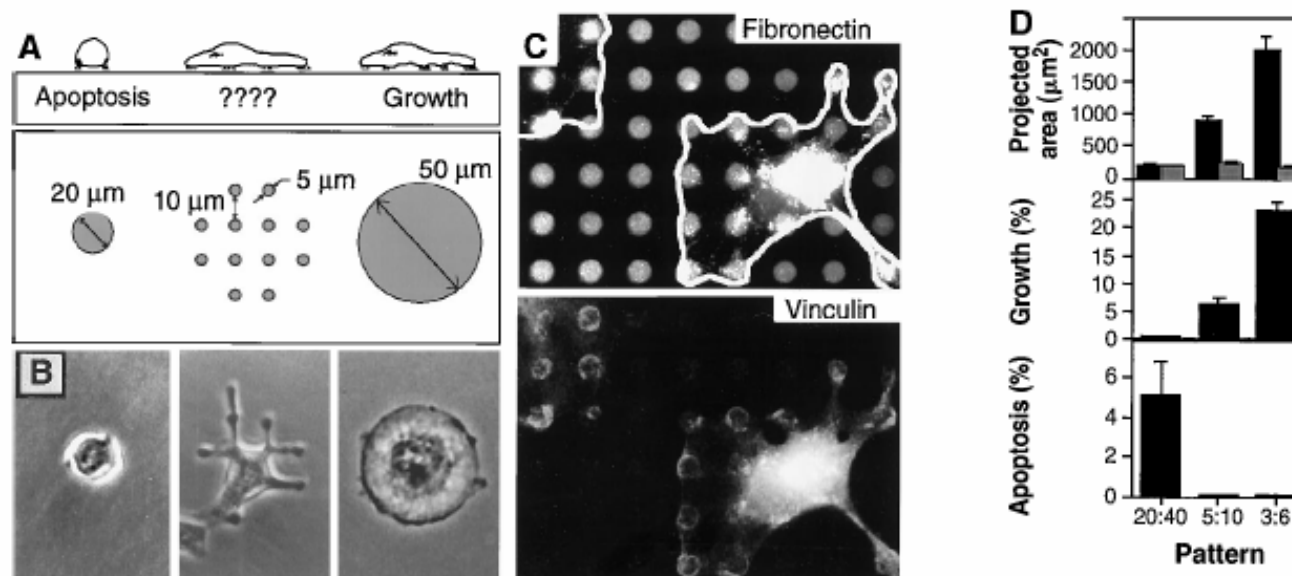


Fig. 3. Cell-ECM contact area versus cell spreading as a regulator of cell fate. **(A)** Diagram of substrates used to vary cell shape independently of the cell-ECM contact area. Substrates were patterned with small, closely spaced circular islands (center) so that cell spreading could be promoted as in cells on larger, single round islands, but the ECM contact area would be low as in cells on the small islands. **(B)** Phase-contrast micrographs of cells spread on single 20- or 50- μm -diameter circles or multiple 5- μm circles patterned as shown in (A). **(C)** Immunofluorescence micrographs of cells on a micropatterned substrate stained for FN (top) and vinculin (bottom). White outline indicates cell borders; note circular rings of vinculin staining, which coincide precisely with edges of the FN-coated adhesive islands. **(D)** Plots of projected cell area (black bars) and total ECM contact area (gray bars) per cell (top), growth index (middle), and apoptotic index (bottom) when cells were cultured on single 20- μm circles or on multiple circles 5 or 3 μm in diameter separated by 40, 10, and 6 μm , respectively.



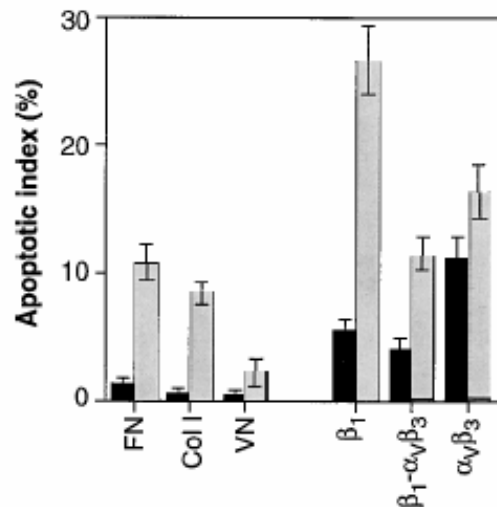


Fig. 4. Role of different integrin ligands in cell shape-regulated apoptosis. Apoptotic indices (percentage positive TUNEL staining) for cells cultured for 24 hours on unpatterned substrates (black bars) or on 20- μ m circles (gray bars) coated with FN, type I collagen (Col I), vitronectin (VN), type I collagen (Col I), vitronectin (VN), anti- β_1 , anti- $\alpha_v\beta_3$, or antibodies to both integrin β_1 and integrin $\alpha_v\beta_3$ (29).

hexadecanethiol [$\text{HS}(\text{CH}_2)_{15}\text{CH}_3$] was printed onto gold-coated substrates with a flexible stamp containing a relief of the desired pattern. The substrate was immersed immediately in 2 mM tri(ethylene glycol)-terminated alkanethiol [$\text{HS}(\text{CH}_2)_{11}(\text{OCH}_2\text{CH}_2)_3\text{OH}$ in ethanol], which coated the remaining bare regions of gold. When these substrates were immersed in a solution of FN, vitronectin, or type I collagen (50 $\mu\text{g}/\text{ml}$ in phos-



Electrochemical Desorption of Self-Assembled Monolayers Noninvasively Releases Patterned Cells from Geometrical Confinements

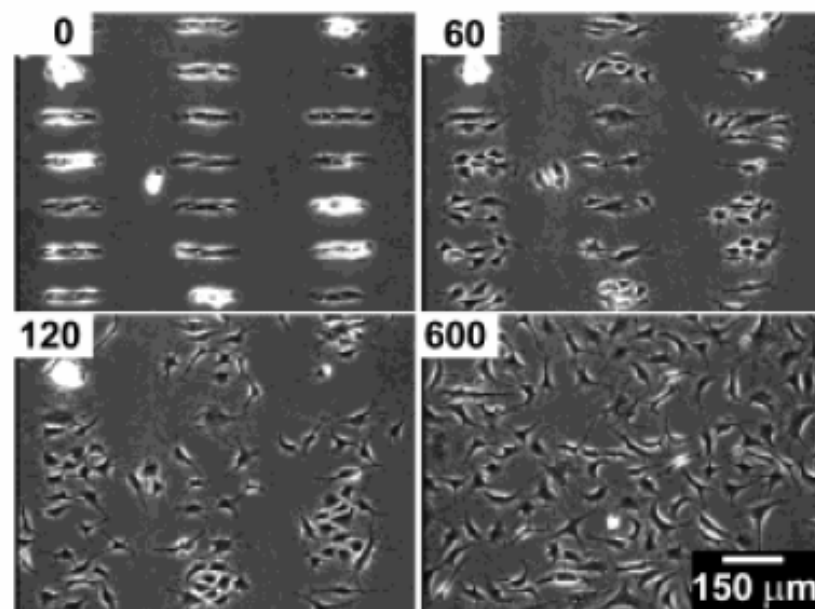


Figure 1. BCE cells were allowed to attach to a surface patterned with C₁₁EG₃ and C₁₈. Application of a cathodic voltage pulse (-1.2 V for 30 s in this case) released the cells from the microislands. The numbers indicate the time elapsed (in minutes) after the voltage pulse.



Directing cell migration with asymmetric micropatterns <http://www.pnas.org/cgi/reprint/102/4/>

PNAS | January 25, 2005 | vol. 102 | no. 4 | 975

Xingyu Jiang*, Derek A. Bruzewicz*, Amy P. Wong*, Matthieu Piel[†], and George M. Whitesides**

*Department of Chemistry and Chemical Biology, Harvard University, 12 Oxford Street, Cambridge, MA 02138; and [†]Department of Molecular and Cell Biology, Harvard University, 16 Divinity Avenue, Cambridge, MA 02138

Contributed by George M. Whitesides, December 2, 2004

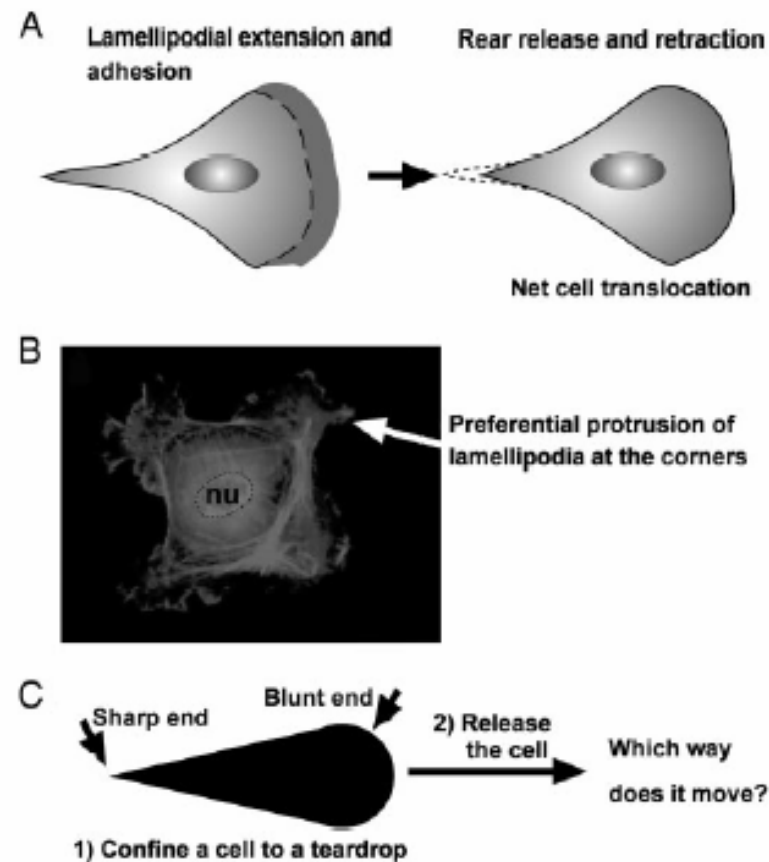


Fig. 1. A problem on cell motility. (A) A cartoon illustration of the migration of a typical mammalian cell on a flat surface. This teardrop shape is found in many types of cells. (B) Cells confined to squares preferentially extend their lamellipodia from the corners. nu, nucleus. (C) If a cell is confined to a shape of teardrop, will the cell preferentially extend its lamellipodia from the sharp end or from the blunt end? If released from confinement, in which direction will it likely move?

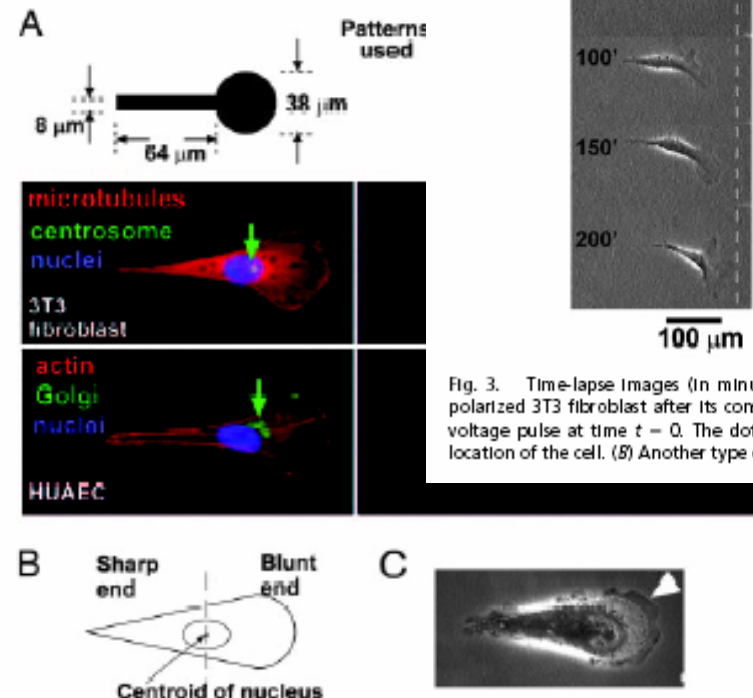


Fig. 2. Asymmetric patterns polarize immobilized cells. (A) The Golgi and the centrosome are located closer to the half of a cell with the blunt end. We used phalloidin, antigolgin, DAPI, antitubulin, and antipericentrin to identify actin (red), the Golgi (green), the nucleus (blue), microtubules (red), and the centrosome (green), respectively. The green arrows indicate the location of centrosomes in 3T3 cells and Golgi in human umbilical artery endothelial cells (HUAEC). (B) We divided the cell into a half with the sharp end and a half with the blunt end by a vertical line drawn at the centroid of the nucleus; >80% ($n = 30$) of the centrosomes and Golgi were localized in the region of the wide end. (C) The lamellipodia of immobilized 3T3 cells tended to extend more from the blunt end as well (arrowhead). The dotted line indicates the edges of the adhesive pattern.

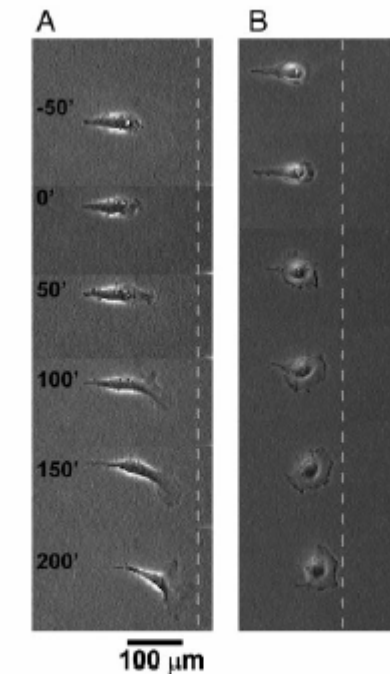


Fig. 3. Time-lapse images (in minutes) show the motility of an initially polarized 3T3 fibroblast after its constraint is released. (A) We applied the voltage pulse at time $t = 0$. The dotted line serves as a reference for the location of the cell. (B) Another type of cell, COS-7, shows similar behavior.



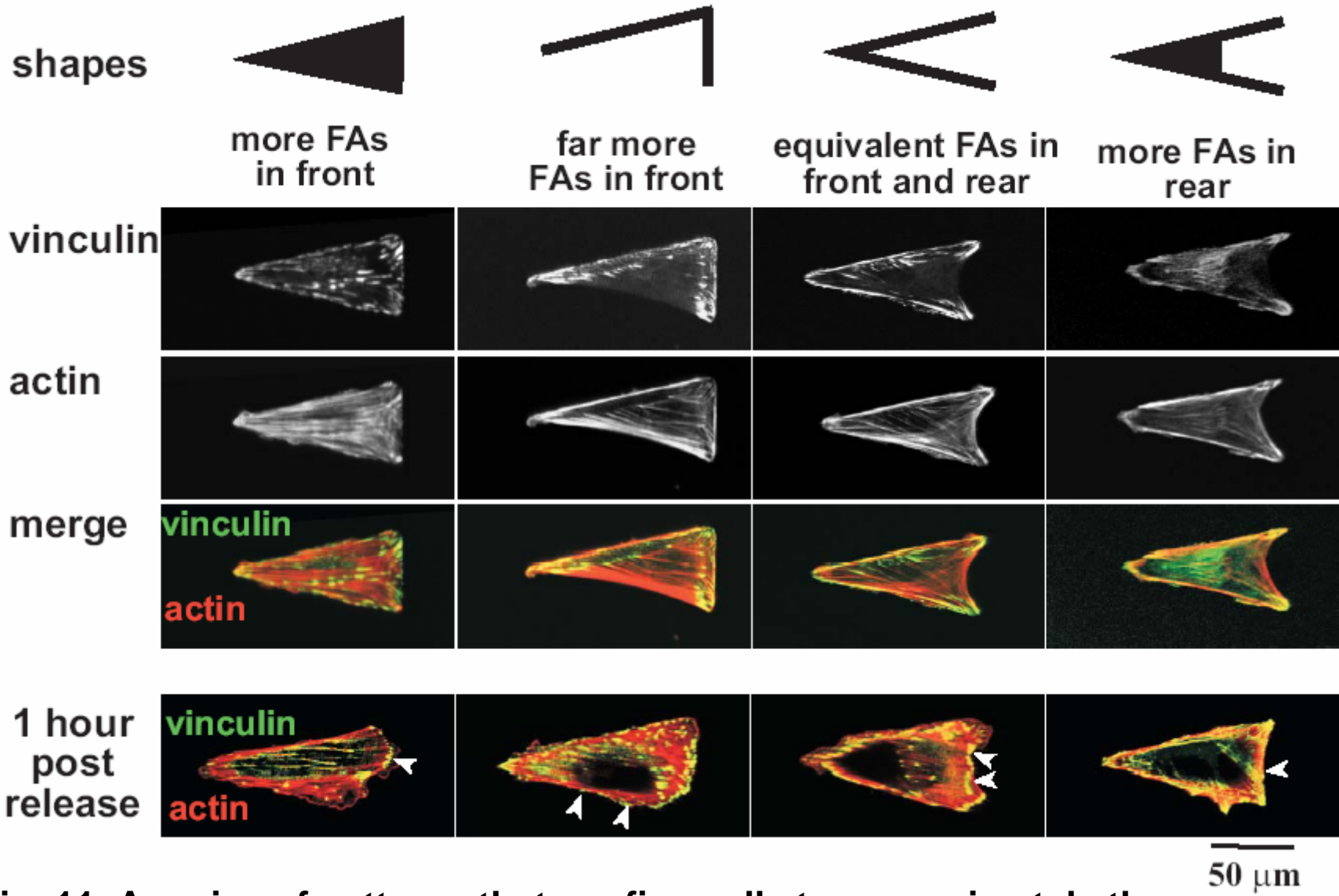


Fig. 11. A series of patterns that confine cells to approximately the same projected geometry (visualized by the actin cytoskeleton) but distribute the focal adhesions (FAs; visualized by immunostaining for vinculin) differently. The bottom row shows that new focal adhesions formed 1 h after release in areas that were inert to attachment of cells prior to release (arrowheads).

Soft-Lithography

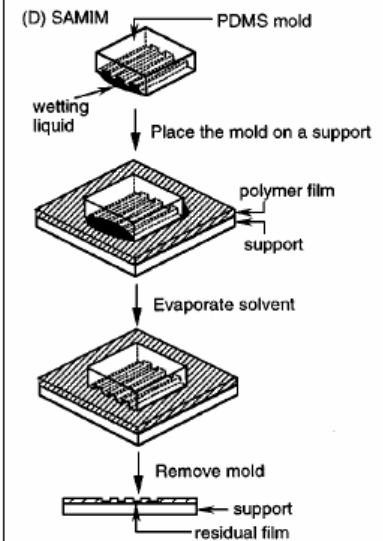
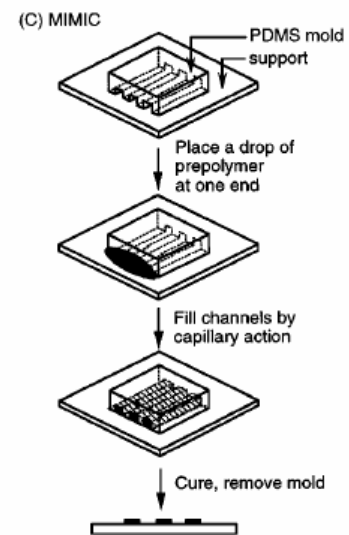
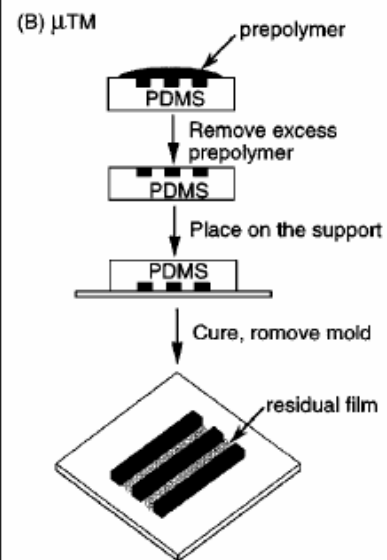
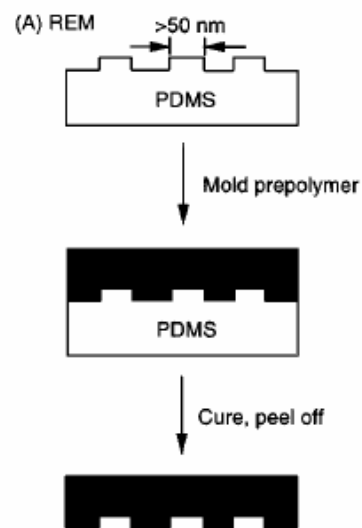
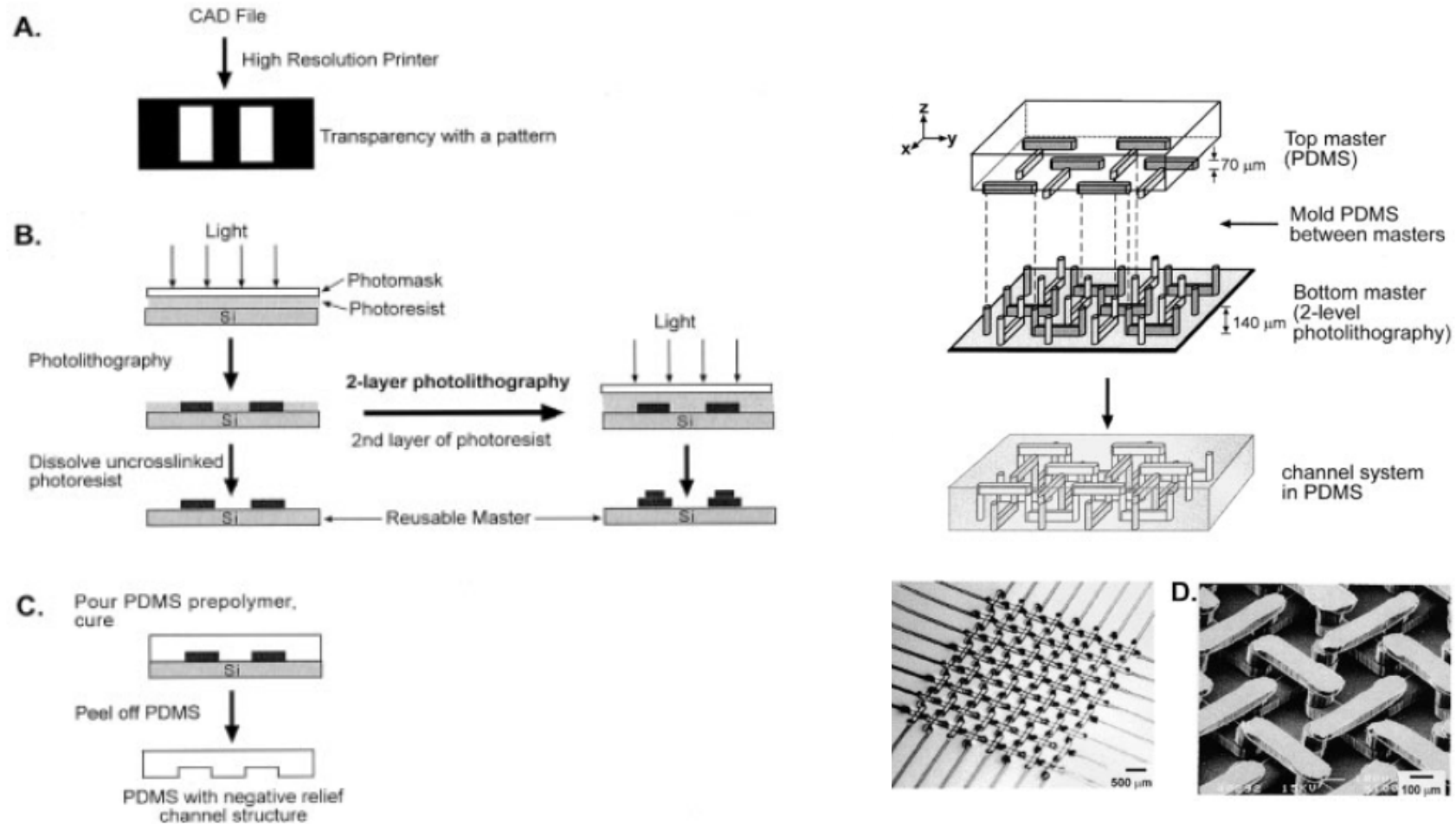


Figure 5 Schematic illustration of procedures for (a) replica molding (REM), (b) microtransfer molding (μ TM), (c) micromolding in capillaries (MIMIC), and (d) solvent-assisted micromolding (SAMIM).



Electrophoresis 2002, 23, 3461–3473



Replication Result

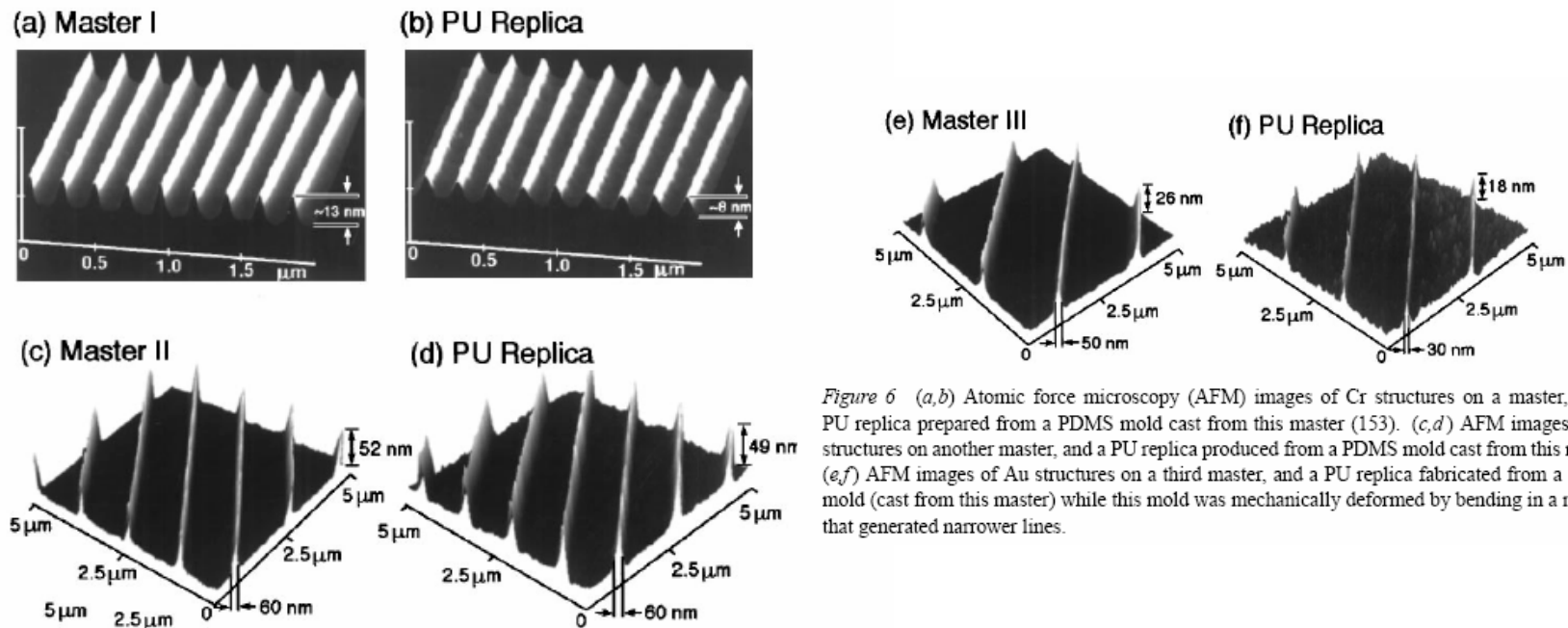


Figure 6 (a,b) Atomic force microscopy (AFM) images of Cr structures on a master, and a PU replica prepared from a PDMS mold cast from this master (153). (c,d) AFM images of Au structures on another master, and a PU replica produced from a PDMS mold cast from this master. (e,f) AFM images of Au structures on a third master, and a PU replica fabricated from a PDMS mold (cast from this master) while this mold was mechanically deformed by bending in a manner that generated narrower lines.

